



**ΠΟΛΥΤΕΧΝΕΙΟ
ΚΡΗΤΗΣ**

Μηχανισμοί και παράμετροι βελτιστοποίησης του κύκλου ζωής των παραδοσιακών άσβεστο-κονιαμάτων

Διδακτορική Διατριβή

Μαρία Αμέντα

Συμβουλευτική επιτροπή: Μαραβελάκη Π.

Κυλίκογλου Β.

Καλλίθρακας-Κόντος Ν.

Εξεταστική επιτροπή: Ιωάννου Ι.

Καλλίθρακας-Κόντος Ν.

Κυλίκογλου Β.

Μαραβελάκη Π.

Μπακόλας Α.

Περδικάτσης Β.

Στεφανίδου Μ.

Χανιά, Ιούλιος 2017



Mechanisms and parameters for life-cycle optimization of traditional lime-based mortars

PhD Thesis
by
Maria Amenta

Chania, July 2017

Acknowledgements

The research work presented in this thesis was carried out at the Institute of Nanoscience and Nanotechnology (INN) of the National Center for Scientific Research “Demokritos” (NCSR “D”) and the School of Architecture of the Technical University of Crete (TUC) under the supervision of Prof. Noni Maravelaki (TUC), Prof. Nikos Kalithrakas (TUC) and Dr. Vassilis Kilikoglou (NCSR “D”). I want to thank them all for giving me the opportunity to carry out this research. I would also like to express my gratitude to the members of the examination committee: Prof. A. Bakolas (National Technical University of Athens), Prof. I. Ioannou (University of Cyprus), Prof. V. Perdikatsis (Technical University of Crete) and Prof. M. Stefanidou (Aristotle University of Thessaloniki) for accepting to contribute to the final and most challenging part of this academic endeavor.

I also want to thank the educational committee of NCSR “Demokritos” for honoring me with a PhD Scholarship four years ago. I feel truly grateful and sad for being one of the last beneficiaries of this kind of scholarship, one that has made the academic development of PhD students for more than three decades possible.

I want to express my deepest gratitude to all the people who have helped and encouraged me during the past years.

First of all, I would like to thank Dr. Vassilis Kilikoglou for giving me the opportunity to work in the Ceramics and Composite Materials (CCM) group and who has been a mentor to me both scientifically and professionally.

My great appreciation goes to my supervisor, Prof. Noni Maravelaki for her support, encouragement and trust throughout the whole course of my research.

I would also like to thank Dr. Ioannis Karatasios who has been my guide from the beginning by helping, encouraging and supporting me in every step of the way.

Many people have offered me tremendous help in this research by sharing knowledge, experience and infrastructure. I want to thank each and every one of them:

Dr. Nikos Boukos (NCSR D) and Dr. Anastasios Traulos (NCSR D) for trusting me with the Scanning Electron Microscope.

Dr. Alexia Karamperi (NTUA) for the AAS measurements and for reminding me the importance of the collaboration between different fields in research.

Dr. George Vekinis (NCSR D) for trusting me to use the INSTRON -100kN compression machine for countless hours and for giving me new perspectives on fracture properties of composite materials.

Prof. Alexis Stefanis (TEI of Athens) for finding the time and giving me access to the Mercury intrusion Porosimeter.

and Alexandra Elbakyan who gave me access to unlimited scientific knowledge.

I also want to thank all members of the Ceramics and Composite Materials (CCM) group, past and present, with whom I spent countless hours these past four years: Dr. Anno Hein, Dr. Lenia Farmakalidou, Dr. Maria Tziotziou, Dr. Dimitris Sioulas and Anastasia Michalopoulou. Without our discussions and their support these past years would have been a lot poorer.

And of course all the researchers, students and personnel of the INN who have always created a friendly and hospitable working environment.

I would also like to express my sincere gratitude to Noemi Mueller (British School at Athens) for being more than a friend these past years and for always helping me see what is important inside and outside the lab.

Finally and most importantly, I want to thank my life-companion, my family and my friends for enduring me these past years. I am eternally grateful for all the love and support they have all given me unconditionally.

Abstract

Cracking is an inherent characteristic of cement-based materials that leads to the reduction of their performance characteristics, thus increasing the need for external interventions. Self healing of cement based materials is a phenomenon that can take place autogenously in mortars and leads to the prolongation of their service-life, as it has also been linked with the longevity of historic mortars. The autogenous self-healing phenomenon can be described by the filling of cracks by healing phases formed by secondary reactions of the mortars own ingredients, without the addition of additional “healing” agents.

Even though the self-healing phenomenon has attracted a lot of attention from the scientific community in recent years, several aspects of the mechanism have not been understood or studied at all. For instance, the healing capacity of hydraulic mortars or the conditions for the occurrence of the autogenous self healing mechanism in these materials have not been determined yet.

In this study, the parameterization of the physicochemical mechanism underlying the occurrence of the autogenous self-healing phenomenon is examined in traditional hydraulic mortars and in historic mortars’ samples.

In this context, this study focuses on the conditions required for the occurrence of the autogenous phenomenon in natural hydraulic lime (NHL) and lime-pozzolan (LP) mortars regarding the binder mineralogy and the humidity conditions. The examination of historic mortars revealed that recurrent patterns exist and the crystal habits of the re-precipitated products depend, among other factors, on the moisture content and on the degree of carbonation of the mortar

During the study of laboratory mortar mixtures, the first-step of the autogenous mechanism; namely the dissolution of calcium-bearing components of the binder was examined by applying an electrochemically accelerated leaching procedure that lead to the identification and monitoring of calcium compounds dissolution, formed during mortar curing.

Moreover, morphological and chemical characterization of the secondary phases produced inside the cracks, was performed, in order to gain a better understanding of the reactions that take place inside the cracks’ space. Additionally, the effect of the autogenous mechanism on the recovery of the mortars’ mechanical properties was

also examined, taking into account factors such as binder mineralogy and the duration of the healing period.

During leaching of NHL and LP specimens the successive dissolution of $\text{Ca}(\text{OH})_2$ and CSH was reported. The dissolution mechanism varies between LP and NHL mortars and it is strongly affected by the curing age of the specimen examined.

It was found that the differences revealed during the leaching of NHL and LP mortars also affect the mechanism of the self-healing phenomenon. Secondary products formed inside cracks were produced by secondary precipitation of calcite or by continued hydration of the cement matrix. Both mechanisms were reported in both NHL and LP specimens, but in different extent. Carbonation is mainly observed in LP specimens whereas hydration is the main mechanism observed in NHL specimens. Prolonged healing period has a favorable impact on the evolution of the autogenous mechanism as higher crack closure was observed.

Humidity conditions affect both the occurrence and the evolution of the self-healing mechanism. Specimens subjected to of water saturation – drying cycles exhibited higher healing potential, as expressed by the formation of secondary products inside the cracks. However the production of secondary phases was evident in specimens cured at 75%RH but not in those cured at 45%RH, suggesting that the presence of humidity above 75%RH can be a sufficient condition for the occurrence of the phenomenon.

Finally, regarding the recovery of mechanical properties due to the self-healing phenomenon, both NHL and LP specimens exhibited a high strength recovery (>90%) after one month healing period, whereas prolonged healing period did not have a substantial impact.

Overall, the parameterization of the autogenous phenomenon as it was performed in this study could lead to a more effective design and application of self-healing mortars incorporating tailor-made “healing additives”.

Περίληψη

Η ανάπτυξη μικρο-ρηγματώσεων είναι ένα κοινό χαρακτηριστικό των κονιαμάτων και αποτελεί ένα από τους κύριους παράγοντες που επιταχύνουν την διάβρωση των υλικών αυτών, μειώνοντας τη διάρκεια του προσδόκιμου ζωής τους.

Η αυτοΐαση των κονιαμάτων είναι ένα φαινόμενο που πραγματοποιείται αυτογενώς στα κονιάματα και μπορεί να οδηγήσει στην παράταση της διάρκειας ζωής τους. Το φαινόμενο αυτό μπορεί να περιγραφεί από την επούλωση των ρηγματώσεων από δευτερογενή προϊόντα, αυξάνοντας έτσι την εσωτερική συνοχή του υλικού και επομένως την αντοχή του στη διάβρωση. Παρόλο που το φαινόμενο της αυτοΐασης έχει παρατηρηθεί σε ιστορικά κονιάματα και έχει συνδεθεί με την μακροβιότητα που παρουσιάζουν, δεν έχει κατανοηθεί επαρκώς.

Τα βασικά ερωτήματα που σχετίζονται με την εξέλιξη του φαινομένου της αυτοΐασης αφορούν στους παράγοντες που επηρεάζουν την εμφάνιση και τη συχνότητα του αυτογενούς μηχανισμού αλλά και τη φύση των δευτερογενώς σχηματιζόμενων προϊόντων στις ρωγμές. Ταυτόχρονα, η δυνατότητα ανάκτησης των μηχανικών ιδιοτήτων των κονιαμάτων κατά την αυτοΐαση τους δεν έχει μελετηθεί και συσχετισθεί με τους προαναφερθέντες παράγοντες.

Η παρούσα μελέτη επικεντρώθηκε στον φυσικοχημικό χαρακτηρισμό του αυτογενούς μηχανισμού σε παραδοσιακά υδραυλικά κονιάματα. Τα παραδοσιακά φυσικά υδραυλικά (NHL) και ασβεστοποζολανικά (LP) κονιάματα χρησιμοποιούνται σε επεμβάσεις συντήρησης στα μνημεία λόγω της υψηλής μηχανικής και φυσικοχημικής τους συμβατότητας με τα ιστορικά κονιάματα.

Σκοπός της παρούσας έρευνας είναι η μελέτη του αυτογενούς φαινομένου σε παραδοσιακά κονιάματα που προσομοιώνουν τη σύνθεση των ιστορικών κονιαμάτων. Πιο συγκεκριμένα, η βαθύτερη κατανόηση του αυτογενούς μηχανισμού επιδιώκεται με βάση τους ακόλουθους στόχους:

- Την παραμετροποίηση της εμφάνισης του φαινομένου της αυτοΐασης σε ιστορικά κονιάματα.

- Την μελέτη της διαδικασίας απασβεστοποίησης όπως λαμβάνει χώρα κατά τη διάρκεια του μηχανισμού έκπλυσης των κονιαμάτων, προσομοιώνοντας έτσι το πρώτο στάδιο του αυτογενούς μηχανισμού.
- Τον προσδιορισμό του τρόπου με τον οποίο αυτή η διαδικασία επηρεάζει τη μικροδομή των κονιαμάτων και των ασβεστιούχων φάσεων μετά την έκπλυση του πορτλανδίτη.
- Την ανάλυση της μορφολογίας και της ορυκτολογίας των προϊόντων αυτοΐασης με μεθόδους μικροσκοπίας και την μελέτη της επίδρασης της μορφολογίας τους από τον χρόνο αυτοΐασης και τις μικροκλιματικές συνθήκες.
- Την ανάπτυξη μεθοδολογίας για την αξιολόγηση της ανάκτησης των μηχανικών αντοχών λόγω του αυτογενούς μηχανισμού αυτοΐασης.
- Την μελέτη της επίδραση της χημικής και ορυκτολογικής σύστασης του συνδετικού υλικού καθώς και του χρόνου αυτοΐασης, στην ανάκτηση των μηχανικών ιδιοτήτων.

Η μελέτη και η κατανόηση των παραπάνω παραμέτρων που επηρεάζουν το φαινόμενο της αυτογενούς αυτοΐασης, έχουν την δυνατότητα να αποτελέσουν τη βάση για έναν πιο αποτελεσματικό σχεδιασμό και εφαρμογή αυτοϊοούμενων κονιαμάτων στις σύγχρονες κατασκευές.

Αρχικά, η εξέταση των αρχαιολογικών δειγμάτων κονιαμάτων προσέφερε τη δυνατότητα μελέτης του φαινομένου όπως εμφανίστηκε φυσικά, καθώς τα υλικά που χρησιμοποιήθηκαν δεν σχεδιάστηκαν για τον συγκεκριμένο σκοπό και οι μηχανισμοί φθοράς και επούλωσης επήλθαν φυσικά με την πάροδο του χρόνου. Το αυτογενές φαινόμενο της αυτοΐασης έχει παρατηρηθεί στις ιστορικές τοιχοποιίες και μπορεί να συσχετιστεί με τη δομική τους ακεραιότητα, με τις πρώτες ύλες που χρησιμοποιήθηκαν καθώς και με τις μικροκλιματικές συνθήκες. Ταυτόχρονα, ο αυτογενής μηχανισμός αυτοΐασης είναι εγγενής ή αυθόρμητος. Ενεργοποιείται ύστερα από φθορά ή βλάβη, ενώ μπορεί το σημείο εκκίνησης του μηχανισμού να είναι μια μεταβολή στις μικροκλιματικές συνθήκες (π.χ. βροχή ή κύκλοι υγρής ξήρανσης).

Η προσέγγιση που ακολουθήθηκε είναι μια αντίστροφη διαδικασία, δηλαδή μία αρχαιομμητική προσέγγιση, η οποία στοχεύει στην συλλογή πληροφοριών σχετικά με τις φυσικοχημικές διεργασίες που έχουν επηρεάσει τα υλικά αυτά για μεγάλες χρονικές περιόδους. Με αυτόν τον τρόπο, οι παράγοντες που ενισχύουν το φαινόμενο

μπορούν να αναπαραχθούν στην παρασκευή και την εφαρμογή σύγχρονων συνθέσεων.

Έτσι, μελετήθηκαν επιλεγμένα δείγματα αρχαιολογικών κονιαμάτων από διαφορετικά μνημεία και ιστορικές περιόδους με βάση τις μικροσκοπικές παρατηρήσεις και με έμφαση στο φαινόμενο αυτοϊασης.

Οι μικροσκοπικές παρατηρήσεις υποδεικνύουν ότι η μορφολογία των προϊόντων που καταβυθίζονται εξαρτάται, μεταξύ άλλων παραγόντων, από την περιεκτικότητα σε υγρασία και από το βαθμό ενανθράκωσης του κονιάματος. Πιο συγκεκριμένα, το φαινόμενο της αυτογενής αυτοϊασης παρατηρήθηκε τόσο σε υδραυλικά όσο και σε αεροπαγή κονιάματα. Τα ασβεστολιθικά αδρανή και τα μικρο-απολιθώματα φαίνεται να αποτελούν ένα ευνοϊκό υπόστρωμα για την κρυστάλλωση του δευτερογενούς ασβεστίτη (χημική και ορυκτολογική συμβατότητα). Ταυτόχρονα, το μέγεθος των ρωγμών καθόρισε σημαντικά την εξέλιξη του φαινομένου, επηρεάζοντας τόσο την κίνηση του διαλύματος των πόρων όσο και την ανάπτυξη των δευτερογενών κρυσταλλικών αποθέσεων. Τέλος, η παρουσία συσσωματωμάτων ασβέστη μπορεί να παρέχει επιπρόσθετα ιόντα Ca^{2+} στο διάλυμα των πόρων, αυξάνοντας σημαντικά την δυνατότητα απόθεσης δευτερογενούς ασβεστίτη.

Στη συνέχεια, μελετήθηκε το πρώτο βήμα του μηχανισμού της αυτοϊασης, και πιο συγκεκριμένα η διαλυτοποίηση ασβεστιούχων συστατικών της κονιάς. Η μελέτη διαλυτοποίησης ή έκπλυσης ιόντων Ca^{2+} πραγματοποιήθηκε μέσω μιας διεργασίας ηλεκτροχημικά επιταχυνόμενης έκπλυσης. Τα αποτελέσματα οδήγησαν στον χαρακτηρισμό των φάσεων, που κατά την έκπλυση τους προσδίδουν ιόντα Ca^{2+} στο διάλυμα και ταυτόχρονα στον συσχετισμό αυτών με την ηλικία των δοκιμίων.

Ειδικότερα, προκειμένου να κατανοηθεί το πρώτο βήμα του αυτογενούς μηχανισμού αυτοϊασης, εξετάστηκε η εξέλιξη της ορυκτολογίας των κονιαμάτων ασβέστη-ποζολάνης (LP) και φυσικού υδραυλικού ασβέστη (NHL) και ο συσχετισμός της με τη διαλυτότητα των ασβεστιούχων συστατικών τους. Ταυτόχρονα μελετήθηκε η επίδραση της διάλυσης των ασβεστιούχων συστατικών τους στα χαρακτηριστικά της μικροδομής των κονιαμάτων και τέλος η επίδραση της τελευταίας από την περίοδο ωρίμανσης των κονιαμάτων.

Παράλληλα, η παραμετροποίηση του αυτογενούς μηχανισμού αυτοϊασης επιχειρήθηκε εστιάζοντας σε συγκεκριμένους παράγοντες που μπορούν να προωθήσουν την εμφάνιση αυτού του φαινομένου, όπως συνθήκες υγρασίας, χρόνος

ωρίμανσης και περίοδος ίασης μετά από την εμφάνιση των ρηγματώσεων. Επιπρόσθετα, πραγματοποιήθηκε ο μορφολογικός και χημικός χαρακτηρισμός των δευτερογενώς σχηματιζόμενων προϊόντων με σκοπό να αναγνωριστούν οι βασικοί μηχανισμοί παραγωγής τους.

Συνδυάζοντας την εξέταση των δειγμάτων στο ηλεκτρονικό μικροσκοπείο σάρωσης (SEM) με την ανάλυση ενεργειακής διασποράς ακτινών X (EDAX), η μορφολογία των δευτερογενών προϊόντων συσχετίστηκε με τη χημική τους σύνθεση.

Ένα άλλο πλεονέκτημα της ανωτέρω προσέγγισης είναι ότι παρατηρείται στο μικροσκόπιο η επιφάνεια των ρωγμών, εξασφαλίζοντας έτσι ότι τα παρατηρούμενα προϊόντα δεν περιορίζονται στην εξωτερική επιφάνεια του δείγματος, παρέχοντας, σε ορισμένες περιπτώσεις, τη χωρική κατανομή των προϊόντων αυτοΐασης.

Η πειραματική διαδικασία περιλαμβάνει την παραγωγή ελεγχόμενης ρωγμής σε δείγματα κονιαμάτων ασβέστη-ποζολάνης (LP) και φυσικού υδραυλικού ασβέστη (NHL) και τον χαρακτηρισμό των δευτερογενών προϊόντων που σχηματίζονται μέσα στη ρωγμή, μετά από διαφορετικές περιόδους αυτοΐασης.

Τέλος μελετήθηκε η δυνατότητα ανάκτηση των μηχανικών ιδιοτήτων των κονιαμάτων μέσω του μηχανισμού της αυτοΐασης λαμβάνοντας υπόψη την ηλικία ρηγμάτωσης και την διάρκεια της περιόδου αυτοΐασης.

Πιο συγκεκριμένα, για να προσδιοριστεί η αποτελεσματικότητα της αυτογενούς αυτοΐασης όπως εκφράζεται από την ανάκτηση των μηχανικών τους ιδιοτήτων, εφαρμόστηκε μια ξεχωριστή μεθοδολογία. Αυτή η μεθοδολογία περιλαμβάνει την εισαγωγή ελεγχόμενης βλάβης στα δείγματα κονιαμάτων ασβέστη-ποζολάνης (LP) και φυσικού υδραυλικού ασβέστη (NHL) και στη συνέχεια - μετά από μια περίοδο αυτοΐασης - την αξιολόγηση της αντιστροφής της βλάβης αυτής με δοκιμή αντοχής σε κάμψη τριών σημείων.

Τα βασικά σημεία που εξετάστηκαν, αφορούν την μεθοδολογία της ρηγμάτωσης, τον έλεγχο του βαθμού βλάβης και της αναπαραγωγιμότητάς του και τέλος την μέτρηση της υπολειπόμενης αντοχής, προκειμένου να συσχετιστεί με την αντοχή του υλικού μετά την περίοδο της αυτοΐασης.

Αρχικά διαπιστώθηκε ότι οι διεργασίες που λαμβάνουν χώρα κατά την αυτοΐαση των φυσικών υδραυλικών (NHL) και ασβεστοποζολανικών (LP) κονιαμάτων είναι η ενανθράκωση και η ενυδάτωση, δημιουργώντας δευτερογενείς ασβεστιτικές ή υδραυλικές ενώσεις αντίστοιχα, κατά μήκος των ρηγματώσεων.

Η αντίδραση ενανθράκωσης οδηγεί στο σχηματισμό ομοιογενών στρωμάτων δευτερογενούς ασβεστίτη στα τοιχώματα ρωγμών. Η εξέλιξη αυτού του μηχανισμού έχει ως αποτέλεσμα την επούλωση ρωγμών μέχρι 60 μm. Κατά τον μηχανισμό ενυδάτωσης, παράγονται δευτερεύουσες υδραυλικές φάσεις διαφορετικής μορφολογίας. Διαπιστώθηκε ότι ινώδεις υδραυλικές φάσεις "χαμηλής πυκνότητας" αρχικά οδήγησαν στην επούλωση μικρο-ρηγματώσεων μέχρι 70 μm. Ωστόσο, δευτερεύοντα υδραυλικά προϊόντα δεν παρατηρήθηκαν κατά την μικροσκοπική παρατήρηση λεπτών και στιλπνών τομών.

Οι αντιδράσεις που συνδέονται με τον αυτογενή μηχανισμό εξαρτώνται από τη διαθεσιμότητα ασβεστιούχων συστατικών στο συνδετικό υλικό και προϋπόθεση για την εναπόθεση του δευτερογενούς ασβεστίτη είναι η παρουσία ιόντων ασβεστίου στο πορώδες διάλυμα.

Τα αποτελέσματα του πειράματος της έκπλυσης υποδεικνύουν ότι η διαθεσιμότητα του ασβεστίου συσχετίστηκε με την ηλικία ρηγμάτωσης, καθώς η σύνθεση της κονιάς διαφοροποιείται λόγω της εξέλιξης των αντιδράσεων πήξης. Τα ιόντα ασβεστίου μπορεί να προέρχονται από τη διάλυση του πορτλανδίτη ($\text{Ca}(\text{OH})_2$), των υδραυλικών φάσεων (CSH) ή του πυριτικού διασβεστίου (C_2S) στην περίπτωση των κονιαμάτων φυσικής υδραυλικής ασβέστου NHL. Οι μηχανισμοί έκπλυσης των κονιαμάτων φυσικής υδραυλικής ασβέστου NHL και των ασβεστο-ποζολανικών κονιαμάτων (LP) παρουσιάζουν ορισμένες διαφορές. Τα ασβεστο-ποζολανικά κονιάματα (LP) πρώιμης ηλικίας, όταν υποβάλλονται σε έκπλυση, παρέχουν τρεις φορές μεγαλύτερη ποσότητα ιόντων ασβεστίου από ότι τα κονιάματα φυσικής υδραυλικής ασβέστου (NHL) πρώιμης ηλικίας. Αντιθέτως, η ποσότητα του εκπλυθέντος ασβεστίου είναι υψηλότερη σε κονιάματα φυσικής υδραυλικής ασβέστου (NHL) μεταγενέστερης ηλικίας, πιθανώς λόγω της δευτερογενούς παραγωγής πορτλανδίτη κατά τη διάρκεια της αντίδρασης ενυδάτωσης ή και δευτερευόντως λόγω της απασβεστοποίησης των υδραυλικών φάσεων CSH.

Η παρατήρηση των διαφοροποιήσεων ανάμεσα στα δευτερογενή προϊόντα που σχηματίζονται μέσα στις ρωγμές, υποδεικνύει τις διαφοροποιήσεις ανάμεσα στους μηχανισμούς αυτοϊασης που επικρατούν σε κονιάματα φυσικής υδραυλικής ασβέστου (NHL) και ασβεστο-ποζολανικά κονιάματα (LP). Στα ασβεστο-ποζολανικά κονιάματα (LP) η παρουσία δευτερογενούς ασβεστίτη παρατηρείται ανεξαρτήτως της ηλικία ρηγμάτωσης του δείγματος. Αντίθετα, η παρουσία ασβεστίτη στα κονιάματα φυσικής υδραυλικής ασβέστου (NHL) παρατηρήθηκε μόνο σε δείγματα

που ρηγματώθηκαν σε μικρή ηλικία. Αυτό θα μπορούσε να σχετίζεται με την διαθεσιμότητα του πορτλανδίτη στη συνδετική κονία.

Ο μηχανισμός ενυδάτωσης ήταν ο κύριος μηχανισμός που συνέβαλε στην παραγωγή δευτερογενών προϊόντων στην επιφάνεια της ρωγμής στα κονιάματα φυσικής υδραυλικής ασβέστου (NHL). Διαπιστώθηκε ότι αρχικά σχηματίζονται «ινώδη» προϊόντα τα οποία, μετά από παρατεταμένη περίοδο επούλωσης, παρουσιάζουν μια πιο πυκνή δομή κερύθρας και βελονοειδείς σχηματισμούς. Στα δείγματα που ρηγματώθηκαν σε μεταγενέστερη ηλικία η παρουσία δομών κερύθρας και βελονοειδών σχηματισμών είναι πιο έντονη, γεγονός που μπορεί να αποδοθεί στην ύπαρξη υψηλότερης ποσότητας υδραυλικών φάσεων στη συνδετική κονία. Αυτό υποδηλώνει έναν κοινό μηχανισμό ενυδάτωσης ανεξάρτητο από το χρόνο ρηγμάτωσης.

Αντίθετα στα ασβεστο-ποζολανικά κονιάματα (LP), παρατηρήθηκε μόνο ο σχηματισμός «ινώδων» προϊόντων CSH, που περιοριζόταν σε δείγματα που υπέστησαν ρηγμάτωση σε μικρή ηλικία, ενώ σε αυτά που ρηγματώθηκαν σε μεταγενέστερη ηλικία ο κύριος μηχανισμός με τον οποίο παράγονται δευτερογενείς φάσεις μέσα σε ρωγμές ήταν η απόθεση δευτερογενούς ασβεστίτη.

Η επίδραση της ηλικίας ρηγμάτωσης εξετάστηκε και σχετικά με την ανάκτηση των μηχανικών ιδιοτήτων των κονιαμάτων. Στα κονιάματα φυσικής υδραυλικής ασβέστου (NHL) παρατηρήθηκε ότι η δυνατότητα αυτοϊασης δεν διαφοροποιήθηκε αισθητά ανάμεσα σε δείγματα που ρηγματώθηκαν μετά από 15 ή 30 ημέρες ωρίμανσης. Ωστόσο, κονιάματα που ρηγματώθηκαν μετά από 210 ημέρες ωρίμανσης επέδειξαν χαμηλότερη η ανάκτηση στις μηχανικές αντοχές.

Η επίδραση της παρατεταμένης περιόδου ίασης έχει ευνοϊκό αντίκτυπο στην εξέλιξη του αυτογενούς μηχανισμού καθώς παρατηρήθηκε η περαιτέρω κρυστάλλωση ασβεστίτη κατά μήκος των ρηγματώσεων. Οι συνθήκες υγρασίας επηρεάζουν τόσο την εμφάνιση όσο και την εξέλιξη του μηχανισμού αυτοϊασης. Τα δείγματα που υποβλήθηκαν σε κύκλους υδατοκορεσμού - ξήρανσης παρουσίασαν αυξημένη δυνατότητα αυτοϊασης, όπως εκφράζεται από το σχηματισμό δευτερογενών προϊόντων μέσα στις ρωγμές. Ωστόσο, η παραγωγή δευτερογενών φάσεων παρατηρήθηκε σε ασβεστοποζολανικά κονιάματα (LP) που κατά την περίοδο ίασης ωρίμασαν σε συνθήκες χαμηλότερης υγρασίας (75% RH) αλλά δεν παρατηρήθηκε σε αυτά σε συνθήκες υγρασίας 45% RH, υποδηλώνοντας ότι οι συνθήκες υγρασίας άνω του 75% RH μπορεί να είναι επαρκής συνθήκη για την εμφάνιση του φαινομένου.

Τέλος, όσον αφορά την ανάκτηση των μηχανικών ιδιοτήτων λόγω του φαινομένου της αυτοϊασης, και οι δύο τύποι κονιαμάτων (NHL και LP) παρουσίασαν υψηλή ανάκτηση (> 90%) των μηχανικών τους αντοχών μετά από περίοδο ίασης ενός μήνα, ενώ η παρατεταμένη περίοδος ίασης δεν είχε κάποια σημαντική επίδραση. Αυτό μπορεί να υποδηλώνει ότι η ανάκτηση των μηχανικών αντοχών ολοκληρώθηκε κατά τον πρώτο μήνα και επομένως η περαιτέρω διάρκεια ίασης δεν είχε κάποια σημαντική επίδραση.

Συνολικά, διαπιστώθηκε ότι η μέγιστη αποτελεσματικότητα του φαινομένου της αυτοϊασης παρατηρήθηκε όταν η ρηγμάτωση των κονιαμάτων πραγματοποιήθηκε σε δείγματα μικρής ηλικίας που στη συνέχεια υποβλήθηκαν σε κύκλους υδατοκορεσμού - ξήρανσης για παρατεταμένη περίοδο ίασης,

Τα αποτελέσματα της παρούσας μελέτης μπορούν να συμβάλουν στην αποτελεσματικότερη σύνθεση και εφαρμογή αυτοϊούμενων κονιαμάτων. Ειδικότερα, ο συσχετισμός της σύστασης της συνδετικής κονιάς με τις αντιδράσεις που επικρατούν στον μηχανισμό της αυτοϊασης (ενυδάτωση ή ενανθράκωση) καθώς και τα χαρακτηριστικά των δευτερογενών προϊόντων που σχηματίζονται μέσα στη ρωγμή, θα μπορούσε να οδηγήσει στο σχεδιασμό κατάλληλων πρόσθετων συστατικών για την ενίσχυση του φαινομένου της αυτοϊασης των κονιαμάτων.

Συνοπτική περιγραφή

Στα Κεφάλαια 1 και 2 εκτίθεται το ερευνητικό πρόβλημα και αναλύονται οι στόχοι της παρούσας διατριβής.

Στο Κεφάλαιο 3 παρουσιάζεται μια εκτεταμένη ανασκόπηση της βιβλιογραφίας σχετικά με τα φαινόμενα αυτοϊασης, όπου τονίζονται τα κύρια ζητήματα στα οποία απαιτείται περαιτέρω έρευνα.

στο Κεφάλαιο 4 παρουσιάζεται η παραμετροποίηση του μηχανισμού της αυτοϊασης όπως παρατηρείται σε ιστορικά δείγματα κονιάματος.

Τα διαφορετικά βήματα του αυτογενούς μηχανισμού προσομοιάζονται και συζητούνται στα κεφάλαια 5-7.

Στο Κεφάλαιο 5, εξετάζεται το πρώτο στάδιο του μηχανισμού της αυτοϊασης, η διαλυτοποίηση ασβεστούχων δηλαδή φάσεων της κονιάς μέσω έκπλυσης. Περιγράφεται η διάταξη ηλεκτροχημικά επιταχυνόμενης έκπλυσης που χρησιμοποιήθηκε για να εξεταστεί η επίδραση της ορυκτολογίας και του χρόνου ωρίμανσης στη διάλυση των ασβεστιούχων φάσεων των κονιαμάτων ασβέστη-ποζολάνης (LP) και φυσικού υδραυλικού ασβέστη (NHL). Η ταυτοποίηση της πηγής των ιόντων ασβεστίου, με την ταυτόχρονη ποσοτικοποίηση τους, συσχετίζονται με τη σύνθεση συνδετικού υλικού και συνεπώς με τις δυνατότητες της εμφάνισης του μηχανισμού της αυτοϊασης.

Η μορφολογία και η ορυκτολογία των δευτερογενών προϊόντων επούλωσης εξετάζεται στο Κεφάλαιο 6. Τα δευτερογενή προϊόντα που σχηματίζονται μέσα σε μικρο-ρωγμές κονιαμάτων ασβέστη-ποζολάνης (LP) και φυσικού υδραυλικού ασβέστη (NHL) χαρακτηρίζονται και συσχετίζονται με τη σύνθεση συνδετικού υλικού κατά τη στιγμή της ρηγμάτωσης, της περιόδου αυτοϊασης και των μικροκλιματικών συνθηκών κατά τη διάρκεια της περιόδου αυτοϊασης.

Στο Κεφάλαιο 7 παρουσιάζεται μια νέα μεθοδολογία για την μελέτη της ανάκτησης των μηχανικών ιδιοτήτων λόγω του μηχανισμού της αυτοϊασης. Τα αποτελέσματα που ελήφθησαν μετά την εφαρμογή αυτής της μεθόδου σε κονιάματα ασβέστη-ποζολάνης (LP) και φυσικού υδραυλικού ασβέστη (NHL) μετά από διαφορετικές περιόδους αυτοϊασης παρουσιάζονται και συζητούνται.

Στο κεφάλαιο 8 παρουσιάζεται και συζητιέται συνδυαστικά το σύνολο των ευρημάτων, ενώ στο κεφάλαιο 9 παρουσιάζονται τα γενικά συμπεράσματα μαζί με προτάσεις για δυνατότητες μελλοντικών ερευνών.

Table of Contents

Acknowledgments	i
Abstract	iii
Περίληψη.....	v
Table of Contents	xiii
Chapter 1: Introduction	1
Chapter 2: Aims and Objectives	7
Chapter 3: Literature Review	11
3.1 Service life and Degradation of building materials/ mortars	11
3.2 General framework and definitions of self-healing phenomena	13
3.3 Mechanisms of self-healing.....	14
3.3.1 Autogenous self-healing	14
3.3.2 Autonomic self-healing.....	17
3.4 Methods used to verify self-healing	20
3.5 Research needs defined	25
References	27
Chapter 4: Self-healing observations in historic mortars	31
4.1 Introduction.....	31
4.2 Materials and Methods	32
4.3 Microscopic observations.....	35
4.4 Discussion	47
4.5 Conclusions.....	52
References.....	53
Chapter 5: Electrochemically accelerated leaching	55
5.1 Introduction.....	55
5.2 Experimental Setup	57
5.2.1 Materials.....	57
5.2.2 Experimental procedure and test setup.....	58

5.2.3 The LIFT method	59
5.2.4 Conductimetry	61
5.2.5 Preliminary measurements	62
5.2.6 Leachate solution analysis by AAS.....	63
5.2.7 Characterization of mineralogical alterations	64
5.2.8 Characterization of microstructural alterations	64
5.2.9 Sample preparation	64
5.3 Results and Discussion.....	65
5.3.1 Current and conductivity monitoring	65
5.3.2 Leachate solution analysis by AAS.....	68
5.3.3 Mineralogical examination	70
5.3.4 Microscopic examination of leached powdered specimens	78
5.3.5 Microstructural alterations and chemical analysis	79
5.4 Conclusions.....	88
References	89
Chapter 6: Microscopic examination of self-healing products	91
6.1 Introduction.....	91
6.2 Materials and Methods	92
6.2.1 Materials.....	92
6.2.2 Crack generation and control	92
6.2.3 Evaluation of crack width in the stereo-microscope	95
6.2.4 Parameters examined	96
6.2.5 Sample preparation for microscopic examination	99
6.3 Results	102
6.3.1 Microscopic observations.....	102
6.3.2 Classification of secondary products by chemical characterization.....	116
6.4 Discussion	118
6.4.1 Effect of curing time prior to cracking on the formation of healing products	118
6.4.2 Effect of Healing Conditions on the formation of healing products	120
6.4.3 Effect of Healing period on the formation of healing products	121
6.5 Conclusions.....	123
References	125

Chapter 7: Recovery against mechanical action	127
7.1 Introduction.....	127
7.1.1 Damage method.....	128
7.1.2 Damage degree and reproducibility.....	128
7.1.3 Residual strength.....	129
7.2 Materials and Methods	130
7.2.1 Sample preparation	130
7.2.2 Methodology	130
7.2.2.1 Hertzian contact stress.....	130
7.2.2.1 Assessment of residual strength	131
7.2.2.2 Groups and parameters studied.....	135
7.2.2.3 Assessment of strength recovery.....	136
7.3 Results and Discussion.....	137
7.3.1 Effect of curing time before damage was introduced (Moment of cracking).....	137
7.3.2 Effect of healing period	141
7.4 Conclusions.....	143
References.....	145
Chapter 8: Discussion	147
Future work	152
Chapter 9: Conclusions	153
Appendix: Preliminary measurements.....	157
List of Figures.....	168
List of Publications and Conference contributions	174

Chapter 1: Introduction

1.1 Research background

Cement-based building materials have been used since antiquity, while the evolution of different types of binding or cementing agents have always been associated with the technological heritage of each historic era (Blezard, 2004). The construction technologies as well as the raw materials were chosen each time according to durability and service life requirements of monuments built structures of different civilizations.

Cement-based materials are still amongst the most widely used construction/building materials worldwide. Service life of cement-based-materials is the period after their application during which their performance remains above safety levels. At the same time, their service-life is limited since several degradation mechanisms affect their durability leading to a gradual declination of their performance overtime (van Breugel, 2012). Nevertheless their service life is shortened due to weathering while, the remedy for building materials' failure is restricted to man-made repairs.

During the recent years, a shift in the way that scientists vision material durability has taken place inspired by the ability of living organism to heal themselves (skin cuts, bone fractures etc.). The focus has shifted from the development of stronger materials, to the development of materials that can reverse micro-damage, thus healing themselves without external intervention. So instead of “*damage prevention*”, “*damage management*” tactics are researched, which points to the modification of materials to “sense” damage and reverse it by intrinsic mechanisms (de Rooij, 2013). In this context, “smart” self-healing materials have attracted much attention.

At the same time, the fact that cement materials are known to have the ability to heal micro-cracks autogenously (Lauer and Slate, 1956; Dhir et al., 1973) has given a new advance in the research of this field. Indeed, the autogenous self-healing mechanism has been identified in historic mortars by several researchers and the abundance of these findings is often associated with the high durability that historic building materials present (Lubelli et al., 2011; Nijland et al., 2011).

Overall, self-healing of cement-based materials is believed to have the potential to have a measurable impact on construction, by prolonging the service-life of structures thus reducing both the maintenance economic and the environmental cost.

Even though the autogenous phenomenon was observed as back as a century ago (Hyde et al., 1889), the understanding of its mechanism has become a priority during the last decade, and has been the subject of numerous publications (Joseph et al., 2011; Li and Herbert, 2012; Muhammad et al., 2016) mostly concentrating on the self-healing properties of Portland cement paste and concrete. Nevertheless, the wide range of cements used with various admixtures, as well as the variety of methods used to verify healing have not always produced consistent observations amongst researchers.

One of the main questions often raised in recent literature (Huang et al., 2013) is the nature of the secondary phases that fills the crack as well as the nature of the secondary reactions that result in the recovery of the microstructure. Carbonation and continued hydration have both been identified as the main self-healing reactions. Jacobsen et al. (1995) observed ettringite, portlandite and CSH as secondary healing products after frost deterioration, whereas Hearn and Morley (1997) attributed the reduction in the permeability of concrete samples to dissolution and precipitation of alkalis. More recently, Schlangen et al.(2006) correlated the crack healing of early-age concrete with ongoing hydration, but Quian et al. (2009) observed only calcite in cracked concrete cured under water. The variety of observations suggests that other issues related to the autogenous mechanism should be further investigated.

The chemical composition of the binder, as well as the evolution of the latter with time, are important factors affecting the self-healing mechanism, which could elucidate the effect of the time when damage occurs, with the material's healing potential (Van Tittelboom et al., 2012). Moreover, the solubility and reactivity of the chemical substances involved in this mechanism, together with the effect that the latter have on the binder microstructure are not yet completely understood.

Besides the composition of the binder, micro-climatic conditions are believed to have a measurable impact on the potential of self-healing. Although, it is agreed amongst researchers that the presence of water is vital in the occurrence of self-healing

mechanism (Neville, 2002; Jiang et al., 2015), the amount and conditions of its delivery are under consideration. Under-water treatment or wet-dry cycles of exposure have promoted optimistic results (Yang et al., 2009) but further research is needed related to structures that lack direct contact with water.

Moreover, recovery of mechanical properties is one of the most important issues that need to be addressed. Different approaches and techniques are applied to induce damage and evaluate the structural recovery after healing. Flexural and tensile splitting are amongst the most usually applied methods. Nevertheless, lack of standardized procedures (Souradeep and Kua, 2016) hinders the comparability between findings.

References

- Blezard Robert G., "The History of Calcareous Cements" in Hewlett, Peter C., ed. *Lea's chemistry of cement and concrete*. 4. ed. Amsterdam: Elsevier Butterworth-Heinemann, 2004. 1-24
- Breugel, K. Van. (2012). Self-healing material concepts as solution for aging infrastructure. *37th Conference on Our World in Concrete & Structures*, 1–17. <http://doi.org/100037009>
- deRooy, M. R., Schlangen, E., & Joseph, C. (2013). Introduction (pp. 1–17). http://doi.org/10.1007/978-94-007-6624-2_1
- Dhir, R. K., Sangha, C. M., & Munday, J. G. L. (1973). Strength and Deformation Properties of Autogenously Healed Mortars. *Journal of the American Concrete Institute*, 70(3), 231–236. <http://doi.org/10.14359/11202>
- Hearn, N., & Morley, C. T. (1997). Self-sealing property of concrete—Experimental evidence. *Materials and Structures*, 30(7), 404–411. <http://doi.org/10.1007/BF02498563>
- Huang, H., Ye, G., & Damidot, D. (2013). Characterization and quantification of self-healing behaviors of microcracks due to further hydration in cement paste. *Cement and Concrete Research*, 52, 71–81. <http://doi.org/10.1016/j.cemconres.2013.05.003>
- Hyde, G. W., & Smith, W. J. (1889). Results of experiments made to determine the permeability of cements and cement mortars. *Journal of the Franklin Institute*, 128(3), 199–207. [http://doi.org/10.1016/0016-0032\(89\)90217-2](http://doi.org/10.1016/0016-0032(89)90217-2)
- Jacobsen, S., Marchand, J., & Hornain, H. (1995). Sem observations of the microstructure of frost deteriorated and self-healed concretes. *Cement and Concrete Research*, 25(8), 1781–1790. [http://doi.org/10.1016/0008-8846\(95\)00174-3](http://doi.org/10.1016/0008-8846(95)00174-3)
- Jiang, Z., Li, W., & Yuan, Z. (2015). Influence of mineral additives and environmental conditions on the self-healing capabilities of cementitious materials. *Cement and Concrete Composites*, 57, 116–127. <http://doi.org/10.1016/j.cemconcomp.2014.11.014>

- Joseph, C., Gardner, D., Jefferson, T., Isaacs, B., & Lark, B. (2011). Self-healing cementitious materials: a review of recent work. *Proceedings of the Institution of Civil Engineers - Construction Materials*, 164(1), 29–41. <http://doi.org/10.1680/coma.900051>
- Lauer, K.R.; Slate, F.O. (1956) Autogenous healing of cement paste. *ACI Journal Proceedings*, 52(6). <http://doi.org/10.14359/11661>
- Li, V. C., & Herbert, E. (2012). Robust Self-Healing Concrete for Sustainable Infrastructure. *Journal of Advanced Concrete Technology*, 10(6), 207–218. <http://doi.org/10.3151/jact.10.207>
- Lubelli, B., Nijland, T. G., Van Hees, R. P. J., & TU Delft: Architecture: RMIT and Media Studies. (2011, December). Simulation of self-healing of dolomitic lime mortar. Retrieved from <http://resolver.tudelft.nl/uuid:31e6db06-69e0-443b-bba9-b19f4d7b2018>
- Muhammad, N. Z., Shafaghat, A., Keyvanfar, A., Abd. Majid, M. Z., Ghoshal, S. K., Mohammadyan Yasouj, S. E., ... McCaffer, R. (2016). Tests and methods of evaluating the self-healing efficiency of concrete: A review. *Construction and Building Materials*, 112, 1123–1132. <http://doi.org/10.1016/j.conbuildmat.2016.03.017>
- Neville, A., 2002. Autogenous Healing—A Concrete Miracle? *ACI* 24, 76–82.
- Nijland, T. G., Larbi, J. a, Hees, R. P. J. Van, & Lubelli, B. (2007). Self Healing Phenomena in Concretes and Masonry Mortars □: a Microscopic Study. *Proceedings of the First International Conference on Self Healing Materials 18-20 April 2007, Noordwijk Aan Zee, The Netherlands*, (April), 1–9.
- Qian, S., Zhou, J., de Rooij, M. R., Schlangen, E., Ye, G., & van Breugel, K. (2009). Self-healing behavior of strain hardening cementitious composites incorporating local waste materials. *Cement and Concrete Composites*, 31(9), 613–621. <http://doi.org/10.1016/j.cemconcomp.2009.03.003>
- Schlangen, E., Heide, N. ter, & Breugel, K. van. (2006). Crack Healing of Early Age Cracks in Concrete. In M. S. KONSTA-GDOUTOS (Ed.) (pp. 273–

284).Springer Netherlands. Retrieved from
http://link.springer.com/chapter/10.1007/978-1-4020-5104-3_32

Souradeep, G., &Kua, H. W. (2016).Encapsulation Technology and Techniques in Self-Healing Concrete.*Journal of Materials in Civil Engineering*, 4016165. [http://doi.org/10.1061/\(ASCE\)MT.1943-5533.0001687](http://doi.org/10.1061/(ASCE)MT.1943-5533.0001687)

Van Tittelboom, K., Gruyaert, E., Rahier, H., & De Belie, N. (2012). Influence of mix composition on the extent of autogenous crack healing by continued hydration or calcium carbonate formation. *Construction and Building Materials*, 37, 349–359.
<http://doi.org/10.1016/j.conbuildmat.2012.07.026>

Yang, Y., Lepech, M. D., Yang, E.-H., & Li, V. C. (2009).Autogenous healing of engineered cementitious composites under wet–dry cycles.*CementandConcreteResearch*, 39(5), 382–390.

Chapter 2: Aims and Objectives

2.1 Aims and Objectives

The aim of the present research is the study and understanding of the parameters that affect autogenous self healing in order to apply them in modern construction and enhance the phenomenon. The autogenous phenomenon in combination with induced self-healing by the incorporation of tailor-made supplementary materials can maximize the service-life of mortars.

In this context the study of the autogenous healing phenomenon in traditional mortars that simulate the composition of historic mortars is pursued. More specifically, a better understanding of the autogenous mechanism is pursued by setting the following objectives:

- To parameterize the occurrence of the self-healing phenomenon in historic mortars.
- To gain insight, on the decalcification process which occurs during leaching of traditional mortars, by simulating the first step of the autogenic mechanism.
- Determine how this process affects mortar microstructure and which phases are affected after the depletion of portlandite.
- Analyze the morphology and mineralogy of self-healing products by means of microscopy and determine how their occurrence is affected by healing time and micro-climatic conditions.
- Development of an applicable methodology for assessing the recovery of mechanical strength due to the autogenous healing mechanism.
- Determine the effect of the chemical and mineralogical composition of the binder as well as healing time, in the recovery of mechanical properties.

The study and understanding of all the above will allow a better “control” of the phenomenon and provide the baseline for a more effective design and application of self-healing agents in modern constructions.

2.2 Strategy-Outline

The present dissertation is composed of seven chapters as presented in Fig. 2.1. An extended review of the literature concerning self-healing phenomena in cement-based materials is presented in Chapter 3 and the main open issues in need for further research are emphasized.

The parameterization of the self-healing mechanism as it is observed in historic mortar samples is presented in Chapter 4. The main parameters are highlighted and implemented in the experimental protocol.

The different steps of the autogenous mechanism are simulated and discussed in Chapters 5-7.

In Chapter 5, an electrochemically accelerated leaching procedure was used to examine the influence of mineralogy and curing time on the dissolution of Ca-bearing phases of lime-pozzolan and NHL mortars. The identification of the source of the calcium ions, together with the quantification of the latter are correlated with the binder composition and thus its healing potential.

The morphology and mineralogy of secondary healing products is examined in Chapter 6. The secondary products formed inside cracks of lime-pozzolan and NHL mortars are characterized and correlated with the binder composition at the time of cracking, the healing period and the micro-climatic conditions during healing.

In Chapter 7, a new methodology for assessing the recovery of mechanical properties after healing is presented. The results obtained after applying this method on lime-pozzolan and NHL mortars after different curing and healing periods are presented and discussed.

Chapter 8 provides a summary of findings together with proposals for enhancing the self-healing potential of lime-pozzolan and NHL mortars.

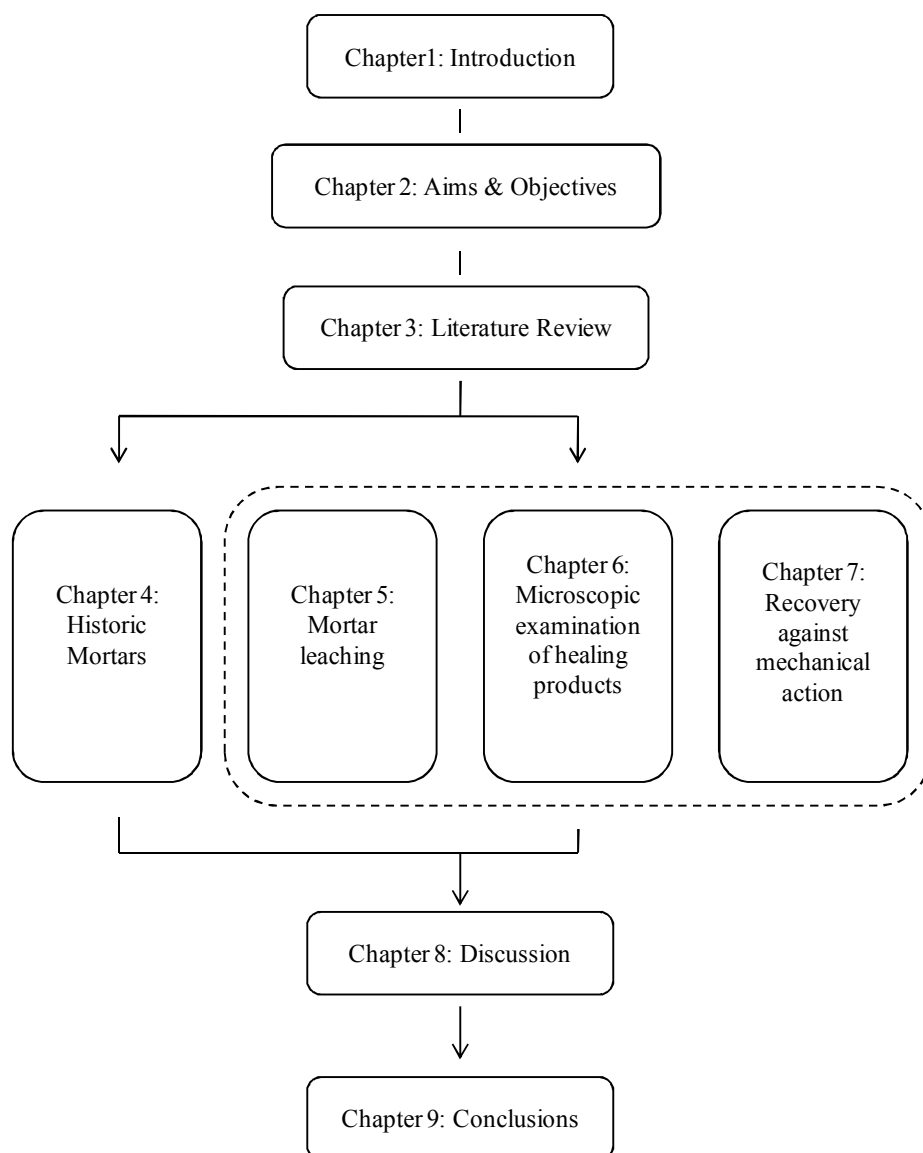


Figure 2.1: Thesis outline

Chapter 3: Literature Review

3.1 Service life and Degradation of building materials/ mortars

A common characteristic of cement-based materials, concerning their durability, is their susceptibility to micro-cracks, which are generated even from the first few days of application. This is usually caused due to intrinsic factors (Holt and Leivo, 2004) most commonly due to water loss and shrinkage mechanisms during setting or -in subsequent periods - due to external parameters mechanical loads or other environmental factors. Early age shrinkage cracking is unavoidable in cement-based materials and although these cracks, may not be considered as a material failure, could lead to further degradation and decreased durability, as micro-cracks make the structure more vulnerable to both mechanical stress, environmental actions and aggressive agents responsible for deterioration mechanisms, thus making their imminent repair or restoration necessary.

Loss of performance is caused by a number of degradation mechanisms that affect the material's microstructure. Those mechanisms are usually classified into three main categories: (i) mechanical, (ii) chemical and (iii) biological.

Mechanical degradation may occur during crystallization of soluble salts (Pye and Schiavon, 1989; Lubelli and de Rooij, 2009) or during freeze-thaw cycles (Yang et al., 2006). Interaction with air-pollutants (Sabioni et al., 2001; Schiavon et al., 2004), decalcification or leaching (Glasser et al., 2008), are the main chemical degradation mechanisms. While colonization of microorganisms (Shirakawa et al., 2004), fungi or bacteria, may lead to further chemical and mechanical degradation. All of the above mechanisms are greatly accelerated by the presence of micro-cracks in the cement matrix.

Performance of cement-based materials is often presented graphically with time as a curve pointing to gradual degradation. In figure 3.1, a typical degradation graph is presented along with the required repairs (Van Breugel, 2012).

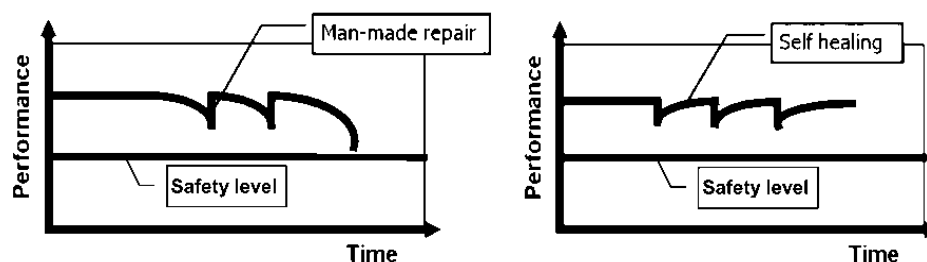


Figure 3.1: Performance of concrete material with elapse of time where traditional cement-based materials requiring man-made repairs are contrasted with self-healing cement-based materials. (Van Breugel, 2012)

After the application of the traditional cement-based materials, its gradual degradation begins which leads to a point where man-made repair is necessary in order to maintain its performance above the safety level. After the first intervention another degradation cycle begins which eventually leads to a second intervention. This is repeated as long as the structure is in use. In contrast, self-healing materials may reverse the effect of micro-damages intrinsically without the need of external interventions.

Required maintenance of structures is usually performed only after the above deterioration mechanisms have taken place, while man-made repairs aiming to reverse their effects have to be employed every few years. This strategy requires not only a substantial economical dependence but also entails a high risk of performance failure (Li and Herbert, 2012).

Traditionally, cement research focused in the development of stronger materials to address durability issues. This is described as *Damage prevention philosophy* (van der Zwaag, 2007) and is characterized by the need to create stronger materials, so that the load needed to damage them, cannot be reached. In this point of view no damage is acceptable.

Recently, inspired by the way biological organisms have the ability to heal themselves up to a certain level of damage; a new approach is pursued in the field of material science, that of *Damage management*. This concept is based on the employment of smart materials that have the ability to “sense” and repair micro-damages as they occur.

In the building material sector, development of self-healing cement is a promising strategy for expanding the service life of structures, as micro-cracks that are considered the initial cause of most deterioration mechanisms, are eliminated.

3.2 General framework and definitions of self-healing phenomena

Self-healing according to the definition proposed by the RILEM Technical committee (Rooij et al., 2013) is “any process by the material itself involving the recovery and hence improvement of a performance after an earlier action that has reduced the performance of the material”.

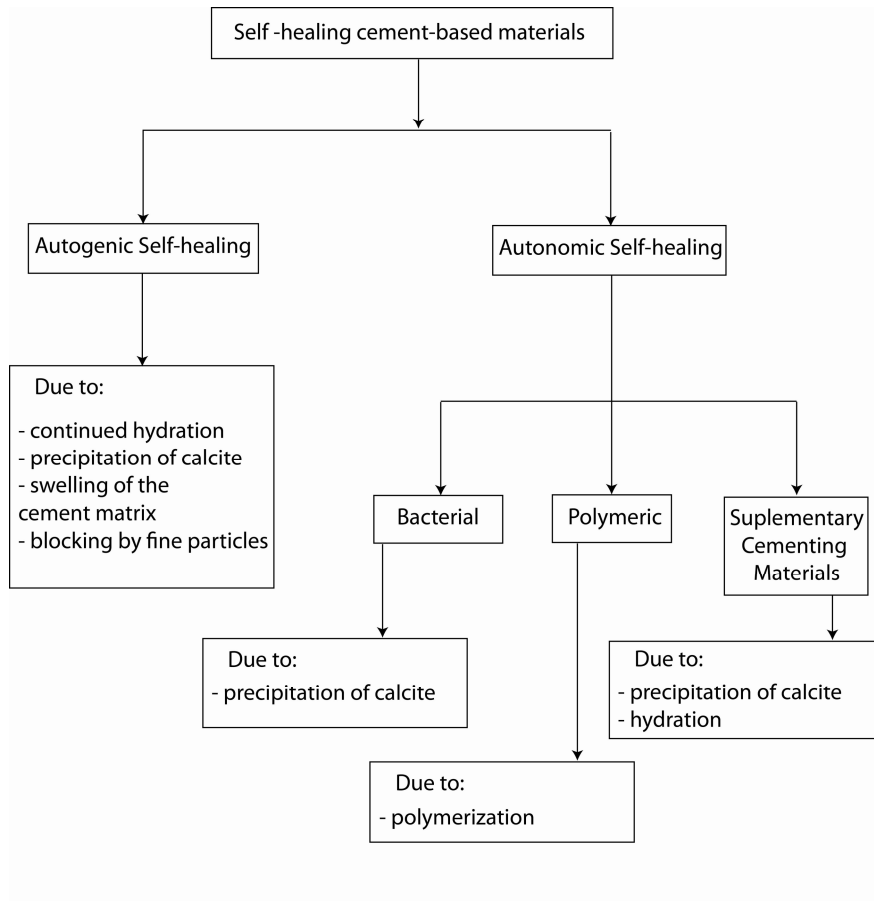


Figure 3.2: Autogenic and autonomic self-healing mechanisms.

In the case of cement-based materials this process can be autogenic which means that “it occurs from the materials own components without external intervention and the self-healing process takes place as a natural mechanism without these materials being specifically designed for this purpose”. In mortars and concretes this phenomenon takes place in the binder matrix where secondary products are formed inside cracks and voids thus repairing the continuity of the microstructure and sealing the material of deleterious substances.

In the recent years, a number of engineered additions are evolved to induce self-healing properties in cement-based materials. It is defined as autonomic self-healing “*when the recovery process uses materials components that would otherwise not be present in the material*”.

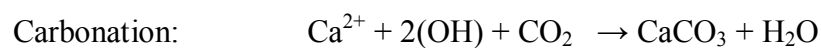
A classification chart of the main self-healing mechanisms studied is presented in figure 3.2.

3.3 Mechanisms of self-healing

3.3.1 Autogenous self-healing

Cement-based materials have the ability to heal their defects in an autogenic way. The prolonged durability of historic lime-based mortars applied centuries ago, is also attributed to their self-healing capacity (Nijland, 2007).

A reduction of crack width may result by physical, mechanical or chemical causes (fig. 3.3). However, it is the chemical mechanism that is the most significant as it is the most efficient in repairing of the microstructure (Edvarsen, 1999). The importance of water presence is also substantial. As water penetrates through cracks and voids of the binder matrix calcareous substances can be dissolved and transported in damaged areas where they react further to produce secondary healing products. The main element involved in these reactions is calcium. Calcium compounds dissolve in pore water producing calcium ions which either react with water dissolved carbon dioxide (CO₂) producing Calcite (CaCO₃) or participate in the hydration mechanism producing secondary hydration products. Calcium hydroxide may also precipitate directly as Portlandite (Ca(OH)₂) (Neville, 2002).



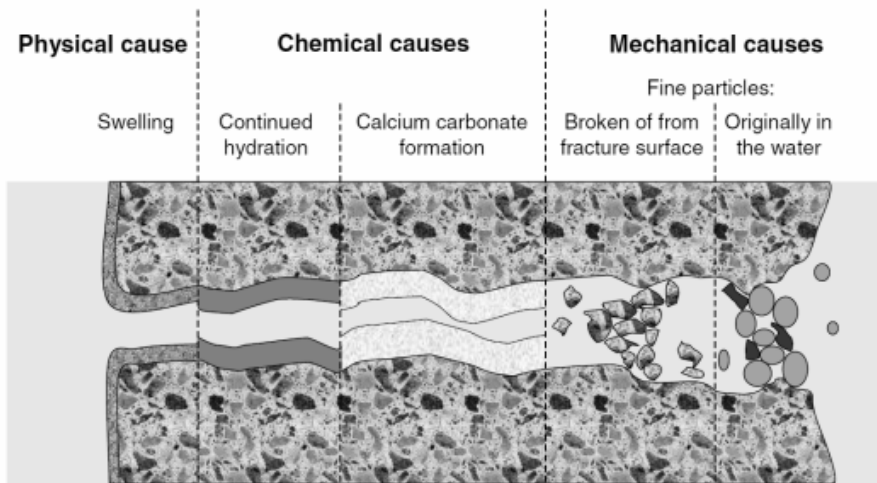


Figure 3.3: Different causes that can lead to autogenic self-healing (Reinhardt et al., 2013)

This phenomenon is autogenic, which means that these materials have the ability to heal micro-defects in their microstructure by filling the cracks with their own generic materials, as described earlier in paragraph 3.2. A simplified description of the phenomenon involves carbonation or hydration mechanisms (Edvarsen, 1999); cracks are filled with either calcium carbonate or hydration products, which derive from the carbonation of calcium hydroxide or by further reaction of non-hydrated phases inside the mortar matrix respectively.

The autogenous self-healing mechanism has been observed over a century ago in Portland cement concrete by Hyde (1889). Since then numerous studies have concentrated on the autogenous self-healing properties of Portland cement.

The main parameters associated with the autogenous phenomenon, most commonly examined are: the presence of water, the crack width, addition of fly ash, addition of lime, age of specimen when the cracking occurs, period of healing, temperature, hardness of water.

- Source of calcium ions

As Ca-bearing phases exhibit a range of solubility values (depending always on the pH and temperature of the pore solution), it is expected that self-healing ability of a mixture will also depend on the stage of carbonation and/or hydration progress in the binder matrix. During carbonation, portlandite is transformed into calcite which is a much less soluble mineral. In hydraulic binders the produced C-S-H and C-A-H

phases are also susceptible to dissolution but, as they are less soluble than portlandite, the dissociation of Ca begins after the dissolution of the latter (Adenot, 1991). With respect to the theoretical assumption that chemical reactions take place inside the crack space described earlier, an important parameter to be studied is the availability of the chemical species involved. More specifically the concentration of calcium ions in the pore solution should be a decisive factor since the carbonate content is not a limiting factor (Edvardsen, 1999). Water could contain a small concentration of calcium ions but in order saturation to be achieved the main source of calcium would be the calcium-bearing components of the binder. In the study of Huang and Ye (2014) was found that the mineralogy of the reaction products of self-healing induced with saturated Ca(OH)_2 solution is similar to that caused by distilled water, but the efficiency was improved. This suggests that calcium ions play the most significant role on the evolution of the autogenic phenomenon.

- Secondary products

The characterization of the healing products is of prime importance as it constitutes the first step towards the comprehension of the autogenous phenomenon. Calcium carbonate has been identified as the main secondary product filling the crack by several studies as well as the presence of portlandite (Lauer, 1956; Lubelli, 2011). At the same time, hydration has also been reported as a self-healing mechanism with ettringite and CSH as the main secondary products (Jacobsen, 1995). Recent studies (Huang et al., 2013) have concluded that in Portland cement paste only hydration products are observed together with portlandite which is also produced during hydration. It is clear that secondary products are depended on the mechanism that predominates (carbonation or hydration) which has not been sufficiently studied and correlated with factors affecting it.

- Effect of relative humidity

The presence of water, which is a crucial parameter of the self-healing phenomenon (Hearn, 1998) (Yang, 2009), varies in the natural environment of structures. It could be present in excess e.g. in underwater structures, or at different atmospheric humidity levels as atmospheric humidity or through capillary actions. Several researchers examined the evolution of the mechanism when the specimens are completely immersed under-water (Tsangouri et al., 2013; Hilloulin et al., 2016) or after wet/dry

cycles (van Tittelboom et al., 2012; Jiang and Yuan, 2015) and found that direct contact with water and water saturation constitute favorable conditions for self-healing. However, water can also be present in the form of atmospheric humidity and variation in the atmospheric humidity levels are known to affect the rate of hardening reactions of hydraulic binders (Karatasiotis et al., 2012). Nevertheless, the effect of relative humidity on the advancement of the autogenic mechanism is not yet studied.

- Curing period/ healing period

An additional parameter that should not be neglected is time, especially in lime-based mortars where non-reacted components may be present for months or years after the initial application of the mortar. Today, it is not yet entirely understood whether this phenomenon can take place only in the first stage of a mortar life (Schlangen, 2006) when there still are unreacted components, or whether it is possible to be the result of secondary dissolution and re-precipitation of hydration or carbonation products.

3.3.2 Autonomic self-healing

Aiming to prolong the life-cycle of building materials the incorporation of healing agents inside the mortar matrix is gaining a lot of attention recently and a variety of materials are tested as to their healing properties. Autonomous self-healing can be distinguished between: (i) bacterial self-healing, using microorganisms, (ii) self-healing by incorporating mineral admixtures - supplementary cementing materials and (iii) self-healing by incorporating polymeric materials (Fig. 3.2)

In order to achieve a realistic expansion of their service life healing agents have to remain inactive for long periods without deteriorating or reacting while their activation has to be triggered as damage occurs (Souradeep and Kua, 2016). This is achieved by inserting into the cement mixture the healing agent protected inside capsules (encapsulation) or hollow tubes (vascular system). In either case, during a crack formation, the protective layer breaks and the activated agent is released inside the crack, repairing it (Fig. 3.4).

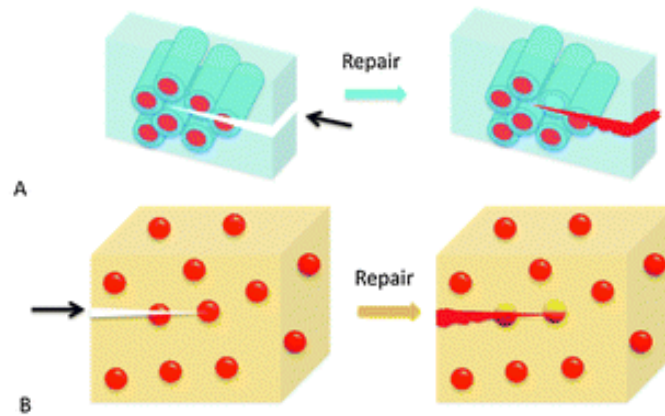
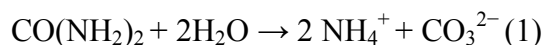


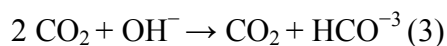
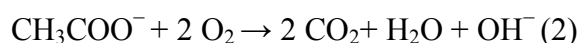
Figure 3.4: Hollow fibers (A) and encapsulation techniques (B) as implemented on self-healing materials (Yang and Urban, 2013).

- Bacterial concrete

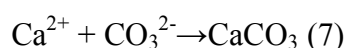
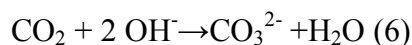
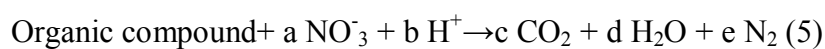
The use of bacteria as a self-healing agent in concrete has been one of the most promising research fields in the last decade (Seifan et al., 2016). The basic idea is that calcium carbonate is produced in the cement matrix as a product of the bacterial metabolic cycle. A large number of different bacteria have been studied as healing agents. Most of them can be classified into three major categories in respect to the source of materials consumed during the process. The main distinction is made between the hydrolysis of urea (1), oxidation of organic acids (2-4) and nitrate reduction (5-7) (De Muynck, et al., 2010, Knorre and Krumbein, 2000).



Formation of calcium carbonate in the presence of calcium acetate is shown in Eqs.2-4



Minerals are precipitated through oxidation of organic compounds by the reduction of nitrate (NO_3^-) via denitrifying bacteria.



Bacterial self-healing presents several advantages as its high efficiency (De Muynck et al., 2010). The main challenge remains the incorporation of the bacteria spores and nutrients in the cement matrix. Bacterial life expectancy decreases rapidly soon after cement setting (Jonkers, 2007). Therefore researchers are studying the immobilization of bacteria inside inert materials which protects bacterial spores during setting and hardening of the cement binder but at the same time have the ability to release them when a crack occurs.

Another question is also the presence of excessive ammonium in the concrete matrix, related with the ureolytic metabolic cycle of bacteria that increases the risk of salt damage by conversion to nitric acid (Siddique and Chahal, 2011).

- Mineral admixtures

Mineral admixtures such as fly ash and slag hydrate are used as supplementary cementitious materials to induce further hydration mechanisms. The main characteristic of these materials is that they react slower than Portland cement thus acting as reactive healing agents in the crack surface.

They chemically interact with the cement matrix producing hydration and carbonation products. They are categorized in two groups: crystalline and expansive admixtures.

Crystalline admixtures (ACI Committee 212, 2010) can be considered as a type of permeability reducing admixtures, usually hydrophilic. Sisomphon K. et al (2012) used a synthetic cementitious material called “crystalline additive” to promote healing. The general process can be described by the following equation where a crystalline promoter, M_xR_x , reacts with tricalcium silicates and water to produce modified calcium silicate hydrates and a pore-blocking precipitate, $M_xCaR_x-(H_2O)_x$.



Mineral admixtures that its reaction products are larger than the original admixture are called expansive admixtures. Several expansive admixtures have been investigated as self healing agents e.g. magnesium oxide (MgO), calcium sulfoaluminate ($Ca_4(AlO_2)_6SO_4$), anhydrite ($CaSO_4$).

These materials are encouraged as healing agents in recent years as be they are relatively low-cost and considered chemically compatible to cement materials (Kanellopoulos et al., 2015).

The main disadvantage of the use of mineral admixtures is that the healing agent is consumed during cement hydration so their encapsulation is necessary. Moreover, additional cracking may occur during the expansion reaction (Suradeep and Kua, 2016).

- Polymeric materials

Adhesives agents such as epoxy, methylmethacrylate (MMA), polyurethane foam (PU), cyanoacrylate and superabsorbent polymers (SAPs) have been tested as healing agents by several researchers (De Belie and van Tittelboom, 2010; van Tittelboom, 2011). One or two or multi-components polymers have been studied to optimize healing efficiency, viscosity and successful supply inside the crack.

It has been found that polymeric materials have a relatively high efficiency but present three drawbacks: (i) they are not chemically or mechanically compatible with cement materials, meaning that cracks may propagate around or within them (ii) they often contain formaldehydes and isocyanides which can raise health and safety issues and (iii) they are expensive, especially SAPs which can cause further damage to the cement matrix upon expansion.

3.4 Methods used to verify self-healing

In order to study the self-healing phenomenon macroscopic together with microscopic methods have to be applied. Self-healing efficiency is commonly studied indirectly by measuring the permeability, strength or durability against deleterious substances of damaged and consequently “healed” specimens. At the same time, direct microscopic, chemical and mineralogical analyses have proven indispensable for the understanding of the physicochemical mechanisms.

Microscopy is one of the most widely used techniques for the characterization of cementitious materials and its proven to be a useful tool in the assessment of both damage degree and healing capacity of these materials (Çopuroğlu, 2013). Optical and Scanning electron microscopy (SEM) are both used in self-healing materials research. Both techniques have advantages and disadvantages, so it is best to be used in combination.

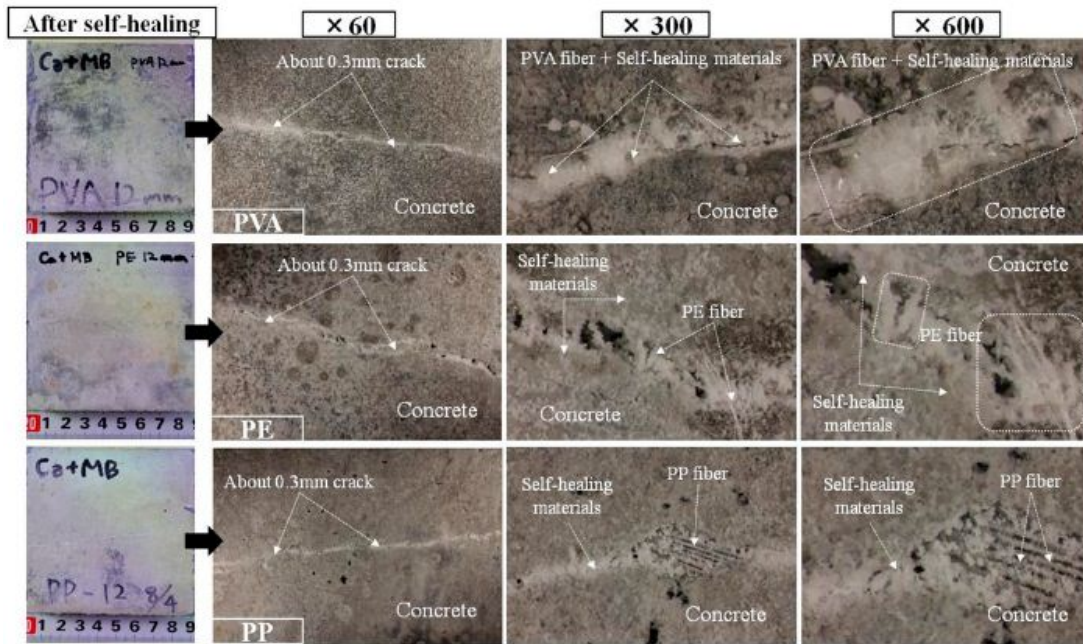


Figure 3.5: Crack closure observed by optical microscopy in concrete samples with different kind of fibers (Choi et al, 2016).

Optical microscopy offers the possibility of larger field of view observations, thus allowing a more complete assessment of the sample condition (Fig 3.5-3.6). Another advantage is related to the discrimination of minerals by observing their characteristic variations of color, in contrast to SEM where differences in mineralogy are discriminated by different shades of gray. Both these characteristics are essential to the study of self-healing mechanism as it offers the visualization of the full length of a crack and at the same time a notable contrast between the cement matrix and the secondary phases.



Figure 3.6: Discrimination of binder, aggregates and secondary precipitated calcite inside crack by polarized light microscopy. 50x magnification (2.7 x 1.4 mm), cross polarized light (Bridge, Amsterdam) (Lubelli et al, 2011)

Nevertheless, SEM is extensively used as high resolution and large depth of field are essential to the characterization of the morphology of secondary products. Moreover, SEM is usually combined with Energy dispersive X-ray spectroscopy (EDS) which allows the simultaneous chemical characterization of different phases.

Usually it is used for the observation of polished sections of damaged samples after the healing treatment, in order to visualize crack closure (Fig.3.7).

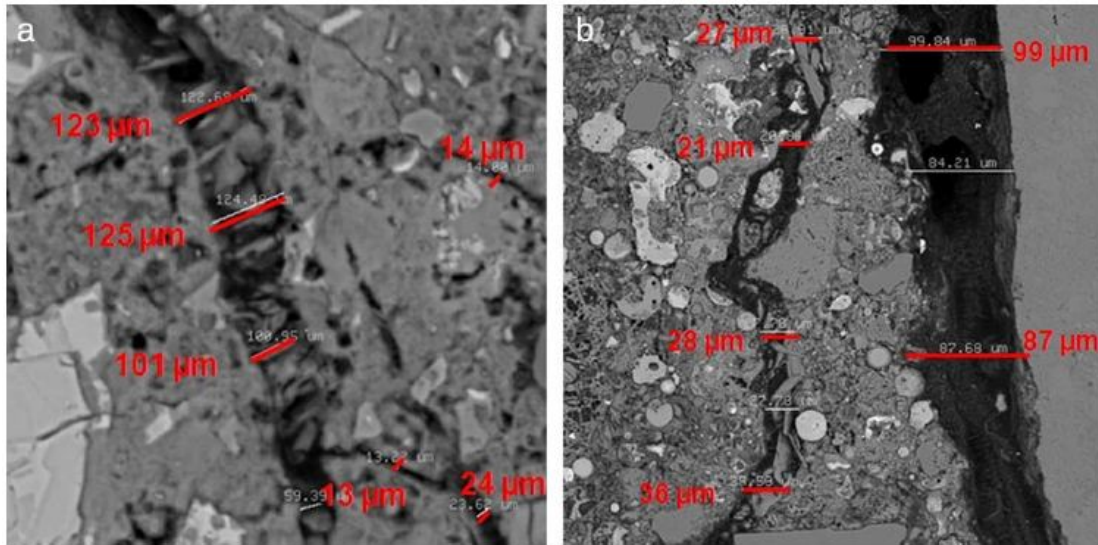


Figure 3.7: Observation of crack healing in fly-ash concrete samples by SEM (Jozwiak, 2015).

Recently Huang and Ye (2012) have used SEM to observe secondary healing products formed on the surfaces of polished samples (Fig. 3.8). By applying this method quantification of secondary products was possible as well.

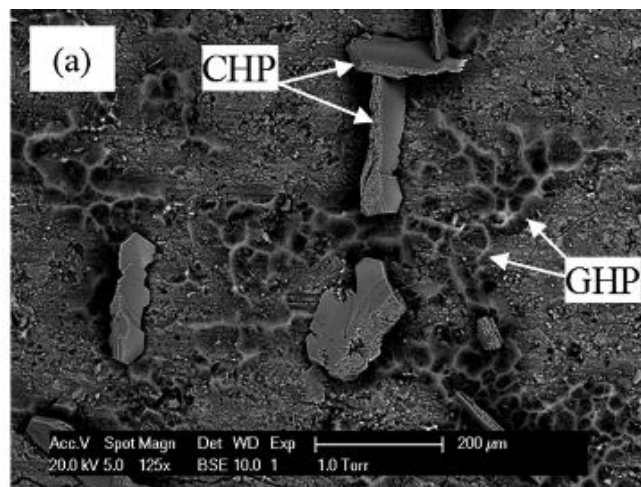


Figure 3.8: Observation of portlandite (CHP) and hydration products on the surfaces of polished samples by SEM (Huang and Ye, 2012).

Permeability measurements have been employed in the study of the self-healing mechanism as proof of recovery against environmental actions (Reinhardt et al., 2013). In earlier studies of the autogenous mechanism the focus was mainly on the self-sealing properties of concrete (Clear 1985, Edvarsen 1999, Hearn and Morley 1997, Hearn 1998) which was studied and evaluated in relation with the decrease of water permeability or leak-tightness of test specimens (Fig.3.9). In the above studies a constant supply of water was the cause of the healing-mechanism and the observations were correlated with the reduction of the flow.

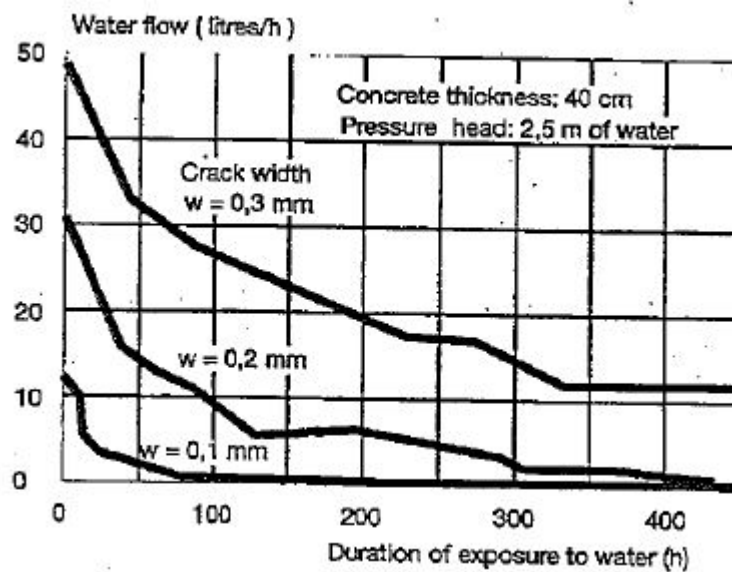


Figure 3.9: Relation between and water flow and time for different crack widths (Edvarsen 1999)

Since then, several new water permeability test equipments have been developed, including high-pressure setups and monitoring by means of neutron radiography (Fig.3.10) (Snoeck et al. 2012).

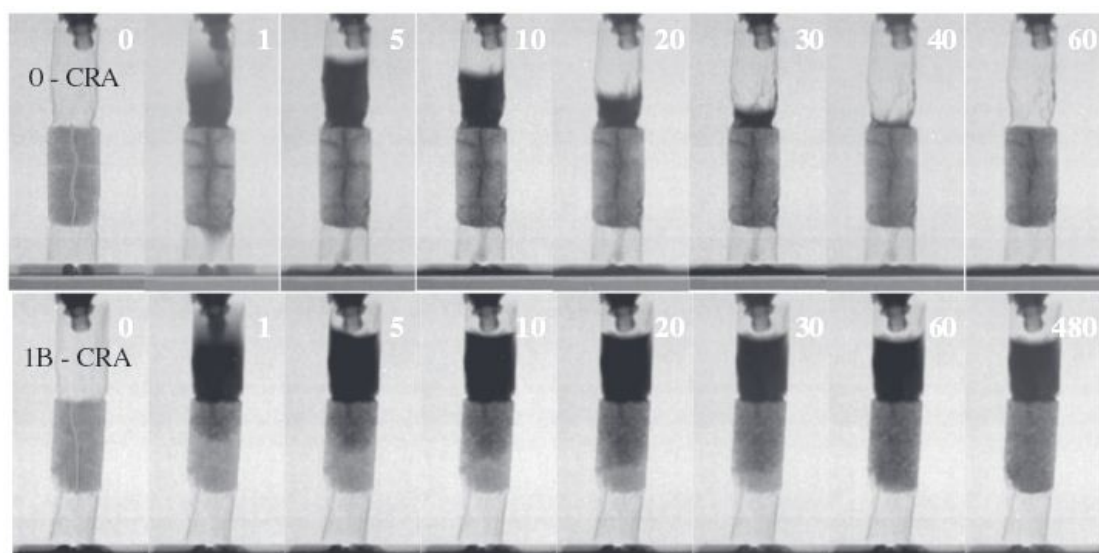


Figure 3.10: Visualization of water permeability test by neutron radiography. Time is expressed in seconds. (Snoeck et al., 2012)

Regain of strength is one of the main challenges related to self-healing materials research as it is an essential condition to the enhancement of service life. Even a complete filling of a crack microscopically, or the reduction of permeability, is not considered as sufficient healing, if cracks continue to propagate around or through the healing material.

In order to assess healing, mechanical damage has to be induced in a controlled way. Controlled cracks are created usually by means of flexural and tensile splitting tests. Crack width and length has to be reproducible for the production of multiple specimens that bear the same damage degree and can be later compared as to their healing properties. This has been proved to be a challenge since the heterogeneous nature of cement materials may be the cause of inconsistent damage to different specimens. Two methods are often used to measure crack-damage in the literature (Çopuroğlu, 2013). The first relies on linear variable differential transformers (LVDTs) that are fixed on the bottom and either sides of the specimens under flexural stress and measure the crack opening (fig 3.11). Nevertheless during unloading crack width tend to decrease due to elastic properties. The second relies on applying a prearranged load on the specimens lower than the maximum load. This method is more dependable on the potential micro-defects inherent to cement matrix and may produce specimens with varying crack characteristics and residual strength especially in lower strength cement-based materials.

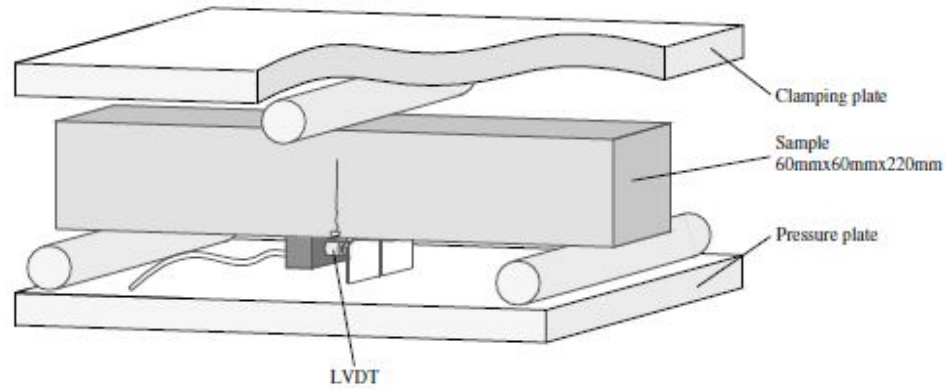


Figure 3.11: Test apparatus for measuring crack width using LVDTs. (Çopuroğlu, 2013)

3.5 Research needs defined

A state-of-the-art literature review is presented in this chapter. The need for further research towards the autogenic mechanism and the main open issues related with self-healing mechanisms are summarized below.

Firstly, a lack of research towards the autogenic mechanism on traditional hydraulic or pozzolanic mortars is evident. Although the autogenic mechanism has been correlated to the high durability of historic structures, very few simulations have been attempted. The longevity of these materials combined with the excess of free lime in their binder composition could provide valuable data related to the factors affecting the autogenous mechanism.

Moreover, autogenous self-healing mechanism studies do not address the issue of the source of calcium ions, neither the possible alteration of microstructure due to dissolution of calcareous phases. A better understanding of the mechanism requires the research of the first step of the mechanism, namely the dissolution of calcareous phases which might be one of the factors that set the limitations for the occurrence of the autogenous mechanism.

Finally, although there are many methods applied to verify the healing-efficiency of cement-based materials, the lack of standardized procedures is evident. One of the main open issues is the evaluation of the recovery of mechanical properties as the introduction of controlled damage in specimens still remains open.

Regarding the autonomous mechanism, several autonomic self-healing agents have a great potential towards efficient healing of cracks, especially mineral admixtures and bacterial concrete; but the efficiency of these admixtures is compromised if they are directly mixed in the binder. A promising solution is the encapsulation of these healing agents inside inert micro-capsules, however further research is needed regarding their encapsulation techniques.

References

- ACI Committee 212 Report on chemical admixtures for concrete, American Concrete Institute (ACI) (2010), pp. 46–50 vol. Chapter 15, no. Report ACI 212-3R-10
- Blaiszik, B. J., Kramer, S. L. B., Olugebefola, S. C., Moore, J. S., Sottos, N. R., & White, S. R. (2010). Self-Healing Polymers and Composites. *Annu. Rev. Mater. Res.*, *40*, 179–211. <http://doi.org/10.1146/annurev-matsci-070909-104532>
- Choi et al Effective Crack Control of Concrete by Self-Healing of Cementitious Composites Using Synthetic Fiber 2016
- Çopuroğlu, O., Schlangen, E., Nishiwaki, T., Tittelboom, K.V., Snoeck, D., Belie, N.D., Rooij, M.R. de, (2013): “Experimental Techniques Used to Verify Healing”, in: Rooij, M. de, Tittelboom, K.V., Belie, N.D., Schlangen, E. (Eds.), *Self-Healing Phenomena in Cement-Based Materials*, RILEM State-of-the-Art Reports. Springer Netherlands, pp. 19–63.
- De Muynck, W., De Belie, N., & Verstraete, W. (2010). Microbial carbonate precipitation in construction materials: A review. *Ecological Engineering*, *36*(2), 118–136. <http://doi.org/10.1016/j.ecoleng.2009.02.006>
- Glasser, F. P., Marchand, J., & Samson, E. (2008). Durability of concrete — Degradation phenomena involving detrimental chemical reactions. *Cement and Concrete Research*, *38*(2), 226–246. <http://doi.org/10.1016/j.cemconres.2007.09.015>
- Hilloulin, B., Legland, J.-B., Lys, E., Abraham, O., Loukili, A., Grondin, F., ... Tournat, V. (2016). Monitoring of autogenous crack healing in cementitious materials by the nonlinear modulation of ultrasonic coda waves, 3D microscopy and X-ray microtomography. *Construction and Building Materials*, *123*, 143–152. <http://doi.org/10.1016/j.conbuildmat.2016.06.138>
- Holt, E., & Leivo, M. (2004). Cracking risks associated with early age shrinkage. *Cement and Concrete Composites*, *26*(5), 521–530. [http://doi.org/10.1016/S0958-9465\(03\)00068-4](http://doi.org/10.1016/S0958-9465(03)00068-4)
- Huang, H., & Ye, G. (2014). Self-healing of cracks in cement paste affected by additional Ca²⁺ ions in the healing agent. *Journal of Intelligent Material Systems and Structures*, *26*(3), 309–320. <http://doi.org/10.1177/1045389X14525490>

- Hyde, G.W. and Smith, W.J., 'Results of experiments made to determine the permeability of cements and cement mortars', J. of the Franklin Institute Philadelphia (1889) 199-207
- Jiang, Z., Li, W., & Yuan, Z. (2015). Influence of mineral additives and environmental conditions on the self-healing capabilities of cementitious materials. *Cement and Concrete Composites*, 57, 116–127. <http://doi.org/10.1016/j.cemconcomp.2014.11.014>
- Jonkers, H. M. (2007). *Self Healing Concrete: A Biological Approach* (pp. 195–204). Springer Netherlands. http://doi.org/10.1007/978-1-4020-6250-6_9
- Jozwiak-Niedzwiedzka, D. (2015). Microscopic observations of self-healing products in calcareous fly ash mortars. *Microscopy Research and Technique*, 78(1), 22–29. <http://doi.org/10.1002/jemt.22440>
- Kanellopoulos, A., Qureshi, T. S., & Al-Tabbaa, A. (2015). Glass encapsulated minerals for self-healing in cement based composites. *Construction and Building Materials*, 98, 780–791. <http://doi.org/10.1016/j.conbuildmat.2015.08.127>
- Knorre, H., & Krumbein, W. E. (2000). Bacterial Calcification. In *Microbial Sediments* (pp. 25–31). Berlin, Heidelberg: Springer Berlin Heidelberg. http://doi.org/10.1007/978-3-662-04036-2_4
- Li, V. C., & Herbert, E. (2012). Robust Self-Healing Concrete for Sustainable Infrastructure. *Journal of Advanced Concrete Technology*, 10(6), 207–218. <http://doi.org/10.3151/jact.10.207>
- Lubelli, B., & de Rooij, M. R. (2009). NaCl crystallization in restoration plasters. *Construction and Building Materials*, 23(5), 1736–1742. <http://doi.org/10.1016/j.conbuildmat.2008.09.010>
- Lubelli, B., Nijland, T.G., van Hees, R.P.J.: Self-healing of lime based mortars: microscopy observations of case studies. *Heron* 56(1/2), 75–91 (2011)
- N. De Belie, K. Van Tittelboom, Self-healing concrete: suitability of different healing agents, *Int J. 3 R's* 1 (2010) 12–21.
- Neville A. Autogenous healing – a concrete miracle? *Concr Int* 2002;24(11):76–82.
- Pye, K., & Schiavon, N. (1989). Cause of sulphate attack on concrete, render and stone indicated by sulphur isotope ratios. *Nature*, 342(6250), 663–664. <http://doi.org/10.1038/342663a0>

- Reinhardt, H. W., H. Jonkers, K. Van Tittelboom, D. Snoeck, N. De Belie, W. De Muynck, W. Verstraete, J. Wang, and V. Mechtcherine. "Recovery against Environmental Action." In *Self-Healing Phenomena in Cement-Based Materials*, edited by Mario de Rooij, Kim Van Tittelboom, Nele De Belie, and Erik Schlangen, 65–117. RILEM State-of-the-Art Reports 11. Springer Netherlands, 2013.
- Rooij, M. R. de, E. Schlangen, and C. Joseph. "Introduction." In *Self-Healing Phenomena in Cement-Based Materials*, edited by Mario de Rooij, Kim Van Tittelboom, Nele De Belie, and Erik Schlangen, 1–17. RILEM State-of-the-Art Reports 11. Springer Netherlands, 2013.
- Sabbioni, C., Zappia, G., Riontino, C., Blanco-Varela, M. T., Aguilera, J., Puertas, F., K. Van Balen, and E. E. Toumbakari. (2001). Atmospheric deterioration of ancient and modern hydraulic mortars. *Atmospheric Environment*, 35(3), 539–548.
[http://doi.org/10.1016/S1352-2310\(00\)00310-1](http://doi.org/10.1016/S1352-2310(00)00310-1)
- Schiavon, N., Chiavari, G., & Fabbri, D. (2004). Soiling of limestone in an urban environment characterized by heavy vehicular exhaust emissions. *Environmental Geology*, 46(3-4), 448–455. <http://doi.org/10.1007/s00254-004-1046-8>
- Seifan, M., Samani, A. K., & Berenjjan, A. (2016). Bioconcrete: next generation of self-healing concrete. *Applied Microbiology and Biotechnology*, 100(6), 2591–2602.
<http://doi.org/10.1007/s00253-016-7316-z>
- Shirakawa, M. A., Loh, K., John, V. M., Silva, M. E. S., & Gaylarde, C. C. (2011). Biodeterioration of painted mortar surfaces in tropical urban and coastal situations: Comparison of four paint formulations. *International Biodeterioration & Biodegradation*, 65(5), 669–674. <http://doi.org/10.1016/j.ibiod.2011.03.004>
- Siddique, R., & Chahal, N. K. (2011). Effect of ureolytic bacteria on concrete properties. *Construction and Building Materials*, 25(10), 3791–3801.
<http://doi.org/10.1016/j.conbuildmat.2011.04.010>
- Sisomphon, K., Copuroglu, O., & Koenders, E. A. B. (2012). Self-healing of surface cracks in mortars with expansive additive and crystalline additive. *Cement and Concrete Composites*, 34(4), 566–574. <http://doi.org/10.1016/j.cemconcomp.2012.01.005>
- Snoeck, D., Steuperaert, S., Van Tittelboom, K., Dubruel, P., & De Belie, N. (2012). Visualization of water penetration in cementitious materials with superabsorbent polymers

- by means of neutron radiography. *Cement and Concrete Research*, 42(8), 1113–1121.
<http://doi.org/10.1016/j.cemconres.2012.05.005>
- Souradeep, G., & Kua, H. W. (2016). Encapsulation Technology and Techniques in Self-Healing Concrete. *Journal of Materials in Civil Engineering*, 04016165.
[http://doi.org/10.1061/\(ASCE\)MT.1943-5533.0001687](http://doi.org/10.1061/(ASCE)MT.1943-5533.0001687)
- Tsangouri, E., Aggelis, D. G., Van Tittelboom, K., De Belie, N., & Van Hemelrijck, D. (2013). Detecting the activation of a self-healing mechanism in concrete by acoustic emission and digital image correlation. *TheScientificWorldJournal*, 2013, 424560.
<http://doi.org/10.1155/2013/424560>
- Van Breugel, K. (2012). Self-healing material concepts as solution for aging infrastructure. *37th Conference on Our World in Concrete & Structures*, 1–17. <http://doi.org/100037009>
- Van Breugel, K. (2012). Self-healing material concepts as solution for aging infrastructure. *37th Conference on Our World in Concrete & Structures*, 1–17. <http://doi.org/100037009>
- Van Tittelboom, K., De Belie, N., Van Loo, D., & Jacobs, P. (2011). Self-healing efficiency of cementitious materials containing tubular capsules filled with healing agent. *Cement and Concrete Composites*, 33(4), 497–505.
<http://doi.org/10.1016/j.cemconcomp.2011.01.004>
- Van Tittelboom, K., Gruyaert, E., Rahier, H., & De Belie, N. (2012). Influence of mix composition on the extent of autogenous crack healing by continued hydration or calcium carbonate formation. *Construction and Building Materials*, 37, 349–359.
<http://doi.org/10.1016/j.conbuildmat.2012.07.026>
- Yang, Y., & Urban, M. W. (2013). Self-healing polymeric materials. *Chemical Society Reviews*, 42(17), 7446. <http://doi.org/10.1039/c3cs60109a>
- Yang, Z., Weiss, W. J., & Olek, J. (2006). Water Transport in Concrete Damaged by Tensile Loading and Freeze–Thaw Cycling. *Journal of Materials in Civil Engineering*, 18(3), 424–434. [http://doi.org/10.1061/\(ASCE\)0899-1561\(2006\)18:3\(424\)](http://doi.org/10.1061/(ASCE)0899-1561(2006)18:3(424))

Chapter 4: Self-healing observations in historic mortars

4.1 Introduction

Mortars have been part of our architectural heritage for millennia and have been used to meet a wide variety of structural needs, e.g. as joint mortars or plasters, lining material in cisterns, aqueducts and wells or as substrate in frescoes. Archaeological mortars dating as back as the Neolithic period have been preserved and studied thus providing us with valuable information regarding the technological evolution of architecture and craftsmanship.

Microscopy analysis of historic mortars has made possible the detailed understanding of their physical characteristics with special emphasis in microstructure (Elsen, 2006), porosity, inclusions, as well as the potential degradation mechanisms. In this context, microscopic examination of historic mortars encouraged the research of technological trends (Moropoulou et al., 2000a, Stefanidou et al., 2012) over the centuries as well as enabled the observation of secondary mechanisms that take place over extensive periods of time, such as degradation mechanisms or secondary products forming in the binder matrix.

Although several researchers have observed microscopically the precipitation of secondary calcite in cracks and voids of lime mortars (Anderegg., 1942), it was only recently linked with the enhanced durability of historic masonry and the autogenic mechanism of self-healing (Callebaut et al., 1999). Limited research has been performed regarding the evaluation of self-healing phenomena in historic mortars. For instance, Moropoulou et al. (2000b) during the examination of Byzantine monuments in Kiev observed that secondary calcite precipitated in cracks - formed during earthquakes - has enhanced the masonry durability over the centuries by reversing earthquake micro-damage to the masonry.

Moreover, two more recent systematic studies performed by Nijland et al. (2007) and Lubeli et al. (2011) focused on 19th century lime-based mortar samples in the Netherlands, showed that:

- The presence of free lime is a prerequisite for the self-healing process to occur.

- Prolonged wet periods followed by dry periods appear to be favorable conditions.
- Besides calcite, portlandite may also be observed as secondary crystallized product that could further react to produce calcite.

The examination of archaeological samples offers the possibility to study this naturally occurred phenomenon, since neither the materials used were designed for this particular purpose nor they were deliberately damaged and cracked.

In this chapter, a detailed study of selected samples is presented based on microscopy observations of specimens of archaeological mortars from different monuments and historical periods focused on the self-healing phenomenon. The approach taken is a reverse process i.e. an archaeo-mimetic approach, which aims firstly to offer information regarding the physico-chemical processes that affect these materials over long periods of time such as in historic structures, and consequently to use this information in order to optimize new material technology .

4.2 Materials and Methods

Twenty samples of representative historic mortars (Table 4.1) from monuments located in six different regions of Greece (Fig.4.1) were examined focusing on the study of the autogenous self-healing phenomenon. The monuments were built in different historic periods, dating from the late Hellenistic to 19th century (Fig 4.2), while mortar samples originate from a multitude of uses such as lining material in water tanks, tombs or baths and joint mortars or plasters in internal and external walls (Table 4.1).

Regarding the micro-climatic conditions, during sampling, the proximity of the masonry to water was taken into account, since water is one of the most important parameters linked with the occurrence of the autogenous phenomenon. The porous network of mortars is known to allow the movement of the pore solution through the material, thus the autogenous phenomenon could take place even in parts of the masonry that are not directly wetted. More specifically, the samples were collected and classified depending on whether they were in direct contact with water, or if water presence is limited to condensation of humidity and diffusion through capillary pores. Besides microclimatic conditions, other parameters studied are:

- chemical composition of the binder (e.g. hydraulic or air-hardening)
- type of aggregates,
- morphological characteristics of cracks and
- formation and morphology of the secondary self-healing products.

Samples of historical mortars were studied in polished sections and fracture surfaces in a scanning electron microscope (FEI Quanta-Inspect) coupled with Energy-dispersive X-ray spectroscopy (SEM / EDX) in order to study their microstructure as well as the chemical composition of individual components and secondary formed products.

Moreover, thin sections were examined in the petrographic microscope, in order to identify the mineralogy, morphology and distribution of secondary products, along with the morphological characteristics of the cracks where the phenomenon is observed.

Table 4.1: List of samples

Sample	Monument	Region	Historic Period	Sampling
Ag 2	Kastraki excavation	Agathonisi	3rd–1st cent. BC	Tank A-lining mortar
Ag 5	Kastraki excavation	Agathonisi	"	Tank A-lining mortar
Ag 14	Kastraki excavation	Agathonisi	"	TankB - lining mortar
Ag 17	Kastraki excavation	Agathonisi	"	TankB - lining mortar
Ag18	Kastraki excavation	Agathonisi	"	TankB - lining mortar
Ag 20	Kastraki excavation	Agathonisi	"	TankB - Joint mortar
FISK 3	Fiskardo-Roman tomb	Agathonisi	3 rd cent. BC-6 th cent. AD	External lining mortar
FISK 6	Fiskardo-Roman bath	Agathonisi	"	Joint mortar
SAM1	Sami-Roman bath	Kefalonia	"	External lining material
SAM2	Sami-Roman bath	Kefalonia	"	Joint mortar
SAM6	Sami-Roman bath	Kefalonia	"	External lining material
SAM 15	Sami-Basilica	Kefalonia	6 th cent. AD	Foundation

DFM-3	Daphni Monastery	Athens	6 th -11 th cent. AD	Fortification wall
DFM-6	Daphni Monastery	Athens	"	"
DFM-8	Daphni Monastery	Athens	"	"
PK 5	Lady of the Castle Cathedral	Rhodes	7 th cent. AD	Interior wall lining 2.6 m.
PK 9	Lady of the Castle Cathedral	Rhodes	"	Interior wall lining 1.6 m
PK 17	Lady of the Castle Cathedral	Rhodes	"	Interior wall lining ~10 m
XD 1	Aghios Nikolaos	Chalki	19 th cent. AD (1861)	Joint mortar
XE 2	Aghios Nikolaos	Chalki	"	External lining material



Figure 4.1: Locations of the monuments

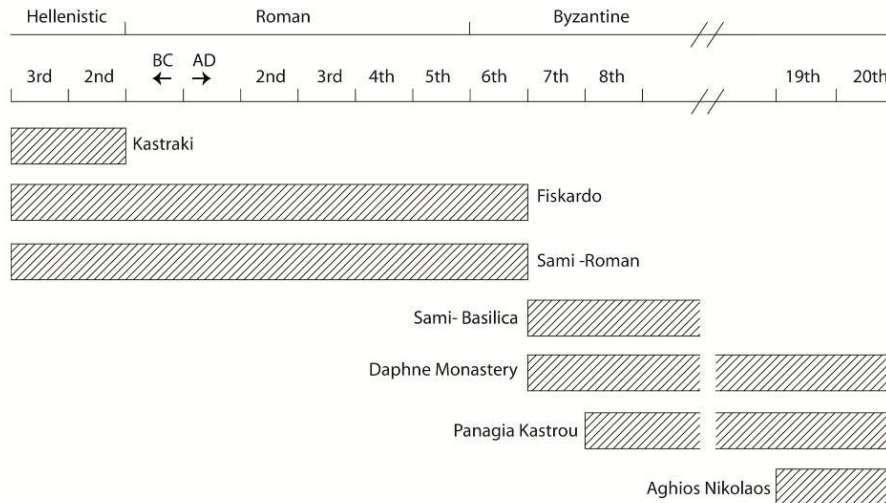


Figure 4.2: Chronological diagram of the monuments

4.3 Microscopic observations

- Agathonisi - Kastraki excavation

Excavations in the Kastraki area in the island of Agathonisi have identified this region as the Ancient Tragaia, a fortified settlement first inhabited during the late 4th millennium BC. During the 2nd century BC, the site was rebuilt under Roman influence, and multiple structures such as cisterns, tanks, as well as enhanced fortifications were dated to that era (Fig 4.3) (Triantafyllidis, 2015).



Figure 4.3: Terrace 1; citadel with cistern; Late Hellenistic–Early Roman period (Triantafyllidis, 2015)

Sampling: The samples examined were part of two tanks lined with hydraulic plaster built during that period and were used for water retaining. More precisely, six samples from two tanks were analyzed, two samples from the first tank (Ag 2, Ag 5) and four samples from the second (Ag14, Ag 17, Ag 18, Ag20).

All mortar samples examined were similar regarding their composition; they consist of aerial binder combined with a variety of natural calcareous and alumino-siliceous aggregates. In some samples (e.g. Ag20a), the presence of Mg was identified, which points to a mixed dolomitic binder. Moreover, the presence of micro-cracks and voids was abundant in all samples. Crack widths do not exceed 100 μm , although it is frequently interrupted by larger voids. Re-precipitated calcite is observed growing on voids' and cracks' walls (Fig. 4.4-4.9). Micro-cracks up to 100 μm are partially or totally filled with CaCO_3 . Both sparitic and micritic calcite are observed.

The placement of these mortars as lining material inside the tanks suggests that, during the functional period of the tanks, they were submerged under water for long periods of time followed by dry periods when the tanks were empty.

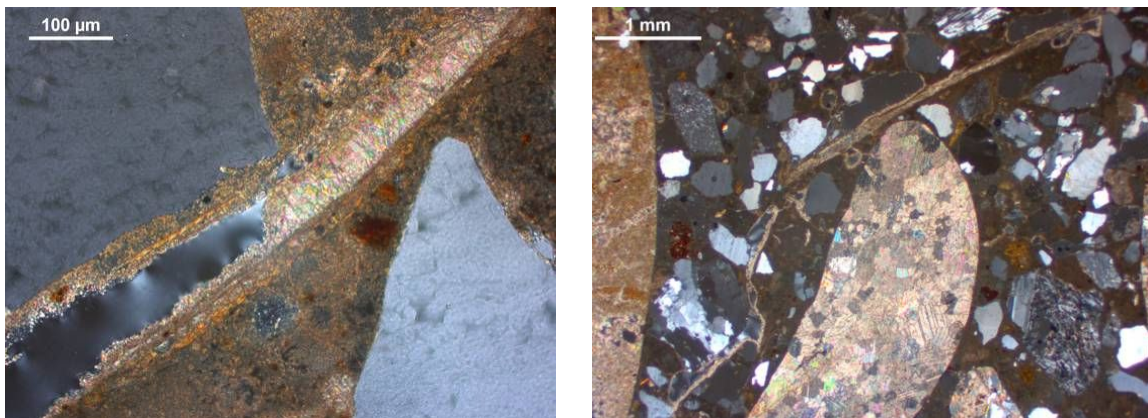


Figure 4.4 (Left): Secondary calcite precipitated filling a crack of 100 μm width. Micritic calcite can be seen precipitated on the crack walls where the crack is only partly filled.-Ag2

Figure 4.5 (Right): Overview of a crack (150 μm width) interrupted by larger voids. Parts of the crack are completely filled with secondary calcite whereas the wider parts are only partially filled. Ag5

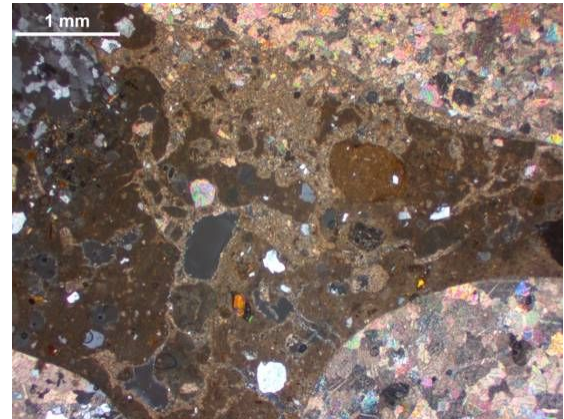
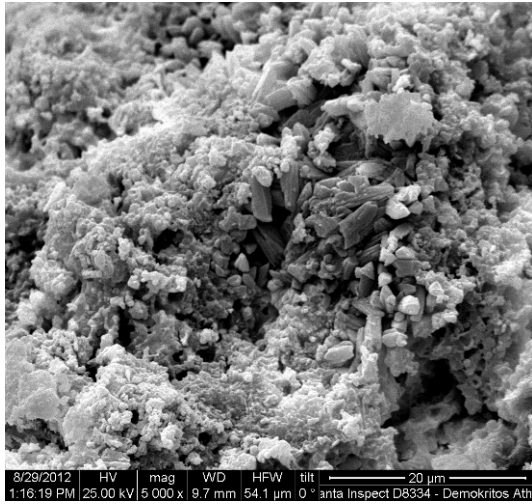


Figure 4.6 (Left): Well crystallized secondary calcite crystals precipitated inside a void-Ag 14

Figure 4.7 (Right): Secondary calcite precipitated in the binder and calcareous aggregates' interface - Ag17

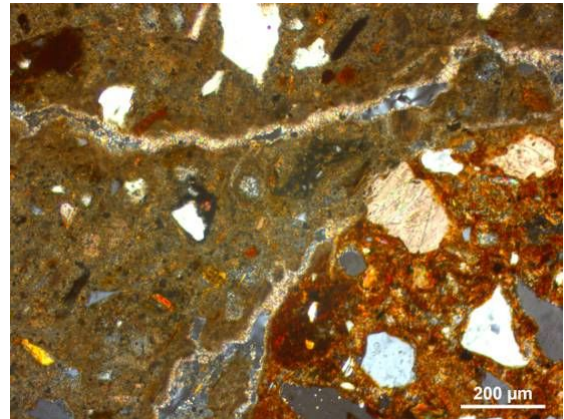
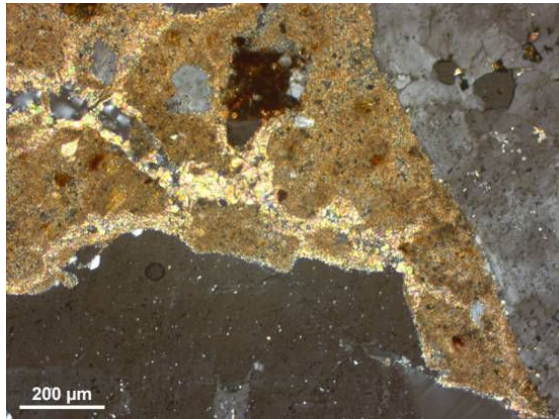


Figure 4.8 (Left): Well crystallized sparitic and micritic calcite filling a 150µm crack - Ag18

Figure 4.9 (Right): Overview of a partly filled crack (100µm width) by a homogeneously crystallized calcite - Ag20

- Cephalonia -Fiskardo excavation

Fiskardo has been identified as the Roman city of Panormos. In this area several Roman monuments were unearthed including a Roman Agora, mausolea and a theatre/conservatory.

Sampling: Two samples were examined, namely, one was lining material from the external masonry of a Roman tomb (F3) (Fig.4.10), and the second was joint mortar from the Roman baths (F6).

Both mortars were characterized by a high binder to aggregate ratio, and dense microstructure. The binder used in the external masonry of the roman tomb (F3) was aerial lime combined with rounded aggregates of a mixed alumino-siliceous nature.

The mortar used in the roman baths (F6) was mixed with crashed ceramic aggregates, while a small amount of fossilized marine microorganisms is also present.

Both samples showed signs of an extended network of micro-cracks and large voids and maximum crack width is 100 μm . Large calcite crystals ($\sim 100 \mu\text{m}$) were observed to grow on the walls of large voids, whereas smaller cracks (60-80 μm), usually linking voids, are completely filled with calcite (Fig. 4.11-4.12).



Figure 4.10: Roman tomb in Fiscardo excavation

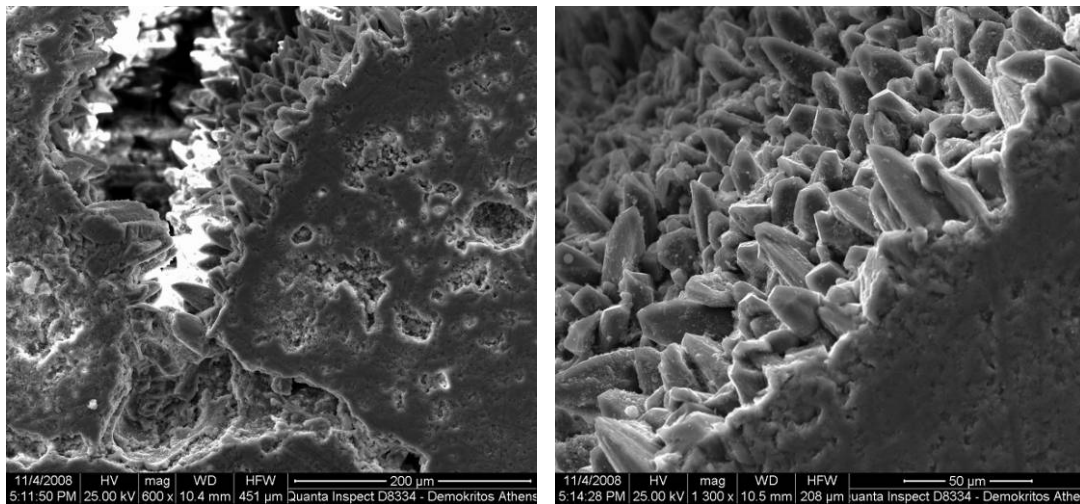


Figure 4.11: (Left) Well crystallized calcite crystals ranging in size up to 50 μm inside a large void; (Right) Detailed microphotograph of the crystals microstructure-F3

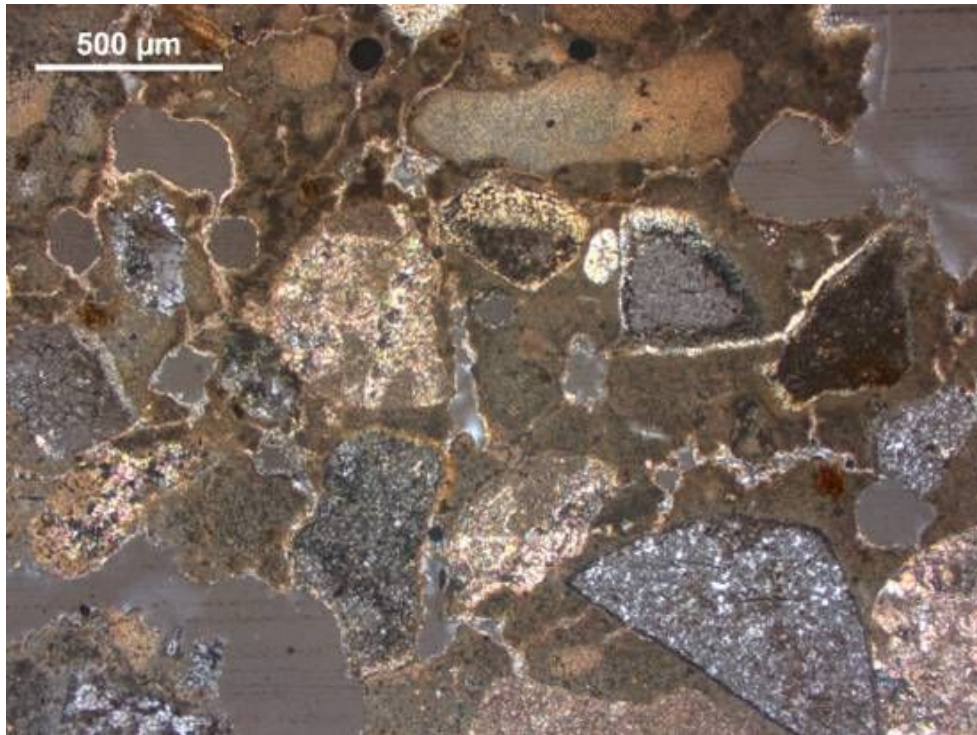


Figure 4.12: Extended network of microcracks partially filled with secondary calcite –F6

- Cephalonia-Sami excavation and Basilica

Sami is considered to be an urban center in Cephalonia that was continuously used from the Early Helladic to Early Christian period. Multiple Roman as well as Byzantine monuments were unearthed during excavations, including Roman baths and the foundations of a Byzantine basilica church (YPPO, 2012).

Sampling: Three samples from the roman baths were examined, two lining mortars from the external masonry of the structure (S1, S6) and a joint mortar(S2).Furthermore, one sample was examined from the basilica’s foundation (S15).

In all mortar samples, the binder is aerial lime combined with natural rounded aggregates, except one lining mortar (S6) in which no aggregates except straw were added. Moreover, the mortar used in the basilica’s foundation (S15) is characterized by the addition of aggregates of larger diameter and lower percentage of binder, thus exhibiting higher porosity. This may be the reason for soil material being present inside the binder matrix.

Furthermore, lime lumps are frequent in all samples in parallel to magnesium being present in the composition of the binder, suggesting a common way of preparing and mixing of the raw materials as well as a local common source of limestone.

Micro-cracks are not observed regularly and the binder matrix is very cohesive. Re-crystallized calcite is grown inside the walls of voids or small cracks that are completely filled. Distinctive crystallized prismatic calcite crystals were observed in higher magnification at the scanning electron microscope inside voids (Fig 4.13-4.15).

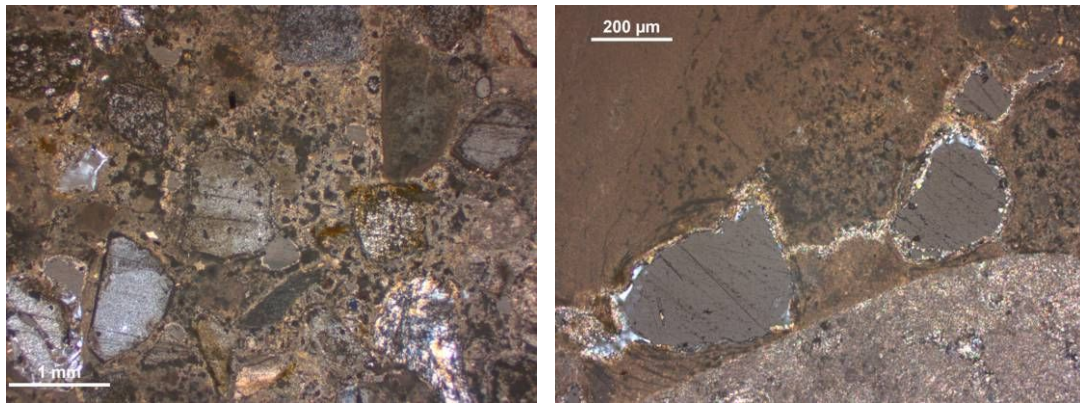


Figure 4.13 (Left): Extended network of microcracks partially filled with secondary calcite-S1

Figure 4.14 (Right): Completely healed crack bridging two large pores. A homogenous layer of calcite precipitation can be seen on the pore walls - S15

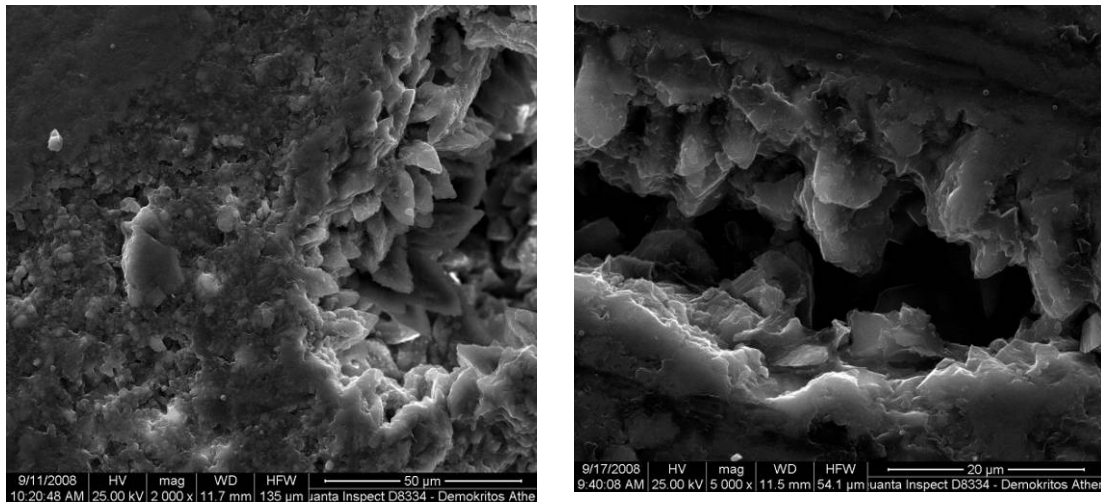


Figure 4.15: Calcite crystals growing on the voids' walls (Left) S2 (Right) S6

- *Athens-Daphni monastery*

Daphni monastery is a UNESCO world heritage site, located in Athens on the side of the ancient street that leads to Eleusis. The main monastery was built during the 6th cent. AD and was enclosed by strong defensive walls. Since then it was continuously used as a Christian monastery (11th cent. AD) while later was used as a garrison during the Greek revolution. After that it was briefly used as a mental hospital (1883-85). It took heavy damage by earthquakes in 1889 and 1897. Restoration works have been conducted since the late 19th century but have been enhanced after the 1999 earthquake.

Sampling: Samples of joint mortars were collected from the exterior fortification walls (Fig 4.16). In all samples an extensive network of micro-cracks was observed. Crystallization of micritic calcite crystals can be seen partially or completely filling cracks of maximum 100 μm (Fig 4.17- 4.19).



Figure 4.16: Exterior fortification walls of Daphni monastery (Commons wikimedia, 2011).

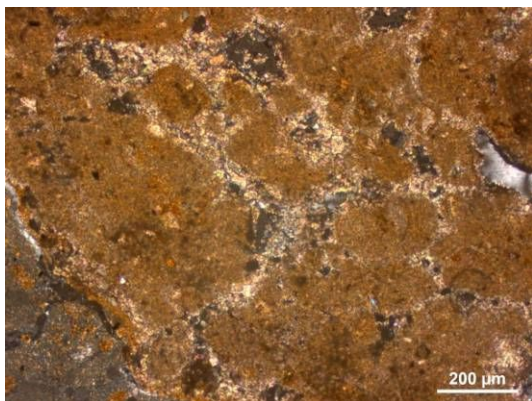


Figure 4.17 (Left): Extended network of microcracks and voids partially or completely filled by secondary micritic calcite. D3

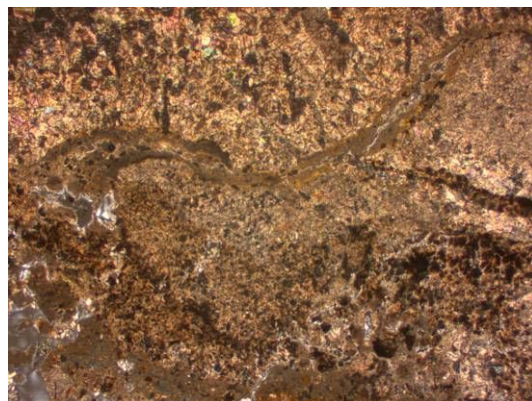


Figure 4.18 (Right) Microcrack of varying diameter (max. 100 μm) filled by secondary calcite. D6

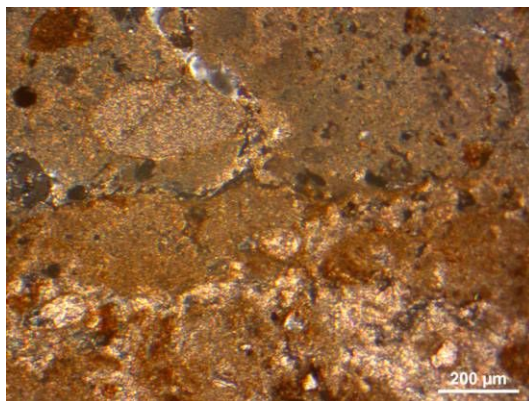


Figure 4.19: Network of microcracks and voids partially filled by secondary micritic calcite. D8

- Rhodes-Lady of the Castle Cathedral (Panagia Kastrou)

The original core of the building was probably erected in the 11th cent.AD and belonged to the type of cruciform church with a dome. After Rhodes' conquest by the Knights, the Byzantine church was reconstructed and took the form of three-aisled Gothic basilica with transept. The east side of the temple abuts the sea fortification. During the Turkish occupation, the church was converted into a mosque and named Enteroum Mosque.

Sampling: The three samples examined were lining mortars collected from the interior northern wall at different heights (1.6, 2.6 and 10 meters).

All mortars were characterized by a mixed hydraulic binder composition with the addition of a variety of natural aggregates (calcareous, dolomitic, siliceous and igneous aggregates) with the addition of marine fossilized microorganisms. Moreover,

the presence of sodium chloride salts was pronounced. Networks of micro-cracks are observed in all samples along with large voids (Fig 4.20-4.24). Calcite is recrystallized filling almost completely micro-cracks up to 100 μm . Both micritic and sparitic forms of calcite are grown in neighboring cracks while well-crystallized prismatic crystals were observed in higher magnification under the scanning electron microscope.

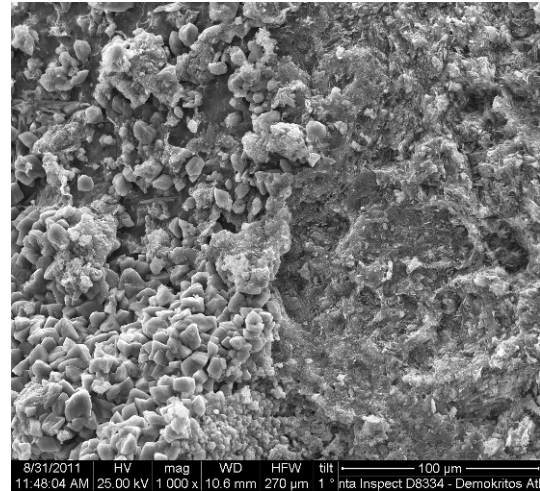
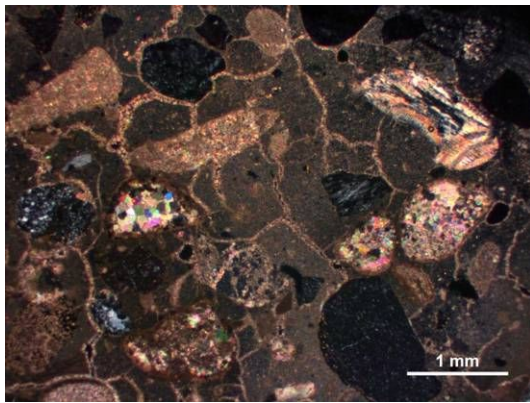


Figure 4.20 (Left): Extended crack network completely filled by secondary calcite. Micritic and sparitic calcite crystals are present - PK5

Figure 4.21 (Right): Microstructure of re-crystallized calcite on a pore surface - PK5

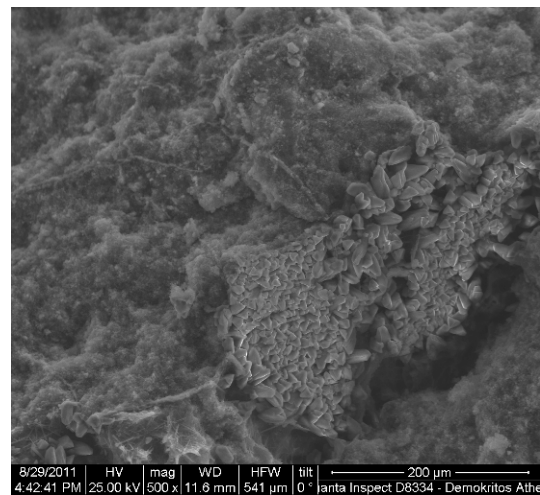
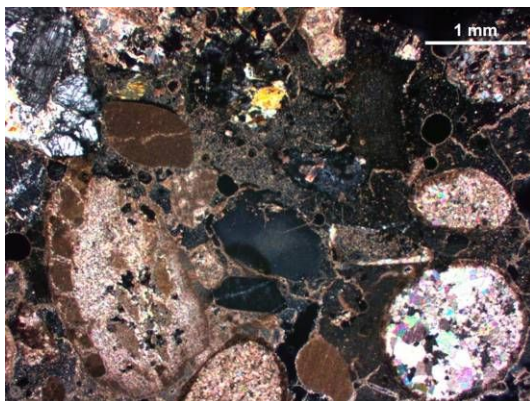


Figure 4.22 (Left): Re-crystallization of calcite inside cracks and voids in the vicinity of microfossils and calcareous aggregates –PK9

Figure 4.23 (Right): Micrograph of sparitic calcite on a crack wall–PK9

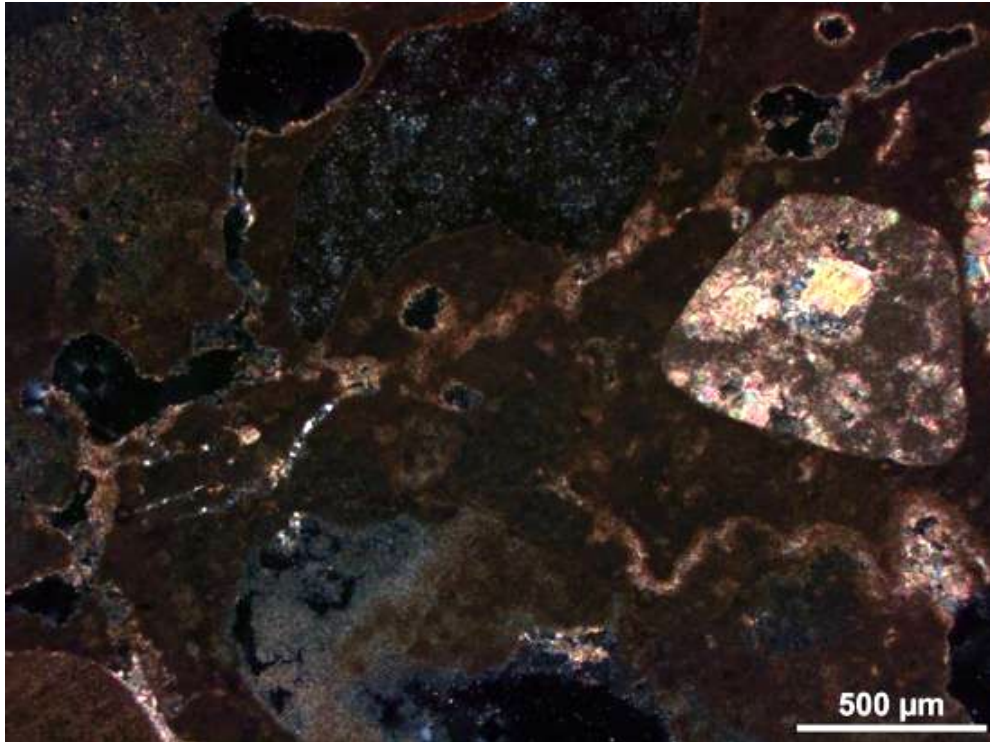


Figure 4.24: Secondary sparitic calcite crystals in the vicinity of lime lump filling completely a 50μm width crack.-PK17

- Chalki - Aghios Nikolaos

St. Nicolas is the main church of Emborio, port of Chalki, built in 1861 with marble parts from the ancient temple of Apollo.

Sampling: Two samples were examined, a joint (XD1) and a lining mortar (XE2). XD1 is characterized by dense microstructure and its composition was assessed to be aerial lime combined with a mixture of natural rounded aggregates of calcitic and aluminosiliceous nature. The presence of lime lumps is also observed.

The lining mortar (XE2) is aerial lime with a weak hydraulic character combined mainly with calcareous aggregates. Some areas of the joint mortar sample (XD1) exhibit a highly corroded microstructure. The lining mortar sample (XE2) exhibit cohesive structure; few micro-cracks are observed with less than 60 μm maximum width.

Leaching and re-crystallization of calcium carbonate was observed in the joint mortar sample (XD1). In both samples micritic calcite is re-crystallized filling micro-cracks and small voids completely (Fig. 4.25-4.27).

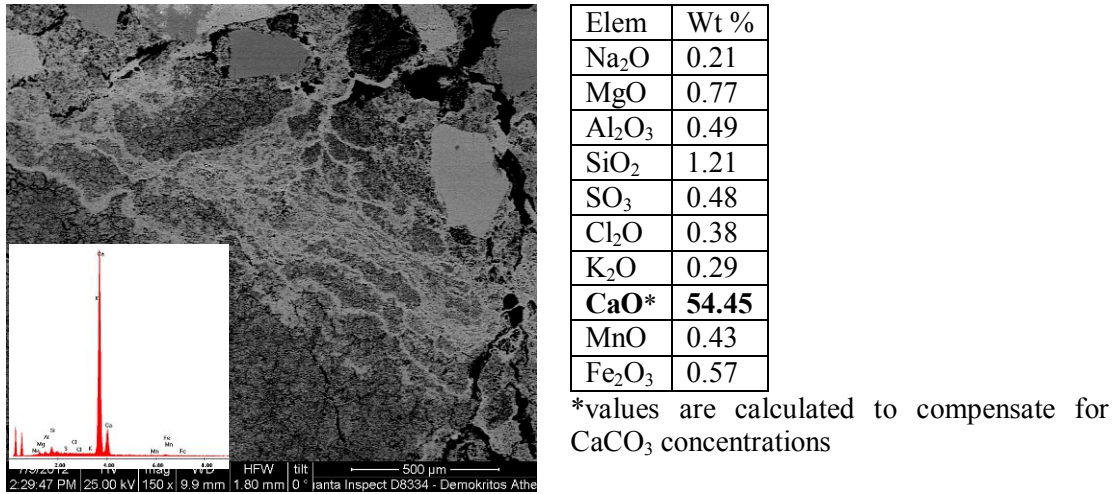


Figure 4.25: (Left) Leached secondary calcite partly repairing damaged microstructure. (Right) Chemical analysis of precipitated calcite –XD1

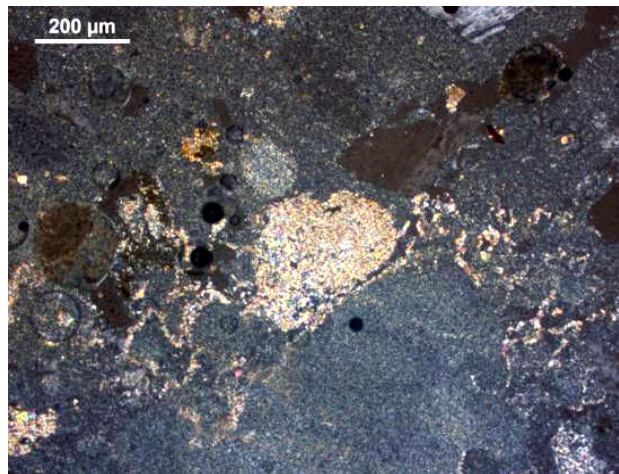


Figure 4.26 (Left): Secondary calcite precipitated around a lime lump XD1

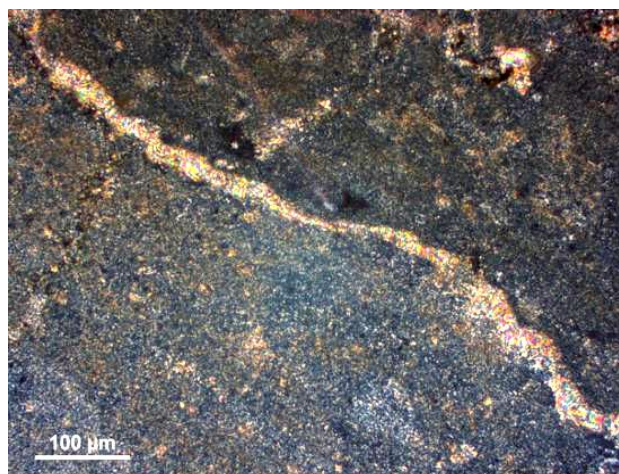


Figure 4.27 (Right): Overview of a completely filled crack (80µm maximum width) by homogeneously crystallized calcite-XE2

Chemical characterization by energy dispersive X-ray analysis (EDAX) of the mortar samples examined in this chapter is presented in Table 4.2.

Table 4.2: Chemical characterization of historic mortars

	Na ₂ O	MgO	Al ₂ O ₃	SiO ₂	P ₂ O ₅	SO ₃	Cl ₂ O	K ₂ O	CaO*	TiO ₂	MnO	Fe ₂ O ₃
Ag 2	1.6	5.2	3.7	11.4	4.2	2.9	0.8	0.4	37.2	0.3	0.4	2.7
Ag 5	1.6	2.5	2.1	5.1	3.1	2.2	1.2	0.4	44.7	0.6	0.3	1.2
Ag 14	1.4	1.8	2.8	4.9	8.7	4.9	0.6	0.3	40.2	0.3	0.7	2.0
Ag 17	0.3	1.8	11.1	24.2	1.9	0.3	2.4	1.2	29.4	0.5	0.5	3.3
Ag 18	1.0	1.7	3.8	8.4	1.6	1.2	0.5	1.0	44.3	0.5	0.3	0.9
Ag 20	1.7	2.5	4.0	8.3	4.8	2.5	1.0	0.4	40.2	0.4	0.3	2.3
FISK 3	0.7	1.1	0.7	2.3	0.8	0.5	0.5	0.2	51.8	nd	nd	0.6
FISK 6	0.8	1.0	2.6	5.8	0.6	0.7	0.8	0.5	48.6	nd	nd	0.6
SAM1	0.7	0.8	1.2	2.1	1.2	1.3	0.7	0.6	50.8	nd	0.1	0.7
SAM2	0.9	2.0	0.8	2.2	1.5	1.6	0.7	0.9	49.7	nd	0.1	0.5
SAM6	0.9	0.9	1.0	1.3	nd	1.5	0.8	0.5	51.8	nd	0.1	0.6
SAM 15	0.9	1.5	1.9	3.2	1.3	0.7	0.6	0.5	49.6	nd	0.1	0.8
PK 5	nd	4.8	1.4	13.3	0.3	0.6	1.6	0.2	42.9	nd	0.1	1.1
PK 9	1.3	1.1	1.6	9.8	0.7	1.3	0.3	0.2	46.3	0.1	0.1	0.9
PK 17	2.5	3.5	2.7	11.2	nd	nd	1.3	0.6	42.9	nd	0.5	1.1
XD 1	0.2	0.8	0.8	1.9	nd	0.2	0.2	0.2	53.0	nd	0.3	0.9
XE 2	0.6	1.2	0.7	1.1	nd	0.9	0.5	0.2	52.8	nd	0.2	0.3

*values are calculated to compensate for CaCO₃ concentrations

4.4 Discussion

Correlating the sampling position with the samples' microscopic characterization, specific parameters related to the autogenic self-healing phenomena are identified and discussed.

Micro-climatic conditions

The materials examined were sampled from a wide variety of sampling positions. Mortar samples from Kastraki, Sami and Fiskardo were unearthed during archaeological excavations, suggesting that they were buried for several centuries. At the same time mortars from Daphni, Rhodes and Chalki were sampled from masonry exposed ranging from two as much as fourteen centuries. Moreover, these mortars were part of diverse structures (fortification, foundation lining in tanks or baths) which indicates a different proximity to water during their use and/or being subjected to wet-dry cycles. More specifically, the phenomenon was observed both in buried structures and standing masonry as well as in external and internal walls.

Crack width and Length

Crack characteristics are essential in the evolution of the self healing phenomenon (Reinhardt and Jooss 2003). The samples examined showed secondary crystalline formations in cracks up to 150 μm . Evidently, the cracks that were completely filled with re-crystallized products did not exceed 100 μm . This is even more evident in some cases where the crack width differentiates lengthwise (Figure 4.29). In that case, there is a homogeneous precipitation of 80 μm along the crack surface that effectively fills cracks of equal or less width, whereas larger voids are not completely filled. The calcite's precipitation homogeneity suggests that it was produced simultaneously, resulting in the complete filling of the crack's narrowest parts, blocking the pore solution from reaching the crack's wider parts.

Irregularity of the crack could also be a factor as sharp edges (Fig.4.30) provide nucleating points (Lauer and Slate, 1956).

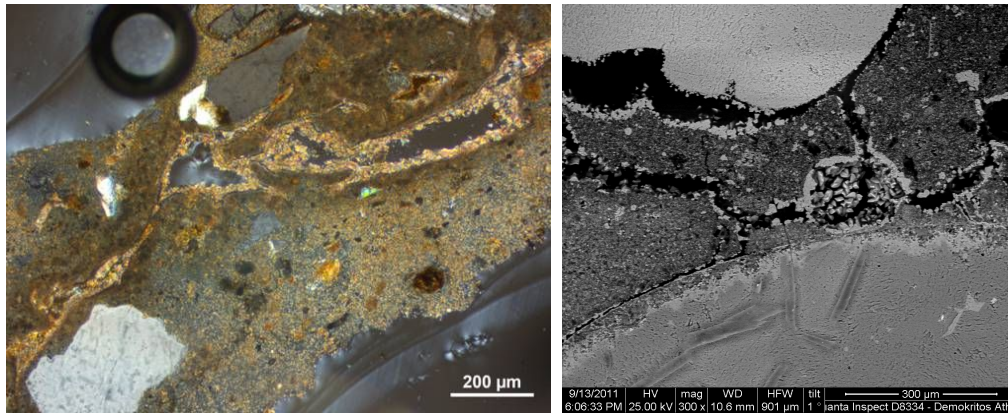


Fig. 4.29 (Left): Secondary calcite evenly precipitated along the sides of a crack - oik 20b

Fig. 4.30 (Right): Irregular cracks provide nucleating points for the precipitation of calcite PK5

Type of secondary products

Secondary products formed inside the cracks and voids of the specimens examined were found to be calcium carbonate, nevertheless crystal form and size varied noticeably. More specifically, micrite and sparite were observed (Fig 4.31 left) coinciding with a notable variance in crystal size.

This is probably due to the fact that crack width also affects the size of the formed crystals. In figure 4.31 (right) the crystals' size can be observed to be directly proportionate to the volume available. This is a complex phenomenon in all probability due, among other parameters, to the different flow of pore solution through different sized cracks. Because crystal diameter is related to the rate of precipitation, larger pores allow the pore solution to enter for a longer period of time thus providing more Ca^{2+} ions to precipitate and increase the size of the calcite crystals. In the same manner, smaller pores or cracks would heal more rapidly sealing off the pore solution.

No secondary hydraulic phases were detected, even in the mixed hydraulic binder samples (e.g. Lady of the Castle Cathedral – PK 5).

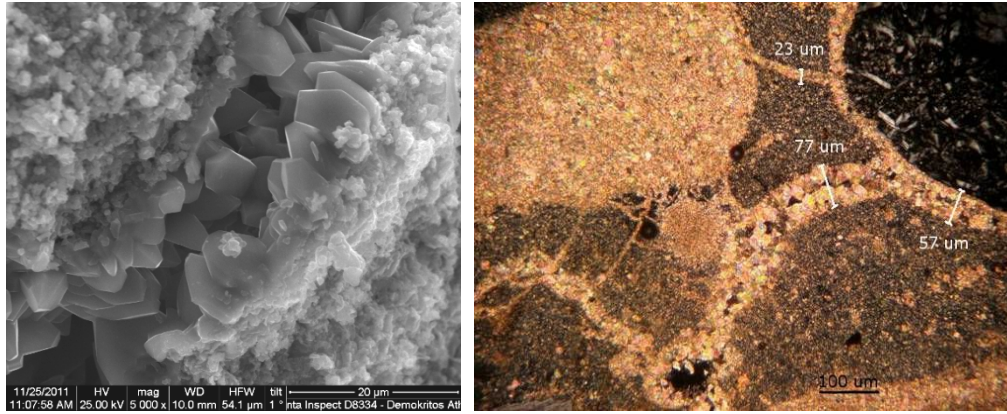


Figure 4.31(Right): Well formed sparitic calcite crystals. (Left) Calcite crystals of different morphology formed, corresponding to the crack width.

Binder composition

Binder composition of historical mortars was studied in polished sections of the samples at a scanning electron microscope equipped with energy dispersive X-ray spectroscopy (SEM / EDAX). Although the mortars examined are distinguished by variations in the chemical composition of the binder, the presence of self-healing phenomenon was verified in both aerial and mixed hydraulic mortars.

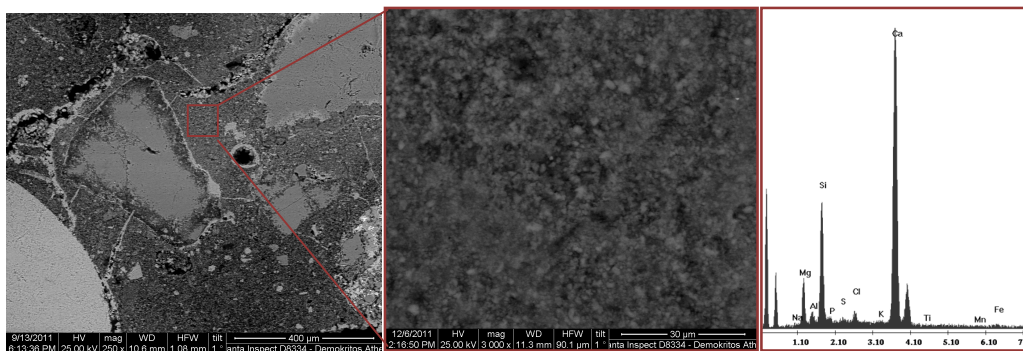


Figure 4.32: An extensive network of micro-cracks partially or completely filled by secondary calcium carbonate was observed in samples with higher magnesium concentration – Detail of the area EDAX analysis was performed (PK5)

Additionally, in the case of dolomitic mortars, (Fig. 4.32), the presence of magnesium seems to affect the phenomenon's development (Lubelli et al, 2011). Although the exact mechanism is not known, calcite crystallization could be enhanced due to the presence of magnesium (Loste et al., 2003).

Moreover, the presence of lime lumps could be a favorable condition, as poorly mixed binder hinders the carbonation process. Un-carbonated lime lumps could thus provide secondary healing products in the occurrence of damage fracture.



Figure 4.33 (Right): Overview of a crack (20-30μm width) filled with secondary calcite possibly due to the presence of a lime lump-XE2

Type of aggregates- inclusions

Self-healing phenomena were encountered in mortars with either calcareous and/or siliceous aggregates. However the presence of calcareous aggregates or fossils may provide nucleating points for calcite precipitation (Figure 4.34 - 4.37). The exact mechanism is not clear, but the compatibility of the substrate is known to enhance crystallization (Lanas et al., 2004). Additionally, the crystals' formation similarity between the calcitic grains and the secondary calcite inside the cracks points to this direction.

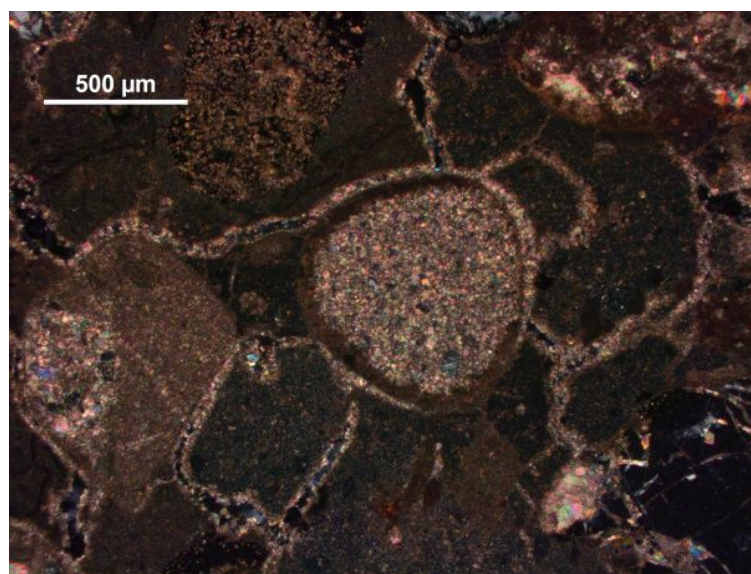


Figure 4.34: Network of cracks completely or partially filled with secondary calcite around a calcitic grain



Figure 4.35: Secondary calcite formed around a fossil, possibly providing (supplying) the neighboring cracks with Ca^{2+} ions.

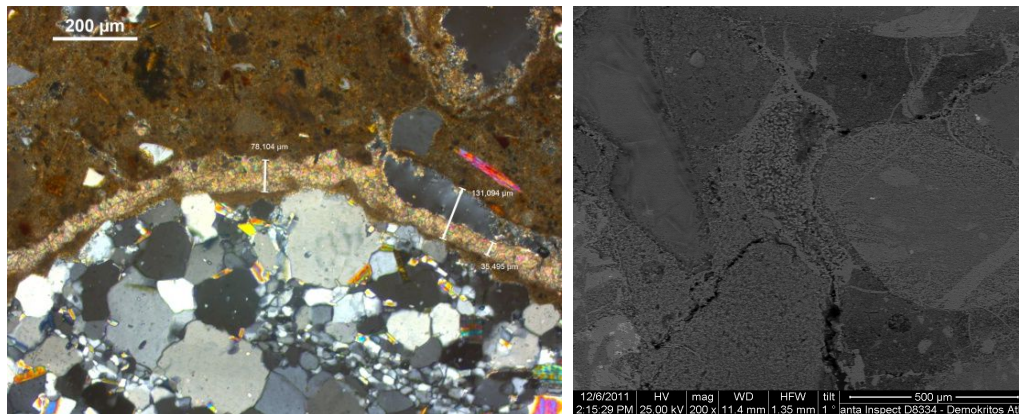


Figure 4.36: Secondary calcite crystallized in the interface between binder and siliceous aggregates Ag20-(Left), PK5-(Right).



Figure 4.37: Secondary sparitic calcite precipitated around a microfossil filling a void of maximum width $150 \mu\text{m}$ - Ag20

4.5 Conclusions

It is noteworthy that archaeological mortars exhibit remarkable consistency and durability, in contrast to modern compatible compositions tested in laboratory.

The study of deterioration and self-healing mechanisms in historic mortars are essential for understanding the evolution process and the parameters that affect self-healing.

The autogenic self-healing phenomenon has been observed in abundance in historic structures and can be correlated, not only to the structural integrity of the latter but also, to the raw materials originally used as well as the structures' micro climatic conditions.

At the same time, the autogenic self-healing mechanism is intrinsic or spontaneous; is activated after wear or damage while a variation in microclimatic conditions (e.g. rain or wet-dry cycles) can be the starting point of the mechanism.

Based on the mortars studied, the following conclusions are drawn:

- The phenomenon of autogenous self-healing was observed in both hydraulic and air-hardening mortars.
- Calcareous aggregates and fossils appeared to be a favorable substrate for the re-crystallization of calcite (chemical and mineralogical compatibility).
- The size of the cracks greatly affected the development of the phenomenon, determining both the movement of the pore solution as well as the crystalline deposits' growth
- The presence of lime lumps may provide pore solution with additional Ca^{2+} ions, greatly enhancing the re-crystallization of calcite.

The results obtained indicate that some recurrent patterns exist and the crystal habits of the re-precipitated products depend, among other factors, on the moisture content and on the degree of carbonation of the mortar.

References

- Ahn, T.-H.(2016). Ceramic Processing Research Investigation of natural crack healing phenomena on historical masonry mortars. *Journal of Ceramic Processing Research*, 17(1), 59–66.
- Anderegg, F. O. Autogenous healing in mortars containing lime. ASTM bulletin , 116 (1942) p.22 as cited in Lubeli et al (2011)
- Callebaut et al. (1999) Petrographical, mineralogical and chemical investigation of 17th and 19th century lime mortars in the St. Michael's church (Leuven, Belgium) in Peter Bartos, Caspar Groot, John J. Hughes PRO 12: International RILEM Workshop on Historic Mortars: Characteristics and Tests, RILEM Publications, 2000
- Commons.wikimedia.org. (2011). *File:External wall Dafni.jpg - Wikimedia Commons*. [online] Available at:

https://commons.wikimedia.org/wiki/File:External_wall_Dafni.jpg?uselang=el
[Accessed 4 Aug. 2016].
- Elsen, J. (2006). Microscopy of historic mortars—a review. *Cement and Concrete Research*, 36(8), 1416–1424. <http://doi.org/10.1016/j.cemconres.2005.12.006>
- Lanas, J., Pérez Bernal, J. L., Bello, M. A., & Alvarez Galindo, J. I. (2004). Mechanical properties of natural hydraulic lime-based mortars. *Cement and Concrete Research*, 34(12), 2191–2201. <http://doi.org/10.1016/j.cemconres.2004.02.005>
- Lauer and Slate. “Autogenous Healing of Cement Paste.” *ACI Journal Proceedings* 52, no. 6 (1956)
- Lubelli B. et al “Self-healing of lime based mortars: microscopy observations on case studies” *HERON* 56 (2011),75-92
- Moropoulou, A., Bakolas, A., Bisbikou, K. (2000). Investigation of the technology of historic mortars. *Journal of Cultural Heritage*, 1(1), 45–58. [http://doi.org/10.1016/S1296-2074\(99\)00118-1](http://doi.org/10.1016/S1296-2074(99)00118-1)
- Moropoulou, A., Cakmak, A. S., & Lohvyn, N. (2000). Earthquake resistant construction techniques and materials on Byzantine monuments in Kiev. *Soil Dynamics and Earthquake Engineering*, 19(8), 603–615. [http://doi.org/10.1016/S0267-7261\(00\)00021-X](http://doi.org/10.1016/S0267-7261(00)00021-X)

- Moropoulou, A., Labropoulos, K., Moundoulas, P., Bakolas, A. (2006).the contribution of historic mortars on the earthquake resistance of byzantine monuments.In *Measuring, Monitoring and Modeling Concrete Properties* (pp. 643–652). Dordrecht: Springer Netherlands. http://doi.org/10.1007/978-1-4020-5104-3_78
- Nijland T., Larbi J., van Hees R.P.J., Lubelli B., de Rooij M., Self-healing phenomena in concrete and masonry mortars, *Proceedings of the 1st International Conference on Self Healing Materials*, Noordwijk, The Netherlands, 2007, 18-20 April 2007
- Pavlos Triantafyllidis Archaeological researches on Milesian Agathonisi in the Dodecanese, Greece
- Reinhardt, Hans-Wolf, and Martin Jooss.“Permeability and Self-Healing of Cracked Concrete as a Function of Temperature and Crack Width.” *Cement and Concrete Research* 33, no. 7 (July 2003): 981–85. doi:10.1016/S0008-8846(02)01099-2.
- Singh, M., Vinodh Kumar, S., Waghmare, S. A., &Sabale, P. D. (2016). Aragonite–vaterite–calcite: Polymorphs of CaCO₃ in 7th century CE lime plasters of Alampur group of temples, India. *Construction and Building Materials*, 112, 386–397. <http://doi.org/10.1016/j.conbuildmat.2016.02.191>
- Stefanidou, M., Papayianni, I., &Pachta, V. (2012). Evaluation of inclusions in mortars of different historical periods from greek monuments. *Archaeometry*, 54(4), 737–751. <http://doi.org/10.1111/j.1475-4754.2011.00645.x>
- Thirumalini, S., Ravi, R., Sekar, S. K., &Nambirajan, M. (2015). Knowing from the past – Ingredients and technology of ancient mortar used in Vadakumnathan temple, Tirussur, Kerala, India. *Journal of Building Engineering*, 4, 101–112. <http://doi.org/10.1016/j.jobe.2015.09.004>
- YPPO-Greek Ministry of culture (2012). *2000 - 2010 Excavations of the Ephorates of Antiquity*. [online] (in greek) Available at: http://www.yppo.gr/0/anaskafes/pdfs/LE_EPKA.pdf [Accessed 20 Feb. 2017].

Chapter 5: Electrochemically accelerated leaching of lime-pozzolan and NHL mortars

5.1 Introduction

In this chapter, the first step of the autogenous self-healing phenomenon is discussed. Namely the dissolution of Ca-ions in the binder matrix, that is essential for the formation of secondary healing phases inside microstructural defects of the binder matrix. For this purpose, an electrochemically accelerated leaching procedure was used to examine the influence of mineralogy and curing time on the dissolution of Ca-bearing phases of lime-pozzolan and NHL mortars.

Self-healing is a multi-step mechanism which involves the dissolution of and re-precipitation of minerals in cracks and voids present in the cement matrix, thus contributing to the enhancement of durability and long-term performance of the material (Hearn 1998). More specifically autogenic self-healing which occurs spontaneously in cement based mortars, is the result of the dissolution of unreacted portlandite (Ca(OH)_2) and the movement of calcium ions through the pore solution - which under favorable conditions - reacts producing secondary phases in cracks and voids, improving the cohesion of the material (Nijland, 2007).

In order to earn a better understanding of the autogenous mechanism the study of the first step, namely the dissolution of Ca-bearing phases, is essential. The first step in the study of self-healing the mechanism is the identification of available ingredients of mortars and the study of their solubility, as it is determined both by the composition of mortars and their curing period.

Binder leaching is a phenomenon frequently observed in cement-based materials and can be summarized as a mass transfer of cement components outside the cement matrix due to contact with water or aggressive solutions. More specifically, it is observed in external masonry, bridges and other structures that have direct contact with water and is encountered more often in young masonry in the first few months after the mortar application (Banfill et al., 2016). The dissolution of soluble phases of the binder after contact with water can lead to an increase in total porosity and

consequently in higher water absorption and decrease of mechanical strength (Forster et al., 2014).

Leaching of cementitious materials is broadly studied as part of their degradation mechanisms and relevant studies focus mainly on their durability aspects. Nevertheless, it can also be identified as the first step of the self-healing mechanism which takes place in cement and concrete (Nijland, 2007; Reinhardt and Jooss, 2003). Traditional mortars, are characterized by high concentration of portlandite ($\text{Ca}(\text{OH})_2$) (Cazzala et al., 2000). The main reactions that take place during mortar hardening are carbonation of portlandite by the atmospheric CO_2 and the hydraulic reaction between portlandite and the silicon and aluminum phases which are either present in the hydraulic lime or in a pozzolanic material. These reactions are controlled by the humidity conditions (Karatasios et al., 2010) and are relatively slow compared to those taking place in Portland cement. This often leads to the observation of reactive portlandite present in the binder matrix long after its application, which is susceptible to leaching due to its higher solubility.

Leaching or decalcification naturally occurs after the exposure of cementitious materials to water (e.g. rain, humidity condensation). Since it is a relatively slow process, it is often simulated under accelerated conditions in the lab (Glasser et al., 2008). There are various leaching techniques commonly used to test the durability of a cement mortar during the leaching process. A method most commonly used (Carde et al., 1996), involves the exposure of specimens to ammonium nitrate (NH_4NO_3), a strong acidic solution which increases the solubility of the cement matrix by the formation of the highly soluble $\text{Ca}(\text{NO}_3)_2$.

For the purposes of this study an electrochemically accelerated method was used which consists of the application of voltage across the mortar specimens. This method was first developed by Saito et al. (1992) in order to assess long term integrity of concrete structures and in order to create long term durability projection for underwater repositories. In his study it was found that leaching was accelerated by a factor of 60 times higher than that of a system without potential gradient (Saito et al., 1992).

The principle of this method, also known as “leaching induced by forced transport” (LIFT) is the accelerated dissolution of binder phases by electrophoresis. Due to the potential gradient, cations and anions are forced towards the cathode and anode respectively. This creates a chemical instability in the pore solution of the cement

mortar, thus forcing towards a further dissolution of binder phases. Although under natural conditions both cations and anions are moved towards the same directions this does not cause any recorded alteration on the degradation mechanism. This method is used in various studies (Castellote et al., 2003; Faucon et al., 1998; Saito et al., 1998; Saito and Deguchi, 2000) and it was found to be reliable and efficient regarding both the chemical and the mechanical alterations related to decalcification.

The aim of this chapter is to provide an insight on the decalcification process which occurs during leaching of lime-pozzolan and natural hydraulic lime mortars, simulating the first step of the autogenic mechanism observed in historic mortars.

More specifically, in order to understand the first step of the autogenous self-healing mechanism, specific parameters are examined:

- The evolution of the setting phases mineralogy in LP and NHL mortars and its correlation to the solubility of Ca-bearing components
- The effect of the dissolution of Ca-bearing components on the microstructural characteristics of LP and NHL mortars and
- How the latter is influenced by the curing period of the materials.

5.2 Experimental Setup

5.2.1 Materials

Two groups of mortar mixtures were prepared, one with a natural hydraulic lime (St. Astier NHL5) and one with a commercially available lime powder (KRINOS SA) and a natural pozzolan of volcanic origin (Dalkafoukis) in 1:1 ratio, as described in Appendix A. In both mixtures standard sand [CEN 196-1] was added as aggregate in a cement/aggregate ratio 1:3 (w/w).

LP and NHL mortar mixtures were subsequently cast in cylindrical moulds (2.8 cm in diameter and 3 cm in height). The mixtures were stored in a temperature and humidity control maturation chamber at 20 ± 1 °C and $90 \pm 1\%$ RH. In order to study the effect of the curing period on the decalcification process, specimens were cured for different periods varying from 24 hours to one year.

Moreover, Merck $\text{Ca}(\text{OH})_2$ powder (96%) was used for reference experiments and methodology optimization and calibration.

5.2.2 Experimental procedure and test setup

The “leaching induced by forced transport” (LIFT) electrochemical acceleration method was used for studying the leaching process of NHL and LP mortars. In the setup used for this method the mortar specimen is placed between Plexiglas (PMMA) containers of 2 liters capacity each. In each container an electrode is placed- a Fe electrode (cathode) and a Pt electrode (anode) (fig.5.1). The two electrodes are connected to a DC power source and a potential difference (an electric field) is applied. According to primary experimental trial voltage was set at 30V.

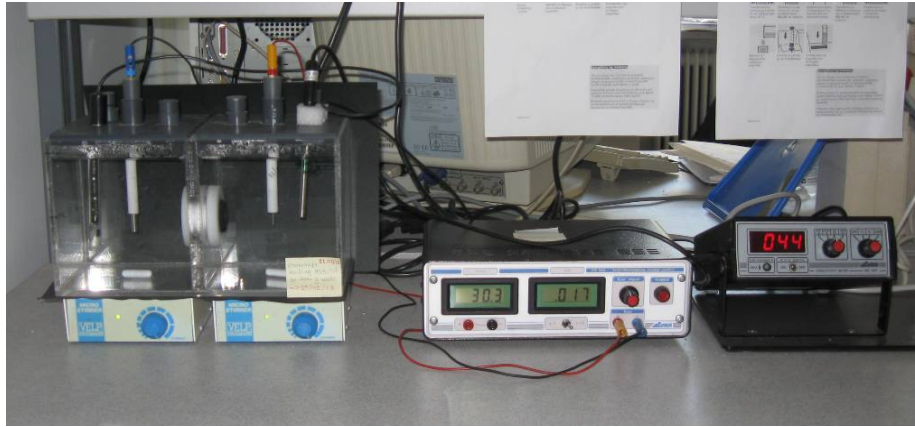


Figure 5.1: Electrochemical accelerated leaching setup. (LIFT)

Additionally, a second series of tests was performed, where powdered samples of mortars were tested in the same setup. Powdered samples due to their higher specific surface allowed the study of mineralogical /chemical alterations that take place during the leaching process, eliminating microstructural factors that affect the dissolution. The powder suspension was added in the container where the anode electrode is placed. To avoid powder transfer in the cathode tank, a filter disk (DURAN[®], D=30mm, por 4) was placed between the two containers its pore size (max. pore size 10 - 16 μm) allows ions to pass through while blocking any powder particles. Powder samples were produced by crashing and grounding mortar specimens in an agate mortar. Subsequently aggregates were separated by sieving to obtain the fraction <63 μm which corresponds to the binder fraction.

All tests performed in cylindrical and powder specimens are summarized in Table 5.1. Cylindrical specimens were tested after three time intervals. For NHL mixture, cylindrical specimens were tested after 15, 60 and 120 days, whereas for LP mixture, after 30, 60 and 120 days. LP specimens did not display the appropriate consistency at 15 days of curing, so specimens cured for 30 days before they were firstly tested.

Table 5.1: Curing periods of tested specimens

Mixture	Curing period	Cylinder Leaching	Powder Leaching
LP	7		+
	14		+
	30	+	+
	60	+	+
	90		+
	120	+	+
	200		+
	360		+
NHL	7		+
	14	+	+
	30		+
	60	+	
	90		+
	120	+	+
	180		+

5.2.3 The LIFT method

Due to the potential difference applied across the specimen, cations move towards the cathode (Fe) (Fig 5.2). This causes the chemical equilibrium to shift in the pore water towards the dissolution of more cations. The movement of ions is recorded as electrochemical current between the two electrodes. Similarly the increase of ions in the cathode tank due to leaching was recorded conductometrically using a

conductivity electrode that was placed inside the cathode tank. During tests, current and conductivity were monitored continuously (every 120 seconds). Provided that it is a “closed” test, were no external interaction or invasive measurement is performed during the test period, the monitoring of current and conductivity provides the possibility to observe the evolution of the phenomenon in real-time.

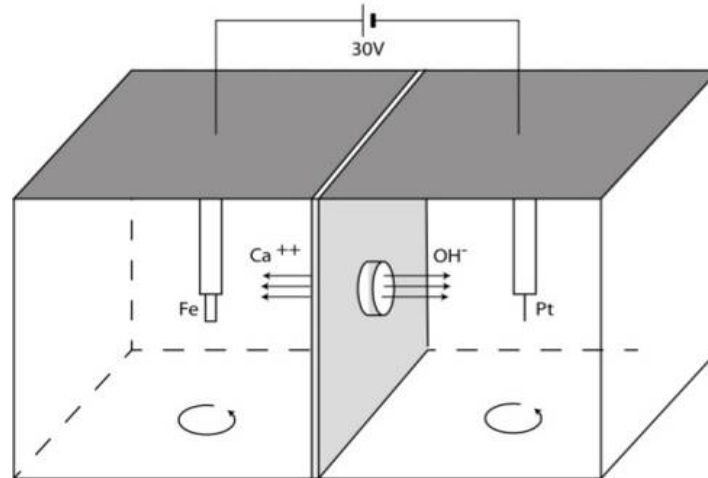


Figure 5.2: Design of the electrochemical accelerated leaching setup. (LIFT)

During the electrochemically accelerated leaching procedure under constant voltage of 30V, the movement of the leached ions is expressed as current. When expressed as a function of leaching time, its value starts from near zero miliampere (mA) and follows an increasing trend until a maximum value after which, declines (fig. 5.3a). The distinctive peak formed is considered characteristic of the dissolution rate of each specimen. Similarly conductivity, which is measured in the cathode tank, also starts from near-zero values (microsiemens, $\mu\text{S}/\text{cm}$) and follows a sigmoidal curve where a saturation point is reached at maximum point where it forms a plateau (fig. 5.3b).

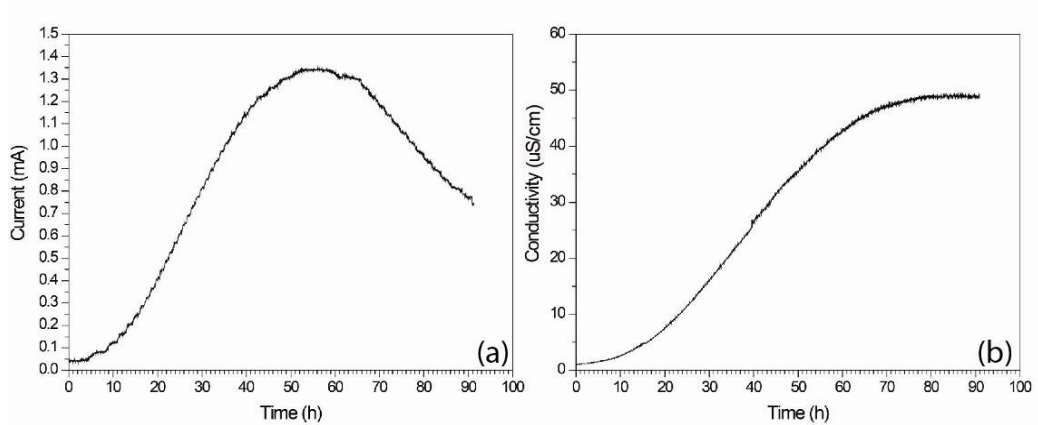


Figure 5.3: A typical example of current (a) and conductivity (b) monitoring as function of leaching period.

Characteristic curves, obtained during current and conductivity monitoring, were used in this experimental setup as a method to determine the end-point of the leaching procedure which was set after conductivity reached the maximum value.

Monitoring of current and conductivity also serves as a semi-quantitative assessment of the effect of the leaching procedure on the specimens tested. More specifically, maximum values of current and conductivity were assessed for each leaching test and were correlated with the curing period of the specimen tested.

5.2.4 Conductimetry

Electrolytic conductivity was monitored throughout the experiment by means of a conductimetry electrode (conductimeter).

The conductance of a material is the ability of a material to conduct electric current and in the case of solutions, conductivity measurements can be linked directly with its ion concentration.

The conductance of an electrolyte solution can be calculated from :

$$G = \kappa * \frac{A}{L}$$

Conductivity (κ) is the conductance of a 1cm^3 cube of the liquid

As the conductivity cell consists of two parallel sheets of platinum, fixed in position by being sealed into the sides of the measuring cell, which determine the edges of the

conductor whereas the surface of each one represents its cross-section. The distance between the two electrodes must be constant during the determination.

L/A is known as cell constant (K_{cell}),

$$K_{\text{cell}} = \frac{L}{A}$$

By measuring the conductance of an electrolyte solution, knowing the cell constant, conductivity is calculated according to the following equation:

$$G = \frac{\kappa}{K_{\text{cell}}}$$

The dimensions of κ is $\text{cm}^{-1}\Omega^{-1}$ or Siemens/cm

In order to correlate conductivity measurements with ion concentration, a set of $\text{Ca}(\text{OH})_2$ solutions was prepared and measured conductometrically. More specifically Calcium hydroxide (96.0% Merck) was used to prepare solutions of ranging from 0 to 500 mg/L $\text{Ca}(\text{OH})_2$.

The correlation was linear in a wide range of concentrations (Fig. 5.4), verifying that conductimetry can be a suitable measurement method for the purposes of this experiment.

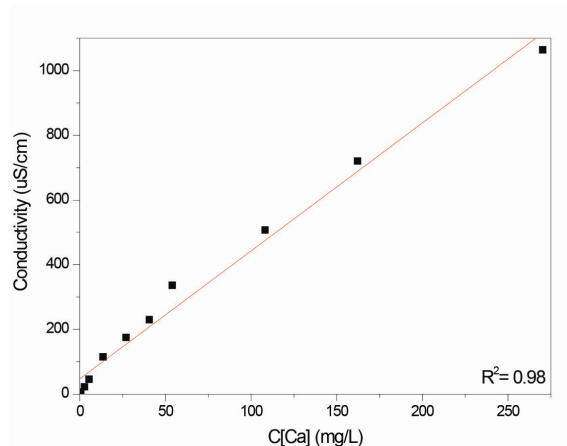


Figure 5.4: Linear correlation of Ca concentration with conductivity values.

5.2.5 Preliminary measurements

A series of leaching tests was performed on calcium hydroxide powder (96.0% Merck) suspensions of 50, 250, 500 and 1000 mg/L. By analyzing these measurements the optimum concentration of the powder suspensions was decided. Larger concentration produced higher noise to the conductivity electrode signal (Fig.5.5) and at the same time lower than expected values of conductivity were measured when 1000 mg/L was tested (Fig.5.6). A suspension concentration of 500 mg/L was considered optimal.

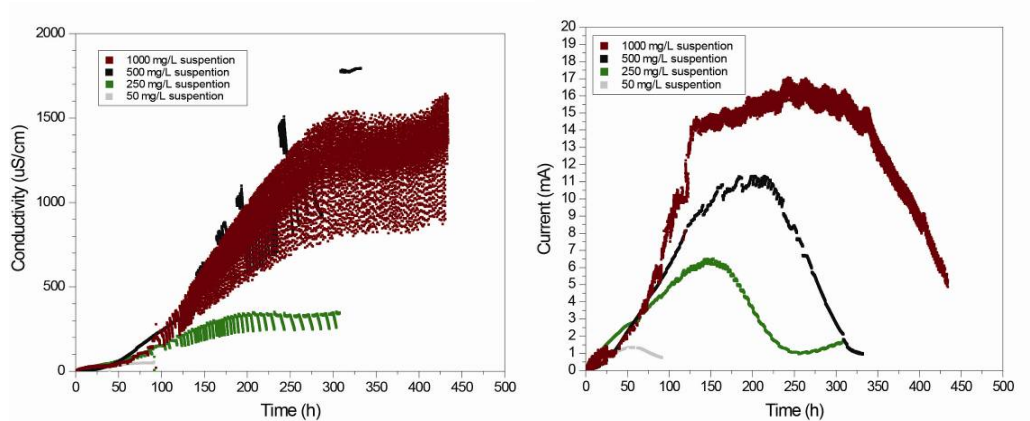


Figure 5.5: Current and conductivity values measured during the leaching tests of calcium hydroxide suspensions.

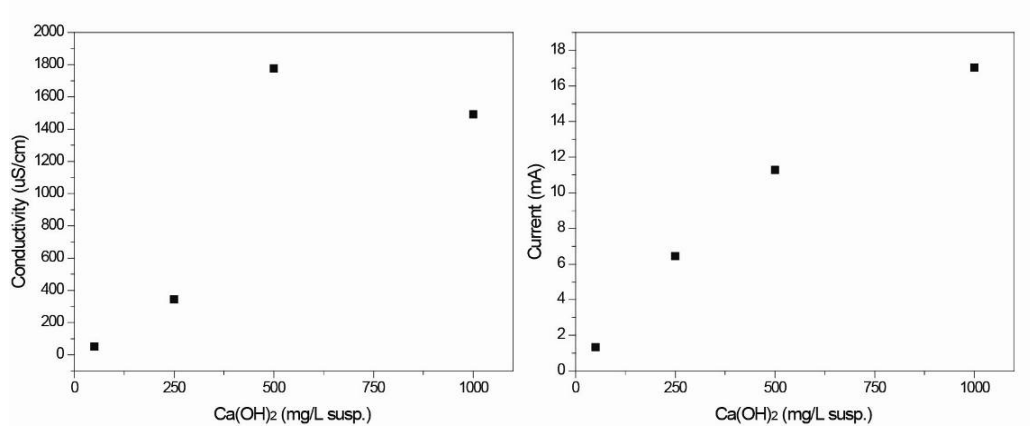


Figure 5.6: Maximum values of current and conductivity measured during leaching of calcium hydroxide suspensions.

5.2.6 Leachate solution analysis by AAS

After the end of the leaching experiment the leachate solution was collected and analyzed by means of atomic absorption spectroscopy (AAS) with air–acetylene flame technique in a Varian AA 240FS flame atomic spectroscopy system. Calcium concentration was determined which can provide information regarding the amount of Ca-bearing phases dissolved and at the same time correlate it AAS findings with conductivity measurements.

5.2.7 Characterization of mineralogical alterations

After the end of each leaching experiment both cylindrical and powdered leached specimens were analyzed by x-ray diffraction (XRD) and thermogravimetric analysis (DTA/TG) to assess any mineralogical alterations as well as the evolution of carbonation and hydration through time and identify and quantify the setting products. XRD analysis is used for the qualitative characterization of mineral phases in cementitious materials, whereas thermogravimetric analysis is used to quantify the main cement components, namely calcite and portlandite calcium silicate hydrates. FTIR measurements were performed in leached powdered samples as well as reference samples after consecutive curing periods using a Bruker Alpha FTIR spectrometer in ATR mode.

5.2.8 Characterization of microstructural alterations

Scanning electron microscopy (SEM) combined with energy dispersive X-ray analysis (EDX) was performed using a FEI Quanta Inspect scanning electron microscope. Polished sections and powder samples were examined to identify changes in microstructure as well as in Ca/Si ratio due to leaching.

Moreover, micro structural analysis was performed on leached cylindrical specimens and alterations in total pore volume and pore size distribution were assessed by mercury intrusion porosimetry (MIP) by a Quantachrome Poremaster- Automatic Pore Size Analyzer.

5.2.9 Sample preparation

More specifically, in order to characterize potential microstructural or mineralogical differences lengthwise along the axis of the cylindrical specimens, during leaching, samples were obtained from both ends of the specimens. In order to assure consistency, samples for all of the above analysis techniques were collected from the specimens by dividing each in eight equal parts (fig. 5.7). Samples obtained from the part in contact with the cathode tank are denoted with (P) whereas the ones obtained from the part in contact with the anode tank are denoted with (L).

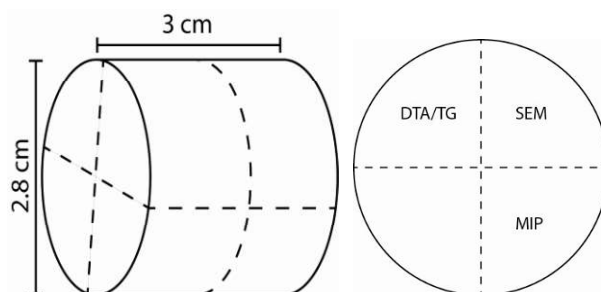


Figure 5.7: Sample preparation

Regarding the leaching tests applied to powdered specimens, a different procedure was applied. After the completion of the leaching period, the leached powder suspension was filtered under vacuum using a Buchner funnel and the collected powder (L) was dried under vacuum.

In both experimental series, reference samples (R) were analyzed which corresponds to the state of the leached specimen before the leaching treatment.

5.3 Results and Discussion

5.3.1 Current and conductivity monitoring

The results obtained by monitoring the current and the conductivity during leaching, show the correlation between the curing time of the specimens -which corresponds to different stages of the evolution of the reactions that take place during hardening- with their response to accelerated leaching, i.e. their dissolution rate. Maximum conductivity and current values recorded during the experiments performed both on cylindrical and powder specimens are plotted, in order to compare (understand) the effect of pore structure and specific surface area on the leaching process.

Regarding the cylindrical specimens (Fig. 5.8) current and conductivity values show a clear decline with the curing time of the specimens tested for LP and NHL specimens. This is in line with related research studies focusing on binder leaching that demonstrate that the evolution of the hardening reactions during curing, results in less soluble products, thus specimens cured for longer period of time are less susceptible to leaching (Banfill et al 2016).

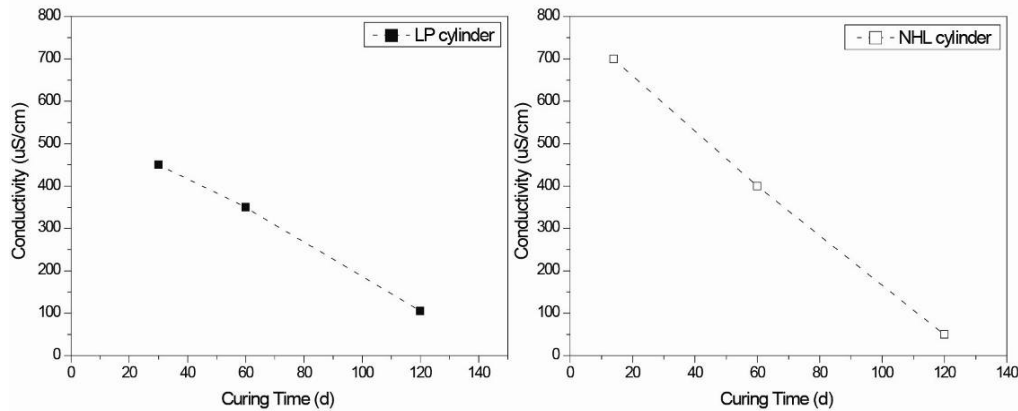


Figure 5.8: Maximum values of conductivity measured as function of curing period of the cylindrical specimens

Similarly, maximum conductivity values obtained by leaching of powdered samples present a similar trend (Fig. 5.9). Nevertheless, conductivity values obtained during leaching of NHL powdered samples that were cured for more than three months (90 days), show an increase and attain values almost equal to conductivity values measured in early-age specimens (7 days).

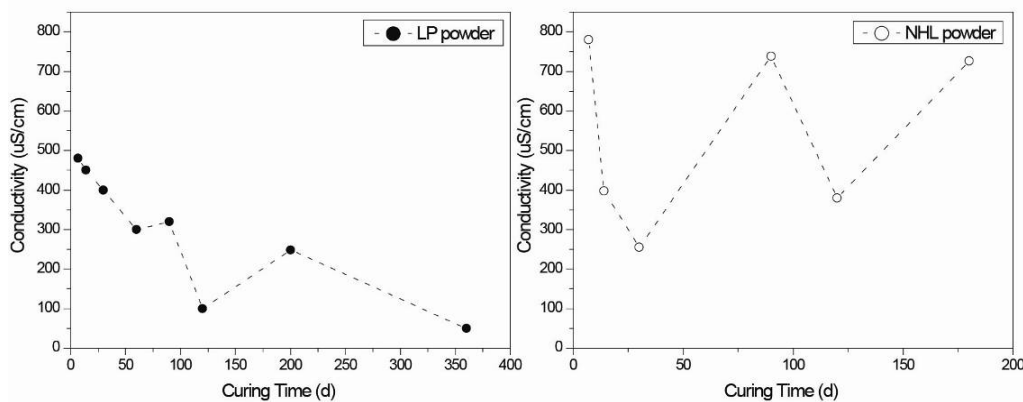


Figure 5.9: Maximum values of conductivity measured as function of curing period of the powdered specimens

This was further investigated by thermogravimetric (DTA/TG) analysis (fig. 5.10) of reference NHL and LP samples. It is evident that during NHL hydration, portlandite is produced. Henceforth, the increase in conductivity reported above (fig. 5.9) could be attributed to the production of portlandite which is added to the soluble phases of the binder matrix.

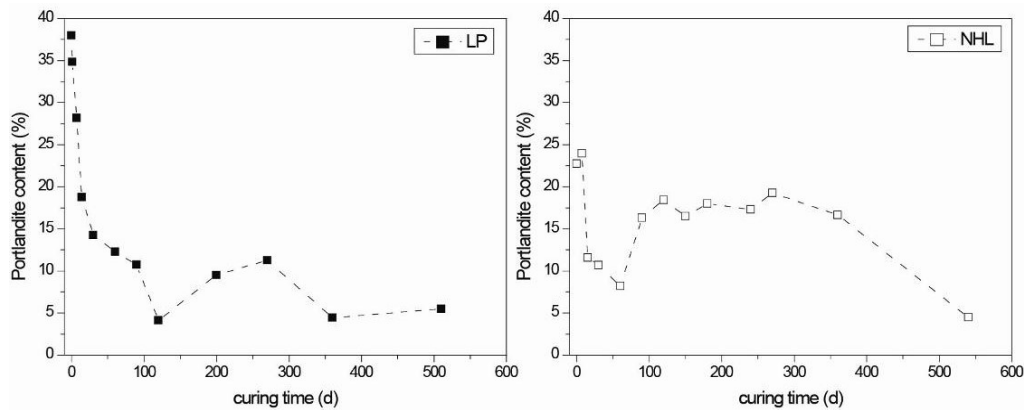


Figure 5.10: The evolution of the content (%) of portlandite as was calculated by thermogravimetric analysis of LP and NHL reference mortars during the first 18 months (540 d) of curing.

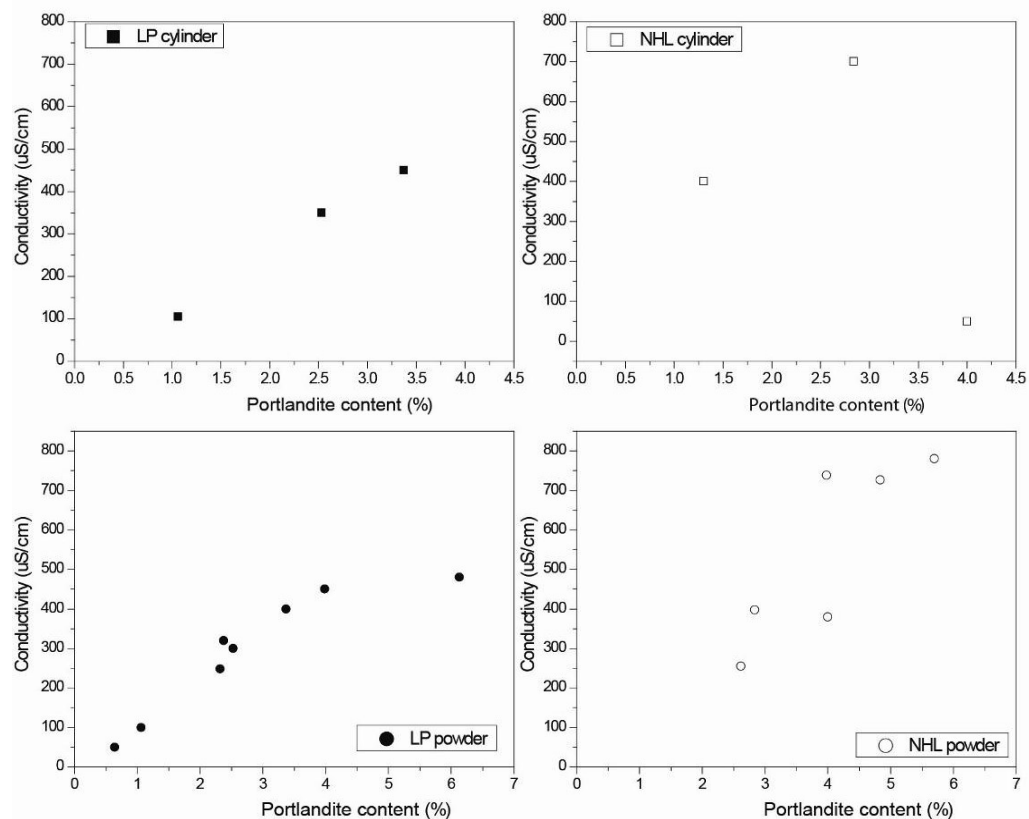


Figure 5.11: Correlation of the available portlandite as measured by DTA/TG in reference specimens with the maximum conductivity values measured during leaching.

By correlating measured conductivity values and portlandite concentration of reference samples measured by DTA/TG (Fig 5.10) some further observations were made (Fig 5.11). The concentration of leached cations (expressed as conductivity) in LP cylindrical and powdered specimens is correlated to the portlandite content measured by DTA/TG. This suggests that regarding LP specimens, portlandite is the main phase dissolved, during the leaching test.

Regarding the NHL specimens, the results obtained do not suggest a straight correlation between the concentration of leached ions and the available portlandite. This indicates that other soluble phases besides portlandite, such as C-S-H could add to the total conductivity measured during leaching.

5.3.2 Leachate solution analysis by AAS

Calcium concentration of the leachate solution (cathode solution) derived from both cylindrical and powdered specimens, was measured by means of atomic absorption spectroscopy (AAS) after the end of each test. Cathode solutions sampled after leaching test of NHL and LP cylindrical specimens exhibited a similar trend. Specimens cured for longer period are less susceptible to calcium leaching indicating the formation of more thermodynamically stable products.

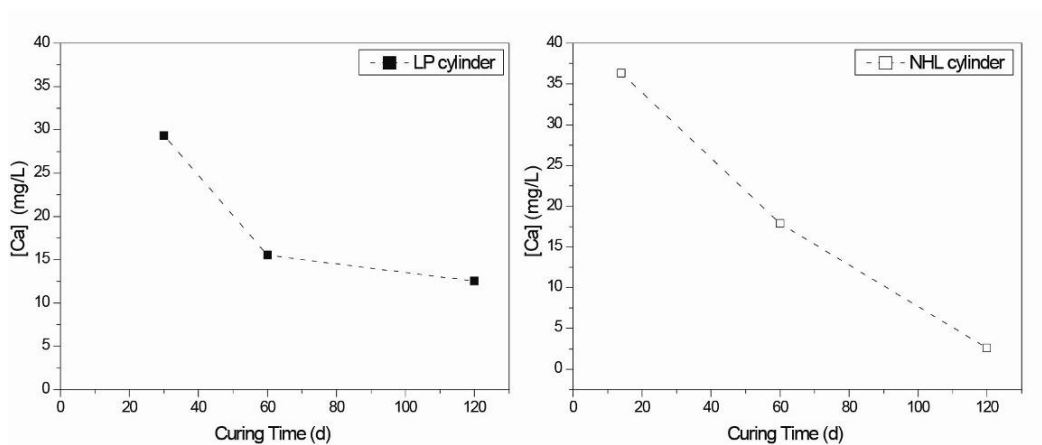


Figure 5.12: Calcium concentration in the leachate solution measured by AAS, as a function of curing period of the cylindrical specimens tested

Similarly, calcium concentration measured in LP powder leachate solutions presents a slight increase in specimens cured for 200 days. This could also be attributed to secondary portlandite produced during hydration reaction.

Accordingly, in NHL powdered samples leachate solutions this increase is much more profound and is observed at 90 days cured samples probably due to the higher surface area of the powdered samples.

By comparing the Ca^{2+} values in powder and cylindrical specimens, it seems that the later provide only an indication of the potential amount of cations that could be leached.

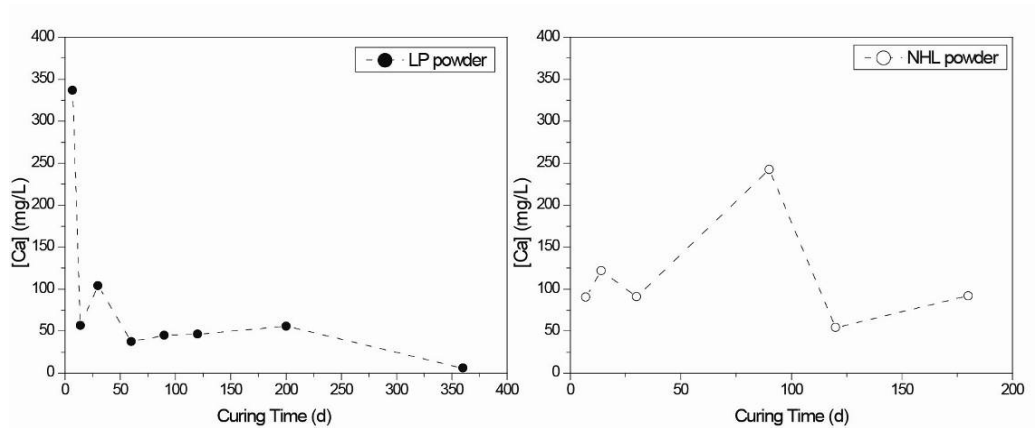


Figure 5.13: Calcium concentration in the leachate solution measured by AAS, as a function of curing period of the powdered specimens tested

5.3.3 Mineralogical examination (X-ray Diffraction, Thermogravimetric analysis, FTIR)

5.3.3.1 Mineralogical analysis -XRD

After each leaching experiment, mineralogical analysis was performed on the leached powder samples and its composition was contrasted with that of the reference sample. The comparison of diffractograms from reference and leached material (Fig. 5.14) reveal the alterations of mineralogical phases.

In reference specimens portlandite (P), calcite (C), dicalcium silicate (C_2S) and calcium silicate hydrates (CSH) were identified. More precisely, in NHL reference samples the presence of portlandite is evident even in samples cured up to 180 days before leaching, whereas in LP specimens, portlandite is not observed after 90 days. In all cases, portlandite is not observed in any of the diffractograms of the leached specimens. In NHL mortars dicalcium silicate (C_2S) is also identified in reference samples, while it is not present after leaching. In LP mortars C_2S is not expected to be part of its composition, as the hydraulic phases are produced by the hydraulic reaction between silicon and aluminum oxides (present in the pozzolanic material) and lime (portlandite). Pozzolanic compounds are viewed in LP diffractograms ca. 27-28 °2 θ (degrees) and seem to be resistant to leaching.

Besides calcite, hydraulic products are also present in leached specimens' diffractograms in NHL and LP specimens alike suggesting a higher resistance to leaching.

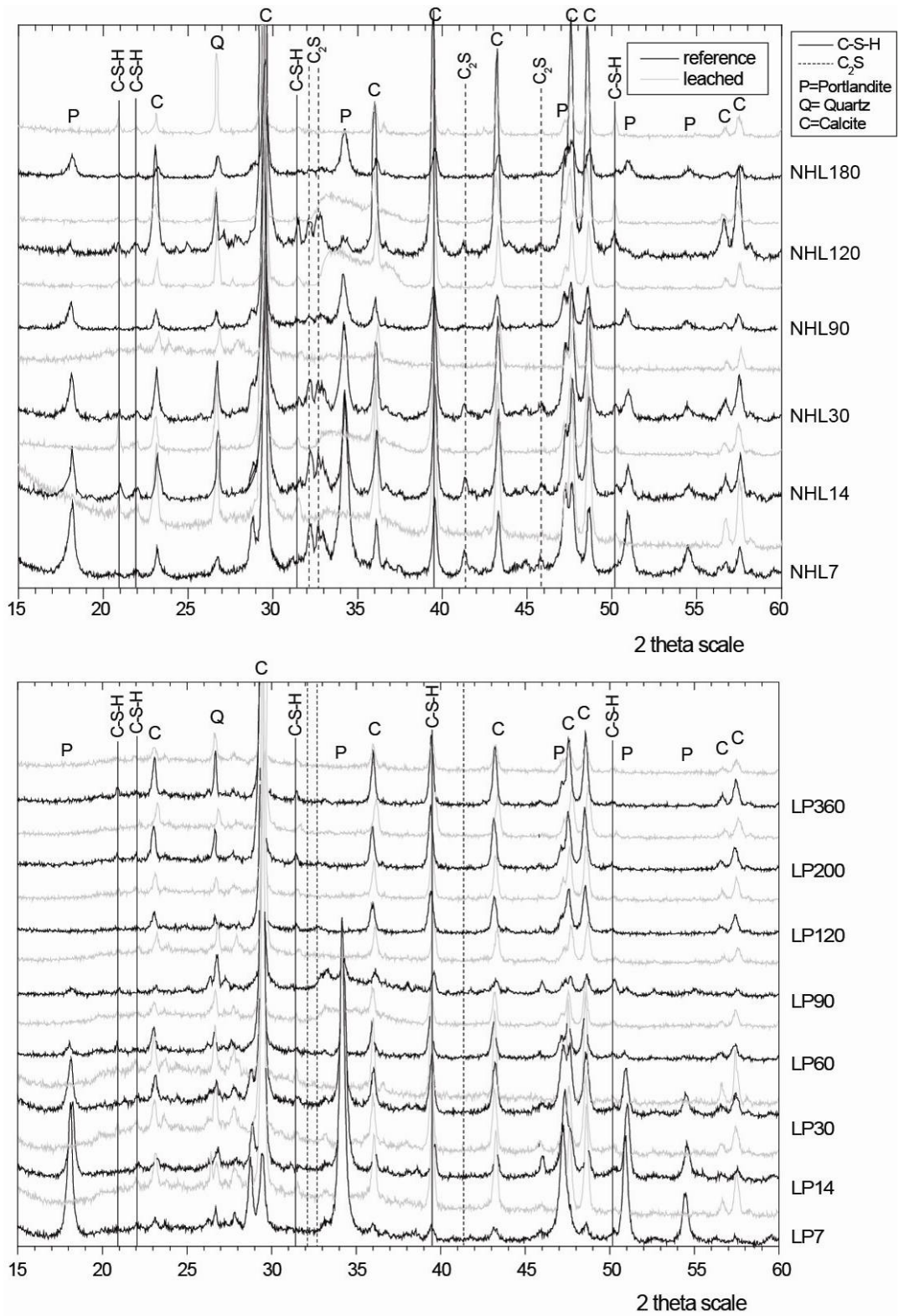


Figure 5.14: Diffractograms of reference (black line) and leached (gray line) powder NHL and LP specimens

5.3.3.2 Thermogravimetric analysis- DTA/TG

Similar to XRD analysis, thermogravimetric analysis was performed on leached samples and was contrasted with the measurements of the reference samples. Thermogravimetric analysis was selected as a method to quantify the main phases present in the binder, namely calcite, portlandite and C-S-H (Fig. 5.15). The quantification method relies on the fact that certain compounds undergo an alteration due to temperature gradient and this is expressed as mass loss. More specifically, on the temperature range 150-350 dehydration of hydraulic phases is reported, on the temperature range 350-450 dehydration of portlandite and on the temperature range 450-800 decarboxylation of CaCO_3 takes place (Giergiczny, 2006; Bakolas et al., 2006; Bruno et al., 2004). Therefore, mass loss % that corresponds to each temperature range can be correlated with the concentration of each compound in the sample.

DTG curves represent the first derivative of TG, and can serve as a reliable method to pinpoint exactly at what temperature range different thermal phenomena take place.

By thermogravimetric analysis both cylindrical (Fig. 5.16) and powder samples (Fig. 5.17-5.18) were analyzed, while quantified results are shown on Table 5.2 respectively.

By examining the DTG curves of LP and NHL cylindrical specimens, (Figure 5.16) the decrease or depletion of portlandite is verified in both sides of the specimens (L and P) whereas calcite and C-S-H phases do not present significant alterations after leaching (Table 5.2).

Similarly, DTG curves of LP powder leached specimens corroborate the depletion of portlandite. However, DTG curves of NHL and LP leached powdered specimens present a mass loss at the temperature range 150-400. This mass loss is attributed to the loss of bound water to amorphous silica (Kappert et al., 2014). Amorphous silica is the end product of CSH decalcification which takes place during leaching after the depletion of portlandite (Adenot and Buil, 1992; Glasser et al., 2008; Faucon et al., 2007). More precisely, Saito et al. reported the complete dissolution of CSH phases, identifying only SiO_2 as an ingredient; whereas other studies (Faucon et al., 1998; Phung et al., 2016) describe decalcification of CSH phases as a higher silicate polymerization.

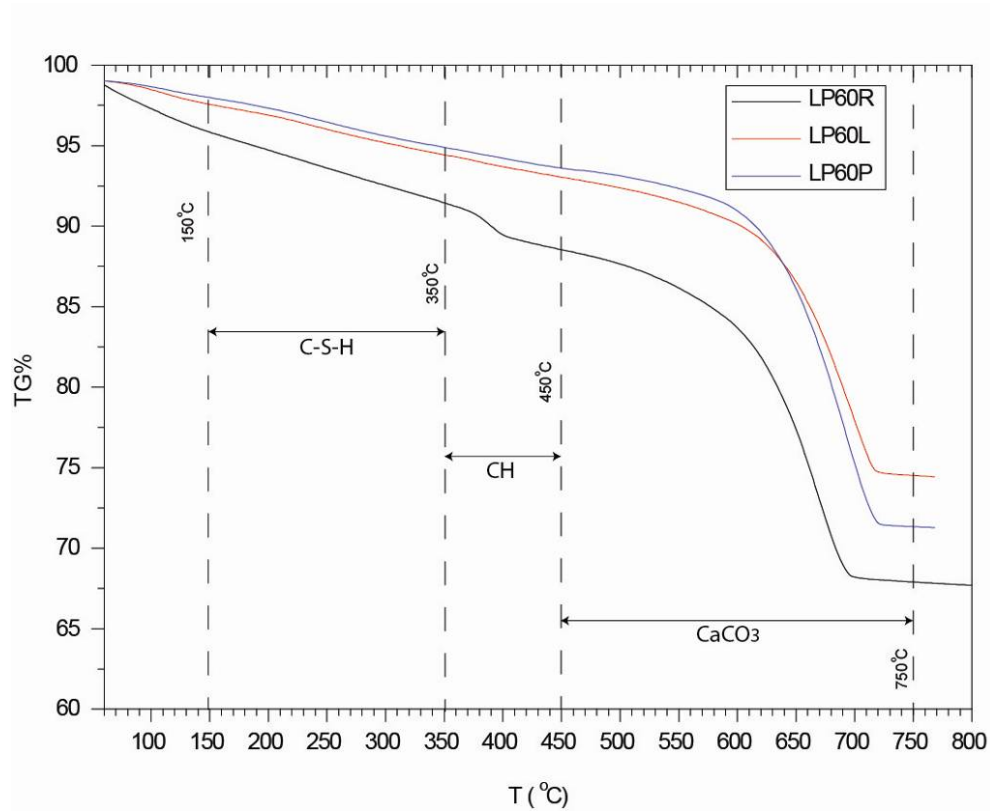


Figure 5.15: Temperature ranges used for the quantification of binder components on leached and reference cylindrical specimens.

Table 5.2: Mass loss calculated by TG% curves during specific temperature ranges for LP and NHL cylindrical specimens

	(°C)	LP30			LP60			LP120		
		R	L	P	R	L	P	R	L	P
C-S-H	<350	3.9	7.3	7.9	3.5	4.2	4.2	3.7	5.3	4.1
Ca(OH) ₂	350→450	3.5	0.7	2.3	2.9	1.0	1.3	1.1	0.8	0.6
CaCO ₃	450→800	13.7	13.8	12.3	20.4	18.7	22.0	23.0	19.2	19.6

	(°C)	NHL15			NHL60			NHL120		
		R	L	P	R	L	P	R	L	P
C-S-H	<350	4.2	7.4	7.8	6.50	6.2	3.6	6.5	5.3	4.8
Ca(OH) ₂	350→450	2.9	2.4	1.7	1.4	0.8	0.8	1.6	1.5	1.4
CaCO ₃	450→800	20.2	20.4	24.8	26.1	26.8	30.1	27.9	24.7	31.6

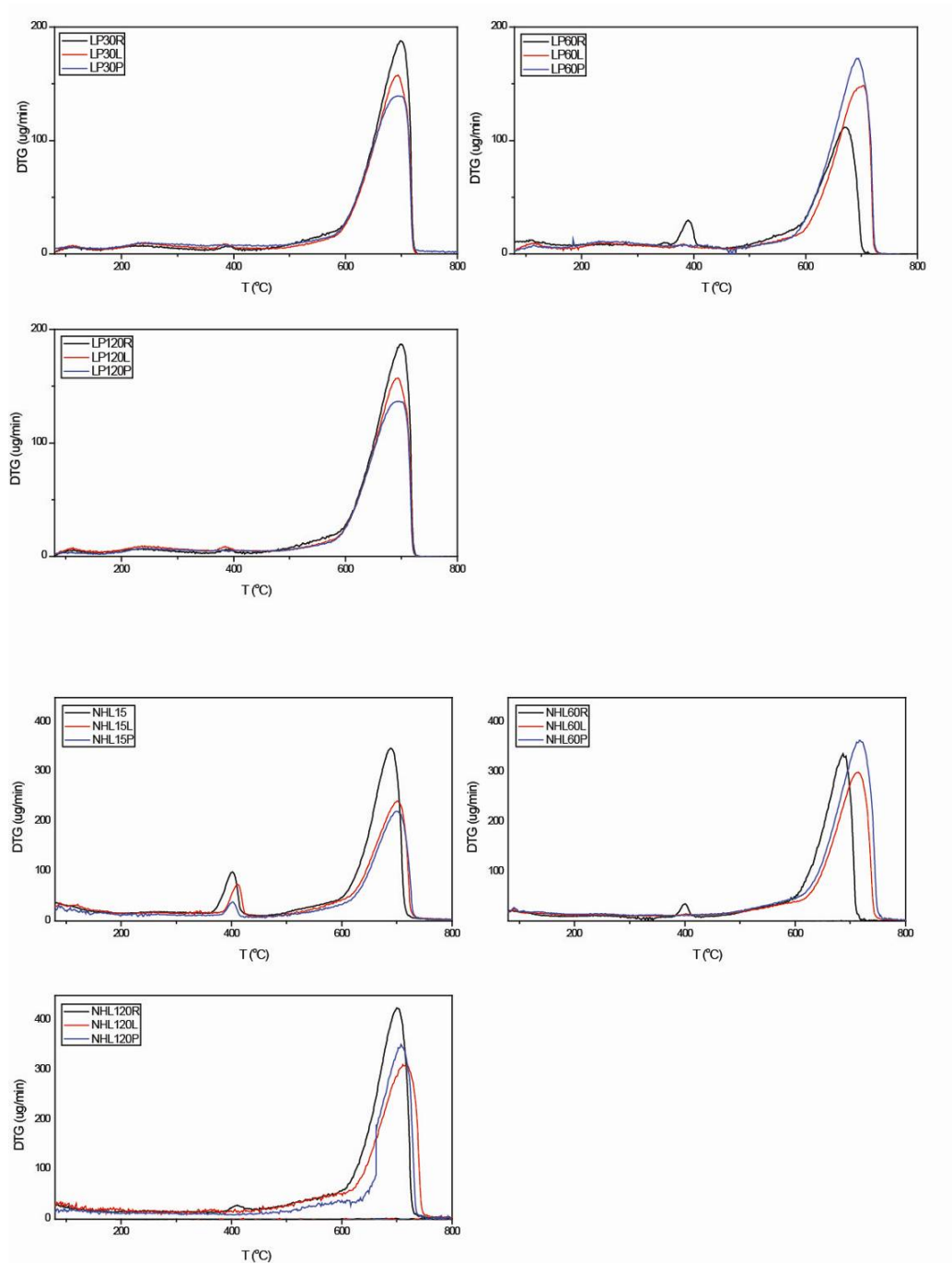


Figure 5.16: DTG of LP and NHL cylindrical specimens before (black line) and after leaching from both sides of the specimen. (L-red line and P-blue line)

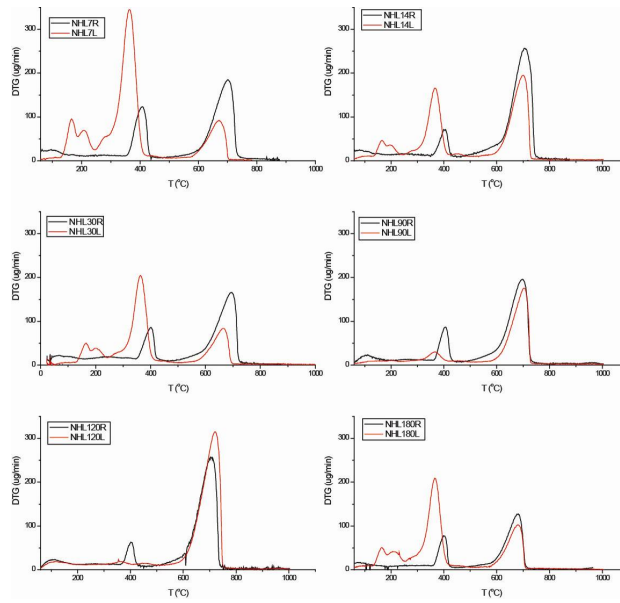


Figure 5.17: DTG of NHL powder specimens before (black line) and after (red line) leaching.

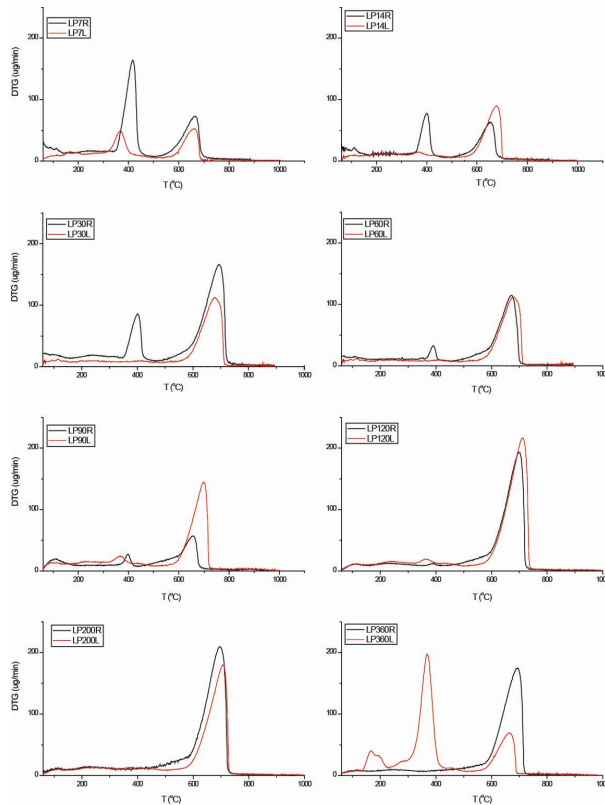


Figure 5.18: DTG of LP powder specimens before (black line) and after (red line) leaching.

5.3.3.3 FTIR spectroscopy

Leached powder samples were analyzed by means of FTIR in order to assess possible alterations in the binder phases. FTIR spectra of both NHL and LP specimens exhibited bands associated with carbonates, calcium hydroxide and CSH (Fig 5.19). More specifically, symmetric and asymmetric stretch of CO_3 deformation are observed at 712 and 874 cm^{-1} respectively while a third band at 1407 cm^{-1} is also attributed to asymmetric stretch of CO_3 . Moreover, Si–O stretching bands at 1010 cm^{-1} are attributed to calcium silicate hydrates (CSH) and at 3645 cm^{-1} a typical OH-stretching, sharp peak is also observed corresponding to Ca-OH in portlandite.

In FTIR spectra of the leached samples, the Si–O stretching band observed at 1010 cm^{-1} is shifted to higher wave numbers and in some samples multiple minima are observed between 1010 and 1300 cm^{-1} . This is attributed to higher polymerization of Si in CSH, due to decalcification of the latter (Kan et al., 2010). This phenomenon, namely the polymerization of C-S-H is recognizable by the broadening of the Si–O stretching band and its shift to higher wave numbers or even the observation of more minima in the same band.

Moreover the alteration of C-S-H phases due to leaching as it is observed in these FTIR spectra can be correlated with the DTA/TG analysis results of the respective specimens, as both analyses results indicate the decalcification of CSH which leads to the formation of amorphous silica.

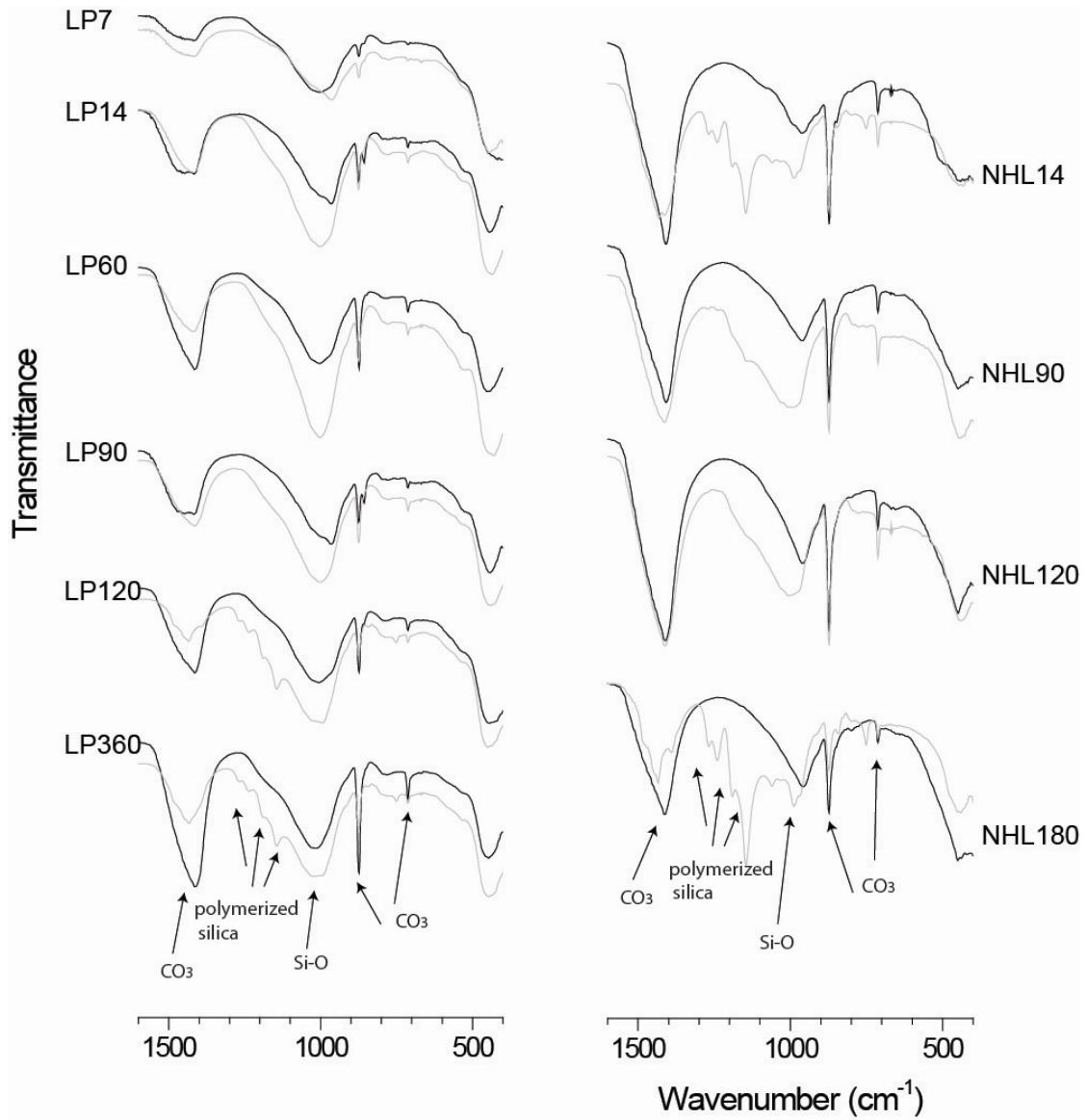


Figure 5.19: FT-IR spectra of ground NHL and LP specimens before (black line) and after (gray line) leaching.

5.3.4 Microscopic examination of leached powdered specimens

Leached powdered specimens were examined at the SEM and were contrasted with not-leached reference samples. The decalcification of both LP and NHL powder specimens was confirmed by Energy dispersive X-ray spectroscopy (EDAX), calculating the Ca/Si ratio.

In both LP and NHL leached samples microphotographs reveal the morphological alterations due to leaching.

After the end of the leaching test, a clear reduction in the particle size of leached powders is observed. Additionally, EDAX spot analysis revealed the decalcification process that has taken place which is expressed by the Ca/Si ratio. Bulk analysis showed that the Ca/Si ratio has dramatically decreased in the samples examined. More specifically, for leached LP and NHL powder specimens this ratio decreases from 2.89 to 0.57 and from 0.98 to 0.29 respectively.

In a more detailed analysis, two main morphological types of particles were observed which could be identified in both NHL and LP powder specimens (Details on Fig 5.20 and 5.21). Spot analysis performed on type A particles confirmed that their morphological characteristics are the result of complete decalcification as the Ca/Si ratio was calculated 0.1 and 0.08 for LP and NHL specimens respectively. Likewise, type B particles also exhibited similar morphological characteristics in LP and NHL specimens and in both cases their diameter varies around 20 μm . Their Ca/Si ratio was calculated at 0.79 and 0.5 for LP and NHL specimens respectively.

The aforementioned observations could be in agreement with the results derived from FTIR and DTA/TG analysis of the respective specimens. The distinctive morphological characteristics of type A particles could be attributed to higher polymerization of Si due to decalcification of C-S-H phases which is also advocated by their low Ca/Si ratio.

Moreover it is noteworthy that even though untreated LP and NHL binders have very distinct chemical and morphological characteristics (Appendix A), accelerated leaching of cured specimens results in very similar characteristics, both morphological and chemical.

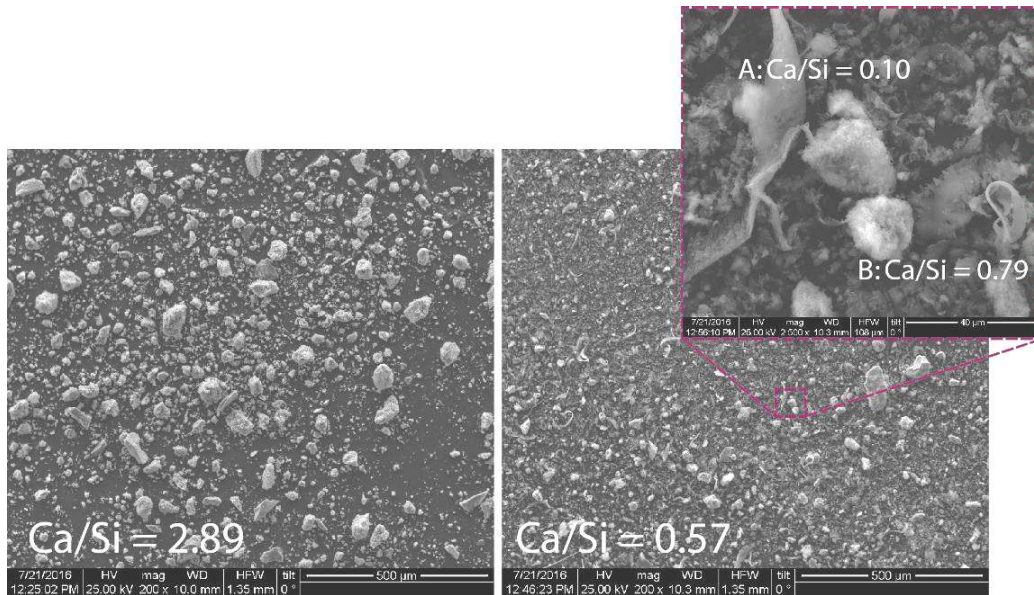


Figure 5.20: Microphotographs of reference (left) and leached (right) powder LP specimens. Ca/Si ratio is result of bulk analysis during SEM examination. In detail microphotograph, the two main particle types are presented along with their measured Ca/Si ratio.

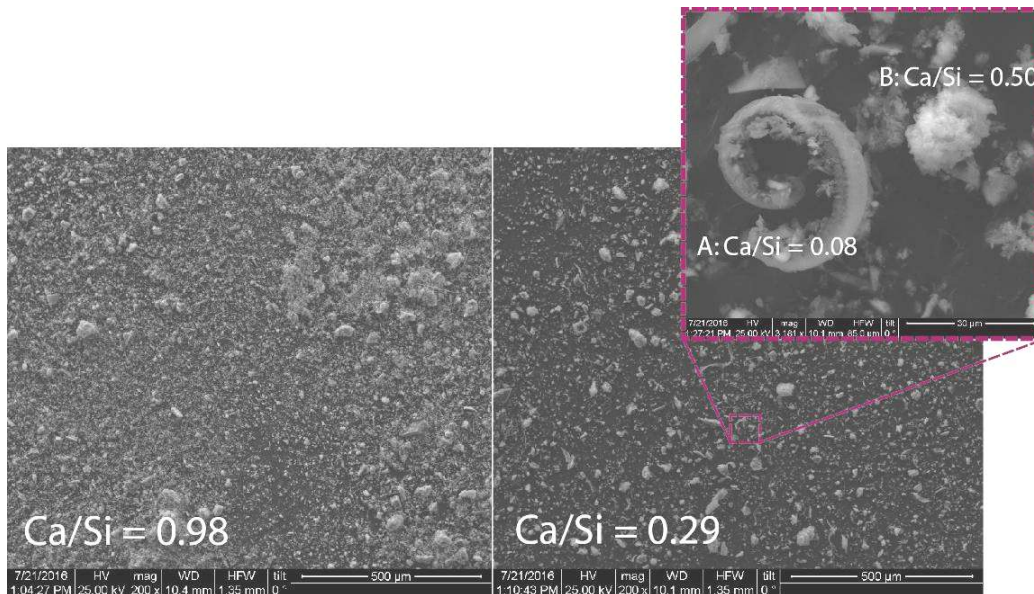


Figure 5.21: Microphotographs of reference (left) and leached (right) powder NHL specimens. Ca/Si ratio is result of bulk analysis during SEM examination. In detail microphotograph, the two main particle types are presented along with their measured Ca/Si ratio.

5.3.5 Microstructural alterations and chemical analysis (MIP, SEM/EDAX)

Characterization of the degraded specimens was performed at the stereoscope (Leica S6D stereo microscope) before and after the leaching process (Fig. 5.22-5.23). Both ends of the specimens were marked in order to compare specific areas on the level of degradation.

The degradation is visible macroscopically on the surface in contact with the anode solution (L) as the binder is absent and aggregate coherence is loosened. This causes an additional loss of material even after the end of the leaching test. This situation is comparable in NHL and LP specimens and is consistent, irrespective of the curing time of the specimens prior to the test.

The surface in contact with the cathode solution (P) is not visibly degraded, and there are no signs of material loss. On the contrary, a crystallized layer is observed, which is homogenous in the case of NHL mortars but relatively dispersed in LP mortars.

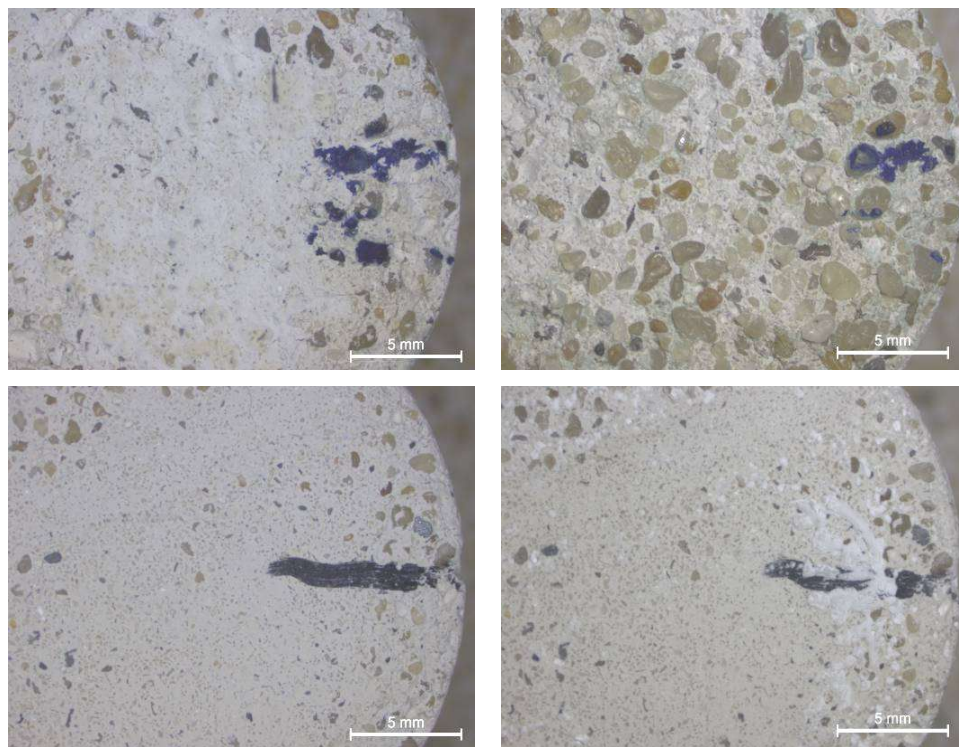


Figure 5.22: LP specimens as captured before (left) and after (right) leaching. On top the surface in contact with the anode solution (L) and at the bottom the surface in contact with the cathode solution (P)

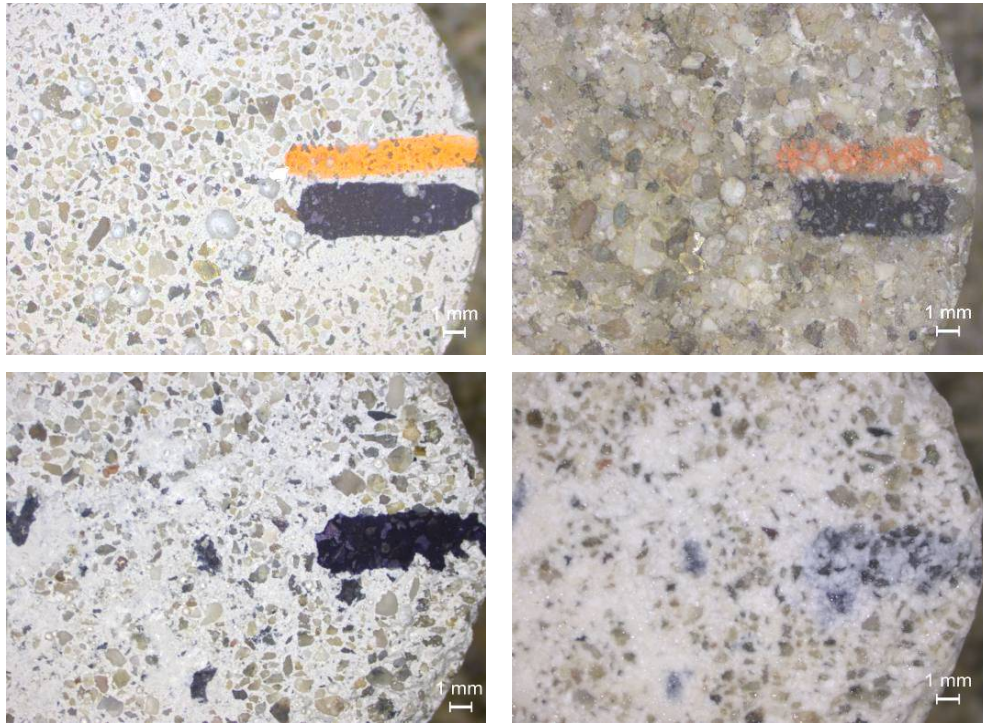


Figure 5.23: NHL specimens as captured before (left) and after (right) leaching. On top the surface in contact with the cathode solution (L) and at the bottom the surface in contact with the anode solution (P)

5.3.5.1 Scanning Electron Microscopy

Observations of polished sections and fresh fractures of both ends of the leached specimens (namely L and P) at the SEM revealed the heterogeneity of the microstructure of the specimens after leaching.

Similarly to the stereomicroscope observations, on the surface of the specimens in contact with the anode solution (P) a precipitated layer of pure calcite crystals (fig. 5.24) was observed along the surface. The morphology of the well-formed crystals suggests that they are the result of precipitation of calcite rather than the result of binder carbonation. This is clearly seen in Fig. 5.24 (left) a, where a layer of well-formed sparitic calcite is precipitated on a substrate of micritic calcite which is common especially in the outer surface of mortars. Similarly in Fig. 5.24 (right) sparitic calcite of distinct crystal sizes is precipitated suggesting a multi-step precipitation mechanism.

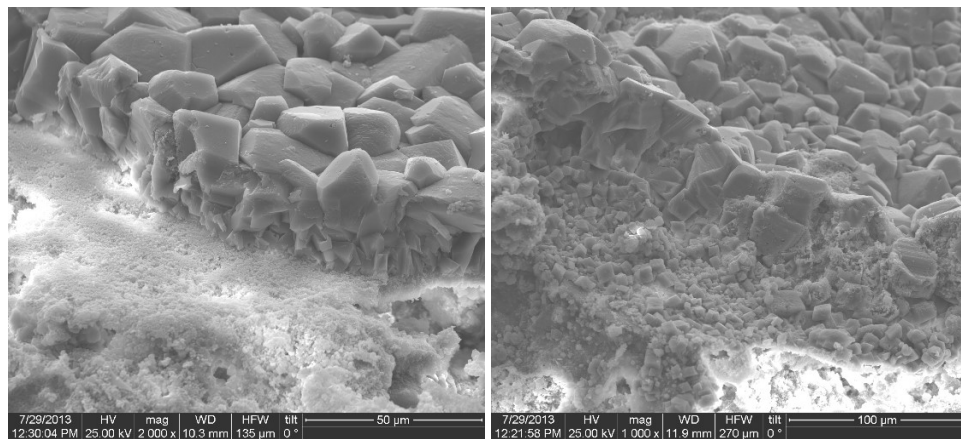


Figure 5.24: Microphotograph of the specimen's surface in contact with the anode solution (P) is characterized by a precipitated layer of pure calcite crystals

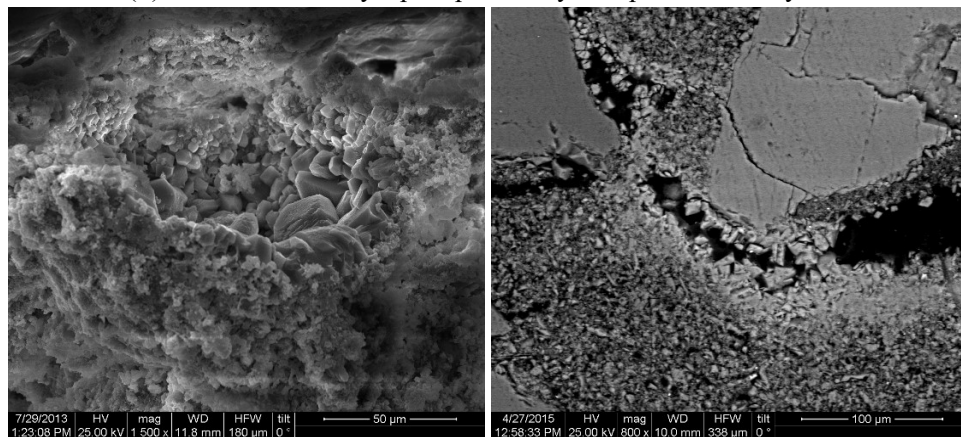


Figure 5.25: Microphotograph of precipitated calcite observed in cracks and voids throughout the sample.

Observation of polished sections of the same specimens (Fig. 5.26-5.27), confirmed the presence of the distinct calcite layer on the surface in contact with the cathode tank, whereas, adjacent to the precipitated layer a highly porous degraded zone was identified.

This mechanism is common in both NHL and LP specimens irrespective of the curing period that preceded the leaching test.

Similarly, the surface in contact with the anode solution (L) is visibly degraded and is characterized by a de-calcified zone. This was corroborated by chemical analysis of the polished sections (Fig. 5.26-5.27). De-calcified zones in LP samples present a thick network of microcracks, whereas in NHL specimens even though material loss is evident in the same zones, micro-cracking is not observed.

The de-calcified zones are easily distinguished in back-scatter mode on the SEM as chemical composition is clearly differentiated. Furthermore, this differentiation is clearer in specimens cured for longer period (120 d) rather than in early age specimens where, both in LP and NHL mortars, the de-calcified zone is not gradual suggesting a different dissolution mechanism.

Moreover, the migration of Ca ions towards the anode is evident in all samples, as precipitated secondary calcite is observed in cracks and voids throughout the sample axis (Fig 5.25). Especially in the case of LP specimens the re-precipitation of calcite is identified on the barrier of the decalcified zone and continues throughout the full length of the specimen reaching the precipitated zone. This is observed more clearly in samples cured for longer period (60 and 120 d).

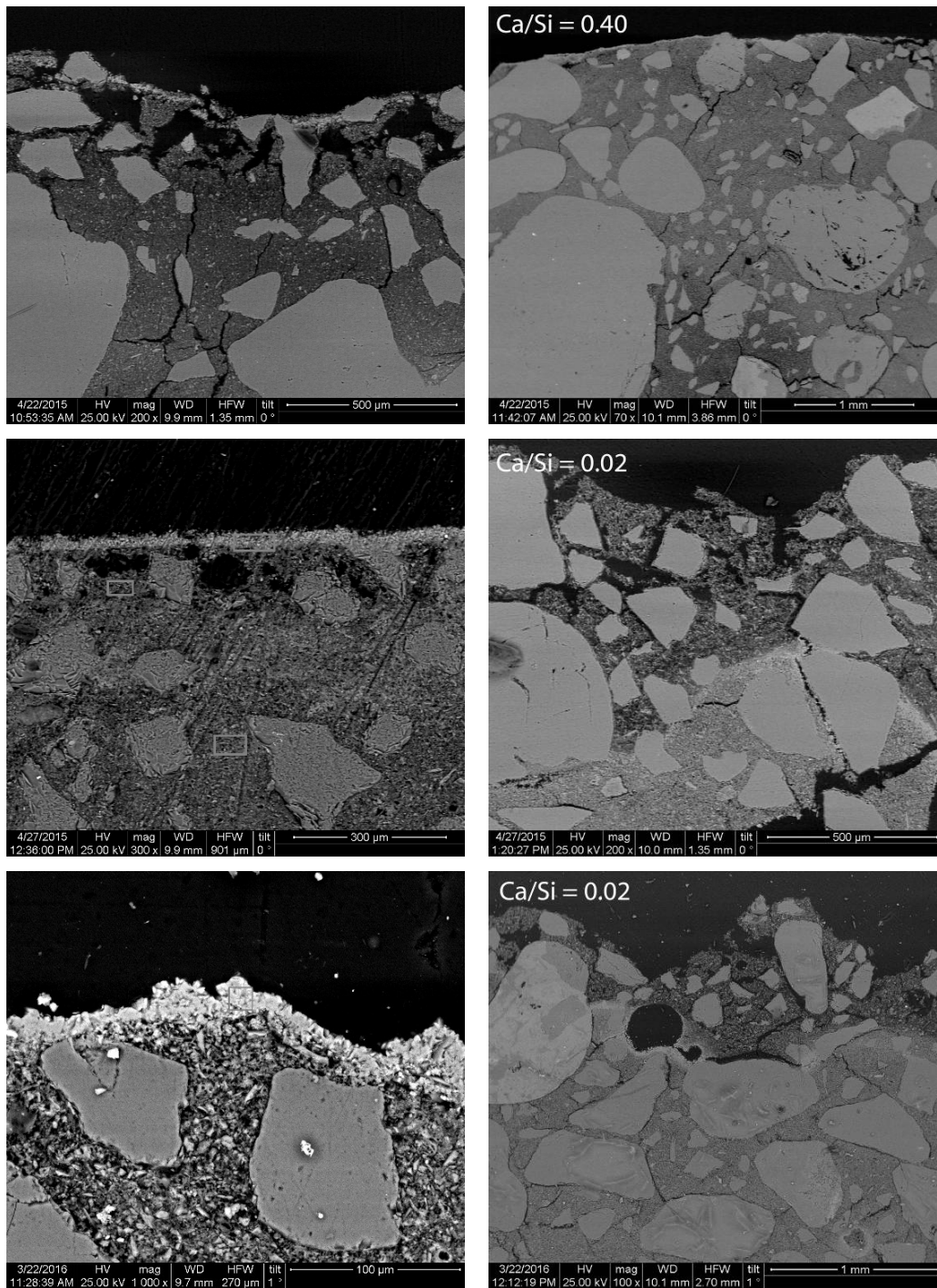


Figure 5.26: Microphotographs of both sides of LP specimens (P-left) (L-right) and Ca/Si ratio calculated by analysis of the leached zone.

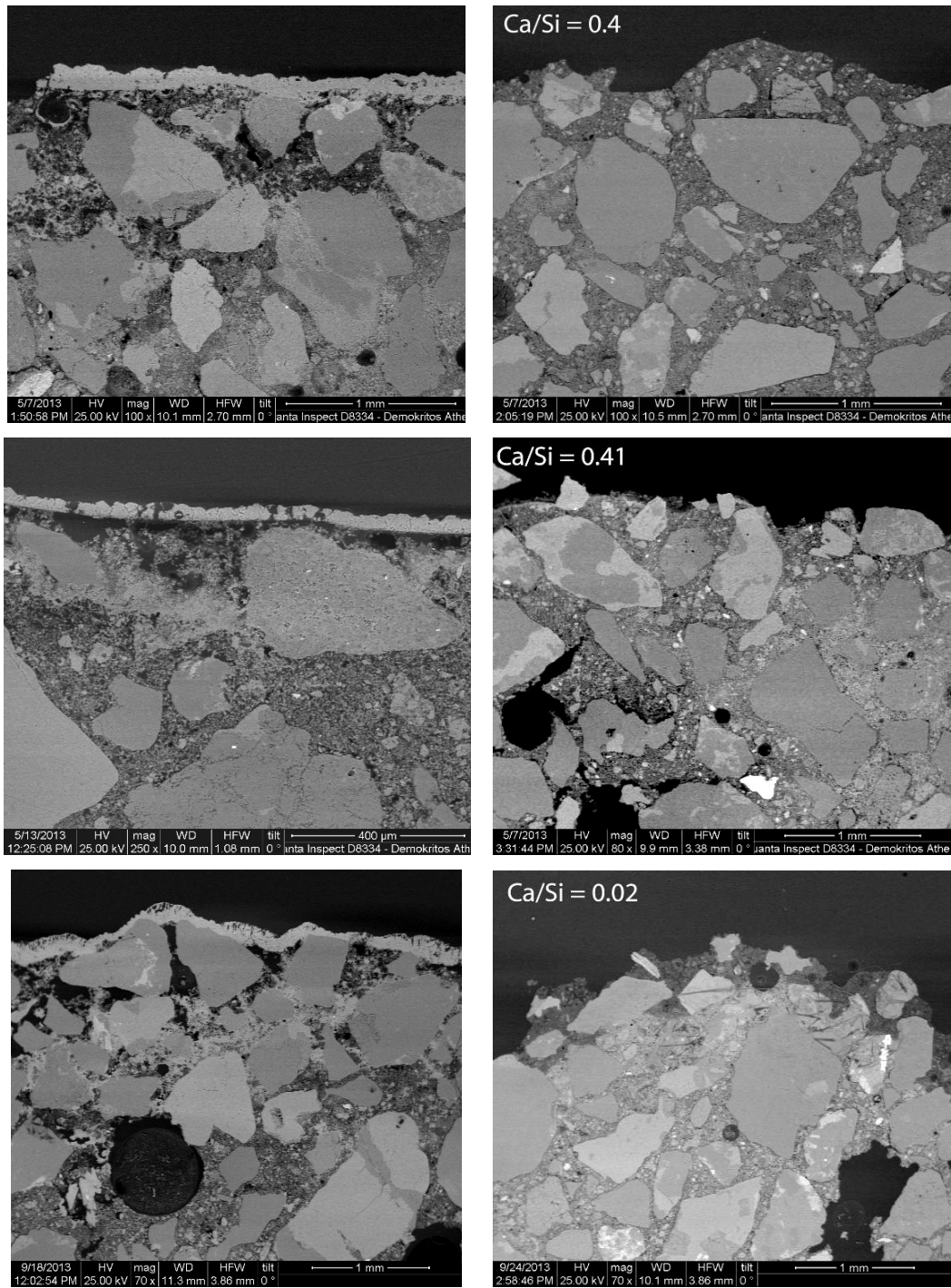


Figure 5.27: Microphotographs of both sides of NHL specimens (P-left) (L-right) and Ca/Si ratio calculated by analysis of the leached zone.

5.3.5.2 Mercury Intrusion porosimetry (MIP)

Microstructural alterations were verified by mercury intrusion porosimetry (MIP) performed in degraded cylindrical specimens. Similar to SEM sample preparation, for MIP leached specimens were separated in two parts so that porosity alterations was assessed for both ends of leached specimens; in contact with the anode and the cathode tank respectively. Total porosity measurements of each part (P or L) when contrasted with each other and with measurements of the reference samples depict clearly the effect of curing time of specimens before leaching on the extent of the degradation (fig. 5.28).

The expected increase in total porosity after leaching is evident in both LP and NHL samples, irrespective of the curing period of the leached specimens. Nevertheless, the extent of that increase is evidently lower for specimens cured for longer period (60 and 120 days), while this trend is common in both LP and NHL specimens. Moreover, when samples collected from the two ends (L and P) of the leached samples are compared, it is evident that the samples taken from the end in contact with the anode tank (L) have in most cases similar or slightly higher porosity than those in contact with the cathode tank (P).

The main difference between LP and NHL specimens is the way that new porosity is formed. More precisely, in early age LP specimens pores larger than 100 μm (low pressure porosimetry) are almost doubled in volume and this is the common for samples taken from both ends of the cylindrical specimens (L and P). At the same time smaller pores (high pressure porosimetry) decrease in total volume which points towards the assumption that degradation is taking place in the full range of pore sizes resulting in the transformation of mesopores to macropores. This can also be deduced by pore size distribution of the same specimens (fig. 5.29). The same trend is observed in degraded LP specimens cured for two or four months (60 and 120 d), but in lower extend.

Similarly, degraded NHL specimens present higher porosity than the reference specimens but the increase is divided between meso- and macro- porosity, which means that meso pores are also created along with macropores.

It is noteworthy that LP and NHL specimens cured for 120 days present similar pore size distribution, as both present a single pore distribution at 0.5-1 μm while a reduction of the amount of smaller pores (< 50 nm) is observed.

The two types of porosity formed in the binder matrix due to Ca-leaching reported; could be attributed to the dissolution of $\text{Ca}(\text{OH})_2$ and is measured as macro-porosity, whereas decalcification of CSH produce micro-porosity and thus does not affect strongly the mechanical properties of the leached specimens (Carde and Francois, 1999; Rimmelé and Barlet-Gouédard, 2010; Phung et al., 2016).

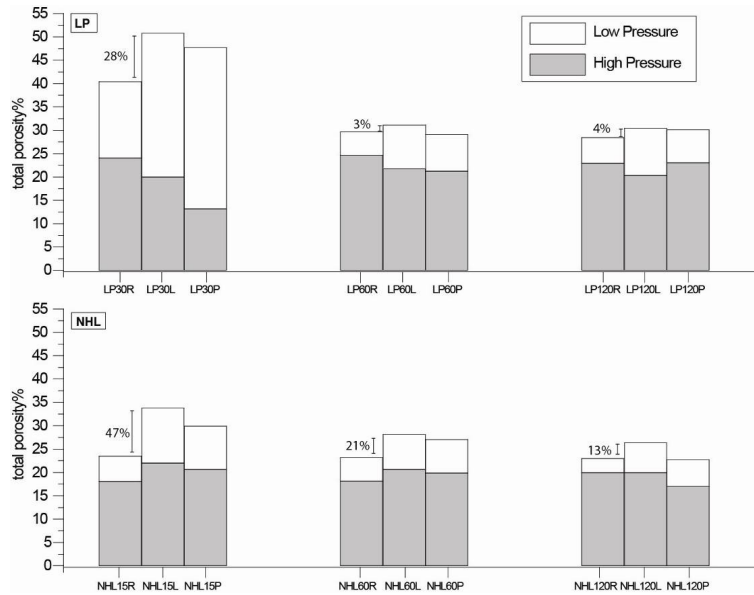


Figure 5.28: Total porosity % of reference and leached LP and NHL cylindrical specimens. The porosity increase % due to leaching on the side of the anode solution (L) is stated.

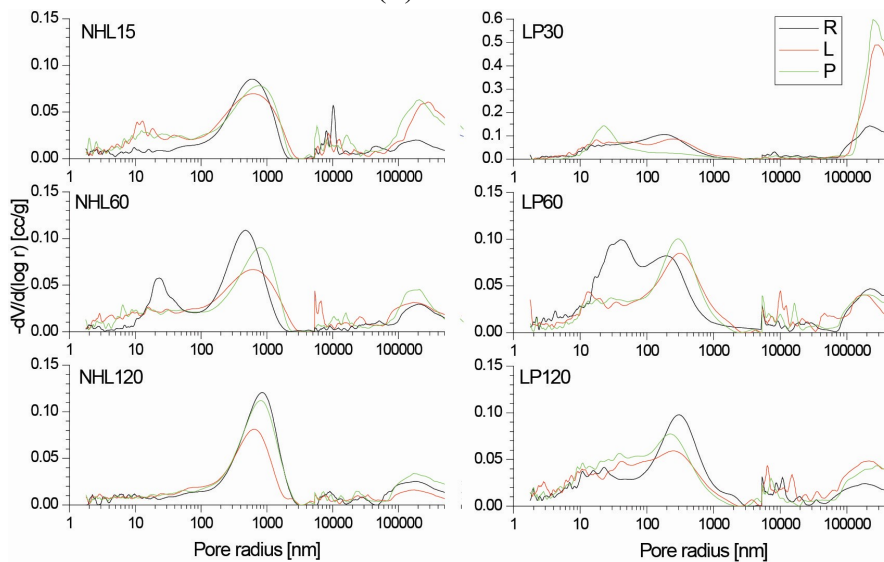


Figure 5.29: Pore size distribution of reference and leached LP and NHL specimens

5.4 Conclusions

In this chapter the dissolution of Ca-bearing phases present in the binder of LP and NHL mortars was studied as this is considered to be the first step in the autogenous self-healing mechanism. The main factor examined was the effect of curing time on the leaching of calcium from these mortars. Thus, by examining the evolution of the mineralogy of LP and NHL mortars after a curing period ranging from a few days to one year and its correlation to the solubility of Ca-bearing components, the following conclusions could be drawn.

Similarly to other studies (Rimmelé and Barlet-Gouédard, 2010; Haga, 2005; Carde et al., 1996) it was found that portlandite is the main component dissolved during leaching. That is to be expected as the solubility of Ca(OH)_2 is orders of magnitude higher than that of calcite.

Ca- leaching or decalcification of cylindrical specimens is proportional to the amount of unreacted portlandite (free lime) present in the binder. However examination of leached of powder specimens revealed that even after the depletion of reactive portlandite, two more mechanisms could be responsible for further providing calcium ions. The first is the production of secondary Ca(OH)_2 due to hydration reaction and the second is the decalcification of C-S-H phases. C_2S may also provide Ca-ions in the case of NHL mortars.

Production of secondary portlandite as a product of hydration reaction is also corroborated by thermogravimetric analysis. The fact that it is not reported during cylindrical leaching testing, could be related to the presence of precipitated secondary calcite inside the pore network of these specimens.

Regarding the microstructural characteristics of leached cylindrical specimens, further conclusions are reached. Leaching of LP and NHL specimens results in an increase in total porosity as expected. However, toughening of the microstructure due to advanced curing periods results in a lower porosity increase during leaching. Moreover, leaching of LP and NHL specimens seems to affect porosity by two different mechanisms. In leached LP specimens the macro porosity is increased, whereas in leached NHL specimens total porosity is mainly attributed to mesoporosity.

References

- Adenot, F., & Buil, M. (1992). Modelling of the corrosion of the cement paste by deionized water. *Cement and Concrete Research*, 22(2–3), 489–496. [http://doi.org/10.1016/0008-8846\(92\)90092-A](http://doi.org/10.1016/0008-8846(92)90092-A)
- Bakolas, A., Aggelakopoulou, E., Moropoulou, A., & Anagnostopoulou, S. (2006). Evaluation of pozzolanic activity and physico-mechanical characteristics in metakaolin-lime pastes. *Journal of Thermal Analysis and Calorimetry*, 84(1), 157–163. <http://doi.org/10.1007/s10973-005-7262-y>
- Banfill, P. F. G., Szadurski, E. M., & Forster, A. M. (2016). Deterioration of natural hydraulic lime mortars, II: Effects of chemically accelerated leaching on physical and mechanical properties of carbonated materials. *Construction and Building Materials*, 111, 182–190.
- Carde, C., & François, R. (1999). Modelling the loss of strength and porosity increase due to the leaching of cement pastes. *Cement and Concrete Composites*, 21(3), 181–188.
- Carde, C., François, R., & Torrenti, J.-M. (1996). Leaching of both calcium hydroxide and C-S-H from cement paste: Modeling the mechanical behavior. *Cement and Concrete Research*, 26(8), 1257–1268. [http://doi.org/10.1016/0008-8846\(96\)00095-6](http://doi.org/10.1016/0008-8846(96)00095-6)
- Castellote, M., Llorente, I., Andrade, C., & Alonso, C. (2003). Accelerated leaching of ultra high performance concretes by application of electrical fields to simulate their natural degradation. *Materials and Structures*, 36(2), 81–90. <http://doi.org/10.1007/BF02479521>
- Cazalla, O., Rodriguez-Navarro, C., Sebastian, E., Cultrone, G., & Torre, M. J. (2004). Aging of Lime Putty: Effects on Traditional Lime Mortar Carbonation. *Journal of the American Ceramic Society*, 83(5), 1070–1076. <http://doi.org/10.1111/j.1151-2916.2000.tb01332.x>
- Faucon, P., Adenot, F., Jacquinet, J. F., Petit, J. C., Cabrillac, R., & Jorda, M. (1998). Long-term behaviour of cement pastes used for nuclear waste disposal: review of physico-chemical mechanisms of water degradation. *Cement and Concrete Research*, 28(6), 847–857. [http://doi.org/10.1016/S0008-8846\(98\)00053-2](http://doi.org/10.1016/S0008-8846(98)00053-2)
- Forster, A. M., Szadurski, E. M., & Banfill, P. F. G. (2014). Deterioration of natural hydraulic lime mortars, I: Effects of chemically accelerated leaching on physical and mechanical properties of uncarbonated materials. *Construction and Building Materials*, 72, 199–207.
- Glasser, F. P., Marchand, J., & Samson, E. (2008). Durability of concrete — Degradation phenomena involving detrimental chemical reactions. *Cement and Concrete Research*, 38(2), 226–246.

- Haga, K., Sutou, S., Hironaga, M., Tanaka, S., & Nagasaki, S. (2005). Effects of porosity on leaching of Ca from hardened ordinary Portland cement paste. *Cement and Concrete Research*, 35(9), 1764–1775.
- Hearn, N. (1998). Self-sealing, autogenous healing and continued hydration: What is the difference? *Materials and Structures*, 31(8), 563–567.
- Kan L.-L., H.-S. Shi, A.R. Sakulich, V.C. Li, (2010) Self-healing characterization of engineered cementitious composite materials, *ACI Mater. J.* 107 (6) 619e626.
- Kappert, E. J., Bouwmeester, H. J. M., Benes, N. E., & Nijmeijer, A. (2014). Kinetic Analysis of the Thermal Processing of Silica and Organosilica. *The Journal of Physical Chemistry B*, 118(19), 5270–5277. <http://doi.org/10.1021/jp502344k>
- Karatasios, I., Amenta, M., Tziotziou, M., & Kilikoglou, V. (2012). The Effect of Relative Humidity on the Performance of Lime-Pozzolan Mortars. In J. Válek, J. J. Hughes, & C. J. W. P. Groot (Eds.) (pp. 309–318). Springer Netherlands. Retrieved from http://link.springer.com/chapter/10.1007/978-94-007-4635-0_2
- Nijland, T. G., Larbi, J. a, Hees, R. P. J. Van, & Lubelli, B. (2007). Self Healing Phenomena in Concretes and Masonry Mortars: a Microscopic Study. *Proceedings of the First International Conference on Self Healing Materials 18-20 April 2007, Noordwijk Aan Zee, The Netherlands*, (April), 1–9.
- Phung, Q. T., Maes, N., Jacques, D., De Schutter, G., & Ye, G. (2016). Investigation of the changes in microstructure and transport properties of leached cement pastes accounting for mix composition. *Cement and Concrete Research*, 79, 217–234. <http://doi.org/10.1016/j.cemconres.2015.09.017>
- Reinhardt, H.-W., & Jooss, M. (2003). Permeability and self-healing of cracked concrete as a function of temperature and crack width. *Cement and Concrete Research*, 33(7), 981–985. [http://doi.org/10.1016/S0008-8846\(02\)01099-2](http://doi.org/10.1016/S0008-8846(02)01099-2)
- Rimmelé, G., & Barlet-Gouédard, V. (2010). Accelerated degradation method for cement under CO₂-rich environment: The LIFTCO₂ procedure (leaching induced by forced transport in CO₂ fluids). *Cement and Concrete Research*, 40(8), 1175–1188. <http://doi.org/10.1016/j.cemconres.2010.03.019>
- Saito, H., & Deguchi, A. (2000). Leaching tests on different mortars using accelerated electrochemical method. *Cement and Concrete Research*, 30(11), 1815–1825.
- Saito, H., Nakane, S., Ikari, S., & Fujiwara, A. (1992). Preliminary experimental study on the deterioration of cementitious materials by an acceleration method. *Nuclear Engineering and Design*, 138(2), 151–155.
- Saito, H., Nakane, S., Tsuji Y. and Fujiwara, A., (1998) ‘Effect of different cements and mix proportions on results obtained with accelerated electrochemical leaching test’, *Concrete Library of JSCE*, 31, 255-273.

Chapter 6: Microscopic examination of self-healing products

6.1 Introduction

In this chapter, a better understanding of the autogenic self-healing phenomenon in laboratory prepared mortar mixtures is presented focusing on the morphological and chemical characterization of the secondary formed products.

As described in Chapter 2, the autogenic self healing mechanism, observed in a wide variety of cementitious materials, has been the subject of various studies in the last decade (van Breugel, 2012, Yildırım et al., 2015), the majority of which are focused on the self-healing ability of Portland cement or ECC (engineered cementitious composites). In contrast, this research focuses on the characterization of secondary products formed when the autogenous phenomenon takes place in lime-pozzolan or natural hydraulic mortars. Nevertheless, despite the differences in the chemical composition of the cement type tested, similar experimental procedures are applied (van der Zwaag, 2007).

More specifically, microscopy is one of the main techniques that enables the discrimination and micro-morphological characterization of the secondary products formed inside cracks. Thus, it is often used for evaluating the efficiency of the self-healing mechanism by measuring the extent of crack-filling by secondary products (Çopuroğlu et al., 2013) in cracks' cross-sections. Additionally, microscopy is used for damage assessment by examining crack characteristics in polished or thin sections of cement samples and is usually combined with length and width measurements.

Huang et al (2015) has recently developed a new methodology by using microscopy as a means for the identification and morphological characterization of secondary self-healing products in Portland cement pastes. By combining scanning electron microscopy examination with energy dispersive spectroscopy, the morphological aspects of secondary products can be correlated with their chemical composition.

Another advantage of the above approach is that the crack surface is observed instead of its cross-section, thus ensuring that the products observed are not limited on the

outer surface of the specimen, providing, in some cases, the spatial distribution of healing products (Suryanto, et al., 2016).

In this chapter, the experimental procedure includes the controlled crack generation in NHL and LP mortar specimens and the characterization of secondary products formed inside the crack after being cured for varying healing periods.

6.2 Materials and Methods

The experimental set-up is aimed on the parameterization of the phenomenon, by simultaneous microscopic examination and elemental characterization of the secondary formed healing products. More precisely special attention was given to the following parameters and how they affect secondary healing products formation:

- cracking age (moment of cracking)
- healing period
- humidity conditions

6.2.1 Materials

LP and NHL mortar mixtures were prepared, as described in appendix A, and were subsequently cast in prismatic moulds (15x15x80 mm). For each mortar mixture prismatic specimens were cast (n=48) and cured at the same temperature and humidity conditions in a controlled chamber (95±5% RH, 20±3°C).

6.2.2 Crack generation and control

In order to study the healing mechanisms, the specimens were damaged by controlled cracking, under three point bending test using an INSTRON -100kN compression machine. A continuous load (100 μ m/min) was applied to all specimens, allowing the controlled deformation of specimens after crack initiation (Fig 6.1).



Figure 6.1: Crack initiation by three point bending.

A set of preliminary tests were conducted in order to correlate displacement values with the width of the crack generated by three-point bending tests. During crack generation special care was given to ensure that the aforementioned displacement would not result in the collapse of the specimen. This was applied in all groups of specimens, as their fracture profiles demonstrate a clear variation in mechanical properties depending on the curing period and the type of binder (Fig. 6.2). In all cases the specimens were unloaded before their load displacement curve became parallel to the displacement axis. At this point the specimens absorb the maximum energy leading to crack propagation, which does not lead to their failure.

After the preparation of 32 cracked specimens for each mixture, the standard deviation of measured strength was calculated to evaluate the homogeneity of each mixture. In Fig 6.3 average strength values are shown together with the calculated standard deviation for each set of specimens. The large number of specimens fractured for each group, combined with a low standard deviation, suggests a high homogeneity amongst the specimens of each group.

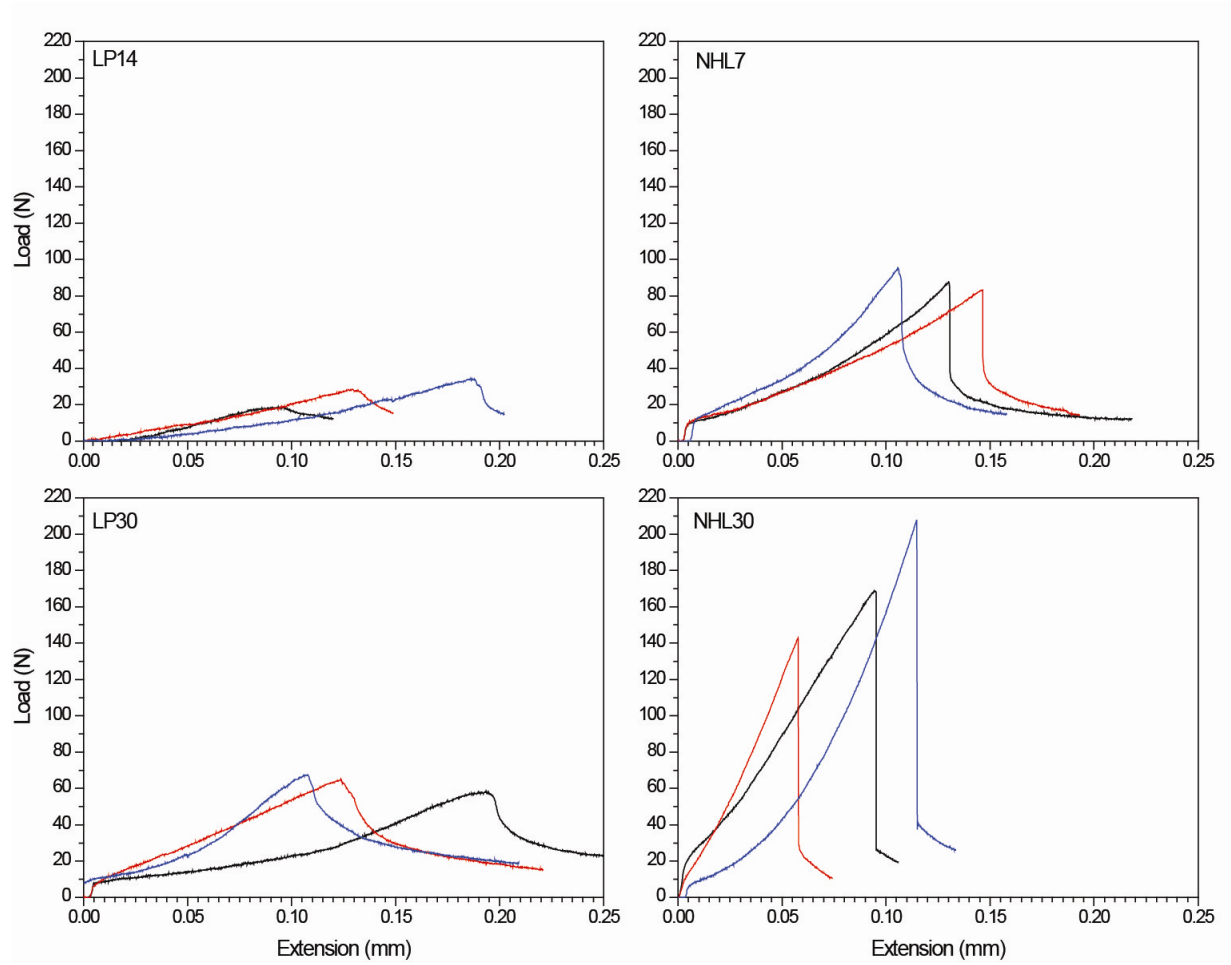


Figure 6.2: Fracture profiles generated by three -point bending

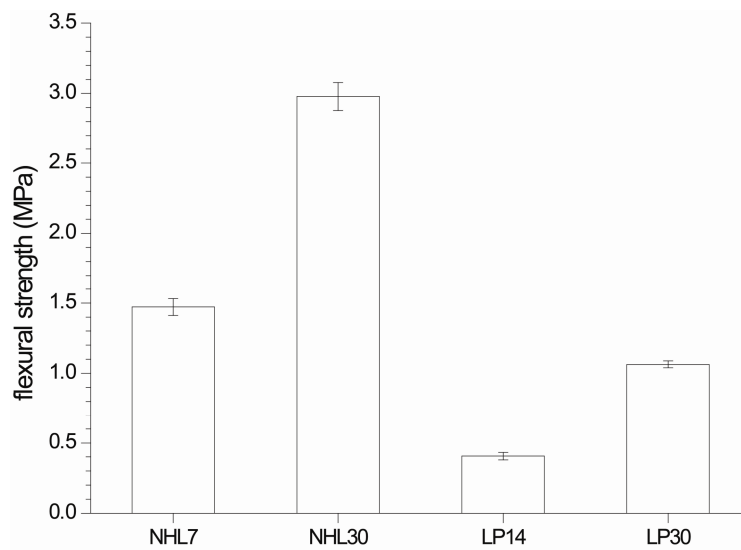


Figure 6.3: Flexural strength and standard deviation measured during crack generation calculated by the average strength values of 32 specimens

6.2.3 Evaluation of crack width in the stereo-microscope

The cracks generated by flexural stress in all the specimens, were recorded at the stereo microscope (Leica S6D) (Fig 6.4), due to the large field of view that provides and thus, the potential of capturing the full length of the crack during the observation of the bottom side of the specimens.

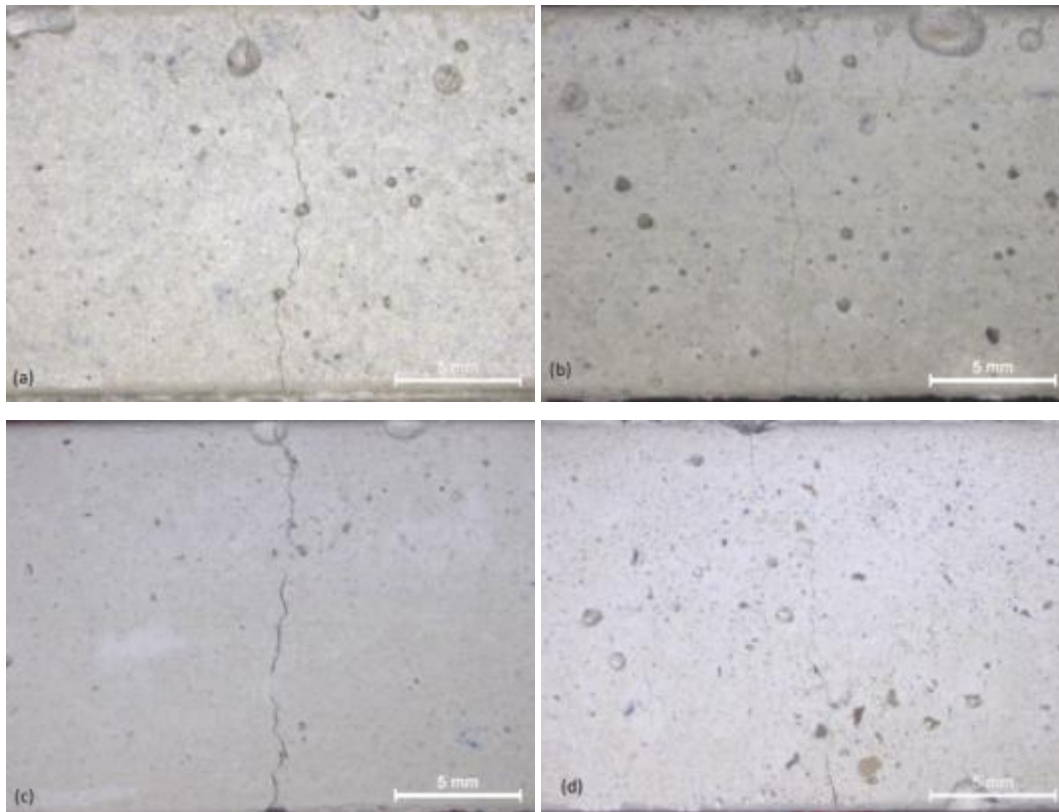


Figure 6.4: Overview of cracks on the bottom side of cracked specimens.

(a) NHL7 (b) NHL30 (c) LP15 (d) LP30

The crack opening was measured in all groups specimens on the bottom side where maximum width is recorded. The measurement was performed using the Leica Application Suite 4.3 software. Cracks of $0.07 (\pm 0.01)$ mm width were measured for all specimens (Fig 6.5). It is noteworthy, that a variation of $10 \mu\text{m}$, measured in the wider part of the crack, is acceptable for the purposes of this experiment as these measurements were performed to produce comparable crack widths in specimens with very distinct fracture properties.

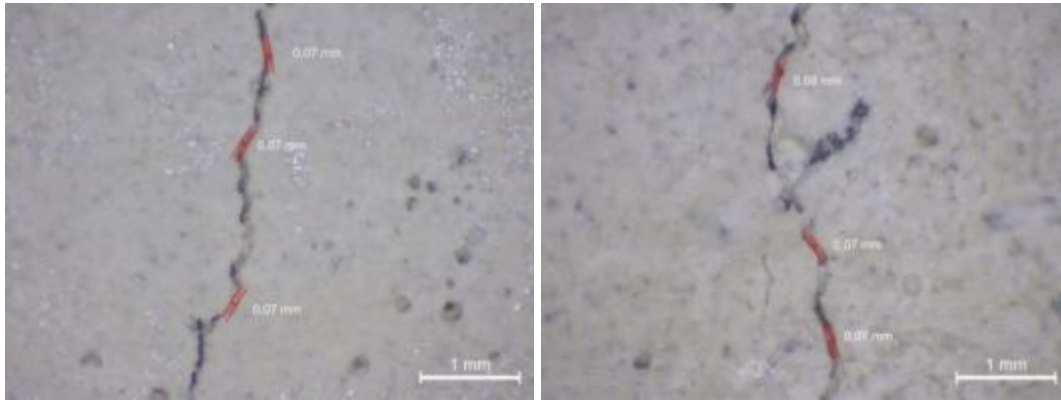


Figure 6.5: Detailed measurement of crack

6.2.4 Parameters examined

The specimens of each mixture (LP and NHL) were then divided in 16 groups of 4 specimens each. In each group one of the following parameters was examined: i) age of the specimens at the time of the crack formation, ii) conditions of healing and iii) healing period, as listed in Table 6.1.

Table 6.1: All groups and parameters examined

Group Code	Binder	Cracking Age (d)	Healing/ curing conditions	Healing/ curing period (d)
NHL73045	NHL	7	45% RH	30
NHL73075	NHL	7	75% RH	30
NHL73095	NHL	7	95% RH	30
NHL730cy	NHL	7	Wet-dry cycles	30
NHL79045	NHL	7	45% RH	90
NHL79075	NHL	7	75% RH	90
NHL79095	NHL	7	95% RH	90
NHL790cy	NHL	7	Wet-dry cycles	90
NHL303045	NHL	30	45% RH	30
NHL303075	NHL	30	75% RH	30
NHL303095	NHL	30	95% RH	30
NHL3030cy	NHL	30	Wet-dry cycles	30
NHL309045	NHL	30	45% RH	90
NHL309075	NHL	30	75% RH	90
NHL309095	NHL	30	95% RH	90
NHL3090cy	NHL	30	Wet-dry cycles	90
LP153045	LP	15	45% RH	30
LP153075	LP	15	75% RH	30

LP153095	LP	15	95% RH	30
LP1530cy	LP	15	Wet-dry cycles	30
LP159045	LP	15	45% RH	90
LP159075	LP	15	75% RH	90
LP159095	LP	15	95% RH	90
LP1590cy	LP	15	Wet-dry cycles	90
LP303045	LP	30	45% RH	30
LP303075	LP	30	75% RH	30
LP303095	LP	30	95% RH	30
LP3030cy	LP	30	Wet-dry cycles	30
LP309045	LP	30	45% RH	90
LP309075	LP	30	75% RH	90
LP309095	LP	30	95% RH	90
LP3090cy	LP	30	Wet-dry cycles	90

6.2.4.1 Cracking age

In order to examine the effect of the curing period prior to cracking on the morphology/type of healing products formed, LP and NHL specimens were cured under controlled humidity conditions (95% RH) for two different time-periods before cracking. For NHL specimens two different curing periods were set after 7 days, for simulating early –age cracking and after 30 days, when portlandite content is lower (based on thermo-gravimetric analysis results) (Fig. 6.6).

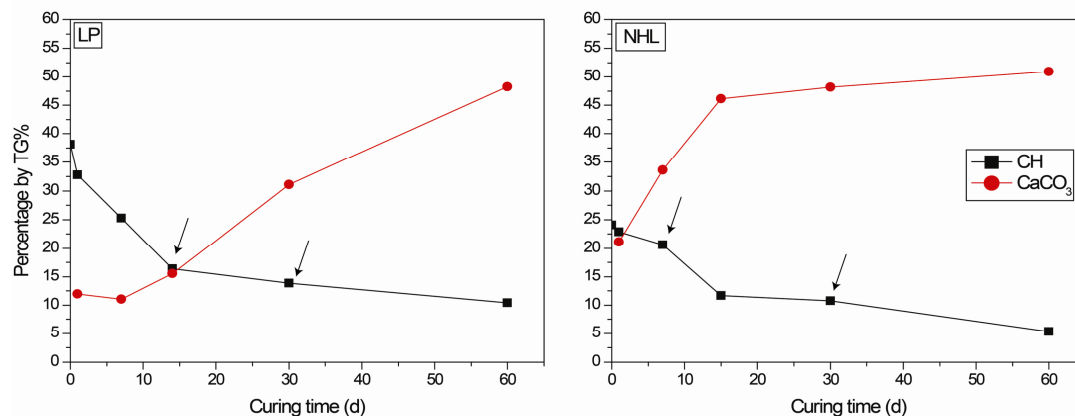


Figure 6.6: The evolution of portlandite and calcite content (wt%), as they were calculated by thermo-gravimetric analysis of LP and NHL reference mortars during the first two months of curing (60 d).

Accordingly, for LP specimens curing periods before cracking were set at 15 and 30 days. Early –age cracking after 15 days curing period was selected in this case, since

LP specimens cured for a shorter period have not yet attained the adequate strength and consistency to be tested and cracked accurately.

6.2.4.2 Healing Conditions

Cracked specimens were cured in four different conditions, in order to simulate different outdoor scenarios. One group of specimens was subjected to wet-dry cycles, which refer to an outdoor environment where masonry is subjected to rainy days followed by a period of drying. Furthermore, three humidity levels were selected in order to understand the effect of relative humidity on the self-healing mechanism. Lower humidity (45% RH) could refer in an arid environment, where long relatively dry periods take place. Higher humidity levels (75 and 95%) refer to two different environmental conditions usually met outdoors.

The specimens were stored in sealed containers, where humidity levels were controlled and stabilized by saturated salt solutions. More specifically, 45% RH was achieved by saturated solution of K_2CO_3 , 75% RH by NaCl and 95% RH by K_2SO_4 . For the wet/dry cycles, the specimens were immersed in tap water for 24 hours and then left to dry for two days in laboratory conditions.

6.2.4.3 Healing period

All cracked specimens were cured for 30 or 90 days after cracking (healing period). For the wet/dry cycles, the specimens were examined after 10 and 30 cycles (30 and 90 days respectively). The observations of secondary products on specimens cured for a 30-day healing period were compared and contrasted to those healed for 90 days in order to study the long term effect of the mechanism. The timeline of cracking-age and healing period for all groups is described in figure 6.7.

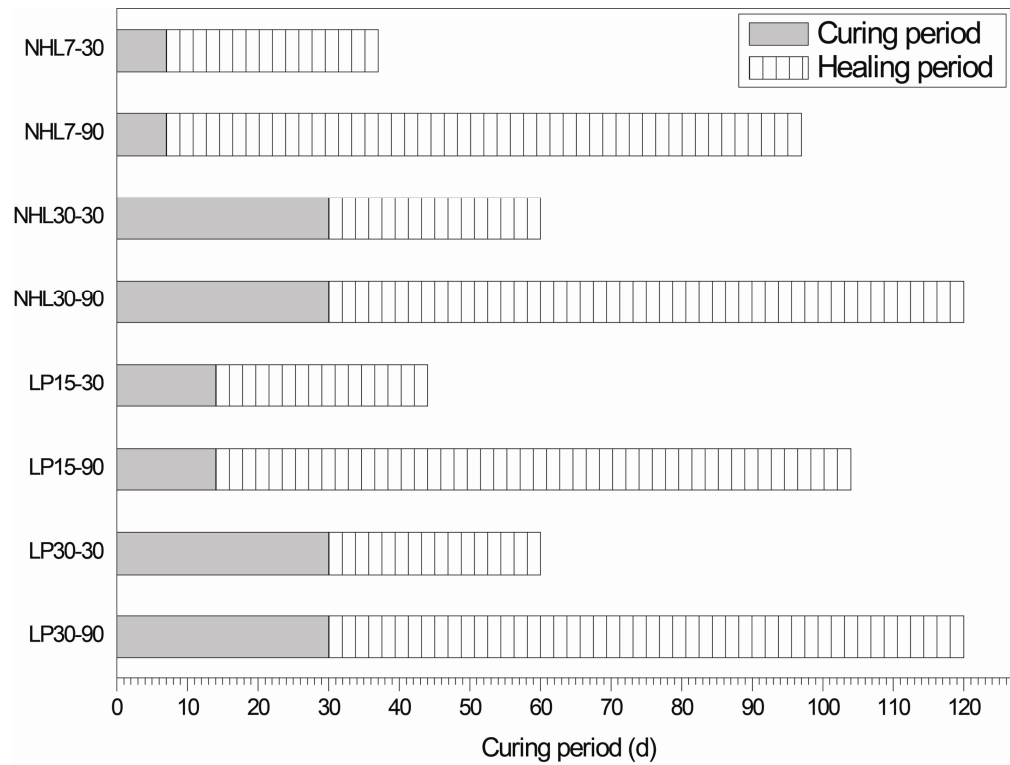


Figure 6.7: Timeline of curing and healing periods

6.2.5 Sample preparation for microscopic examination

At the end of each healing period, healing products formed inside the cracks were examined in a FEI Quanta-Inspect Scanning Electron Microscope, coupled with Energy-dispersive X-ray spectroscopy (SEM/EDAX).

Three samples were prepared for each group. One specimen was used for the characterization of the secondary products morphology by examination of the crack surface (Fig. 6.8) and two more to produce a thin and a polished section of the crack (Fig. 6.10). Similarly to the procedure for the carbonation testing, the specimen was separated in two parts, exposing the crack surface. The one half of the specimen was subsequently cut at a distance approximately 1 cm from the crack surface in order to minimize the sample volume using a diamond cutting wheel.



Figure 6.8: Sample preparation for SEM and polarizing light microscope. One specimen was split in two to reveal the crack surface.

During the sample preparation, the separation of the specimen for the observation of secondary products formed inside the crack would ideally expose healing products on either side of the crack. But it is possible that healing products are separated from one surface during the separation due to their low cohesion with the binder matrix (Fig. 6.9).

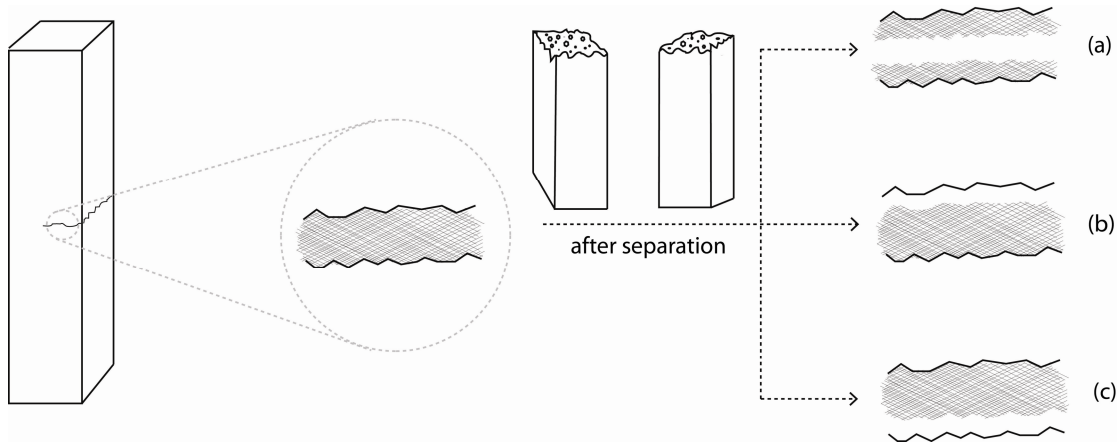


Figure 6.9: Separation of the crack walls might lead to: the observation of secondary healing products in either walls (a) or the detachment from one wall due to low cohesion with the crack surface (b and c)

Moreover, the cross-section of the crack was examined in order to obtain supplementary information regarding the topography of the secondary products inside the cracks. For this reason two specimens were impregnated under vacuum in epoxy resin to produce thin and polished sections of the crack plane.

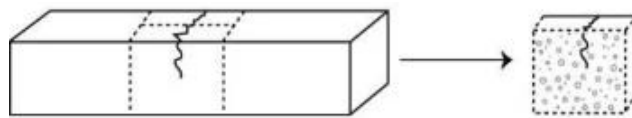


Figure 6.10: Epoxy impregnated specimens were cut vertically to expose a cross-section of the crack (bottom).

6.2.5.1 Impregnation methodology

Since early-age natural hydraulic lime and lime-pozzolan mortar specimens are usually quite friable, they were carefully impregnated to ensure that no further damage would occur on the specimen.

More specifically, after the end of the healing period, the cracked specimen was immersed in a low viscosity epoxy resin inside a vacuum chamber. Afterwards, the epoxy resin was solidified and the specimen was sealed and stabilized, so that no further damage would be inflicted during cutting. Subsequently, in order to minimize the sample volume, it was cut parallel to the crack using a diamond cutting wheel. The specimen was then further immersed in a low viscosity resin and after its hardening; it was cut perpendicular to the crack, thus exposing a cross-section of the crack. The experimental outline is shown in figure 6.11

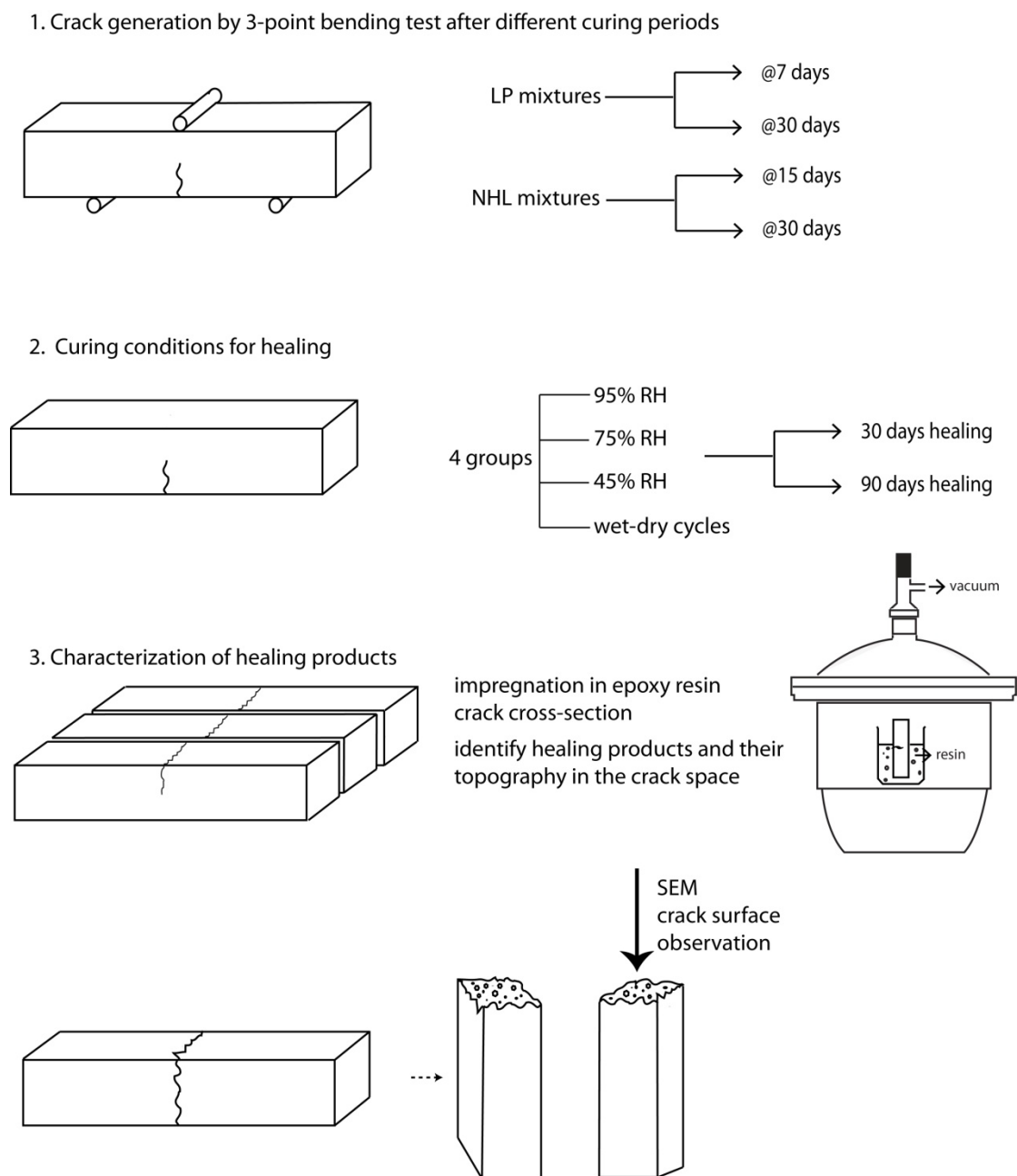


Figure 6.11: Experimental outline

6.3 Results

6.3.1 Microscopic observations

The observation of crack surfaces at the scanning electron microscope (SEM) showed a variety of secondary formed products. Near the surface on the outer part of the crack, a calcite layer is formed and is easily recognizable as it crystallizes on the edge of the specimens. This was also noticeable, when an external view of the crack was observed at the polarizing microscope in reflected light mode (Fig. 6.12). This is a precursor to the autogenous healing, as the diffusion of atmospheric CO_3^{2-} in the pore solution is much higher near the crack mouth than it is inside the crack, thus enabling the precipitation of secondary calcite, creating a sealing layer. This observation is similar to the results of other studies (Huang et al, 2016; Sisomphon, 2012).

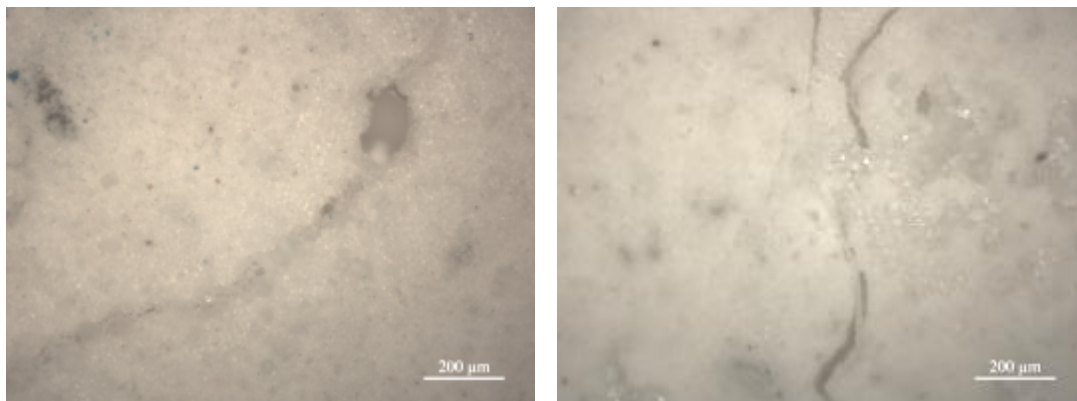


Figure 6.12: Precipitation of secondary calcite on the crack mouth as observed in under polarizing microscope (left-LP, right-NHL)

LP1530

In LP samples fractured at early-age (15 d) and healed for 30 days several secondary products were observed and identified (Fig 6.13). The presence of secondary hydraulic phases is recorded in all different humidity healing conditions with the exception of these at 45% RH. Secondary hydraulic phases form a single uniform layer of interconnected gel-like fibers, which are extended outwards- towards the opposite side of the crack. The density of these products does not vary noticeably depending on the humidity conditions applied.

Uniform layers of secondary hydraulic fiber-like products were formed on different substrates (Fig 6.14). More specifically, such layers were observed on typical micritic calcite in the binder matrix, on the surface of siliceous aggregates but also together with secondary calcite. The morphological similarities of these phases, suggests that there is a common mechanism governing their formation regardless the substrate on which they are formed.

The same morphological characteristics were observed in secondary products bridging microcracks of $\sim 30 \mu\text{m}$ width (Fig 6.15). The density of the interconnected fibers is higher inside the crack, revealing the capability of these networks to form interconnected formations bridging the opposite sides of cracks.

Moreover, a wide variety of CaCO_3 crystal formations were observed varying the humidity conditions implemented during the healing period (Fig 6.16), resulting in different crystalline groups. Well-formed calcite crystals of varying sizes were observed in high humidity conditions, whereas in lower humidity levels (75% RH) vaterite is also observed. The presence of vaterite only in lower humidity conditions could be attributed to the fact that as it is a metastable phase, it transforms to calcite in the presence of water (Zhou et al., 2010).

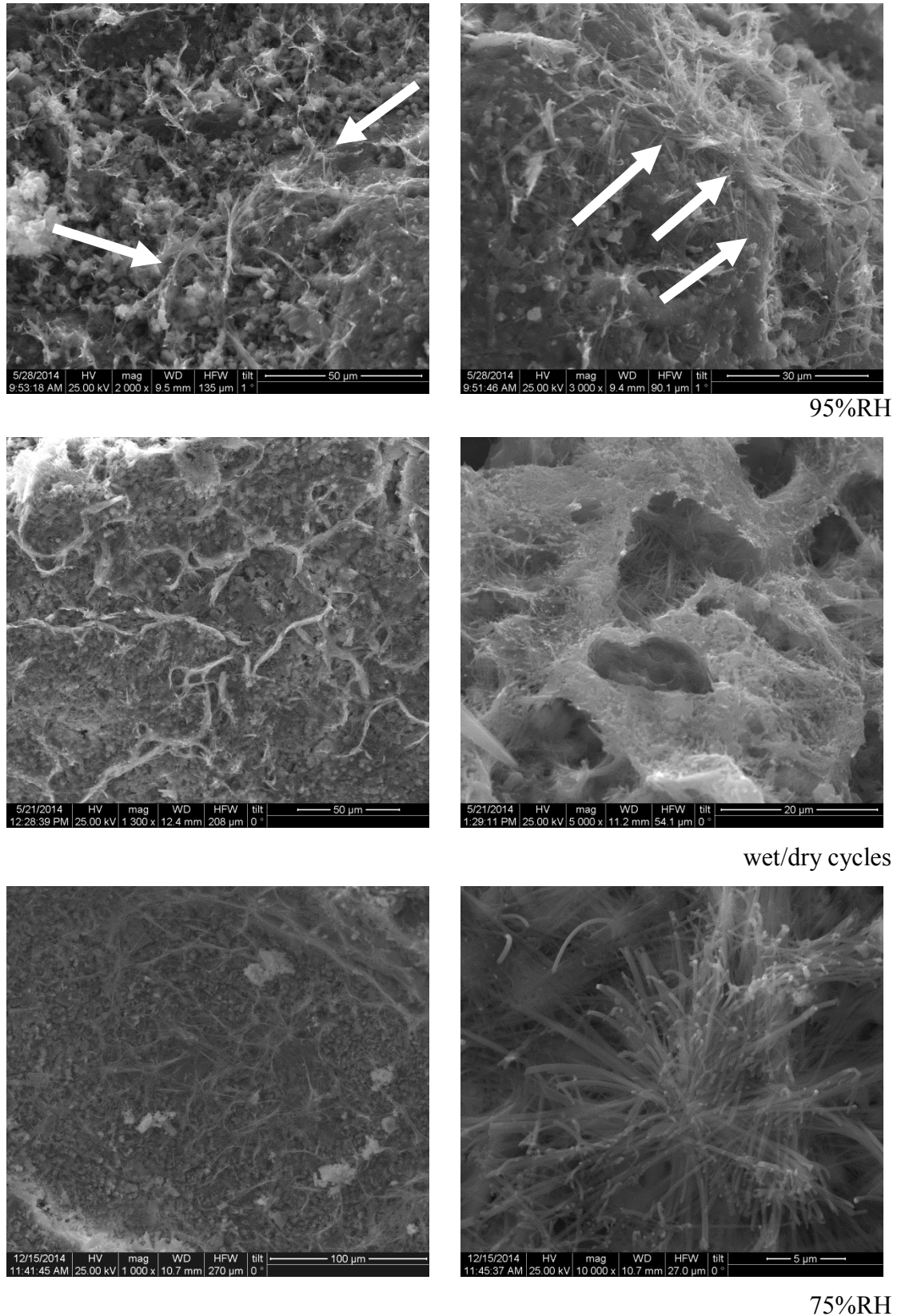


Figure 6.13: Secondary hydraulic phases at different healing conditions (95% RH, 75% RH and wet/dry cycles) develop a single uniform layer of interconnected fibers. In detail: the outward orientation of the fibers.

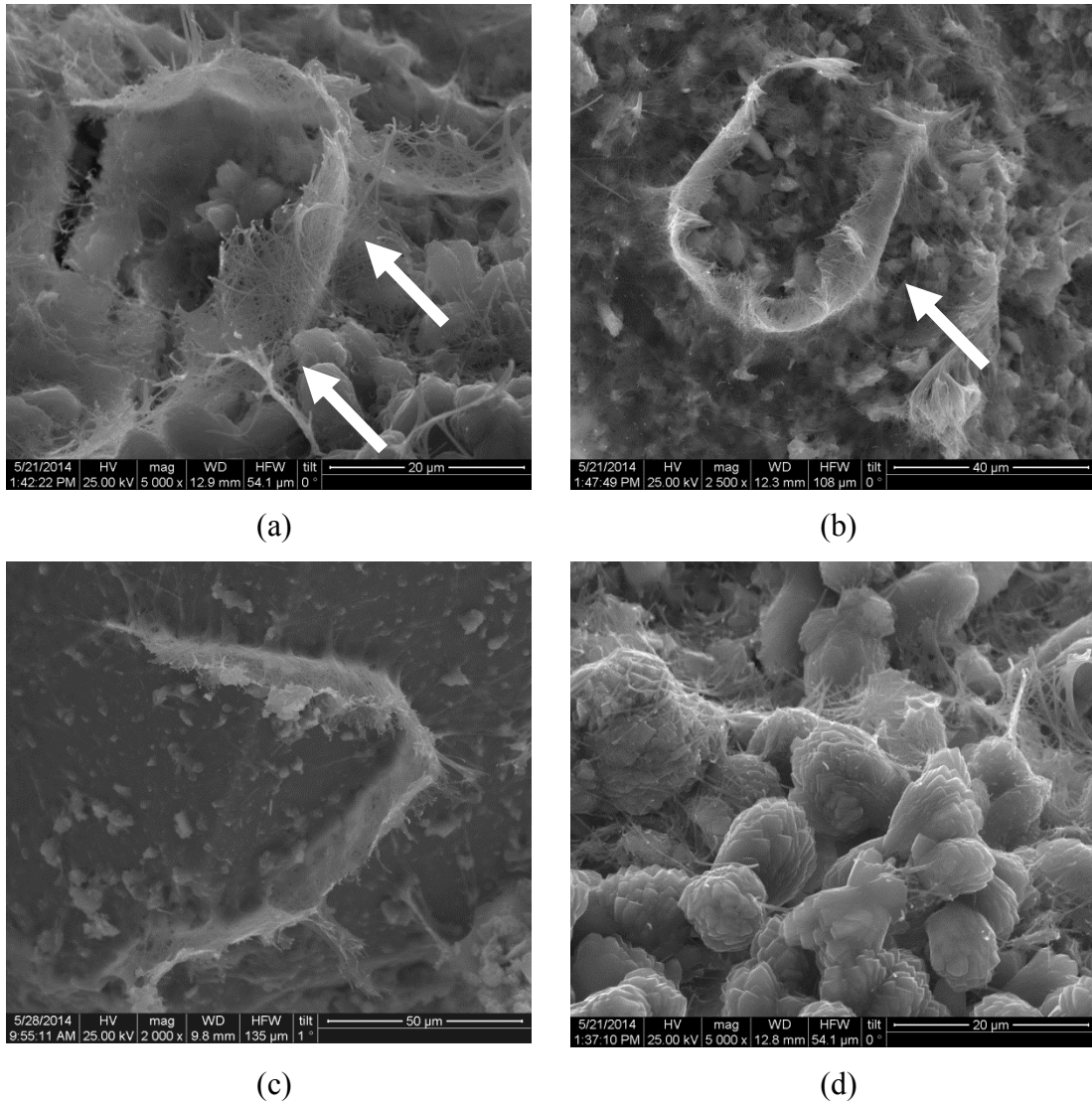


Figure 6.14: Secondary hydraulic phases are formed on various substrates such as (a) and (b) on micritic calcite in the binder matrix, (c) on the surface of aggregates and (d) together with secondary calcite.

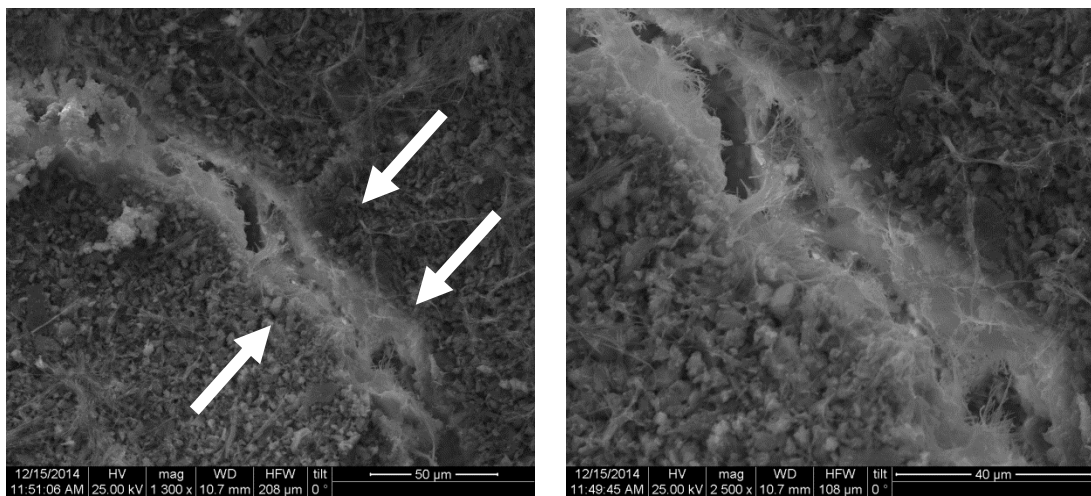
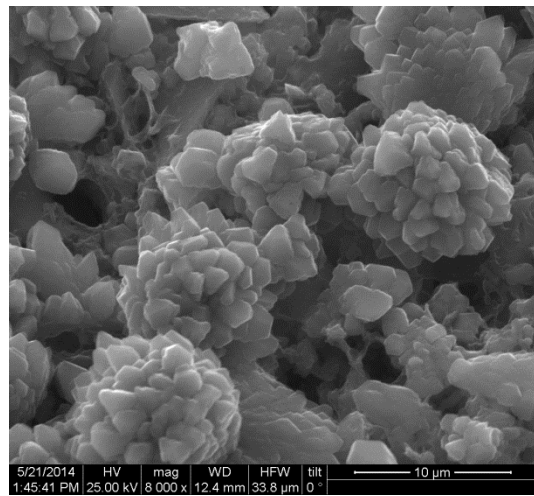
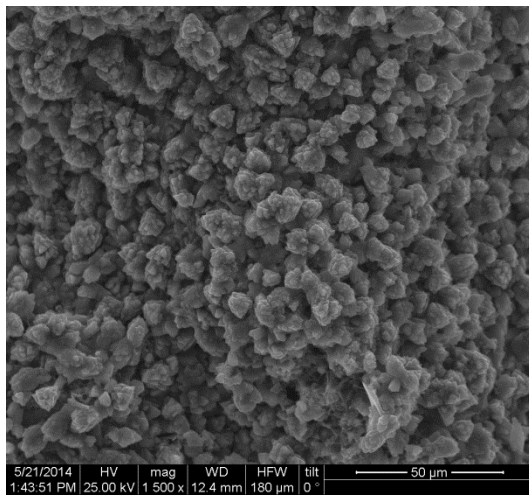
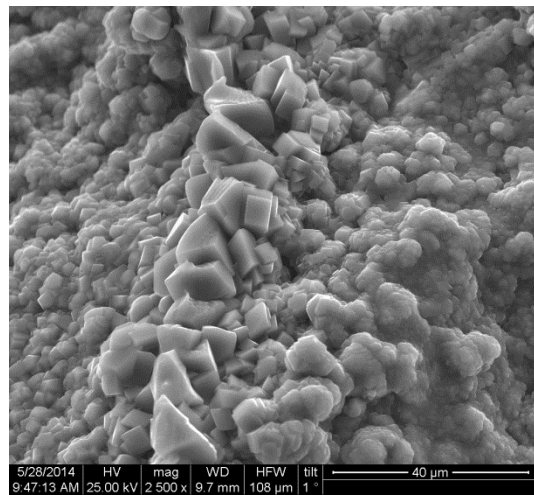
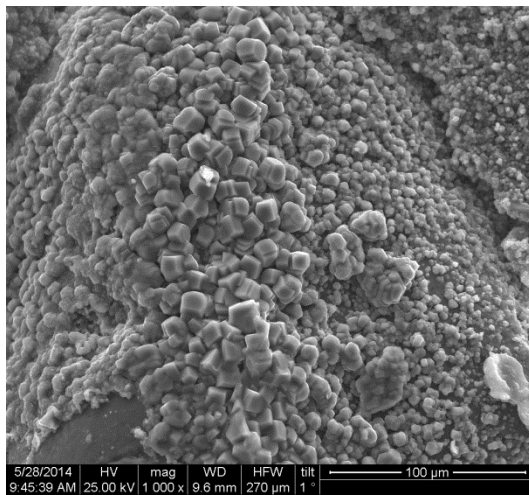


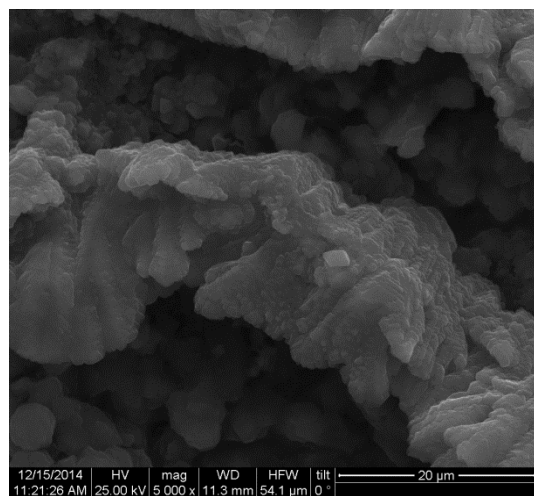
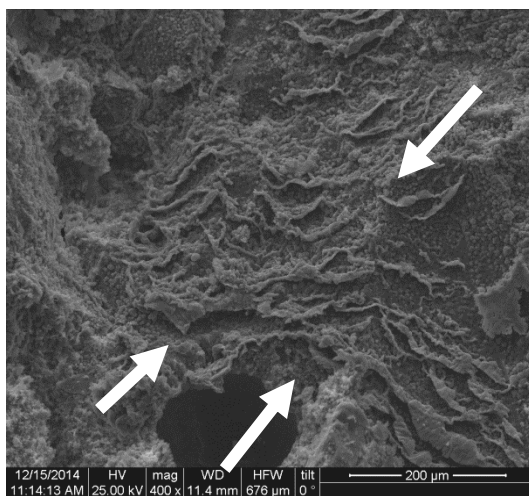
Figure 6.15: Fiber-like secondary hydraulic phases bridging a micro-crack of ~30 μm width.



95%RH



wet/dry cycles



75%RH

Figure 6.16: Morphology of CaCO₃ developed at different humidity levels (95%RH, 75% RH and wet/dry cycles)

LP1590

LP specimens cracked at early age (15 d) and then healed for a prolonged period (90 d) exhibited extended networks of hydraulic phases similar to LP1530 (Fig 6.17), together with extensive secondary calcite zones (Fig 6.18).

Moreover, secondary hydraulic phases were observed bridging cracks identical to the mechanism described for LP1530. However, the microcracks completely healed after 90 days are substantially wider ($\sim 70 \mu\text{m}$) while the healing network appears more dense (Fig 6.19).

Likewise, the extent of the secondary calcite precipitation appears to be more advanced due to the prolonged healing period. In figure 6.20 a part of a secondary calcite precipitation layer is shown. Secondary calcite was formed on both sides of the crack filling their in-between space. Nevertheless due to the separation of the two crack walls, during sample preparation, secondary calcite precipitated on the opposite side of the crack was detached from its substrate. This could be attributed to a low cohesion between precipitated calcite and the binder matrix. It is possible that secondary calcite results by in-situ carbonation of un-reacted portlandite of the cement-matrix, or as this image suggests, by precipitation of calcite from the pore solution. In the latter case, the cohesion of the secondary phases to the binder matrix is expected to be lower.

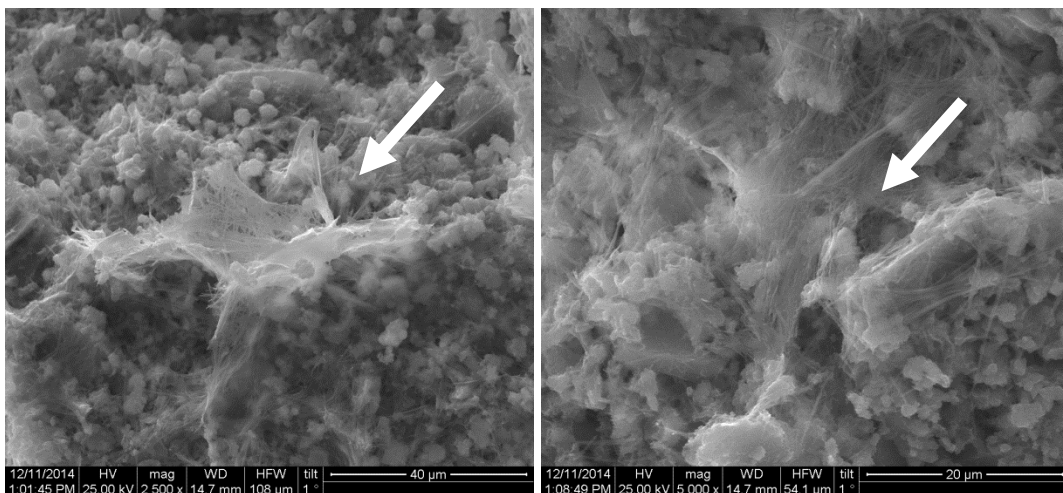


Figure 6.17: Secondary fiber-like hydraulic phases

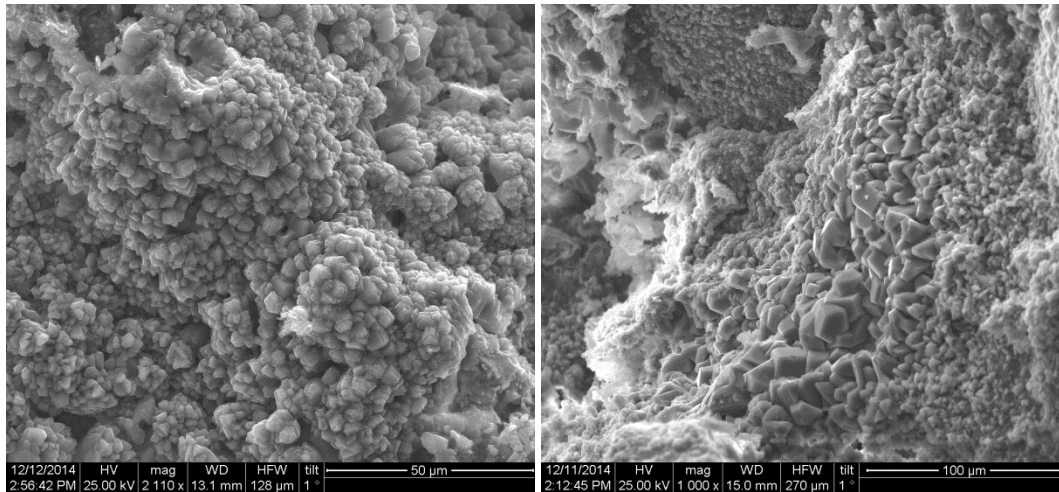


Figure 6.18: Extended zones of secondary calcite precipitation on the crack surface

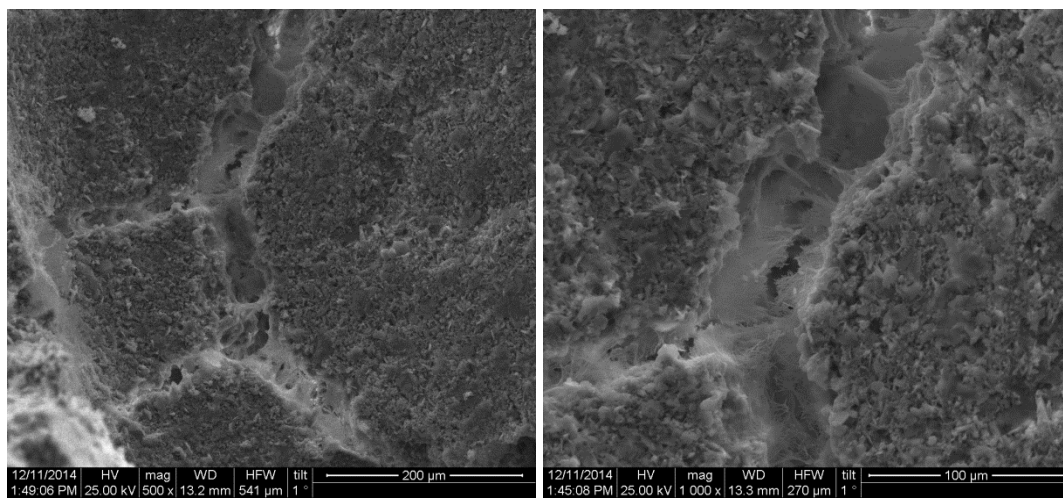


Figure 6.19: Fiber-like secondary hydraulic phases bridging a ~70 µm micro-crack.

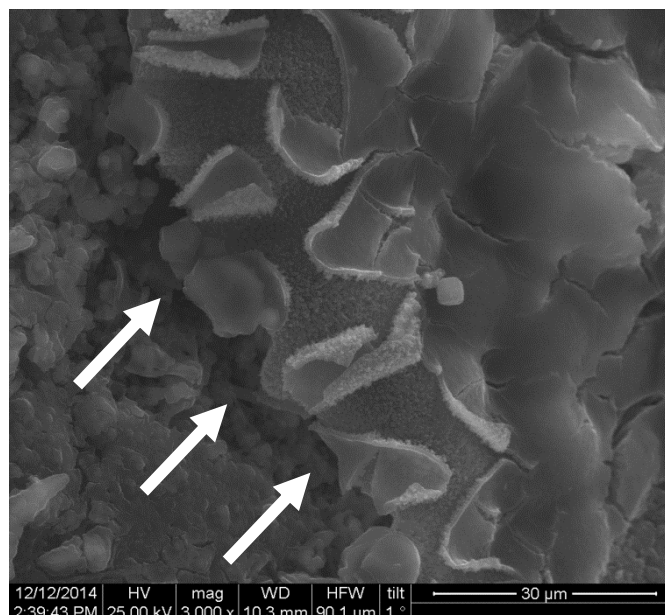
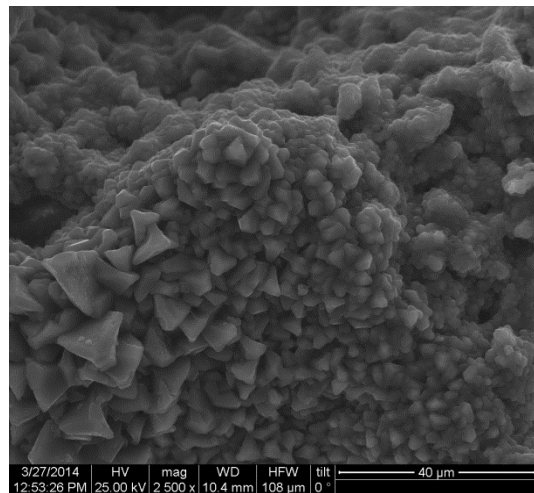
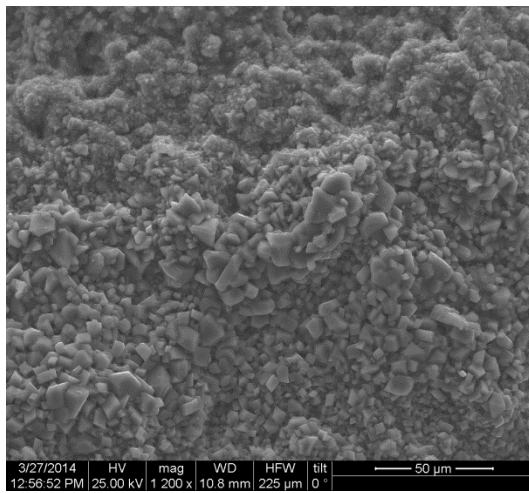


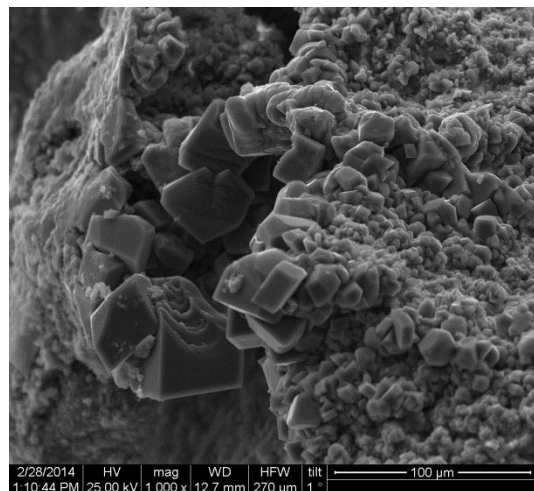
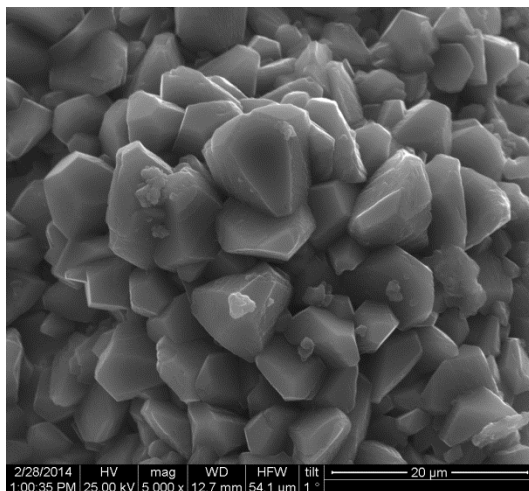
Figure 6.20: Precipitated secondary calcite probably severed during sample preparation. The low cohesion to the binder matrix is evident

LP3030

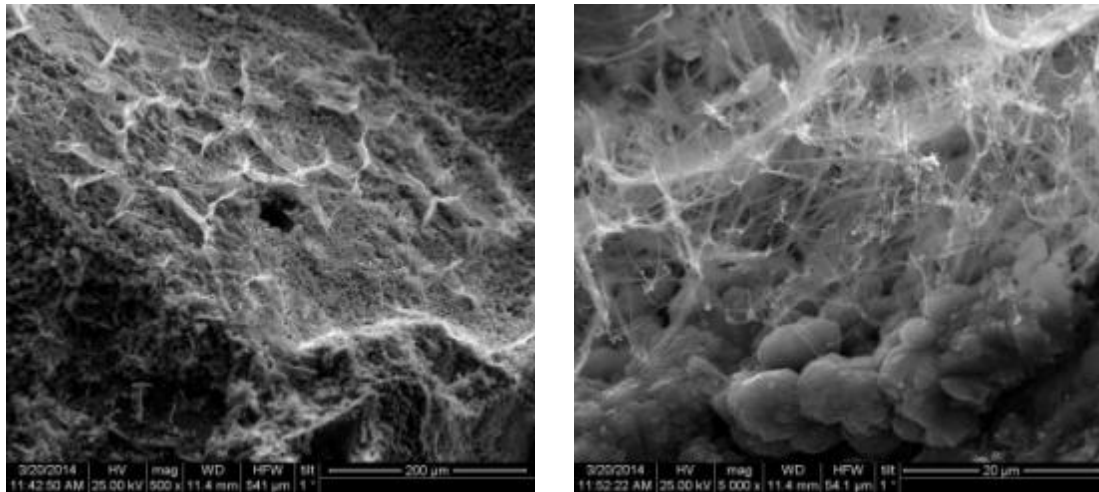
Contrary to the findings in early – age cracked LP specimens, when cracking takes place at later –age (30 d) calcite is the main secondary product observed (Fig 6.21). Hydration products, similar with the ones observed in LP1530 specimens, are observed mainly at humidity levels of 75%RH. This could be related to the availability of unreacted phases in the crack surface at the time that cracking occurs. Higher humidity conditions seem to have a favorable impact on the evolution of the carbonation mechanism. This was also confirmed during the examination of the polished surfaces (Fig.6.22).



wet/dry cycles



95%RH



75%RH

Figure 6.21: Main products formed on the crack surface of LP specimens cracked after 30 days of curing.

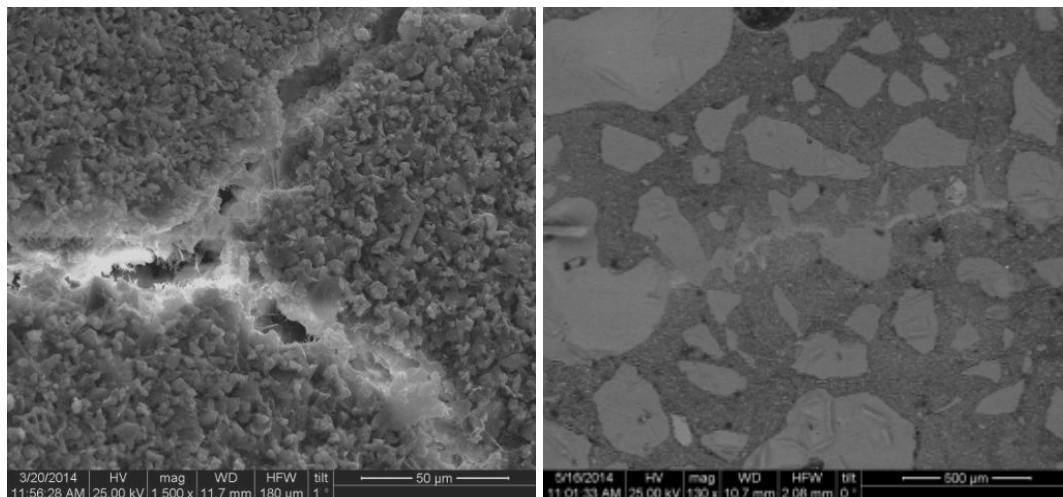


Figure 6.22: Microphotographs of LP303075. Hydration products formed along a smaller perpendicular crack (left) and a micro crack completely filled by calcite (right).

LP3090

Similarly to LP3030, in LP3090 specimens, where an extended healing period was applied, secondary calcite was observed (Fig.6.23). However, the size of calcite crystals were larger (50 μm), compared to the ones observed in LP3030. This suggests that secondary carbonation is an ongoing mechanism during which larger calcite crystals are produced.

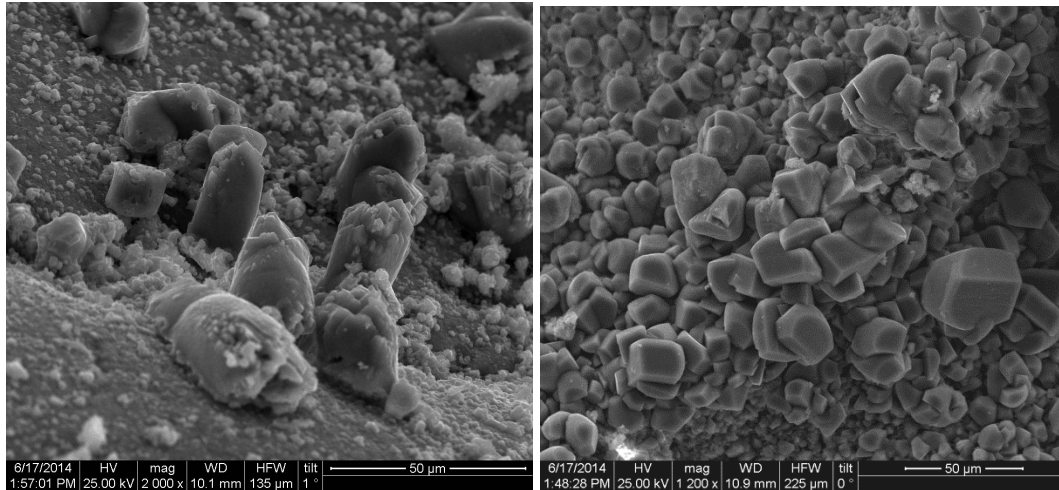


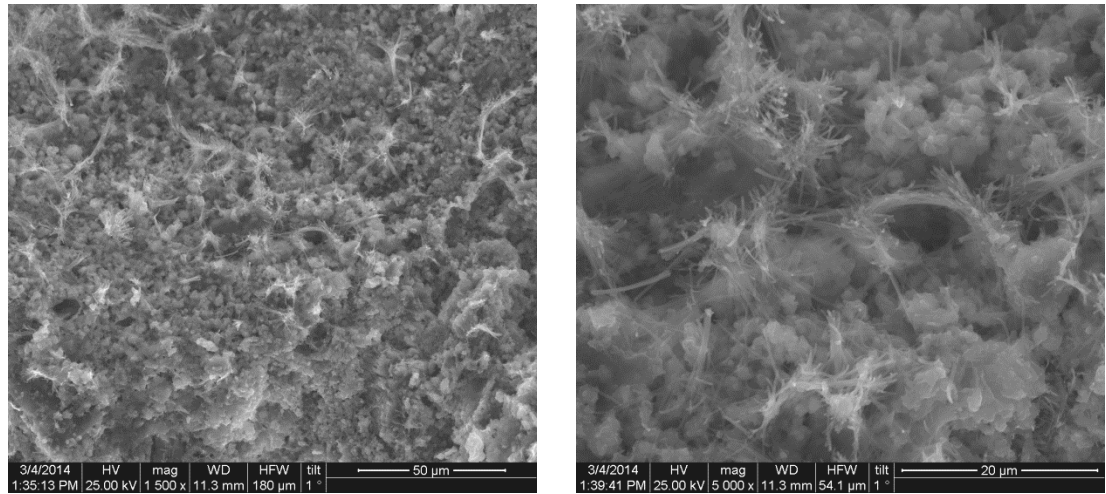
Figure 6.23: Well-formed secondary calcite crystals up to $\sim 50\ \mu\text{m}$ in diameter.

NHL730

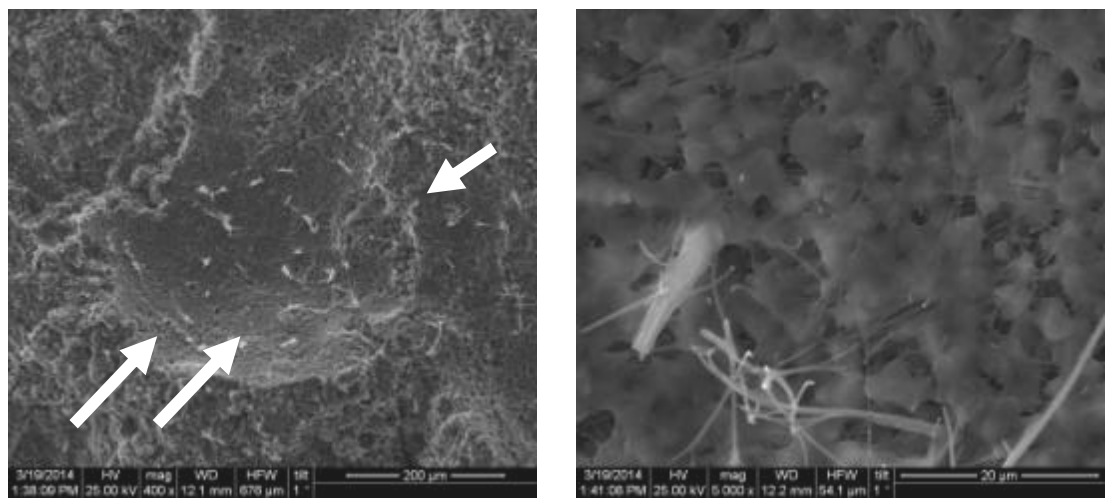
In NHL specimens the presence of secondary hydraulic phases is observed in specimens cured at RH 95% and wet/dry cycles, whereas, no secondary phases were identified in specimens healed under humidity conditions of 75% and 45%RH, suggesting a higher humidity threshold ($>75\%$) for the self-healing phenomenon to take place.

NHL specimens cracked at early age (7 d) and then healed for 30d, similar to LP specimens, exhibited extended networks of hydraulic phases (Fig 6.24) when cured under conditions of 95%RH and wet/dry cycles. In the case of wet/dry cycles the hydraulic phases created separate networks of a bee-hive formation (Fig 6.25). This formation appears more solid, however higher magnification reveals the presence of CSH fibers, suggesting a similar mechanism.

In specimens cured at 95% RH two more types of hydraulic phases were observed. Typical CSH needle-like formations were identified in dense formations (Fig 6.26) throughout the crack surface whereas more sporadically, highly gelatinous hydraulic phases are detected (Fig 6.27). However, the presence of calcite was not obvious on the crack surface, irrespective of the humidity conditions of healing.



wet/dry cycles



95%RH

Figure 6.24: Secondary fiber- like hydraulic phases in NHL specimens cured under wet/dry cycles and at 95%RH.

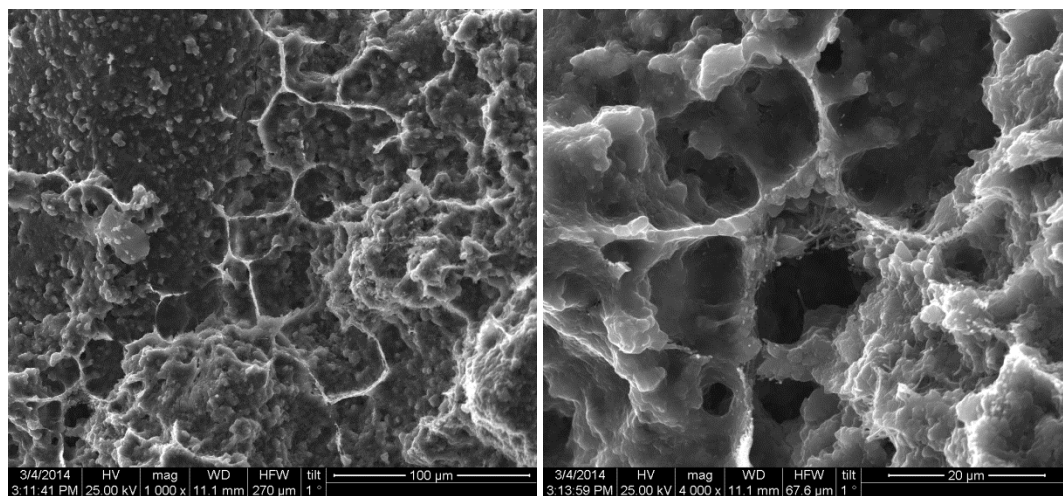


Figure 6.25: Honeycomb formation observed in specimens cured under wet/dry cycles and detail.

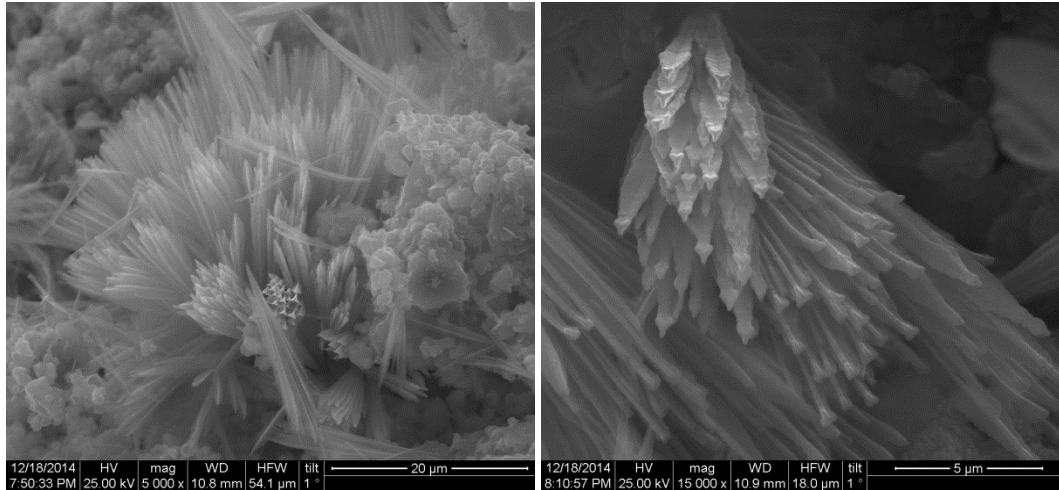


Figure 6.26: CSH needle-like formations observed in specimens cured at 95%RH.

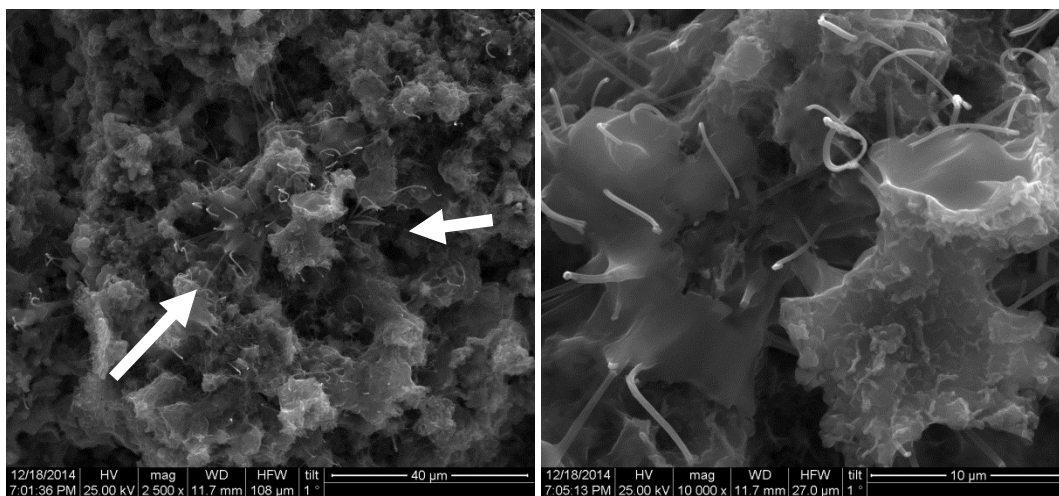


Figure 6.27: Highly gelatinous hydraulic phases in specimens cured at 95%RH

NHL790

In NHL specimens cracked at early age (7 d) and then healed for an extended period (90 d), networks of fiber and needle-like hydraulic phases were observed (Fig 6.28) along with expanded bee-hive formations (Fig. 6.29). The observation of these two types of secondary products suggests that the prolonged healing period results in the accumulation of more dense secondary phases produced by the evolution of the same reactions.

Nevertheless, in specimens healed under wet/dry cycles, the presence of secondary calcite is also predominant (Fig 6.30). It is noteworthy that layers of well-formed calcite crystals are precipitated alongside dense networks of hydraulic phases. This suggests that the carbonation mechanism is facilitated by wet/dry cycles while its evolution is slower.

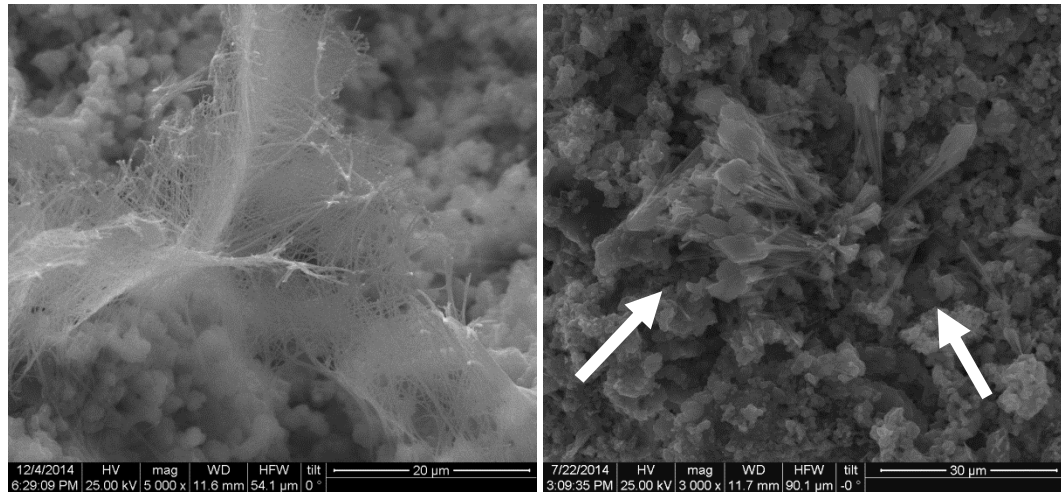


Figure 6.28: Secondary fiber and needle-like hydraulic phases in specimens healed for 90 days.

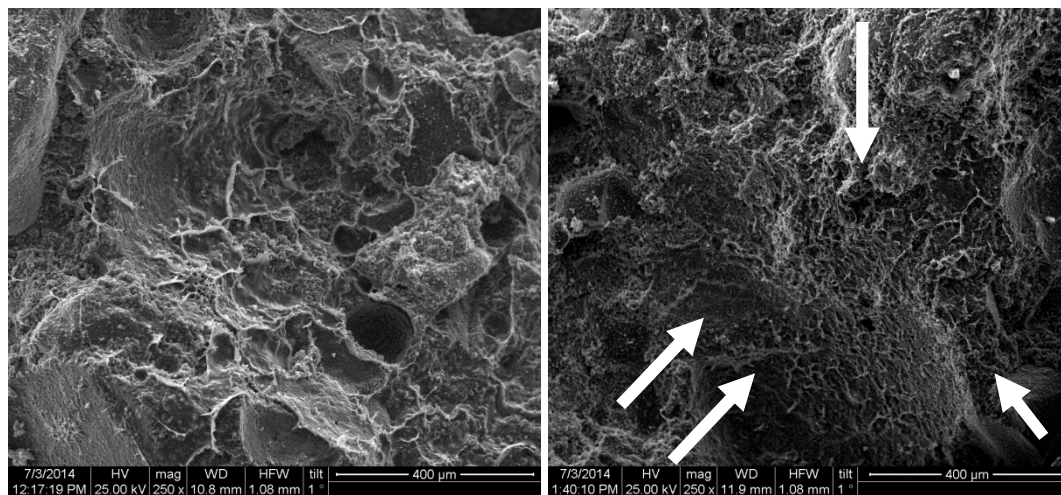


Figure 6.29: Expanded honeycomb formations in specimens healed for 90 days.

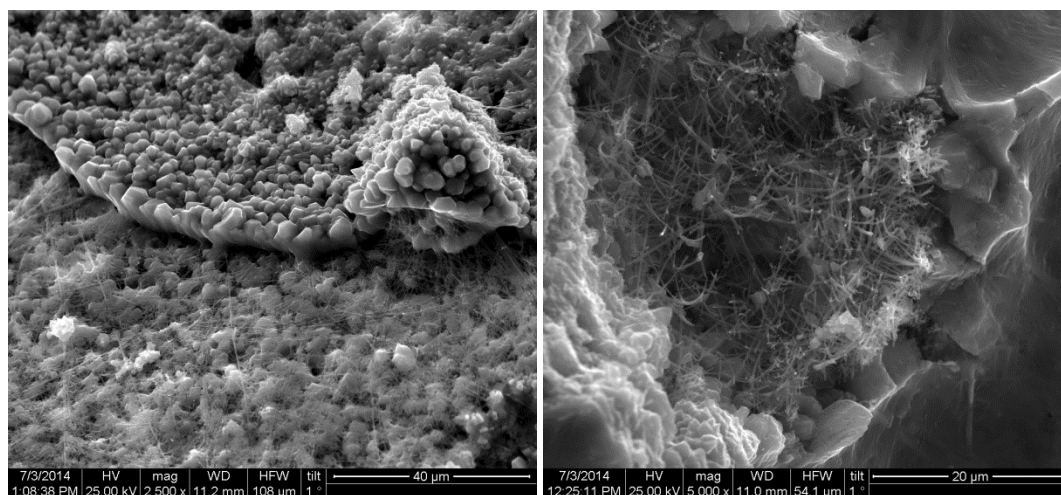


Figure 6.30: Layers of well-formed calcite crystals are precipitated alongside dense networks of fiber-like hydraulic phases, in specimens healed under wet/dry cycles

NHL3030

Contrary to the findings in early – age cracked NHL specimens, when cracking takes place at later age (30 d) needle-like formations are the main secondary products observed. However, more dense conglomerates are detected, which form large crystal-like formations (Fig 6.31).

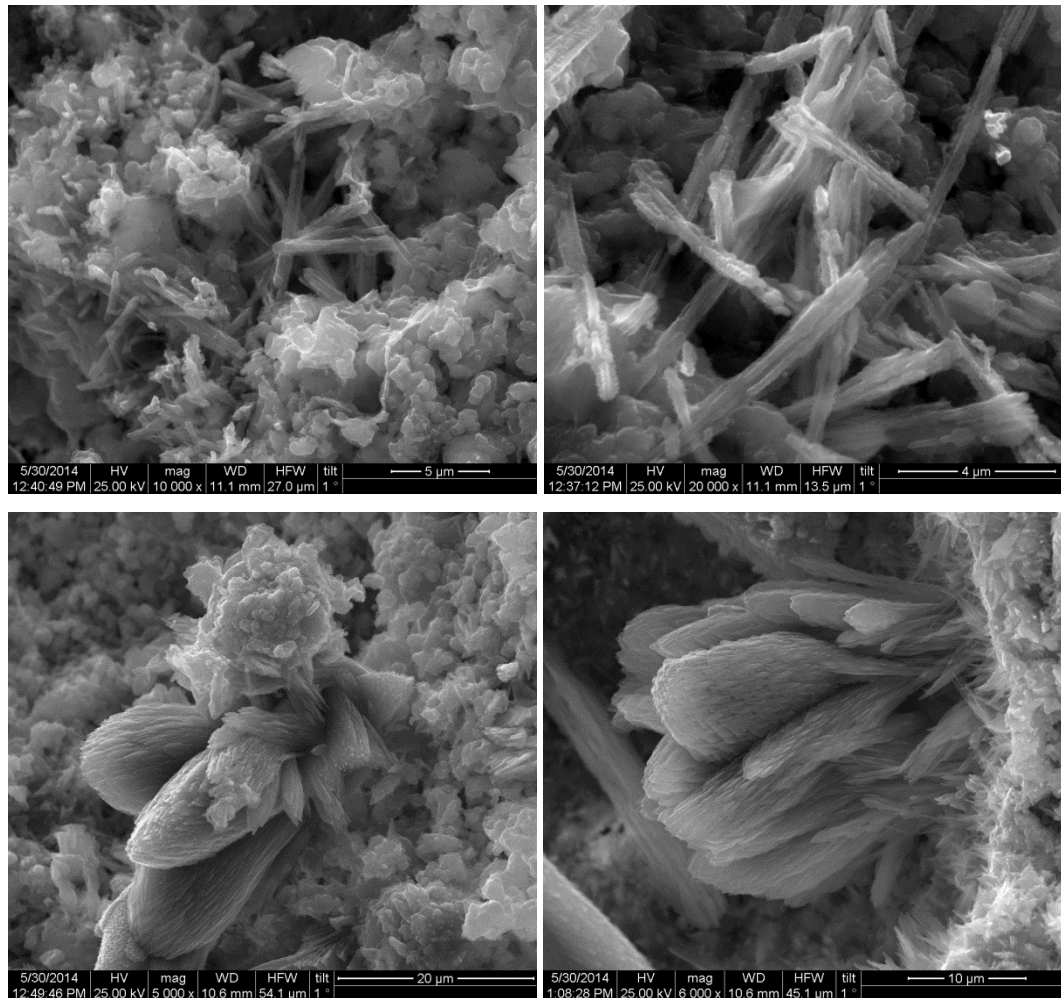


Figure 6.31: Conglomerates of needle-like formations in NHL specimens cracked after 30 days of curing.

NHL3090

The same observations apply to NHL specimens cracked at later age (30 d) but healed for an extended period of 90 days. Needle-like secondary phases are predominant (Fig 6.32), which indicates that this is the main mechanism by which self healing could occur, when cracking takes place at a later age, regardless of the healing period.

Moreover, in contrast with NHL790, the presence of calcite was not detected, despite the prolonged healing period something which was found in NHL 790 and was attributed to the long healing period.

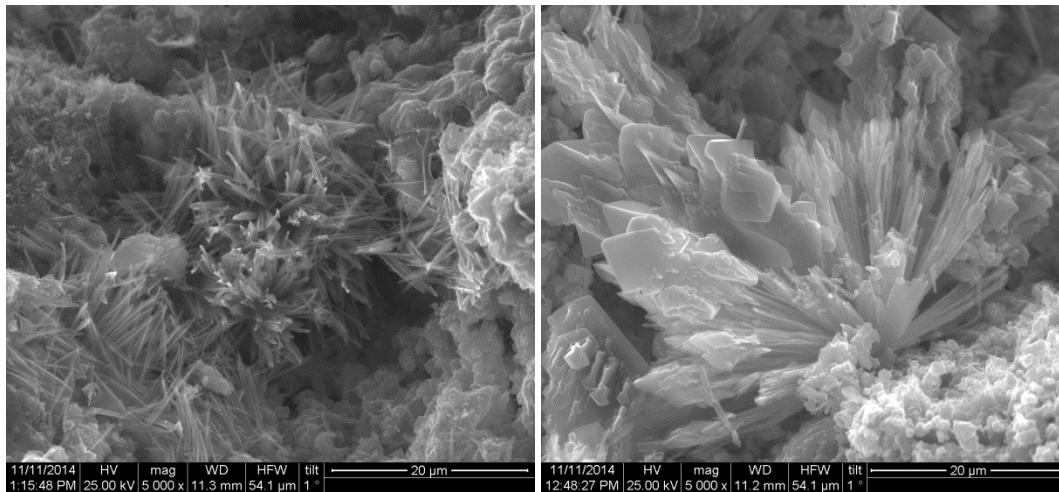


Fig 6.32: Needle-like formations in NHL specimens cracked after 30 days of curing and healed for 90 days.

6.3.2 Classification of secondary products by chemical characterization

The observation of the crack surfaces at the SEM revealed a variety of secondary products formed during each healing condition. The secondary products were classified into two main groups, namely carbonation and hydration products. Chemical examination performed at SEM/EDAX confirmed the two main groups (Fig. 6.33); polymorphs of calcium carbonate are crystal-like products, whereas gel-like products consisted of different hydraulic phases (CSH and CAH).

The classification seen in Figure 6.28 is due to the Ca/Si ratio differentiation between the products analyzed. Ca/Si ratio of crystal-like products, ranging from 13 to 30, is much higher than that of gel-like products, which range from near-zero values up to 7. Gel-like products show a higher dispersion than crystal-like, as to the Al/Si ratio, which suggests that there is a wide variety in the stoichiometry amongst the hydraulic phases.

Secondary phases produced in NHL specimens displayed higher diversity in Al/Si ratio, whereas a sub-group was identified amongst gel-like products, which seem to be richer in aluminum. In contrast, secondary products in LP specimens exhibited a very narrow distribution in regard to Al/Si ratio, whereas a clear separation as to Ca/Si ratio (crystal vs. gel-like products).

The different types of hydraulic phases identified according to their morphological characteristics, correspond to varying Al/Si ratios. Fiber-like hydraulic phases, which were the only-type of secondary hydraulic product identified in LP mortars, display an Al/Si ratio narrow distribution, suggesting a common chemical composition. Whereas, the variety of secondary hydraulic products identified in NHL mortars is expressed by the corresponded variations of Al/Si ratio. Low Al/Si ratio was matched to highly gelatinous hydraulic phases while high Al/Si ratios correspond to needle – like hydraulic phases.

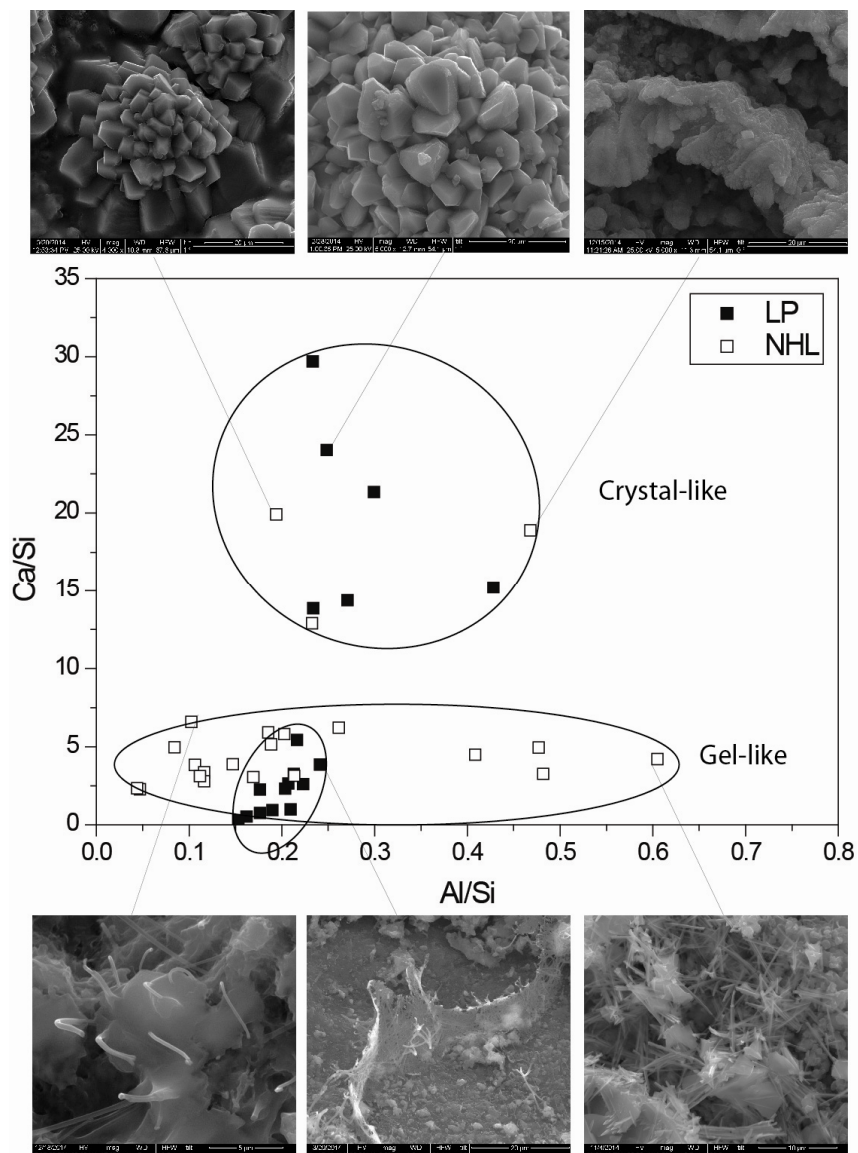


Figure 6.33: Analysis of the secondary products performed by EDAX revealed the two main groups formed in the examined specimens.

6.4 Discussion

The occurrence of different healing products varies between the samples examined, but there are some repetitive patterns than can be recognized.

6.4.1 Effect of curing time prior to cracking on the formation of healing products (Moment of cracking)

The effect of cracking at early-age was studied in specimens cured for 15 (LP) and 7 days (NHL) before cracking, as both mixtures are characterized by a higher amount of reactive portlandite (free-lime), compared with those cracked after 30 days of curing (Fig. 6.6).

In both NHL and LP specimens, when cracked at early age, continued hydration is identified as one of the mechanisms that take place. Hydration products were observed in LP mortars, mainly as fiber-like formations (Fig. 6.34), while their density and distribution frequency is higher for early-age cracked specimens. In NHL mortars, secondary hydraulic products were observed (Fig. 6.34-6.36) regardless of the moment of cracking. Nevertheless, in later-age cracked specimens mainly needle-like hydration products were identified.

This could be attributed to the fact that hydration mechanism is a multi-step mechanism during which CSH products of different morphology are identified (Arizzi and Cultrone, 2012). More specifically, fiber-like CSH products are produced first and are characterized by a highly porous continuous layer that improves the cohesion of the microstructure. Fiber-like or “low-density” CSH tends to occupy larger space, previously occupied by the pore solution (Regourd, 1986). This first step is controlled by the availability of calcium hydroxide in the liquid phase (Odler, 1998). Subsequently, as the concentration of calcium hydroxide decreases, needle-like CSH is produced by unreacted C_2S phases. This type of CSH is referred to as “high-density” C-S-H, and is characterized by lower porosity and a more stable configuration (Jennings et al., 2007) as an interlocking or honeycomb structure (Diamond, 1986). The formation of “high-density” CSH is slower and compared to “low-density” CSH, these products are formed inhomogeneously.

In both NHL and LP mortars cracked at early age the concurrence of higher concentration of portlandite and high humidity conditions, at the time cracking occurred, supported the production of “first-step” fiber-like CSH phases. In the case

of later-age cracking NHL specimens the main product was “second-step” needle-like CSH possibly due to the lower concentration of portlandite.

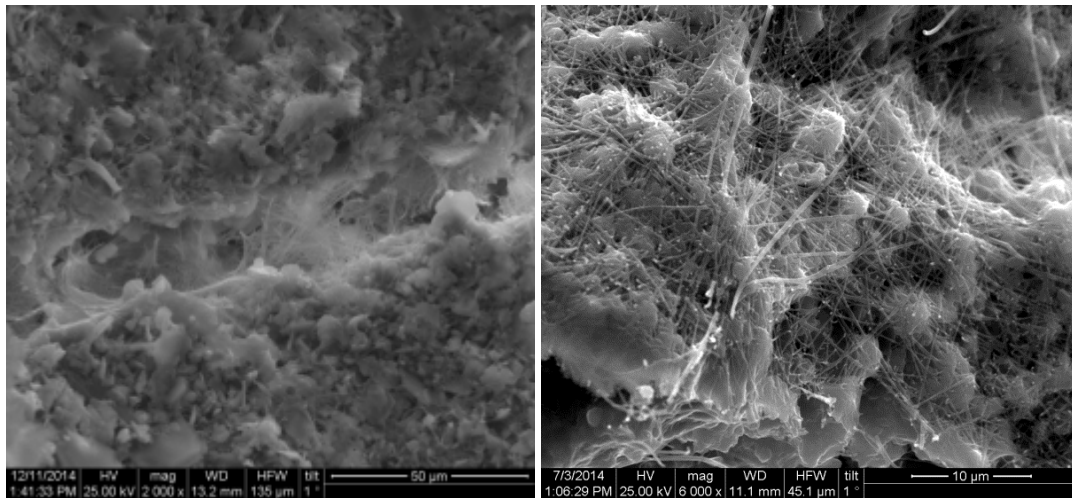


Figure 6.34: First-step, fiber-like or “low-density” CSH forms a continuous layer.

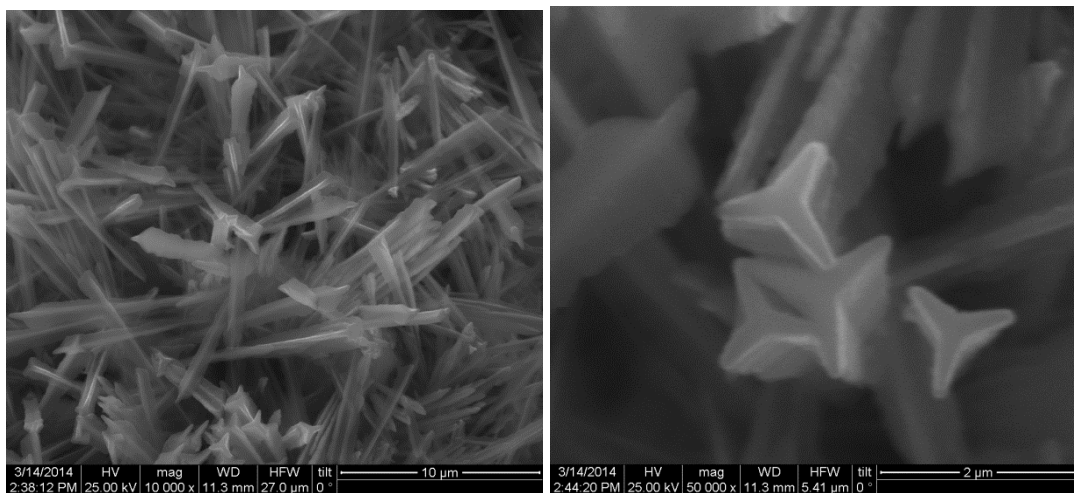


Figure 6.35: Second-step needle-like CSH hydration products and detail

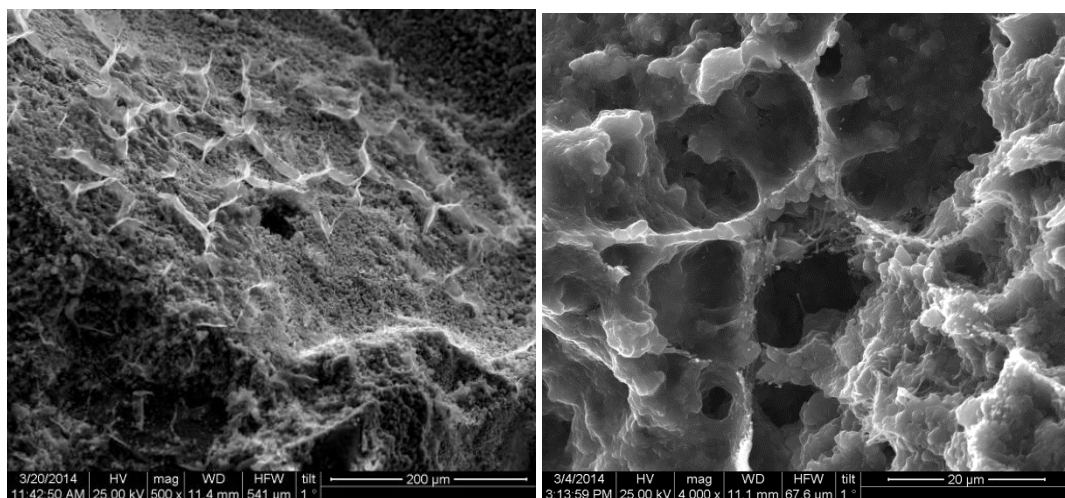


Figure 6.36: Second-step honeycomb CSH formations

The carbonation products display a large diversity in terms of both crystal shape and size (Fig. 6.37). The evolution of the carbonation reaction is controlled mainly by two factors; namely the diffusion of CO_2 in the pore solution and the concentration of portlandite in the binder matrix (Saetta et al., 1994). The moment of cracking affects the secondary precipitation of calcite, as it is correlated with the available portlandite at that time. Furthermore, it is a relatively slow process as it entails the dissolution of available portlandite and the diffusion of CO_2 in the pore water, together with the conditions of precipitation. Moreover, due to the differential diffusion of CO_2 in the water, carbonation tends to begin near the crack mouth and spread from the outside towards deeper in the crack (Sisomphon et al., 2012).

The presence of calcite is observed mainly in LP specimens, whereas in NHL specimens, calcite was largely observed in specimens cracked at early age (7 d) and cured for prolonged period (90 days). However, it was not evident when specimens that were cracked at later-age, even after a prolonged healing period. This could be correlated with the decrease of available portlandite present in the binder between 7 and 30 days of curing.

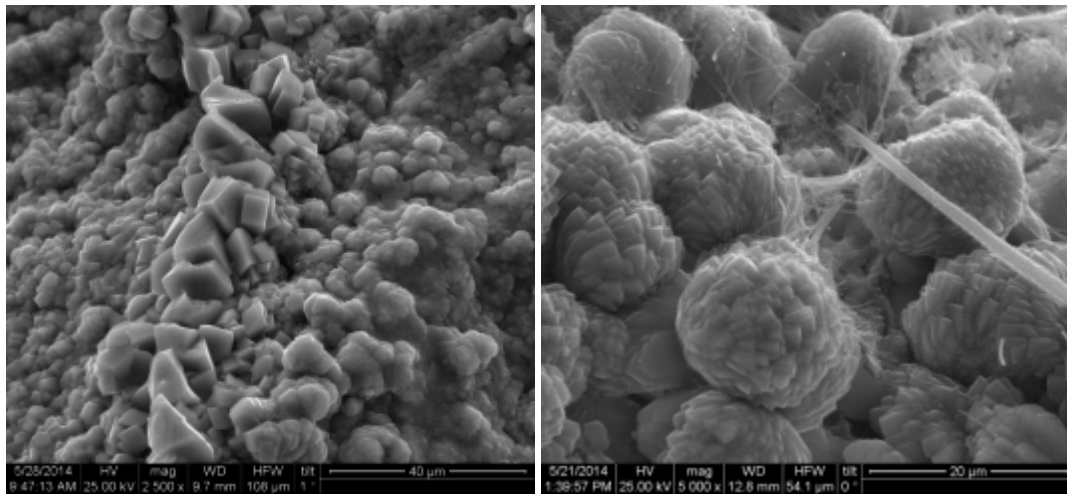


Figure 6.37: Typical patterns of calcium carbonate formations of varying size and morphology.

6.4.2 Effect of Healing Conditions on the formation of healing products

Concerning the effect of humidity level, in samples cured at 45% RH -regardless of their composition, age of cracking and healing period - no secondary products were observed. In the specimens cured at 75% RH, the secondary products were not

observed in NHL mortars, whereas LP mortars revealed an abundance of hydraulic secondary phases.

The precipitation of vaterite was also observed under the same humidity conditions (75%RH). Vaterite is formed as a metastable phase of calcium carbonate. The fact that it is not present in samples cured for an extended healing period (90 days) suggests its transformation to calcite and a multi-step crystallization mechanism.

In later-age cracked LP specimens cured at higher humidity levels (95%RH or wet-dry cycles) the formation of secondary calcite dominates. However, secondary hydration products along with calcite were observed when the same specimens were cured at 75% RH.

Finally, regarding NHL specimens at 75% RH, no major secondary products were observed. Similar mechanism was found to take place when specimens were cured at 95% RH and wet-dry cycles. However, in early age cracked NHL specimens exposed to wet-dry cycles a dense network of “honeycomb” formations was produced and after 90 days of curing, precipitated calcite was identified too (Fig.6.38).

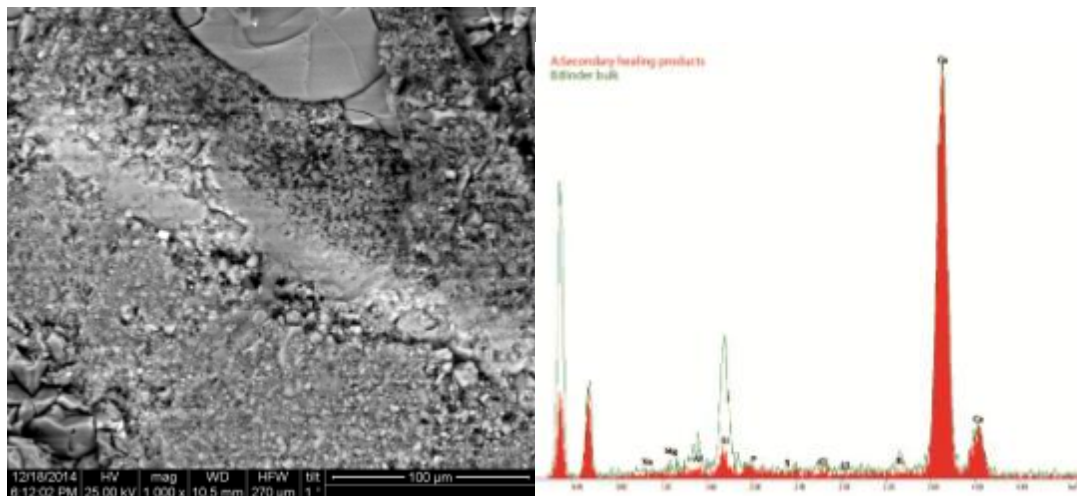


Figure 6.38: Secondary formed calcite in LP mortars completely filling a micro crack (left). Chemical characterization of secondary calcite was also determined by EDAX analysis (right).

6.4.3 Effect of Healing period on the formation of healing products

After prolonged healing period, both carbonation and hydration mechanisms are evolved, especially when early-age cracking occurs. When subjected to wet-dry

cycles and cured at 95% RH, the prolonged healing time resulted in the enrichment of the crack surface with gel-like products. Similarly, fiber-like secondary hydraulic phases were observed bridging wider micro-cracks (Fig. 6.39).

Likewise, the extent of the secondary calcite precipitation appears to be more advanced due to the prolonged healing period. This was corroborated by the observation under polarizing microscope of LP and NHL samples cured by wet/dry cycles in polished sections (Fig. 6.40-6.41). After 30 cycles calcite precipitation was more advanced, which suggests an ongoing mechanism (Fig. 6.41).

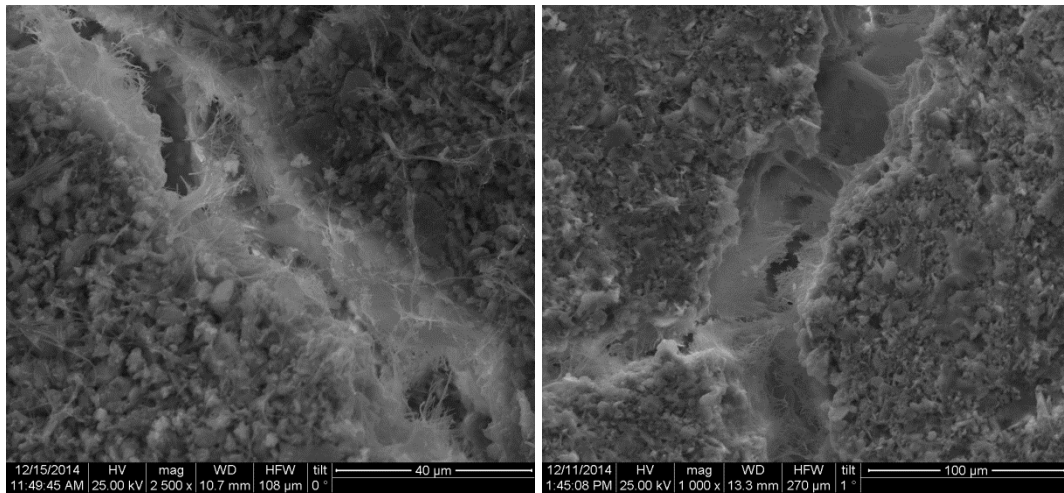


Figure 6.39: Fiber-like secondary hydraulic phases bridging micro-cracks of ~30 and ~70 μm after prolonged healing period.

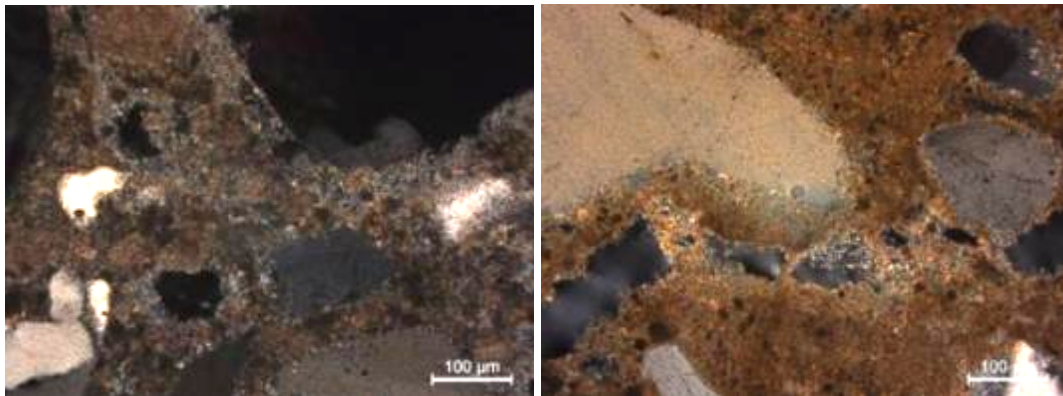


Figure 6.40: Secondary formed calcite in NHL mortars after ten (left-NHL730cy) and thirty wet-dry cycles (right-NHL790cy).

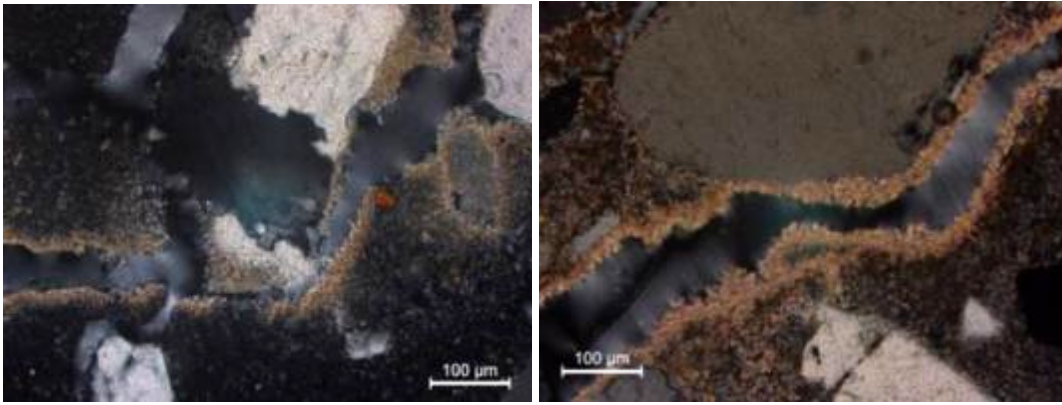


Figure 6.41: Secondary formed calcite in LP mortars after ten (left-LP1430) and thirty wet-dry cycles (right-LP1490). It was observed that the precipitation of calcite advances with additional cycles.

Table 6.3: Synopsis of the main microscopic observations

	Hydraulic products	Carbonated products	Other observations
LP1530	fiber-like CSH	calcite and vaterite	~30 µm crack filled with fiber-like CSH
LP1590	fiber-like CSH	calcite	~70 µm crack filled with fiber-like CSH
LP3030	fiber-like CSH	calcite	~30 µm sparitic calcite
LP3090	fiber-like CSH	calcite	~50 µm sparitic calcite
NHL730	fiber-like and needle-like CSH, bee-hive formations	-	“low-density” CSH
NHL790	fiber-like and needle-like CSH, bee-hive formations	calcite	micro-sparitic calcite
NHL3030	needle-like CSH	-	“high-density” CSH
NHL3090	needle-like CSH	-	Densification of type needle-like CSH hydraulic phases

Conclusions

Regarding the mechanisms responsible for the crack healing by secondary products, two main mechanisms were identified and correlated to the observation of the healing products; continued hydration and precipitation of secondary calcite. Although, autogenic self-healing has been attributed to both these reactions, the underlying mechanisms differ. In particular, continued hydration takes place on the crack surface, provided that reactive phases are present, whereas secondary calcite is precipitated depending on the movement of the pore solution and the solubility of the calcium-bearing phases of the binder matrix.

Nevertheless, it was shown that the availability of portlandite affects both mechanisms. The effect of cracking age was a crucial parameter to the healing efficiency, since it was correlated with the available each time portlandite at the time cracking occurred.

The study of crack surfaces under SEM revealed the presence of carbonates and a large variety of hydration products, depended on the initial composition of the binder. At the humidity level of 75%, the healing products were abundant in LP specimens, whereas in NHL were hardly spotted. Lower humidity conditions (45% RH) found to be inadequate for the evolution of the autogenous healing phenomenon to take place. Nevertheless, under these conditions a high percentage of unreacted components remain active in the mortar matrix, allowing a potential future initiation of the self-healing, when the proper conditions are reached.

Although complete healing of the main crack induced by three point bending, was not observed in any mixture, smaller side-cracks were completely filled with secondary products under specific each-time conditions.

Finally, curing time was found to be of prime importance for early-age cracked specimens, where additional curing time was found to have a substantial effect on the evolution of both mechanisms. Enrichment of the crack surface by secondary hydration products was observed while under-wet dry cycles additional secondary calcite precipitation was observed in the cracks, both in LP and NHL mortars.

Overall, the availability of water during wet-dry cycles enhanced the precipitation of secondary calcite in both LP and NHL specimens, especially when early-age cracking occurred.

References

- Arizzi, A., Cultrone, G., 2012. Aerial lime-based mortars blended with a pozzolanic additive and different admixtures: A mineralogical, textural and physical-mechanical study. *Construction and Building Materials* 31, 135–143.
doi:10.1016/j.conbuildmat.2011.12.069
- Balen, K.V., Gemert, D.V., 1994. Modelling lime mortar carbonation. *Materials and Structures* 27, 393–398. doi:10.1007/BF02473442
- Cizer, Ö., Rodriguez-Navarro, C., Ruiz-Agudo, E., Elsen, J., Gemert, D. V. and Balen, K. V. (2012): “Phase and Morphology Evolution of Calcium Carbonate Precipitated by Carbonation of Hydrated Lime”. *Journal of Materials Science*. Vol.47, No.16, 6151-6165.
- Çopuroğlu, O., Schlangen, E., Nishiwaki, T., Tittelboom, K.V., Snoeck, D., Belie, N.D., Rooij, M.R. de, (2013): “Experimental Techniques Used to Verify Healing”, in: Rooij, M. de, Tittelboom, K.V., Belie, N.D., Schlangen, E. (Eds.), *Self-Healing Phenomena in Cement-Based Materials*, RILEM State-of-the-Art Reports. Springer Netherlands, pp. 19–63.
- Diamond, S., 1986. Cement Paste Microstructure in Concrete. MRS Online Proceedings Library Archive 85. doi:10.1557/PROC-85-21
- Edvardsen, C. (1999): “Water Permeability and Autogenous Healing of Cracks in Concrete.” *ACI Materials Journal* Vol. 96, No. 4, 448–54.
- Hearn, N. (1998): “Self-Sealing, Autogenous Healing and Continued Hydration: What Is the Difference?” *Materials and Structures* Vol.31, No. 8, 563–67.
- Hearn, N., Morley, C.T., (1997): “Self-sealing property of concrete—Experimental evidence”. *Materials and Structures* Vol. 30, 404–411.
- Huang H., Ye G., and Damidot D. (2013): “Characterization and quantification of self-healing behaviors of microcracks due to further hydration in cement paste”. *Cement and Concrete Research* Vol. 52, 71–81.
- Huang, H., and Ye G. (2015) “Self-Healing of Cracks in Cement Paste Affected by Additional Ca²⁺ Ions in the Healing Agent.” *Journal of Intelligent Material Systems and Structures*, vol. 26, No. 3, 309-320
- Jacobsen, S., Marchand, J., Hornain, H. (1995) “Sem Observations of the Microstructure of Frost Deteriorated and Self-Healed Concretes.” *Cement and Concrete Research* Vol. 25, No. 8
- Jennings, H.M., 1983. The Developing Microstructure in Portland Cement, in: GHOSH, S.N. (Ed.), *Advances in Cement Technology*. Pergamon, pp. 349–396.
doi:10.1016/B978-0-08-028670-9.50016-8
- Jennings, H.M., Thomas, J.J., Gevrenov, J.S., Constantinides, G., Ulm, F.-J., 2007. A multi-technique investigation of the nanoporosity of cement paste. *Cement and Concrete Research*, Cementitious Materials as model porous media: Nanostructure and Transport processes July 2005, Centro Monte Verita, Switzerland 37, 329–336.
doi:10.1016/j.cemconres.2006.03.021
- Karatasios, I., Amenta, M., Tziotziou, M., Kilikoglou, V., (2012): “The Effect of Relative Humidity on the Performance of Lime-Pozzolan Mortars”, in: Valek, J., Hughes, J.J.,

- Groot, C.J.W.P. (Eds.), *Historic Mortars*, RILEM Bookseries. Springer Netherlands, 309–318.
- Lauer and Slate. (1956): “Autogenous Healing of Cement Paste.” *ACI Journal Proceedings*. Vol. 52, No. 6
- Lubelli, B., Nijland, T. G. , van Hees R. P. J. (2012): “Simulation of Self-Healing of Dolomitic Lime Mortar,” *Materiali In Tehnologije* Vol.46, No. 3, 291-296.
- Lubelli, B., Nijland, T.G., van Hees, R.P.J. (2011): “Self-healing of lime based mortars: microscopy observations of case studies”. *Heron* Vol. 56(1/2), 75–91.
- Moorehead, D.R., (1986). “Cementation by the carbonation of hydrated lime”. *Cement and Concrete Research* Vol.16, 700–708.
- Nijland, T.G., Larbi, J.A., van Hees, R.P.J., Lubelli, B., de Rooij, M. (2007): “Self-healing phenomena in concretes and masonry mortars: a microscopic study.” In: *Proceedings of the First International Conference on Self-healing Materials*, NoordwijkaanZee, The Netherlands, p. 31
- Regourd, M., 1986. *Microstructure of Cement Blends Containing Fly Ash, Silica Fume, Slag and Fillers*. MRS Online Proceedings Library Archive 85.doi:10.1557/PROC-85-187
- S. Diamond, “The Microstructures of Cement Paste in Concrete,” *Proceedings of the 8th International Congress on the Chemistry of Cement*, Rio de Janeiro, 1986, pp. 122-147.
- Saetta, A.V., Schrefler, B.A., Vitaliani, R.V., 1993. The carbonation of concrete and the mechanism of moisture, heat and carbon dioxide flow through porous materials. *Cement and Concrete Research* 23, 761–772. doi:10.1016/0008-8846(93)90030-D
- Schlangen, E., terHeide, N. and van Breugel, K., (2006): "Crack healing of early age cracks in concrete." In: M.S. Konsta-Gdoutos, Eds. *Measuring, monitoring and modeling concrete properties*. Netherlands: Springer
- Sisomphon, K., Copuroglu, O. and Koenders, E.A.B., (2012). "Self-healing of surface cracks in mortars with expansive additive and crystalline additive." *Cement and Concrete Composites*, Vol. 34, No.4, 566-574.
- van der Zwaag, S. (Ed.). (2007). *Self Healing Materials* (Vol. 100). Dordrecht: Springer Netherlands. <http://doi.org/10.1007/978-1-4020-6250-6>
- van Breugel K. (2012): “Self-healing material concepts as solution for aging infrastructure”. 37th Conference on our world in Concrete & Structures, Singapore. Accessed April 8, 2015.
- Xu, S., Wang, J., Sun, Y., 2015. Effect of water binder ratio on the early hydration of natural hydraulic lime. *Mater Struct* 48, 3431–3441. doi:10.1617/s11527-014-0410-8
- Yang, Y., Lepech, M.D., Yang, E.H., and Li, V.C. (2009): "Autogenous healing of engineered cementitious composites under wet-dry cycles." *Cement and Concrete Research*, Vol. 39, No. 5, 382-390.
- Zhou, G.-T., Yao, Q.-Z., Fu, S.-Q., & Guan, Y.-B. (2010). Controlled crystallization of unstable vaterite with distinct morphologies and their polymorphic transition to stable calcite. *European Journal of Mineralogy*, 22(2).].

Chapter 7: Recovery against mechanical action

7.1 Introduction

In this chapter, the evaluation of self-healing capacity of LP and NHL mortars was attempted focusing on the recovery of their mechanical strength after damage has been inflicted.

In the previous chapter, the self healing capacity of traditional (LP and NHL) mortars was discussed in relation to the secondary products observed on the crack surface. In order to determine the efficiency of the autogenous self-healing as expressed by the recovery of their mechanical properties, a separate methodology was applied. This methodology includes the introduction of controlled damage to the specimens and subsequently – after a healing period- the evaluation of the reversal of that damage by a flexural strength test.

The autogenic mechanism as it is described in the previous chapters may entail different processes; namely continued hydration and precipitation of secondary calcite. The filling of micro-cracks by secondary products results at the same time in the improvement of the cohesion of the damaged areas and in the sealing or protection of the material against aggressive agents (Edvarsen, 1999), but it does not necessarily result in the recovery of the material's mechanical properties, equal to these of an undamaged state.

Due to lack of standard procedures, several methods have been applied in order to assess the recovery of the mechanical properties of cement-based materials after the introduction of damage (Muhammad et al., 2016; Yidirim et al., 2015). The main points considered, when the recovery of strength is studied, are:

- The way damage is introduced
- The control of the damage degree and its reproducibility and
- The measurement of the residual strength, in order to be correlated with the strength of the material after healing

7.1.1 Damage method

The types of strain induced in order to inflict measurable damage on cement-based materials varies between different studies. The main methods adopted are damage by flexural three or four point bending tests (Wanng et al., 2012; Hilloulin et al., 2016), compressive strength tests (De Nardi et al., 2016), and tensile tests (Yang et al., 2011; Li and Li, 2011) or by generating cuts with a rotating blade (Achal et al., 2013).

The aim of all the aforementioned techniques is to create a predetermined defect on the specimens studied, so that the healing capacity of the materials can be assessed according to the reversal of that defect. The types of damage profiles by these techniques are shown in Fig. 7.1.

More specifically, by compressive stress and tensile deformation multiple microcracks are generated which whereas during flexural deformation, material failure derived from the propagation of the main crack.

During the mechanical strain, three typical phases take place, namely elastic deformation, plastic deformation and material failure. For the purposes of the study of self healing properties, damage is inflicted to reach the plastic deformation level (Li et al., 2013), as elastic deformation is reversible producing no damage, whereas after complete failure the specimens are not eligible for further treatment or testing.

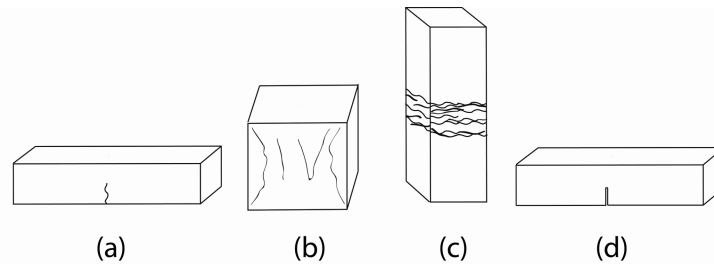


Figure 7.1: Damage profiles generated by different types of strain; (a) flexural, (b) compressive, (c) tensile and (d) cutting.

7.1.2 Damage degree and reproducibility

One of the main challenges faced regarding self-healing and strength recovery of cement-based materials, is the control of the damage degree.

A common method applied is the measurement of flexural or tensile deformation by linear variable differential transformers (LVDT) (Schlangen et al., 2006). In this

method specimens are loaded until the average crack width reaches the desired value and are subsequently unloaded. The cracks partly close with unloading (Aldea et al, 2000). Nevertheless, due to the brittle nature of cement based materials, the crack width is difficult to be controlled (Li et al, 2013).

A similar method is the pre-loading of the specimens at predetermined loads, which corresponds to percentages of its maximum load. This is used when compressive or flexural deformation is applied (De Nardi et al., 2016).

In both the above methods, the specimens -after a predetermined curing period- are tested again, but this time until failure and the maximum load is compared to the one measured during the first cracking. The self-healing efficiency was evaluated by comparing the peak load obtained during the first loading cycle and the reloading cycle (Wang et al., 2012).

Assessing the damage degree is crucial for the reproducibility of the results obtained by each method. The wide variety of cement-based materials studied and consequently the variation of their mechanical properties are partly responsible for the lack of a standard procedure to measure the efficiency of self-healing. In particular, the same crack width generated in different cement-based materials, does not necessarily denote the same damage degree. Especially when low-strength materials are studied, the control of the crack-width is more challenging, resulting in very low reproducibility potential and consequently in an uncertain damage degree assessment.

7.1.3 Residual strength

Damage degree is related to the residual strength of the specimens after damage has been induced. Residual strength of damaged specimens can be measured by immediately reloading them after the predetermined damage is inflicted (De Nardi et al 2016). Therefore, the residual strength of the damaged specimens can be compared to the strength of undamaged specimens. In this case, damage generation method coincides with the method for the damage degree assessment. The measurement of residual strength of specimens is essential for the evaluation of the damage degree as well as for the evaluation of the material's strength recovery.

Residual strength can also be estimated indirectly by ultrasonic pulse velocity (UPV) measurements (Sarkar et al 2014, De Nardi et al 2016). In this case, UPV of damaged

specimens is compared with that of undamaged ones and damage degree is calculated (Zhong et al 2008).

In the present study a new methodology was developed for the assessment of self-healing potential of traditional mortars. The main purpose for this methodology was the disassociation of the damage method from the damage degree measurement. More precisely, the generation of damage is introduced by a localized hertzian stress and the damage degree is assessed by comparing the flexural strength (residual strength) of damaged and un-damaged specimens.

7.2 Materials and Methods

7.2.1 Sample preparation

LP and NHL mortar mixtures were prepared, as described in Appendix A, and were subsequently cast in prismatic moulds (20x20x80 mm). For each mortar mixture prismatic specimens (n=20) were cast and cured in a temperature and humidity controlled chamber ($95\pm 5\%RH$, $20\pm 3^{\circ}C$).

7.2.2 Methodology

7.2.2.1 Hertzian contact stress

Damage was introduced by hertzian stress. A uniaxial stress is applied on a linear one-dimensional plane by a cylindrical bar of equal or greater length as the specimen (Fig. 7.2). A localized deformation is created around the contact point as a constant displacement rate is applied until the predetermined load is reached.

Cement-based materials when exposed to hertzian contact stresses present a similar behavior as when exposed to uniaxial compressive stress (Brezeanu, 2015). As the displacement advances a network of microcracks is generated, until the ultimate failure point is reached and the material collapses. Contrary to compressive stress test, where microcracks are generated throughout the specimen, when hertzian stress is applied, microcracks are formed around the contact point, forming a localized defect. In this way, damage degree can be controlled and reproduced, while the method by

which damage is introduced is disassociated by the measurement of the residual strength.

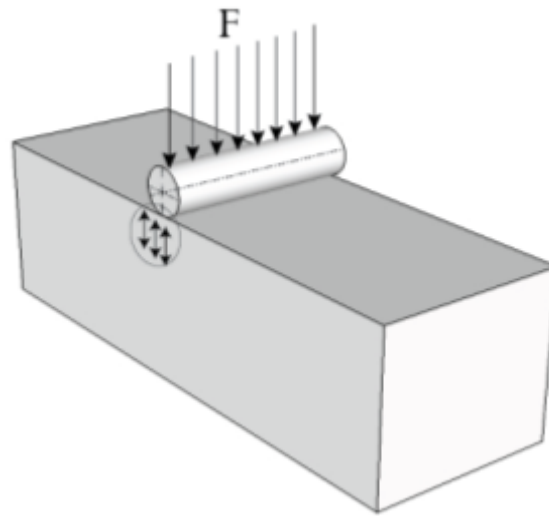


Figure 7.2: Localized damage formed by the application of hertzian stress

7.2.2.2 Assessment of residual strength

Preliminary measurements were performed in order to assess the residual strength of the mortar specimens after damage was introduced by hertzian contact stress.

More specifically for each mixture the application of incremental predetermined loads by hertzian contact stress was followed by three-point bending tests. The measured flexural residual strength was in turn contrasted with the flexural strength of undamaged specimens (Fig 7.3).

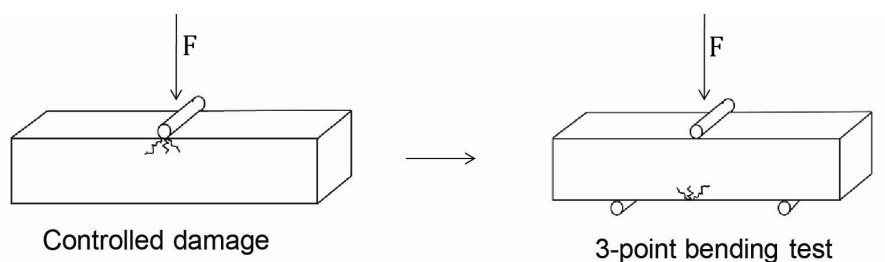


Figure 7.3: Specimens were locally damaged by hertzian contact stress and were subsequently measured as to their residual strength by three point bending test.

For each test the residual strength was calculated by the average of three measurements by the following equation:

$$D_f = \frac{f_0 - f_1}{f_0}$$

where D_f is the damage degree of the specimens, f_1 is flexural strength of specimens after hertzian loading, and f_0 is the flexural strength of undamaged specimens.

Moreover, ultra-sonic pulse velocity (UPV) measurements were conducted on the specimens before and after the hertzian loading, and damage degree was supplementary calculated by the following equation:

$$D_{UPV} = \frac{v_0 - v_1}{v_0}$$

where D_{UPV} is the damage degree of the specimens, v_1 is UPV after hertzian loading, and v_0 is the UPV before loading.

Ultra-sonic pulse velocity was used to assess damage degree in reference and damaged specimens by hertzian stress (Fig 7.5).

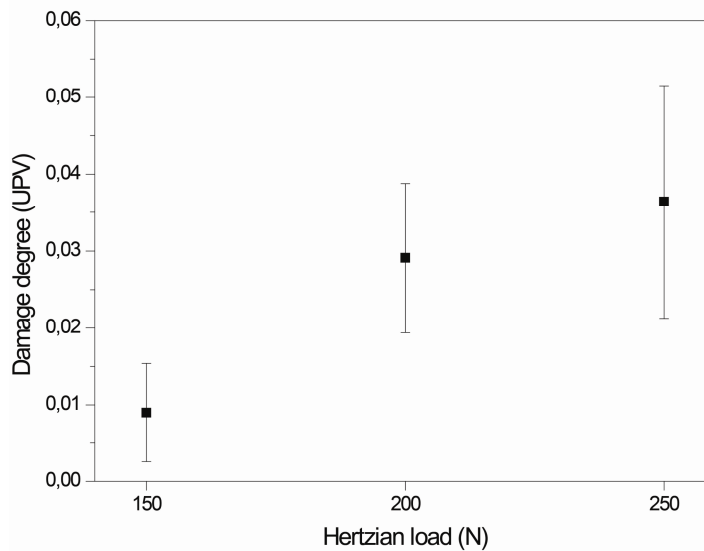


Figure 7.5: Damage degree calculated by UPV after incremental loads applied by hertzian stress on NHL 3030 specimens.

Similarly residual was calculated in each experiment by the flexural tests performed in specimens damaged by hertzian stress and reference undamaged specimens (Fig 7.6).

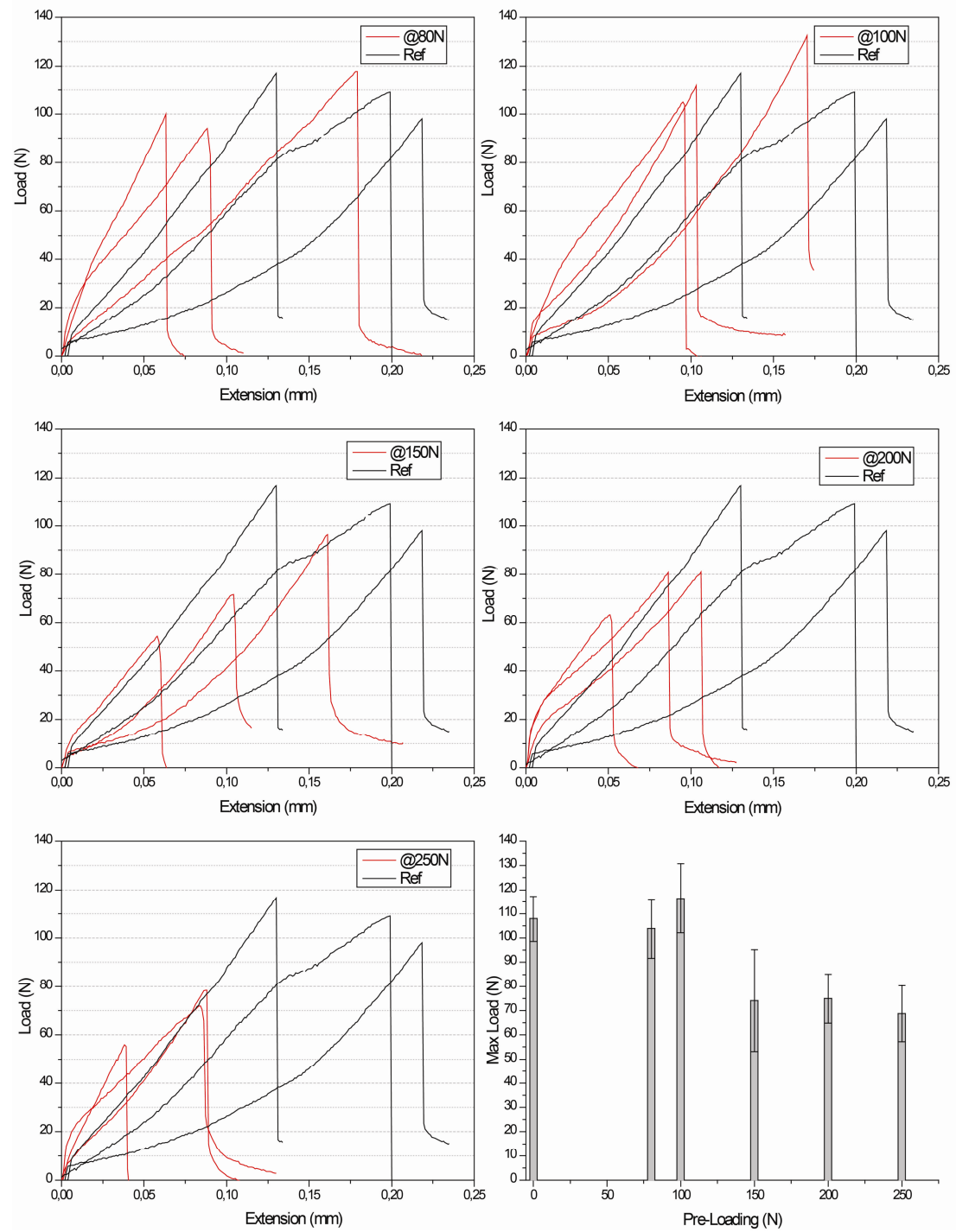


Figure 7.6: Loading curves obtained during three-point bending tests and damage degree calculated by three-point bending tests after incremental loads applied by hertzian stress.

More specifically, for each experiment five hertzian loads were applied and subsequently the flexural strength of the damaged specimens was measured by three-point bending. The residual strength was calculated and compared. The adequate load was the one that produced the lower residual strength without leading to the specimen failure.

Table 7.1: Groups of specimens tested in each experiment for the assessment of mechanical properties recovery due to self-healing.

Groups (n=3)	Hertzian stress test	Flexural strength test	Additional curing period (30d)	Flexural strength test
Reference undamaged after predetermined curing period (A)	-	+	-	-
After Hertzian stress test(B) (residual strength)	+	+		
After predetermined healing period (C)	+	-	+	+
Reference undamaged after predetermined healing period (D)	-	-	+	+

For each experiment after the adequate hertzian load was determined, the following procedure was applied:

More specifically, mortar specimens were initially cured at set time periods in order to assess the healing potential of mortars, four separate groups of specimens (n=3) were tested (Table 7.1). For each group 3 specimens were tested to ensure the reproducibility of the results.

- One reference group (A) was tested by three point bending test at the specific age to determine the flexural strength of undamaged mortars.
- In order to measure the residual strength of damaged specimens, a second group (B) was damaged by hertzian stress test and was consequently tested by three point bending test.

- To assess the healing potential, a third group (C) was damaged by hertzian stress test and was cured in high humidity conditions (95%RH) for the predetermined healing period. After the end of the “healing” period, group C specimens were tested by three-point bending test and their strength after healing was measured
- A group of reference un-damaged specimens (group D), cured under the same conditions as group C and for the same period, was tested also and was contrasted with the healed mechanical properties of group C.

7.2.2.3 Groups and parameters studied

The parameters examined in this chapter are:

- the age of the mortar when the damage occurs
- the healing period

In order to examine the effect of the curing period prior to damage (moment of cracking), NHL and LP specimens were damaged after varying curing periods (Fig. 7.4). Subsequently, damaged specimens were healed at 95%RH for varying periods in order to determine the effect of healing period.

More specifically, NHL mortars were damaged after 15, 30 and 240 days of curing and were subsequently cured for a 30-day healing period before healing capacity was determined. Another group of specimens was damaged at 30 days and was cured for a 210-day healing period in order to study the effect of the duration of the healing period on the healing capacity.

Similarly, LP mortars were damaged after 15, 30 and 90 days of curing and were subsequently cured for a 30-day healing period, in order to assess the healing capacity related to the age of the specimens when damage occurs. Whereas the effect of the duration of the healing period was studied in specimens damaged after 90 days and cured for a 90-day healing period.

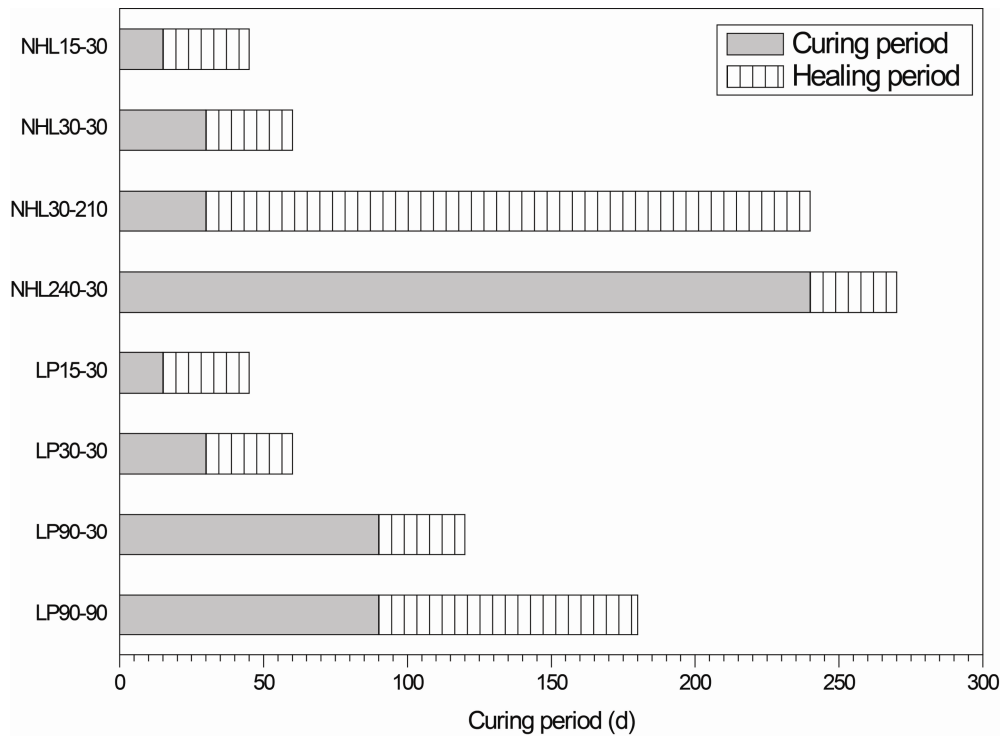


Figure 7.4: Timeline of curing and healing periods

7.2.2.4 Assessment of strength recovery

The recovery of flexural strength was calculated according to the following equation:\

$$H_f = \frac{f_h}{f'_0} \times 100\%$$

where H_f is the strength recovery of the specimens, f_h is flexural strength of specimens after hertzian loading, and f'_0 is the flexural strength of reference undamaged specimens.

7.3 Results and Discussion

7.3.1 Effect of curing time before damage was introduced (Moment of cracking)

NHL specimens damaged by hertzian stress after 15 or 30 days of curing were measured, after a 30-day healing period in high humidity conditions, to evaluate the effect of curing time on the healing efficiency. Moreover a group of NHL specimens was damaged after 240 days and measured after a 30-day healing period according to the previous experiment, to assess the healing potential when damage is introduced at later-age.

When damage was introduced at 15 or 30 days, the hertzian stress applied, resulted in a 36 and 39% reduction respectively in flexural strength (Group B) of the NHL reference specimens. After a 30-day healing under high humidity conditions (95%RH), the damaged specimens have recovered their strength and exhibited improved mechanical properties (Group C).

The healing potential of those specimens was assessed by comparing their flexural strength with that of the reference undamaged specimens, cured under the same conditions (Group D). The results indicate that healed specimens recovered a considerable amount of their flexural strength, exhibiting 90 and 89% of the strength of the reference ones (Fig 7.7 - 7.8). Although, the standard deviation in the case of the healed specimens damaged at 30 days is higher, indicating larger amount of randomly dispersed non-treated flaws.

Regarding the specimens damaged after 240 days, damage degree was set at 15% as higher loads resulted in the complete failure of the specimens. This could be attributed to the stiffening of the microstructure of later –age mortars, which results in a more rigid behavior. However, the improvement of their mechanical properties after the healing period was minimal, suggesting a lower healing potential.

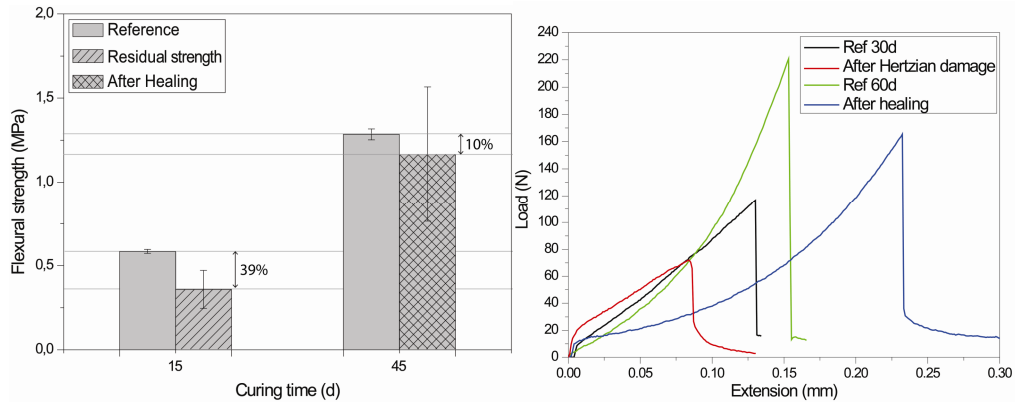


Figure 7.7 (Left): Flexural strength values of NHL specimens, damaged at 15 days. The 30 days healing process in elevated humidity conditions resulted in a significant recovery of their strength. **(Right)** Representative loading curves obtained during three-point bending tests.

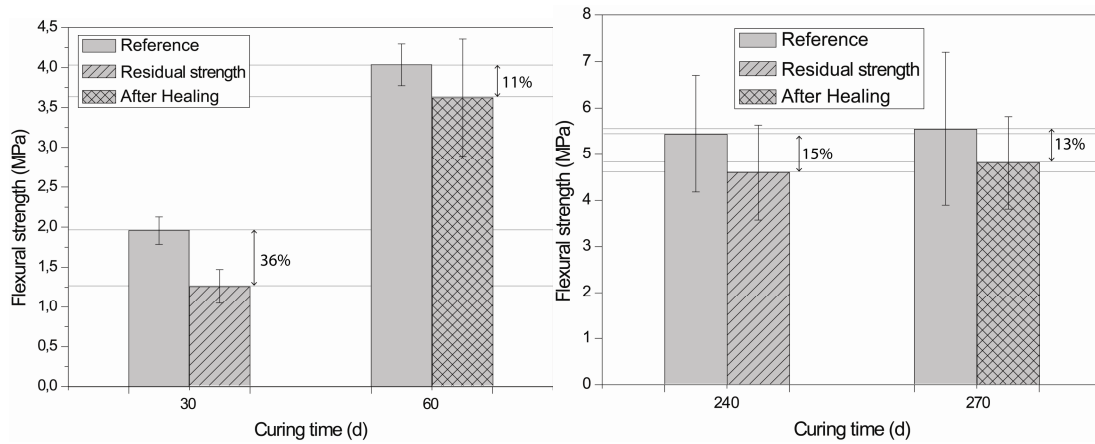


Figure 7.8: Flexural strength values of NHL specimens damaged at 30 and 240 days and healed for a 30 day healing period in elevated humidity conditions.

The interpretation of the curves obtained during three-point bending tests (Fig. 7.7 right) provides a comparison of the elastic properties and thus, the development of microstructure in the different groups. As it was expected, the slope of the damaged specimens is lower than that of the reference ones, exhibiting however an extended tail after crack-damage at maximum load. This is the result of the extended network of micro-cracks created during hertzian damage, which act as crack initiation flaw and drastically reduces the strength of the specimens and at the same time increases the energy dissipation during fracture (energy under the tail). This results in materials with higher toughness which are more resistant to crack propagation than their un-cracked counterparts.

The denser microstructure of the specimens cured for 60 days results in a higher slope, indicating a more brittle microstructure. However, the more interesting behavior is that of the “healed” specimens; the slope of the load curve is between the reference and the damaged one, while the maximum load tends to reach or even overcome in some cases (see *stdev* values in Fig 7.7 - 7.8) that of 60 days. Moreover, the loading curve of the healed specimens present a more brittle fracture suggesting the healing of the micro-cracks network responsible for the more ductile fracture of damaged specimens. The 11% difference of strength values between healed and un-damaged specimens - in combination with the interpretation of three-point bending curves - is a strong indication of the partial healing of the specimens and filling of the micro-cracks network created during hertzian stress. If otherwise, where the extended network of micro-cracks has not been healed, the damaged area would have acted again as a strong crack initiation flaw, resulting in a strength reduction of the same level, close to 40%.

The same experimental procedure was performed in LP specimens damaged by hertzian stress after 15 or 30 days of curing. After a 30 day healing period in high humidity conditions, flexural strength of healed LP specimens was measured to evaluate their healing efficiency.

In both cases, the damage degree was calculated. In specimens damaged after 15 days of curing damage degree was higher due to the low strength brittle nature of early-age LP specimens. The damage produced by hertzian stress could not be recovered during the 30 days healing period in high humidity conditions. Flexural strength measured in damaged specimens revealed that their flexural strength was 26% of that of undamaged specimens cured under the same conditions (Fig 7.9). Nevertheless, their strength was partly recovered which implies that their mechanical properties should be further examined after an extended healing period.

In specimens damaged after 30 days of curing the maximum load applied produced by hertzian stress resulted in a 20% damage degree (Fig 7.9). Higher loads resulted in the complete failure of the specimens. After 30 days of curing the specimens' strength recovery was calculated at 89% of the undamaged specimens cured under the same conditions (Fig 7.9).

Finally, hertzian stress applied after 90 days of curing resulted in a 37% reduction in flexural strength and the respective recovery after a 30 day-healing period was calculated at 98% of the undamaged specimens (Fig 7.9).

Similarly to NHL specimens loading curves of damaged LP specimens suggest the presence of an extended network of microcracks leading to the increase of the energy dissipation during fracture. At the same time loading curve of the healed specimen indicates the healing of the microcracks due to the brittle fracture profile similar to the undamaged reference specimens.

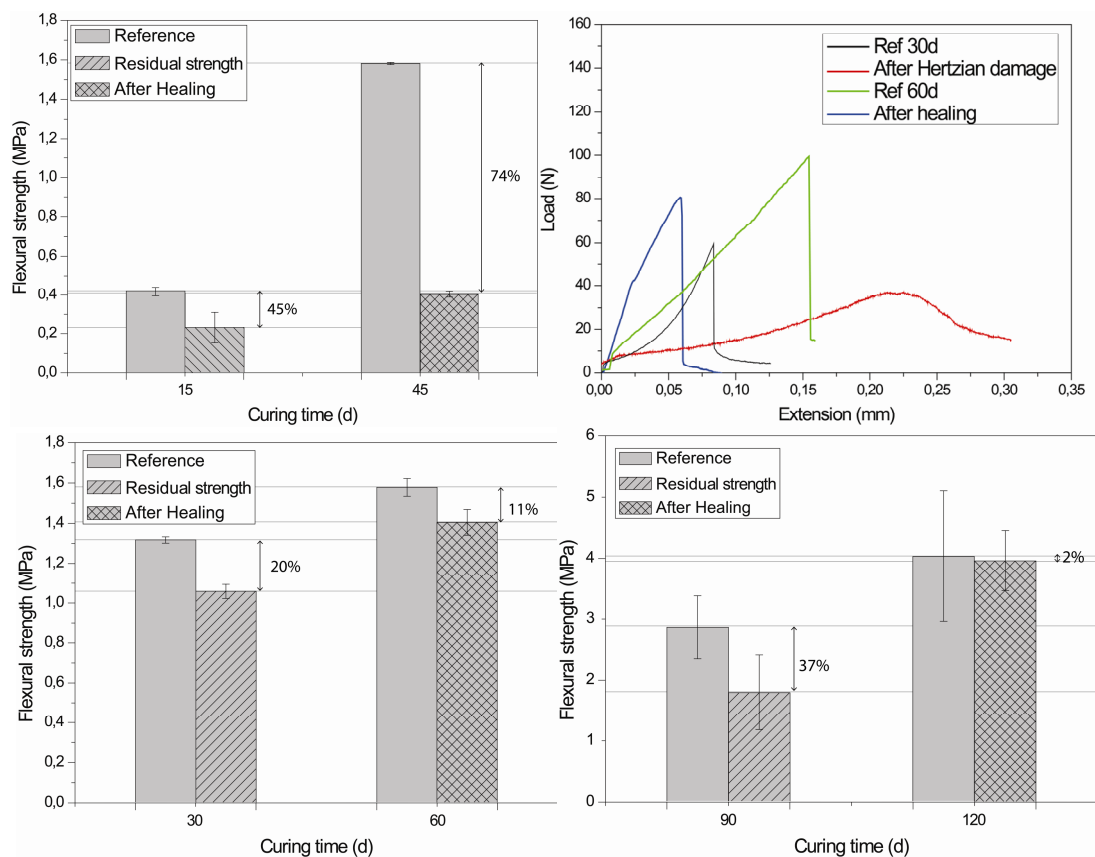


Figure 7.9: Flexural strength values of healed LP specimens damaged at 15 days 30 and 90 days respectively and healed for a 30 day healing period in elevated humidity conditions.

(Top Right) Representative loading curves obtained during three-point bending tests.

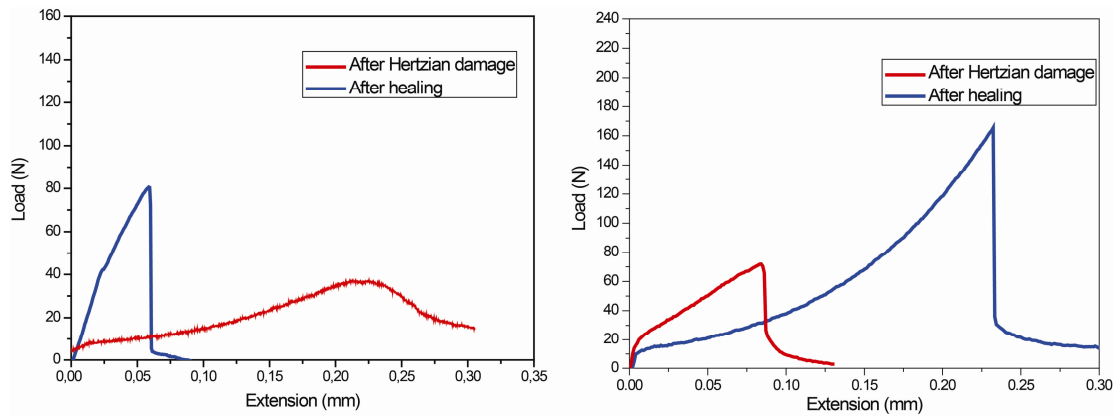


Figure 7.10: Representative loading curves obtained during three-point bending tests of LP (left) and NHL (right) specimens damaged after 30 day curing and healed for another 30 days.

The loading curves recorded during three-point bending tests of damaged and healed specimens can provide some further information concerning the effect of the self-healing mechanism on the mechanical properties of NHL and LP mortars (fig. 7.10).

As it was shown in figures 7.7 and 7.9, the mechanical properties of the healed specimens as expressed by their loading curves present a different fracture mode than their damaged counterparts. Damaged specimens present an extended tail which points to higher energy dissipation due to the presence of the microcracks. Microcracks act as an inherent localized flaw which is responsible for the lower strength values. In contrast, healed specimens present a brittle fracture loading curve which is a strong indication that the localized flaw was reversed. If otherwise, the microcrack network would have caused a higher energy dissipation and a more ductile fracture profile.

7.3.2 Effect of healing period

The effect of the duration of the healing period was studied in NHL mortar specimens cured for 30 days before hertzian stress was applied and subsequently cured for a 30 or 210-day healing period. In both experiments damage degree was the same, as hertzian stress was applied in specimens of the same group.

The 30 days healing period resulted in an 89% recovery of strength of the undamaged specimens, whereas after 210 days (an extension of curing period by six months) the specimens' strength recovery was calculated at 91% of the respective undamaged specimens (Fig 7.11).

Accordingly, the effect of the duration of the healing period was studied in LP specimens damaged by hertzian stress after 90 days of curing and subsequently cured

for 30 or 90 days. After 30 days the average recovery of strength calculated was 98% of the undamaged specimens and after 90 days the respective recovery was 104% (Fig 7.12).

It is noteworthy, that the extended healing period does not have a substantial impact on the recovery of the mechanical properties of NHL or LP mortars indicating that the inflicted damage was reversed during the first month, thus a prolonged healing period did not have a substantial impact on the healing process.

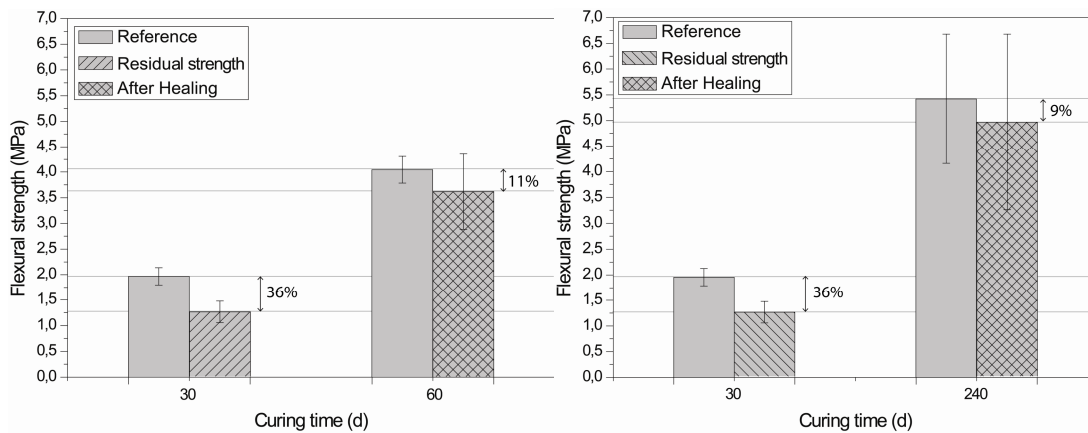


Figure 7.11: Flexural strength values of NHL specimens, damaged at 30 days (left) and subsequently cured for 30 (left) or 210 (right) day healing period respectively under high humidity conditions (95%RH).

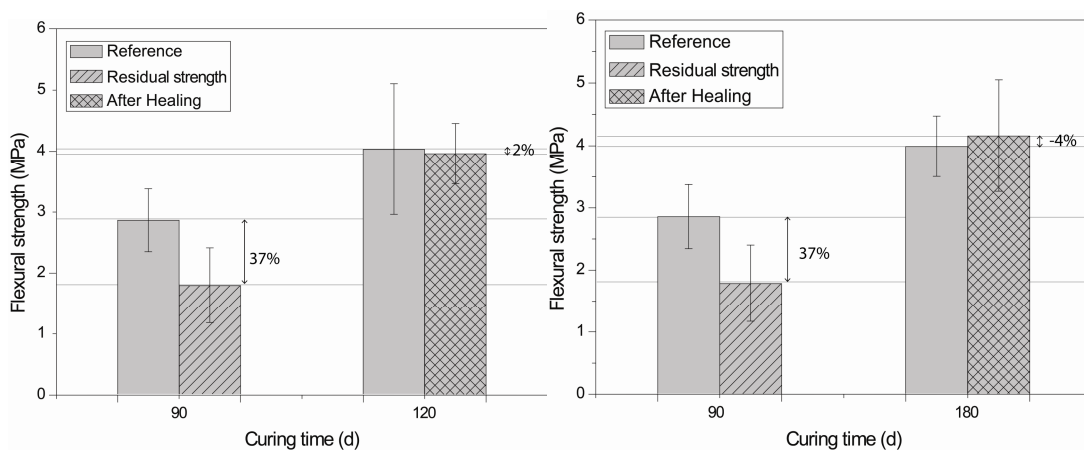


Figure 7.12: Flexural strength values of LP specimens, damaged at 90 days and subsequently cured for 30 (left) or 90 (right) days under high humidity conditions (95%RH).

Table 7.2: Synopsis of strength recovery results

	Curing Period	Healing Period	Damage Degree	Strength Recovery
	(d)	(d)	(%)	(%)
NHL 15-30	15	30	39	90
NHL 30-30	30	30	36	89
NHL 240-30	240	30	15	87
LP 15-30	15	30	45	26
LP 30-30	30	30	20	89
LP 90-30	90	30	37	98
NHL 30-30	30	30	36	89
NHL 30-210	30	210	36	91
LP 90-30	90	30	37	98
LP 90-90	90	90	37	104

7.4 Conclusions

In this chapter a new methodology was applied to determine the healing potential of traditional mortars focusing on the recovery of their mechanical properties.

The methodology applied was developed aiming at the creation of a reproducible defect amongst the specimens of each group and at the same time at the calculation of the damage degree generated by that defect. The autogenic self healing capacity of traditional mortars was examined in NHL and LP specimens damaged after different curing periods and subsequently healed for different predetermined periods (healing periods).

The autogenic self-healing mechanism in NHL and LP mortars, as it was described in Chapter 5 based on microscopy observations, is controlled by both continued hydration and secondary precipitation of calcium carbonate. It is known that the filling of cracks by the respective secondary products can lead to the reduction of water permeability which is crucial for the protection of the mortar against aggressive agents (Ma et al., 2014). Nevertheless it does not necessarily have an impact on the recovery of its mechanical properties.

In this chapter the recovery of mechanical properties was assessed in damaged NHL and LP specimens and the resulted regain of strength indicates that the autogenic healing mechanism is taking place under these curing conditions.

The recovery of mechanical properties suggests that the damage inflicted on the specimens was reversed by the toughening of the microstructure due to the healing of microcracks by secondary phases. Moreover, a high adhesion between the healing phases and the binder matrix is indicated; if otherwise the interface between the secondary phases and the binder matrix would have easily separated and there would be no strength improvement recorded.

This is also indicated by the interpretation of the loading curves of damaged and healed specimens acquired during three-point bending tests. The healed specimens present a brittle fracture profile with no indication of the presence of the localized flaw, in contrast to the damaged specimens where the higher energy dissipation during fracture is the result of the microcrack network induced by herzian stress.

Overall, the main outcomes provided by the interpretation of the results regarding the factors examined, indicate that:

- The age of the specimens during cracking did not affect the healing capacity of NHL mortars damaged at 15 and 30 days. However when damaged after 210 days the recovery of mechanical strength was lower even though the inflicted damage degree was low (15%).
- In LP specimens similar conclusions could not be reached since the damage inflicted varied considerably (20-45%)
- The extended duration of the healing period in NHL specimens resulted in a slight increase of the strength recovery. Taking into account the high strength recovery exhibited after one month of healing, this could indicate that their healing potential was reached during the first month, and an additional curing period does not have any substantial impact.

References

- Achal, V., Mukerjee, A., & Sudhakara Reddy, M. (2013). Biogenic treatment improves the durability and remediates the cracks of concrete structures. *Construction and Building Materials*, 48, 1–5. <http://doi.org/10.1016/j.conbuildmat.2013.06.061>
- Aldea, C.-M., Song, W.-J., Popovics, J. S., & Shah, S. P. (2000). Extent of Healing of Cracked Normal Strength Concrete. *Journal of Materials in Civil Engineering*, 12(1), 92–96. [http://doi.org/10.1061/\(ASCE\)0899-1561\(2000\)12:1\(92\)](http://doi.org/10.1061/(ASCE)0899-1561(2000)12:1(92))
- Brezeanu, L. C. (2015). Contact Stresses between Two Cylindrical Bodies – Cylinder and Cylindrical Cavity with Parallel Axes – Part II: 2D and 3D FEA Comparative Study. *Procedia Technology*, 19, 177–184. <http://doi.org/10.1016/j.protecy.2015.02.026>
- De Nardi, C., Bullo, S., Cecchi, A., & Ferrara, L. (2016). Self-healing capacity of advanced lime mortars. *Advances in Materials and Processing Technologies*, 2(3), 349–360. <http://doi.org/10.1080/2374068X.2016.1191896>
- Edvardsen, C. (1999). Water permeability and autogenous healing of cracks in concrete. *ACI Materials Journal*, 96(4), 448–454. Retrieved from <http://www.scopus.com/record/display.url?eid=2-s2.0-0033167808&origin=inward&txGid=C588B4805824E0504E7CF72DE6D0054E.CnvcAmOODVwpVrjSeqQ%3A1>
- Hilloulin, B., Legland, J.-B., Lys, E., Abraham, O., Loukili, A., Grondin, F., ... Tournat, V. (2016). Monitoring of autogenous crack healing in cementitious materials by the nonlinear modulation of ultrasonic coda waves, 3D microscopy and X-ray microtomography. *Construction and Building Materials*, 123, 143–152. <http://doi.org/10.1016/j.conbuildmat.2016.06.138>
- Li Mo and Victor C. Li. (2011). Cracking and Healing of Engineered Cementitious Composites under Chloride Environment. *ACI Materials Journal*, 108(3). <http://doi.org/10.14359/51682499>
- Li, V. C., Sakulich, A. R., Reinhardt, H. W., Schlangen, E., Van Tittelboom, K., Snoeck, D., ... Nishiwaki, T. (2013). Recovery against Mechanical Actions. In M. de Rooij, K. Van Tittelboom, N. De Belie, & E. Schlangen (Eds.) (pp. 119–215). Springer Netherlands. http://doi.org/10.1007/978-94-007-6624-2_4
- Ma, H., Qian, S., Zhang, Z., 2014. Effect of self-healing on water permeability and mechanical property of Medium-Early-Strength Engineered Cementitious

- Composites. *Construction and Building Materials* 68, 92–101.
[doi:10.1016/j.conbuildmat.2014.05.065](https://doi.org/10.1016/j.conbuildmat.2014.05.065)
- Muhammad, N. Z., Shafaghat, A., Keyvanfar, A., Abd. Majid, M. Z., Ghoshal, S. K., Mohammadyan Yasouj, S. E., ... McCaffer, R. (2016). Tests and methods of evaluating the self-healing efficiency of concrete: A review. *Construction and Building Materials*, 112, 1123–1132.
<http://doi.org/10.1016/j.conbuildmat.2016.03.017>
- Sarkar, M., Chowdhury, T., Chattopadhyay, B., Gachhui, R., & Mandal, S. (2014). Autonomous bioremediation of a microbial protein (bioremediase) in Pozzolana cementitious composite. *Journal of Materials Science*, 49(13), 4461–4468.
<http://doi.org/10.1007/s10853-014-8143-1>
- Schlangen, E., Heide, N. ter, & Breugel, K. van. (2006). Crack Healing of Early Age Cracks in Concrete. In M. S. KONSTA-GDOUTOS (Ed.) (pp. 273–284). Springer Netherlands. Retrieved from
http://link.springer.com/chapter/10.1007/978-1-4020-5104-3_32
- Wang, J., Van Tittelboom, K., De Belie, N., & Verstraete, W. (2012). Use of silica gel or polyurethane immobilized bacteria for self-healing concrete. *Construction and Building Materials*, 26(1), 532–540.
<http://doi.org/10.1016/j.conbuildmat.2011.06.054>
- Yang, Y., Yang, E.-H., & Li, V. C. (2011). Autogenous healing of engineered cementitious composites at early age. *Cement and Concrete Research*, 41(2), 176–183. <http://doi.org/10.1016/j.cemconres.2010.11.002>
- Yıldırım, G., Keskin, Ö. K., Keskin, S. B., Şahmaran, M., & Lachemi, M. (2015). A review of intrinsic self-healing capability of engineered cementitious composites: Recovery of transport and mechanical properties. *Construction and Building Materials*, 101, Part, 10–21. <http://doi.org/10.1016/j.conbuildmat.2015.10.018>
- Zhong, W., & Yao, W. (2008). Influence of damage degree on self-healing of concrete. *Construction and Building Materials*, 22(6), 1137–1142.
<http://doi.org/10.1016/j.conbuildmat.2007.02.006>

Discussion

Self healing is considered one of the main mechanisms that have the potential to prolong the service life of cement-based materials. Even though, autogenic self-healing is encountered in abundance in historic mortars and it has often been linked with the longevity of the monuments, its mechanism is not completely understood yet neither is the self-healing potential of hydraulic mortars. A better understanding of the main factors governing the autogenous phenomenon is a prerequisite for the development of tailor-made “smart” self-healing mortars by utilizing their autogenic self-healing potential.

The main open questions related to the self-healing phenomenon are related to the factors affecting the occurrence of the autogenous mechanism, but also to the nature of the healing products that fill the cracks and finally to the extent of the materials properties recovery after healing.

This research was focused in the physicochemical characterization of the autogenous mechanism in traditional hydraulic mortars. Natural hydraulic (NHL) and lime-pozzolan mortars are regularly used in conservation intervention of monuments due to their high mechanical and physicochemical compatibility with the historic mortars.

The parameterization of the autogenic self healing mechanism was attempted focusing on specific factors that promote the occurrence of this phenomenon as microclimatic conditions, time of cracking and healing period. Additionally a morphological and chemical characterization of the secondary formations was carried out which allowed the identification of the mechanisms taking place within the frame of the autogenic phenomenon. Furthermore, the potential of the self healing mechanism was also examined regarding the recovery of mechanical properties of the mortars.

It was found that the autogenic self healing mechanism in hydraulic mortars takes place by the initiation of two separate reactions; namely carbonation and hydration. Carbonation reaction leads to the formation of homogenous layers of secondary calcite on the crack walls. The extent of this mechanism results in the healing of cracks up to 60 microns. Regarding the hydration mechanism, secondary hydraulic phases are produced exhibiting an outward orientation. It was found that “low-

density” fiber-like hydraulic phases are initially formed bridging cracks up to 70 microns. However secondary hydraulic products were not observed during the observation of thin and polished sections.

The reactions responsible for the autogenous mechanism are controlled by the availability of reactive phases in the binder. A prerequisite for the precipitation of secondary calcite is the presence of calcium ions in the pore solution. Calcium dissolution is considered the first step of the autogenic mechanism and was measured by subjecting mortar specimens to an accelerated leaching process.

The availability of calcium is related to the moment of cracking, as the binder composition may differ due to the evolution of the hardening reactions of the cement matrix. Calcium ions may derive from the dissolution of portlandite (Ca(OH)_2), calcium silicate hydrates (CSH) and dicalcium silicate (C_2S) in the case of NHL mortars. The dissolution mechanisms of NHL and LP mortars present some differences. Early-age lime-pozzolan (LP) mortars, when subjected to leaching, may provide higher amount of calcium ions than early-age NHL mortars. However, the amount of leached calcium is higher in later-age NHL mortars, probably due to the production of portlandite during the hydration reaction and secondarily due to the decalcification of CSH phases.

Consequently, the secondary products formed inside the cracks, as observed at the SEM, also reflect that the main self-healing mechanisms in NHL and LP mortars differ. In LP mortars the presence of secondary calcite is pronounced irrespective of the specimen’s age when the cracking occurred. In contrast, in NHL specimens it was only observed at early-age cracked specimens. This could be related to the availability of free-lime in the binder matrix.

The self-healing hydration mechanism was observed in both LP and NHL mortars. The formation of secondary hydraulic products is also controlled by the mineralogical composition of the binder when cracking occurs. In NHL specimens the hydration mechanism was the main mechanism contributing to the production of secondary products in the crack surface. It was found that “fiber-like” hydration products are formed initially when the cracks are generated in early-age NHL specimens which, after prolonged healing period, present a more dense bee-hive structure and needle-like formations. In specimens cracked at later-age the presence of bee-hive structure

and needle-like products is more profound which could be attributed to the existence of higher amount of hydraulic phases in the binder matrix. This suggests a common mechanism irrespective of the time cracking occurs.

In contrast in LP specimens, only “low density fiber-like” CSH was observed limited to specimens cracked at early-age, whereas in specimens cracked at later-age carbonation was the main mechanism by which secondary phases were produced inside cracks.

Moment of cracking was also examined regarding the recovery of LP and NHL specimens’ mechanical properties. The healing capacity of NHL mortars was not affected by the reduction of the amount of free lime between 15 and 30 days. However when damaged after 210 days the recovery of mechanical strength was lower. In the case of LP mortars definite conclusions regarding the effect of the moment of cracking were not drawn due to the variation of the damage degrees between the experiments.

Another important parameter was the duration of the healing period after damage has been inflicted on NHL and LP specimens. Prolonged healing periods led to the production of more dense secondary formations inside cracks in both LP and NHL specimens. More specifically, the carbonation mechanism in LP specimens was more advanced after a three months-healing period leading to a further decrease of the crack width. In NHL specimens, a prolonged healing period of three months resulted in the observation of secondary calcite, as it was not detected in specimens cured for shorter healing periods. This could suggest that secondary precipitation of calcite requires longer healing periods.

Accordingly, the hydration mechanism as it was observed in NHL specimens led to the observation of denser hydraulic structures namely bee-hive formations and needle-like CSH products. In LP specimens prolonged healing period also resulted in the bridging of wider cracks by fiber-like CSH products.

A summary of the main findings regarding secondary products observed in LP and NHL specimens can be seen in the following table (Table 6.3).

	Hydraulic products	Carbonated products	Other observations
LP1530	fiber-like CSH	calcite and vaterite	~30 μ m crack filled with fiber-like CSH
LP1590	fiber-like CSH	calcite	~70 μ m crack filled with fiber-like CSH
LP3030	fiber-like CSH	calcite	~30 μ m sparitic calcite
LP3090	fiber-like CSH	calcite	~50 μ m sparitic calcite
NHL730	fiber-like and needle-like CSH, bee-hive formations	-	“low-density” CSH
NHL790	fiber-like and needle-like CSH, bee-hive formations	calcite	micro-sparitic calcite
NHL3030	needle-like CSH	-	“high-density” CSH
NHL3090	needle-like CSH	-	Densification of type needle-like CSH hydraulic phases

The effect of the time of cracking can be also discussed in relation to the microstructure of the specimens when damage occurs. Preliminary measurements of capillary coefficient performed on NHL and LP specimens after various curing periods ranging from 7 to 360 days are presented in Appendix A. As it is expected both NHL and LP specimens water capillary values follow an exponential decay. Nevertheless in LP mortars capillary coefficient stabilizes after 60 days of curing indicating a constant volume of capillary pores, whereas in NHL specimens decreases until 360 days of curing which suggests that its microstructure becomes more impermeable with time. The above observations can be linked with the absence or presence of secondary calcite precipitation in NHL and LP mortars respectively according to the age damage occurs.

Similarly, the microstructural differences observed between NHL and LP specimens leaching; namely the higher amount of macropores generated in LP specimens which suggests the predominance of the portlandite dissolution mechanism, in contrast to the increase of micropores in NHL specimens which suggests the decalcification of CSH phases, are in agreement with the healing mechanisms observed in the two mixtures. More specifically, the secondary crystallization of calcite which was more profound in LP specimens, could be related to the higher abundance of dissolved portlandite in the pore solution, whereas the dissolution processes in NHL mortars could promote secondary hydraulic reactions.

The effect of the duration of the healing period was also examined regarding the recovery of mechanical properties. The experimental results suggested that prolonged healing periods could have a favorable impact on the strength recovery of both NHL and LP specimens; but since the recovery of strength was almost complete after the first month of healing, the additional healing time provided a lower increase of strength.

Lastly, the autogenous mechanism is largely controlled by the micro-climatic conditions, and specifically the presence of water. In this study mortar samples were subjected either to wet-dry cycles or different humidity levels (45, 75 or 95%RH). Self healing of microcracks was observed under all conditions except in the specimens cured at 45%RH. In specimens subjected to wet-dry cycles the mechanism was more advanced.

The presence of water, which is considered crucial for the occurrence of the autogenous phenomenon, is often related to the deterioration of mortars through excessive leaching, salt penetration and crystallization or microbial attack. Nevertheless the results of this study suggest that the autogenous mechanism can take place in lower humidity conditions provided that extended healing period is applied. This is corroborated by the observations of healed micro-cracks in historic mortars which were not in direct contact with water. Prolonged periods of high humidity (>75% RH) combined with high content of free-lime which is a common characteristic of these mortars, could result in the filling of micro-cracks by secondary precipitation of calcite.

The data attained during this study, can contribute in the more effective design of self-healing mortars. More specifically, chemical characterization of the binder composition was correlated with the favorable healing mechanism and the characteristics of the secondary products formed inside the crack. Consequently, the above findings could promote the design of tailor-made healing agents incorporated in the binder matrix for enhancing the self healing phenomenon.

Moreover, the results of this study, related to micro-climatic conditions together with the extent of the healing period, are essential for defining both the prospects and the limitations related to the autogenous mechanism, thus leading to a more effective application of these materials.

Future work

The present study focuses on the main parameters affecting the occurrence of the autogenous self-healing phenomenon in hydraulic mortars.

However further research is needed concerning some aspects of the autogenous mechanism. The study of the effect of crack width is not understood yet and crack width limitations are not reported. As it was concluded after observation of the autogenous mechanism in historic mortars, crack width also affects the morphology of the secondary products. In the same context, a better understanding of the effect of the damage degree on the strength recovery is needed. The methodology developed within the framework of this thesis for the assessment of strength recovery could be applied as it incorporates the evaluation of the damage degree.

Moreover, further research is needed in order to implement these findings to an optimized design and application of self-healing mortars bearing tailor-made self-healing agents. More specifically, the addition of supplementary “healing” agents in the binder composition could enhance the self-healing capacity of hydraulic mortars. The composition of these agents can be controlled in order to enhance the secondary formation of carbonation or hydration products in the cracks. Nevertheless, similar studies have shown that in order to achieve a realistic expansion of their service life healing agents have to remain inactive for long periods without deteriorating or reacting while their activation has to be triggered as damage occurs (Souradeep and Kua, 2016¹). This is achieved by inserting into the cement mixture the healing agent protected inside capsules (encapsulation). During a crack formation, the protective layer breaks and the activated agent is released inside the crack, repairing it. However, encapsulation materials and methods have not yet produced sufficient results.

¹ Souradeep, G., & Kua, H. W. (2016). Encapsulation Technology and Techniques in Self-Healing Concrete. *Journal of Materials in Civil Engineering*, 04016165. [http://doi.org/10.1061/\(ASCE\)MT.1943-5533.0001687](http://doi.org/10.1061/(ASCE)MT.1943-5533.0001687)

Conclusions

The autogenous self-healing mechanism is a multifaceted physicochemical mechanism which is controlled by several inherent properties of the mortar (i.e. binder composition, porosity and water absorption) or external conditions (i.e. humidity or water saturation), together with aspects regarding the damage degree.

Within the context of the present thesis, the evaluation of the autogenous self-healing mechanism in hydraulic mortars was accomplished by qualitative and quantitative criteria. The autogenous mechanism was examined by the observation of its end-products in historic mortars but also as an on-going process in laboratory produced mortar mixtures. Moreover, in order to evaluate the strength recovery linked with the autogenous self healing phenomenon a new methodology was applied that enabled the quantitative assessment of the strength recovery correlated with the respective damage degree that was reversed.

The main conclusions of the present study are summarized below:

A: Self-healing phenomenon in historic mortars

- The results obtained during the examination of historic mortars indicate that some recurrent healing patterns exist and the crystal habits of the re-precipitated products depend, among other factors, on the moisture content and on the degree of carbonation of the mortar.
- The abundance of the autogenous self healing phenomenon in historic mortars can be attributed to the high percentages of free-lime in their initial composition which is the main source of Ca^{2+} ions.

B: Dissolution of Ca-compounds

- The key parameter for the occurrence of self-healing in mortars is the availability of Ca^{2+} . These are provided either by leaching or decalcification of LP and NHL specimens and in both cases the amount leached is proportional to the amount of unreacted portlandite (free lime) present in the binder. However after the depletion of reactive portlandite, two more mechanisms

could be responsible for further providing calcium ions. The first is the production of secondary Ca(OH)_2 due to hydration reaction and the second is the decalcification of C-S-H phases. C_2S may also provide Ca-ions in the case of NHL mortars.

- Leaching of LP and NHL mortars results in an increase in total porosity, as expected. However, porosity increase due to leaching is substantially lower when later age (> 60d) specimens are tested. Moreover, leaching of LP and NHL specimens seems to affect porosity by two different mechanisms. In leached LP specimens the macro porosity is increased, whereas in leached NHL specimens total porosity is mainly attributed to mesoporosity.

C: Identification of self-healing products

- Regarding the mechanisms responsible for healing of cracks that may exist in the structure of mortars, two main mechanisms were identified and correlated to the observation of the healing products; continued hydration and precipitation of secondary calcite. Although, autogenic self-healing has been attributed to both these reactions, the underlying mechanisms differ. In particular, continued hydration takes place on the crack surface, provided that reactive phases are present, whereas secondary calcite is precipitated depending on the movement of the pore solution and the solubility of the calcium-bearing phases of the binder matrix.
- The availability of portlandite affects both mechanisms of Ca-rich products formation in the cracks.
- The effect of cracking age was a crucial parameter to the healing efficiency, since it was correlated with the available portlandite at the time cracking occurred.
- Although complete healing of the main crack induced by three point bending, was not observed in any mixture, smaller side-cracks were completely filled with secondary products under specific each-time conditions.
- Humidity was a very important parameter for the successful implementation of the healing mechanisms. It was found that LP mortars benefitted more from humidity than the NHL counterparts since at the humidity level of 75%, the

healing products were abundant in LP specimens, whereas in NHL were hardly spotted. An addition, lower humidity conditions (45% RH) found to be inadequate for the evolution of the autogenous healing phenomenon to take place.

- Overall, the availability of water during wet-dry cycles enhanced the precipitation of secondary calcite in both LP and NHL specimens, especially when early-age cracking occurred.
- As secondary precipitation of calcite is enhanced when specimens are subjected to water saturation (wet/dry cycles), carbonation mechanism might be hindered in NHL mortars due to the decrease of capillary absorption with time.
- Calcite precipitation is enhanced with additional healing period as larger calcite crystals are produced. This is also corroborated by the observations of historic mortars where extended networks of cracks were filled by sparitic calcite.
- Prolonged healing period was found to have a substantial effect on the evolution of both mechanisms. Enrichment of the crack surface by secondary hydration products was observed

D: Regain of strength after self-healing

- The resulted high regain of strength (87-104%) in NHL and LP mixtures, suggests that autogenic healing mechanism is taking place.
- The age of the specimens at the moment of cracking did not affect the healing capacity of NHL mortars when damaged at early stages of curing (15 and 30 days). However when damaged at late stage (210 days) the recovery of mechanical strength was lower even though the inflicted damage degree was low (15%). In LP specimens similar conclusions could not be reached since the damage inflicted varied considerably (20-45%)
- The extended duration of the healing period in NHL specimens resulted in a slight increase of the strength recovery. Taking into account the high strength recovery exhibited after one month of healing, this could indicate that their

healing potential was reached during the first month, and an additional curing period does not have any substantial impact.

In summary, the results of this research have shown that the autogenous self-healing phenomenon occurs during the life-cycle of hydraulic mortars and that it can be enhanced both by environmental and compositional parameters. The implementation of the above mentioned parameters in the parametric design of modern (conservation) mortars can contribute in practice to the enhancement of their life-cycle.

Appendix: Preliminary measurements

In this chapter, NHL and LP mortar samples were examined after successive curing periods ranging from one day to 18 months. The aim is to establish the evolution of chemical and mineralogical composition of NHL and LP mortars as well as their physical and mechanical properties in order to adjust the experimental setup accordingly.

Materials

Two groups of mortar mixtures were prepared, one with a natural hydraulic lime (St. Astier NHL5) and one with a commercially available lime powder (KRINOS SA) and a natural pozzolan of volcanic origin (Dalkafoukis) in 1:1 ratio.

In both mixtures standard sand [CEN 196-1] was added as aggregate in a cement/aggregate ratio 1:3 (w/w).

Characterization of raw materials was performed by means of X-ray diffraction analysis (XRD), Thermo-gravimetric analysis (DTA/TG) and microscopically in a FEI Quanta-Inspect Scanning Electron Microscope coupled with Energy-dispersive X-ray spectroscopy (SEM/EDAX).

Mixtures

Mixtures were prepared according to European standard EN 196-1. Raw materials were mixed in a Bear Varimixer cement mixer for 1.5 minutes in low speed during and 1 minute at high speed. The plasticity of the mixture was measured, each time before molding, in a flow table, according to standard EN 1015-3. The mixtures were stored in a temperature and humidity control maturation chamber at 20 ± 3 °C and $95\pm 5\%$ RH.

Table 1: Mixture composition and flow values are given in

	Lime powder	pozzolan	NHL 5	w/b	b/a	Flow value (cm)
LP	50	50	-	0.76	1/3	16
NHL	-	-	100	0.6	1/3	16

XRD analysis of raw materials

X-ray diffraction analysis was performed in the raw materials used in this study to assess their mineralogical composition. In the lime powder diffractogram the typical peaks of portlandite are observed. Calcite is also present as a minor constituent. The pozzolanic material is composed of illite, quartz, anorthite and albite, which are Si and/or Al rich minerals responsible for the pozzolanic reaction with portlandite in the presence of water.

Diffractogram of natural hydraulic lime (NHL5) revealed the presence of portlandite calcite and quartz, along with dicalcium silicate or belite. The reaction between dicalcium silicate and portlandite is mainly responsible for the hardening of hydraulic binders. Moreover, diffractogram of the standard sand used in this study, confirmed its siliceous nature, while no other phases were detected.

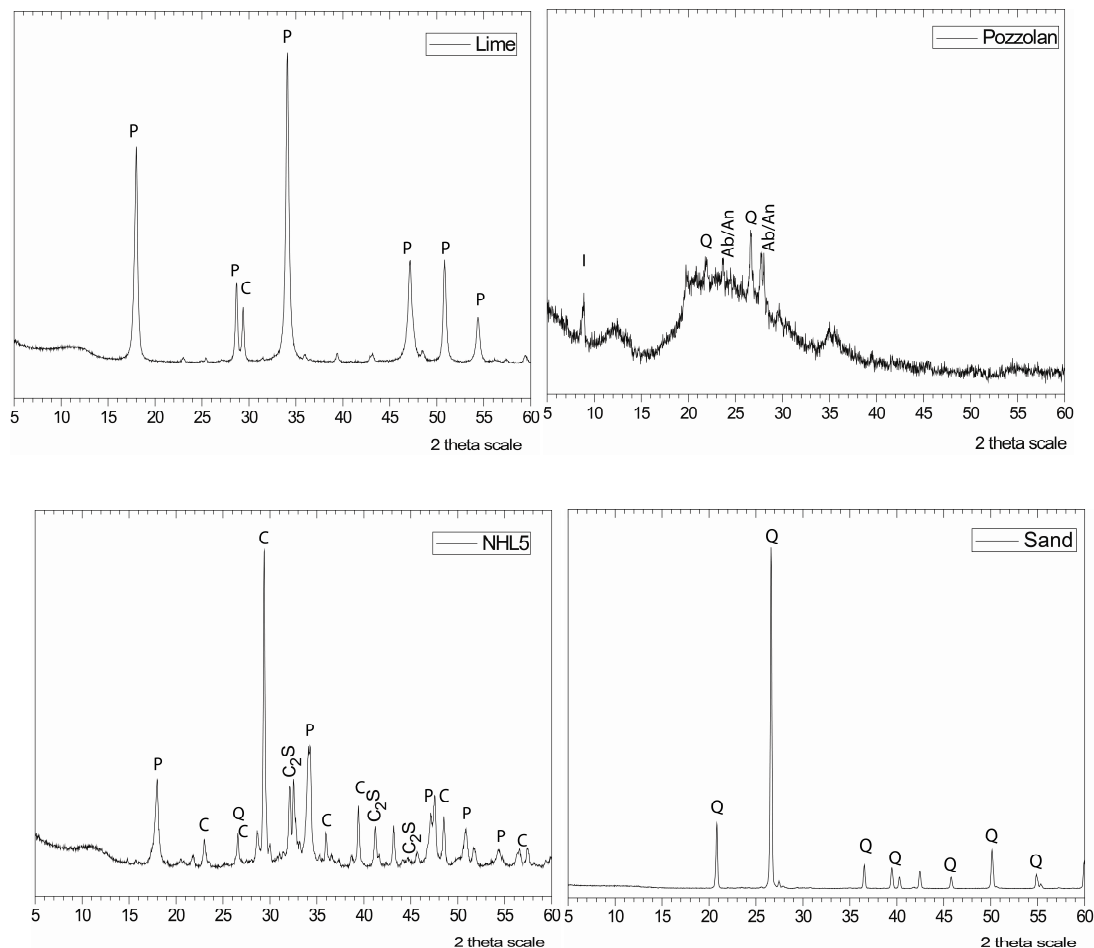


Figure 1: Diffractograms of the raw materials used in this study. P: portlandite, C: calcite, Q: quartz, I: illite, Ab: albite, An: anorthite, C₂S: dicalcium silicate

Chemical characterization of raw materials

Chemical characterization of raw materials was performed at the FEI Quanta-Inspect Scanning Electron Microscope coupled with Energy-dispersive X-ray spectroscopy (SEM/EDAX). Chemical analysis of raw materials is given in Table 2.

Table 2: Chemical characterization of raw materials

		Na ₂ O	MgO	Al ₂ O ₃	SiO ₂	SO ₃	Cl ₂ O	K ₂ O	CaO	TiO ₂	Fe ₂ O ₃	Total
NHL5	Wt %	0.5	1.9	3.15	19.8	1.74	0.22	0.56	70.9	0.17	1.15	100
Lime	Wt %	1.2	2.4	1.23	1.45	2.62	0.25	0.27	90.3	nd	0.32	100
Pozzol.	Wt %	3.1	0.8	13.92	75.1	nd	0.07	4.39	0.7	0.32	1.65	100

Thermal analysis of raw materials

Raw materials were characterized also by means of thermal analysis and their % portlandite and calcite content was quantified. Thermogravimetric (DTG) curves are interpreted in order to define the temperature ranges corresponding to the loss of water (H₂O) from calcium hydroxide (Ca(OH)₂) and carbon dioxide (CO₂) from calcium carbonate (CaCO₃). TG% represents the mass loss (%) during the aforementioned temperature ranges.

Mass percentages of calcium hydroxide (Ca(OH)₂) and calcium carbonate (CaCO₃) are calculated by the following equations:

$$m_{CH} = \frac{m_{CH}^{water} M_{CaO}}{M_{H_2O}} + m_{CH}^{water}$$

$$m_{CaCO_3} = \frac{m_{CaCO_3}^{CO_2} M_{CaO}}{M_{CO_2}} + m_{CaCO_3}^{CO_2}$$

Where: m_{CH} and m_{CaCO_3} are the mass% of calcium hydroxide ($Ca(OH)_2$) and calcium carbonate ($CaCO_3$), m_{CH}^{water} and $m_{CaCO_3}^{CO_2}$ are the mass loss% of water removed from calcium hydroxide and carbon dioxide from calcium carbonate respectively and M_{CaO} , M_{CO_2} and M_{H_2O} are the molar masses of CaO , CO_2 and H_2O respectively.

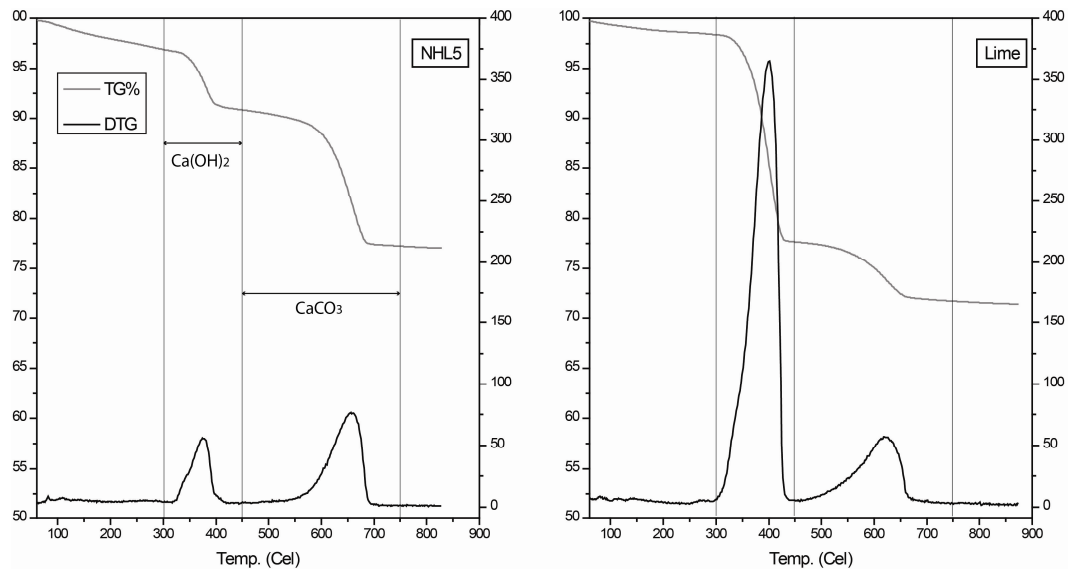


Figure 2: Thermogravimetric curves of the raw materials

Table 3: Quantification of the TG% curves

	NHL5	Lime
m_{CH}	24.96	85.09*
m_{CaCO_3}	30.88	13.55

*Calcium hydroxide calculated by mass % is corresponds to 50% of the LP binder mixture. Therefore portlandite % in the fresh mixture equals to 42.55%.

Monitoring of the mineralogical composition of LP and NHL mortars

The evolution of the main hardening reactions taking place in LP and NHL mortars is monitored by means of X-ray diffraction (XRD), Fourier transform infrared spectroscopy (FTIR) and thermogravimetric (DTA/TG) analysis after predetermined curing periods.

XRD analysis

X-ray diffraction analysis was performed in NHL mortars cured from 7 to 180 days. The presence of portlandite and C_2S is recorded which are the main reactants along with calcite and CSH which are formed during carbonation and hydration reactions respectively. The reduction of the portlandite and C_2S peaks is observed, but a second increase is reported after 120 days in the portlandite peaks, which could be attributed to the formation of portlandite as a hydration product.

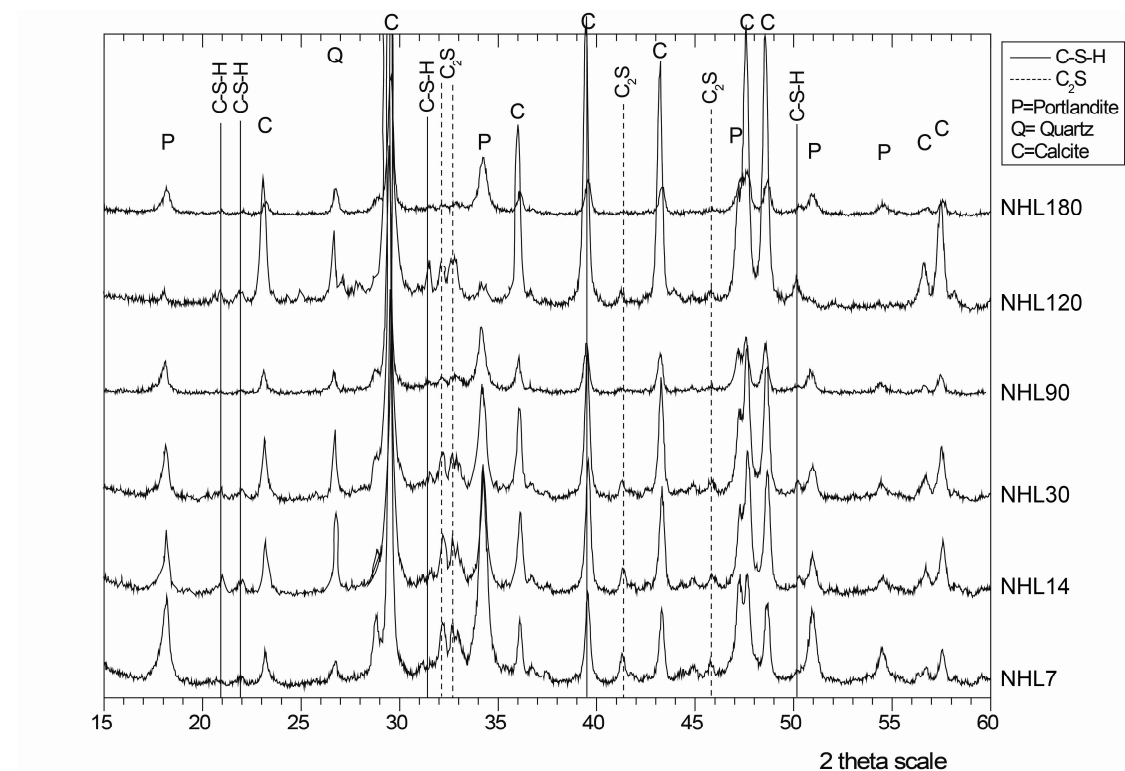


Figure 3: Diffractograms of NHL mortars.

Diffractograms of LP mortars cured from 7 to 360 days present the evolution of hydration and carbonation similarly to NHL mortars. The depletion of portlandite is

evident after 90 days of curing. The presence of calcite and CSH is also reported as the main products formed during hardening. C_2S is not present in LP mortars as the hydration reaction takes place between portlandite and Al / Si rich phases of the pozzolanic material.

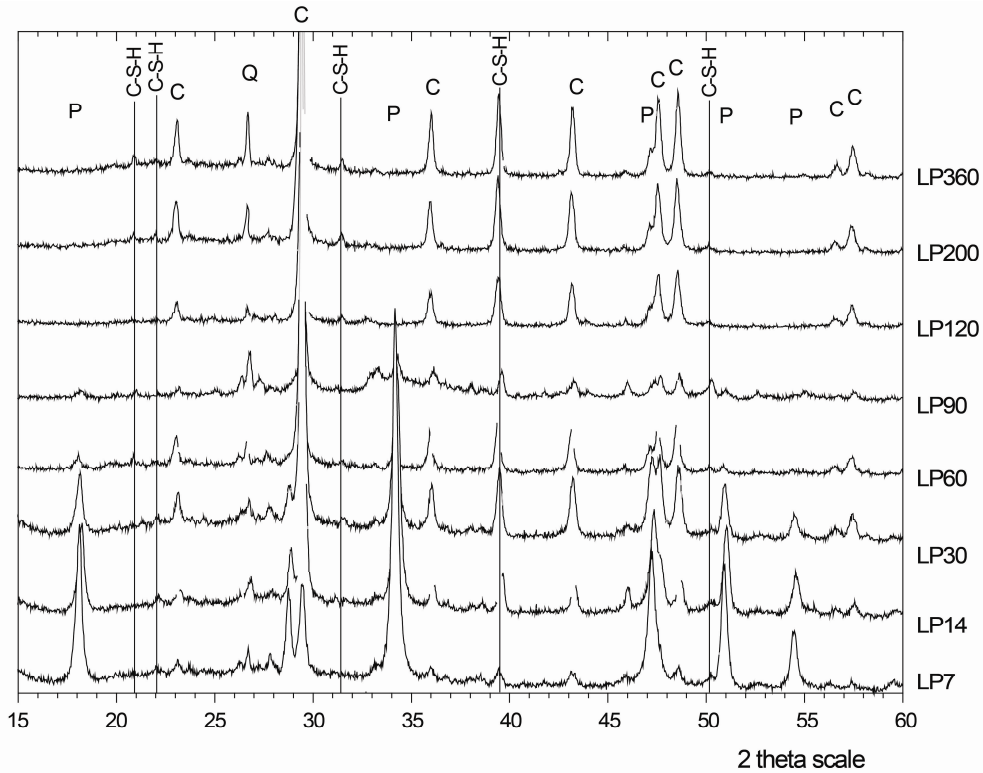


Figure 3: Diffractograms of LP mortars.

FTIR analysis

NHL and LP mortars were examined by means of FTIR spectroscopy in attenuated total reflection (ATR) mode, after varying curing periods. The FTIR spectra of the samples measured are presented in figure 4. The sharp transmittance peak observed at 3645 cm^{-1} corresponds to the stretching vibration of O-H bond of portlandite. The depletion of portlandite is observed in LP mortars, corresponding to the disappearance of that peak after 90 days of curing. Whereas in NHL specimens portlandite is present in all samples, similarly to the XRD observations, possibly due to the formation of portlandite as a hydration product.

The main bands associated with calcite are observed in both LP and NHL mortars' spectra. More specifically, at $712, 872\text{ cm}^{-1}$ typical symmetric and asymmetric

respectively deformations of CO_3 are detected, while a broad band at 1407 cm^{-1} is attributed to CO_3 asymmetric stretching (Kroner et al., 2010).

The broad band observed between 970 and 1010 cm^{-1} are characteristic of CSH hydraulic compounds (Maravelaki-Kalaitzaki et al., 2005).

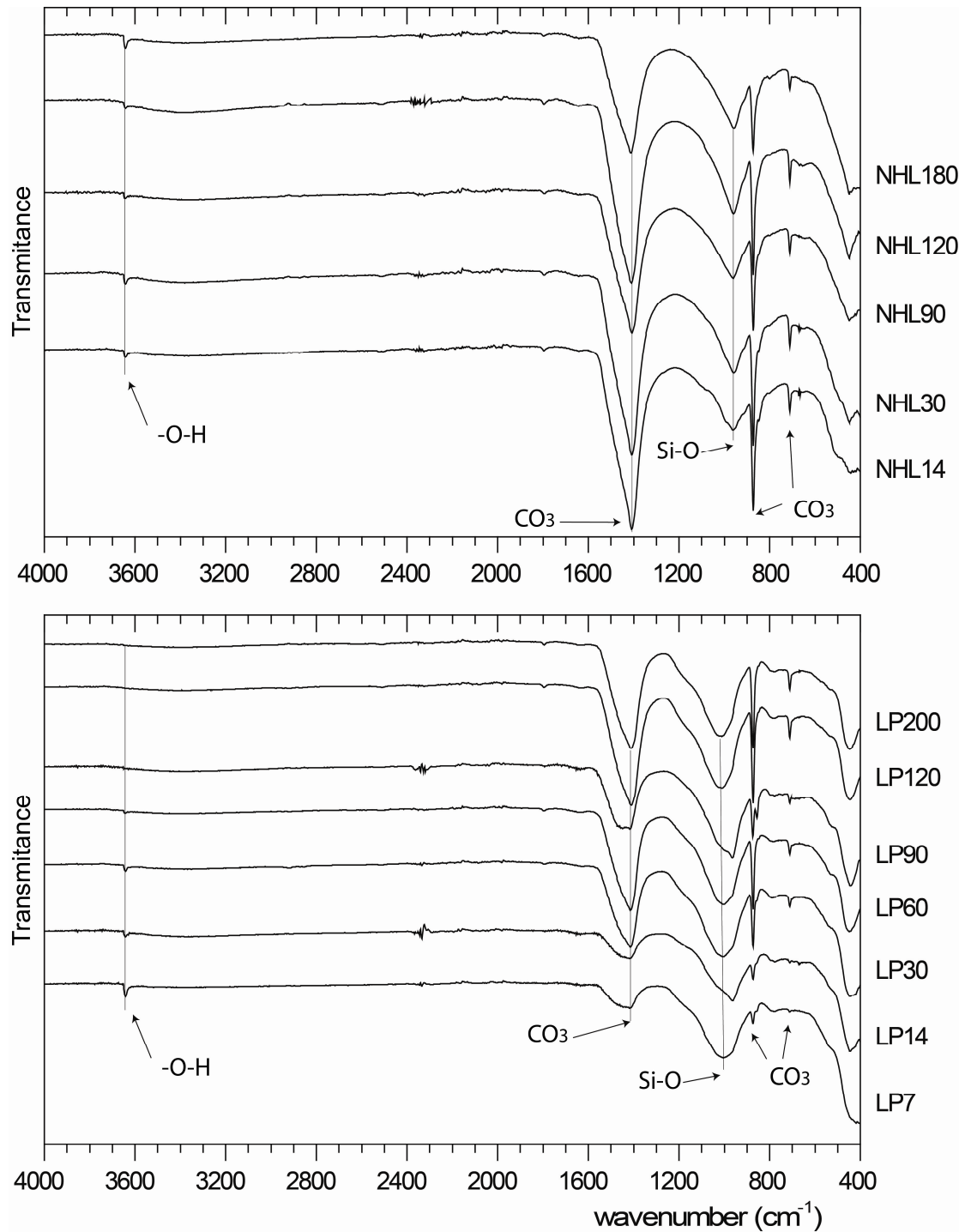


Figure 5: FTIR spectra of NHL and LP mortars after varying curing periods.

Thermogravimetric analysis (DTA/TG)

Thermogravimetric analysis was performed on LP and NHL mortars after varying curing periods. As observed after XRD and FTIR analysis the evolution of portlandite content can be used as an indicator of the setting reactions' progress.

Thermogravimetric analysis was used as described earlier to quantify the portlandite content. The portlandite content % calculated after each curing period is presented in figure. 6. In both LP and NHL mortars two periods can be distinguished. During the first period the portlandite percentage decreases rapidly due to its consumption in the progress of the setting reactions. However in the second period portlandite content presents an increase which is attributed to its formation curing the hydration reaction.

The first period as observed in LP mortars results in the depletion of portlandite close to 10% of its initial content and is defined at the first 120 days of curing. In NHL mortars, portlandite is reduced during the first period to 25% of its initial concentration and is the first period is defined in the first 90 days of curing.

During the second period, the formation of portlandite is more profound in NHL mortars where the portlandite content increases and stabilizes. Whereas in LP mortars the secondary increase is limited.

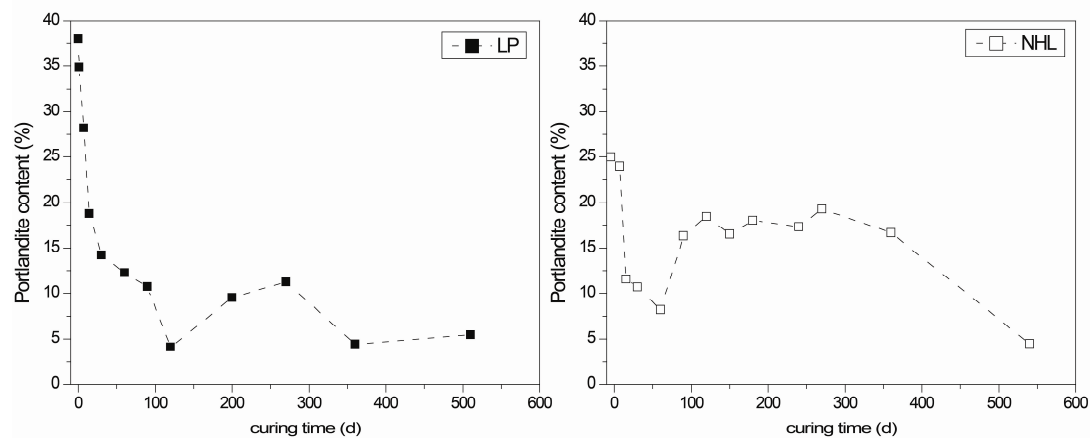


Figure 6: Portlandite content in NHL and LP mortars after varying curing periods.

Microstructural and physical properties of NHL and LP mortars

Total porosity and pore size distribution was assessed by mercury intrusion porosimetry (MIP) in LP specimens cured for 30, 60 and 120 days and NHL specimens cured for 15, 60 and 120 days.

The total porosity was assessed in low and high pressure porosimetry. Low pressure corresponds to pore sizes more than 5 μm and up to 500 μm , whereas by low pressure porosimetry pore sizes from approximately 1 nm to 5 μm .

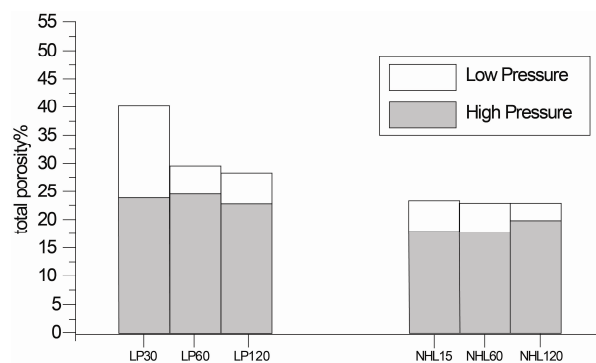


Figure 7: Total porosity of NHL and LP mortars after varying curing periods.

Total porosity (%) of LP mortars decreases with time mainly due to the decrease of macro porosity. NHL mortars do not present a significant variation in total porosity between the different curing periods examined.

Pore size distribution of LP mortars cured for the same periods revealed that the decrease of pore volume can be attributed mainly to pore-sizes larger than 15 μm . Moreover, a wide distribution of pore sizes ranging from 10 nm to 1 μm is observed after 30 days of curing which after additional curing periods is divided into a double distribution from approximately 10 to 100 nm and 100 nm to 1 μm . Pore sizes ranging from 10 to 100 nm, are classified as micropores (Gong et al., 2014), and are decreased after 120 days of curing. Mesopores, ranging from 100 nm to 1 μm , do not present a significant variation.

Similarly in NHL mortars the main variation is attributed to micropores which present an increase in volume only in the specimens cured for 60 days.

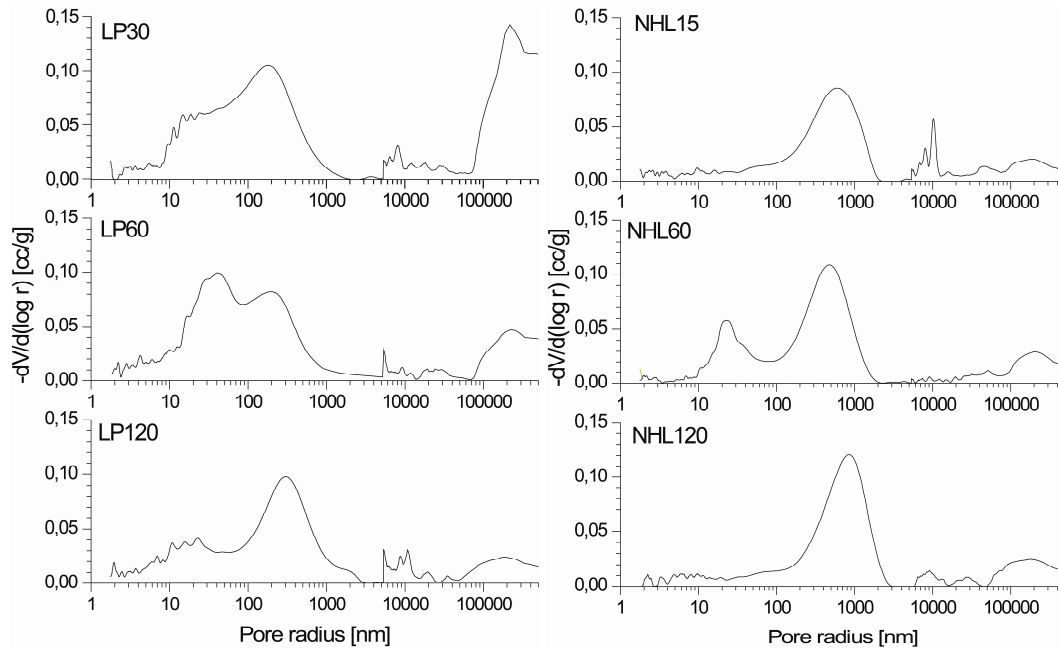


Figure 8: Total porosity of NHL and LP mortars after varying curing periods.

Water absorption by capillary porosity is mainly attributed to the pore ranges between $10 \mu\text{m}$ - 50nm . Water absorption coefficient by capillary was measured in NHL and LP mortar specimens in specimens cured from 7 to 360 days. The water capillary values follow an exponential decay and in LP mortars stabilizes after 60 days of curing, whereas in NHL specimens decreases until 360 days of curing.

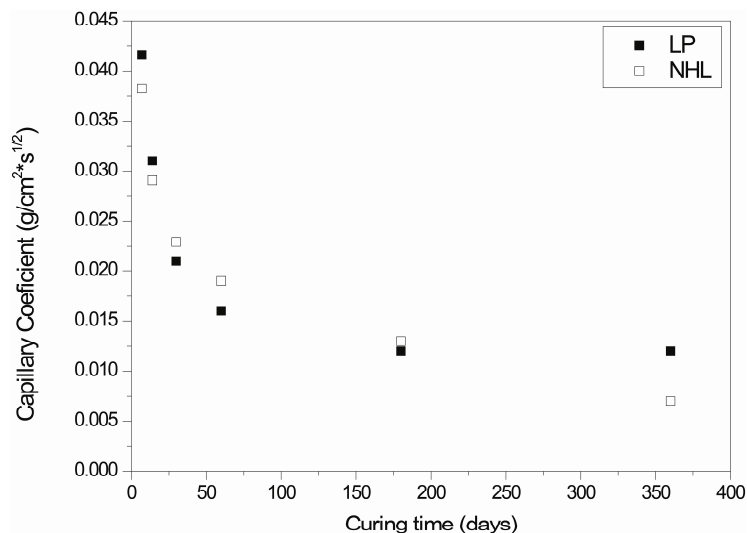


Figure 9: Absorption by capillary of NHL and LP mortars after varying curing periods.

References

- BS EN 1015-3:1999. Methods of test for mortar for masonry. Determination of consistence of fresh mortar (by flow table)
- BS EN 196-1:2005. Methods of testing cement. Determination of strength
- Gong, F., Zhang, D., Sicat, E., & Ueda, T. (2014). Empirical Estimation of Pore Size Distribution in Cement, Mortar, and Concrete. *Journal of Materials in Civil Engineering*, 26(7), 4014023. [http://doi.org/10.1061/\(ASCE\)MT.1943-5533.0000945](http://doi.org/10.1061/(ASCE)MT.1943-5533.0000945)
- Kroner, S., Domenech-Carbo, M.-T., & Mas-Barbera, X. (2009). Hydraulic Lime Mortar in the Ambit of Stone Restoration: Evaluation of Applicability. *Arche: Publicacion Del Instituto Universitario de Restarucion Del Patrimonio de La Universitat Politecnica de Valencia = Arche: The Journal of the Heritage Conservation Institute of the Polytechnical University of Valencia*, (4–5), 181–188
- Maravelaki-Kalaitzaki, P., Bakolas, A., Karatasios, I., & Kilikoglou, V. (2005). Hydraulic lime mortars for the restoration of historic masonry in Crete. *Cement and Concrete Research*, 35(8), 1577–1586. <http://doi.org/10.1016/j.cemconres.2004.09.001>

List of Figures

Figure 2.1: Thesis outline.....	9
Figure 3.1: Performance of concrete material with elapse of time where traditional cement-based materials requiring man-made repairs are contrasted with self-healing cement-based materials.	12
Figure 3.2: The main distinction is made between autogenic and autonomic self-healing mechanisms.	13
Figure 3.3: Different causes that can lead to autogenic self-healing	
Figure 3.4: Hollow fibers (A) and encapsulation techniques (B) as implemented on self-healing materials.....	15
Figure 3.5: Crack closure observed by optical microscopy in concrete samples with different kind of fibers	18
Figure 3.6: Discrimination of binder, aggregates and secondary precipitated calcite inside crack by polarized light microscopy. 50x magnification (2.7 x 1.4 mm), cross polarized light (Bridge, Amsterdam).....	21
Figure 3.7: Observation of crack healing in fly-ash concrete samples by SEM	21
Figure 3.8: Observation of portlandite (CHP) and hydration products on the surfaces of polished samples by SEM	22
Figure 3.9: Relation between and water flow and time for different crack widths	22
Figure 3.10: Visualization of water permeability test by neutron radiography.....	24
Figure 3.11: Test apparatus for measuring crack width using LVDTs.	25
Figure 4.1: Locations of the monuments.....	34
Figure 4.2: Chronological diagram of the monuments.....	35
Figure 4.3: Terrace 1; citadel with cistern; Late Hellenistic–Early Roman period (Triantafyllidis, 2015)	35
Figure 4.4 (Left): Secondary calcite precipitated filling a crack of 100µm width. Micritic calcite can be seen precipitated on the crack walls where the crack is only partly filled.....	36
Figure 4.5 (Right): Overview of a crack interrupted by larger voids. Parts of the crack are completely filled with calcite whereas the wider parts are only partially filled.....	36
Figure 4.6: Well crystallized secondary calcite crystals precipitated inside a void.....	
Figure 4.7 (Right): Secondary calcite precipitated in the binder and calcareous aggregates' interface	37

Figure 4.8 (Left): Well crystallized sparitic and micritic calcite filling a 150 μ m crack	37
Figure 4.9 (Right): Overview of a partly filled crack (100 μ m width) by a homogeneously crystallized calcite	37
Figure 4.10: Roman tomb in Fiscardo excavation.....	38
Figure 4.11: (Left) Well crystallized calcite crystals ranging in size up to 50 μ m inside a large void; (Right) Detailed microphotograph of the crystals microstructure.....	38
Figure 4.12: Extended network of microcracks partially filled with secondary calcite	39
Figure 4.13: Extended network of microcracks partially filled with secondary calcite	40
Figure 4.14 (Right): Completely healed crack bridging two large pores. A homogenous layer of calcite precipitation can be seen on the pore wall.....	40
Figure 4.15: Calcite crystals growing on the voids' wall	40
Figure 4.16: Exterior fortification walls of Daphni monastery	41
Figure 4.17 (Left): Extended network of microcracks and voids partially or completely filled by secondary micritic calcite	42
Figure 4.18 (Right) Microcrack of varying diameter filled by secondary calcite	42
Figure 4.19: Network of microcracks and voids partially filled by secondary calcite	42
Figure 4.20 (Left): Extended crack network completely filled by secondary calcite. Micritic and sparitic calcite crystals are present	43
Figure 4.21 (Right): Microstructure of re-crystallized calcite on a pore surface	43
Figure 4.22 (Left): Re-crystallization of calcite inside cracks and voids in the vicinity of microfossils and calcareous aggregates.....	43
Figure 4.23 (Right): Micrograph of sparitic calcite on a crack wall.....	43
Figure 4.24: Secondary sparitic calcite crystals in the vicinity of lime lump filling completely a 50 μ m width crack.	44
Figure 4.25: (Left) Leached secondary calcite partly repairing damaged microstructure. (Right) Chemical analysis of precipitated calcite.....	45
Figure 4.26 (Left): Secondary calcite precipitated around a lime lump	45
Figure 4.27 (Right): Overview of a completely filled crack (80 μ m maximum width) by homogeneously crystallized calcite.....	45
Figure 4.29: Secondary calcite evenly precipitated along the sides of a crack	48
Figure 4.30: Irregular cracks provide nucleating points for the precipitation of calcite	48
Figure 4.31: Well formed sparitic calcite crystals. Calcite crystals of different morphology formed, corresponding to the crack width.	49
Figure 4.32: An extensive network of micro-cracks partially or completely filled by secondary calcium carbonate was observed in samples with higher magnesium concentration – Detail of the area EDAX analysis was performed.....	49

Figure 4.33 (Right): Overview of a crack (20-30 μm width) filled with secondary calcite possibly due to the presence of a lime lump.....	50
Figure 4.34 : Network of cracks completely or partially filled with secondary calcite around a calcitic grain	50
Figure 4.35 : Secondary calcite formed around a fossil, possibly providing (supplying) the neighboring cracks with Ca^{2+} ions.....	51
Figure 4.36 : Secondary calcite crystallized in the interface between binder and siliceous aggregates.....	51
Figure 4.37 : Secondary sparitic calcite precipitated around a microfossil filling a void of maximum width 150 μm	51
Figure 5.1 : Electrochemical accelerated leaching setup. (LIFT).....	58
Figure 5.2 : Design of the electrochemical accelerated leaching setup. (LIFT).....	60
Figure 5.3 : A typical example of current (a) and conductivity (b) monitoring as function of leaching period.	61
Figure 5.4 : Linear correlation of Ca concentration with conductivity values	62
Figure 5.5 : Current and conductivity values measured during the leaching tests of calcium hydroxide suspensions.....	63
Figure 5.6 : Maximum values of current and conductivity measured during leaching of calcium hydroxide suspensions	63
Figure 5.7 : Sample preparation	65
Figure 5.8 : Maximum values of conductivity measured as function of curing period of the cylindrical specimens	66
Figure 5.9 : Maximum values of conductivity measured as function of curing period of the powdered specimens.....	66
Figure 5.10 : The evolution of the content (%) of portlandite as was calculated by thermogravimetric analysis of LP and NHL reference mortars during the first 18 months (540 d) of curing	67
Figure 5.11 : Correlation of the available portlandite as measured by DTA/TG in reference specimens with the maximum conductivity values measured during leaching.	67
Figure 5.12 : Calcium concentration in the leachate solution measured by AAS, as a function of curing period of the cylindrical specimens tested	68
Figure 5.13 : Calcium concentration in the leachate solution measured by AAS, as a function of curing period of the powdered specimens tested	69
Figure 5.14 : Diffractograms of reference (black line) and leached (gray line) powder NHL and LP specimens	71

Figure 5.15: Temperature ranges used for the quantification of binder components on leached and reference cylindrical specimens.....	73
Figure 5.16: DTG of LP and NHL cylindrical specimens before (black line) and after leaching from both sides of the specimen. (L-red line and P-blue line).....	74
Figure 5.17: DTG of NHL powder specimens before and after leaching	75
Figure 5.18: DTG of LP powder specimens before and after leaching.....	75
Figure 5.19: FT-IR spectra of ground NHL and LP specimens before (black line) and after (gray line) leaching.....	77
Figure 5.20: Microphotographs of reference (left) and leached (right) powder LP specimens. Ca/Si ratio is result of bulk analysis during SEM examination. In detail microphotograph, the two main particle types are presented along with their measured Ca/Si ratio.....	79
Figure 5.21: Microphotographs of reference (left) and leached (right) powder NHL specimens. Ca/Si ratio is result of bulk analysis during SEM examination. In detail microphotograph, the two main particle types are presented along with their measured Ca/Si ratio.....	79
Figure 5.22: LP specimens as captured before (left) and after (right) leaching. On top the surface in contact with the anode solution (L) and at the bottom the surface in contact with the cathode solution.....	80
Figure 5.23: NHL specimens as captured before (left) and after (right) leaching. On top the surface in contact with the cathode solution (L) and at the bottom the surface in contact with the anode solution.....	81
Figure 5.24: Microphotograph of the specimen's surface in contact with the anode solution (P) is characterized by a precipitated layer of pure calcite crystals.....	82
Figure 5.25: Microphotograph of precipitated calcite observed in cracks and voids throughout the sample	82
Figure 5.26: Microphotographs of both sides of LP specimens (P-left) (L-right) and Ca/Si ratio calculated by analysis of the leached zone.....	84
Figure 5.27: Microphotographs of both sides of NHL specimens (P-left) (L-right) and Ca/Si ratio calculated by analysis of the leached zone.....	85
Figure 5.28: Total porosity % of reference and leached LP and NHL cylindrical specimens. The porosity increase % due to leaching on the side of the anode solution (L) is stated	87
Figure 5.29: Pore size distribution of reference and leached LP and NHL specimens	87
Figure 6.1: Crack initiation by three point bending	93
Figure 6.2: Fracture profiles generated by three -point bending	94
Figure 6.3: Flexural strength and standard deviation measured during crack generation calculated by the average strength values of 32 specimens.....	94

Figure 6.4: Overview of cracks on the bottom side of cracked specimens.	95
Figure 6.5: Detailed measurement of crack	95
Figure 6.6: The evolution of portlandite and calcite content (wt%), as they were calculated by thermo-gravimetric analysis of LP and NHL reference mortars during the first two months of curing (60 d).....	97
Figure 6.7: Timeline of curing and healing periods	99
Figure 6.8: Sample preparation for SEM and polarizing light microscope. One specimen was split in two to reveal the crack surface	99
Figure 6.9: Separation of the crack walls might lead to: the observation of secondary healing products in either walls (a) or the detachment from one wall due to low cohesion with the crack surface	100
Figure 6.10: Epoxy impregnated specimens were cut vertically to expose a cross-section of the crack	100
Figure 6.11: Experimental outline.....	101
Figure 6.12: Precipitation of secondary calcite on the crack mouth as observed in under polarizing microscope (left-LP, right-NHL)	102
Figure 6.13: Secondary hydraulic phases at different healing conditions (95% RH, 75% RH and wet/dry cycles) develop a single uniform layer of interconnected fibers. In detail: the outward orientation of the fibers.	104
Figure 6.14: Secondary hydraulic phases are formed on various substrates such as (a) and (b) on micritic calcite in the binder matrix, (c) on the surface of aggregates and (d) together with secondary calcite	105
Figure 6.15: Fiber-like secondary hydraulic phases bridging a micro-crack of ~30 μm	106
Figure 6.16: Morphology of CaCO_3 developed at different humidity levels (95%RH, 75% RH and wet/dry cycles)	106
Figure 6.17: Secondary fiber- like hydraulic phases	107
Figure 6.18: Extended zones of secondary calcite precipitation on the crack surface	108
Figure 6.19: Fiber-like secondary hydraulic phases bridging a ~70 μm micro-crack	108
Figure 6.20: Precipitated secondary calcite probably severed during sample preparation. The low cohesion to the binder matrix is evident.....	108
Figure 6.21: Main products formed on the crack surface of LP specimens cracked after 30 days of curing	110
Figure 6.22: Microphotographs of LP303075. Hydration products formed along a smaller perpendicular crack (left) and a micro crack completely filled by calcite (right)	110
Figure 6.23: Well-formed secondary calcite crystals up to ~50 μm in diameter.....	111
Figure 6.24: Secondary fiber- like hydraulic phases in NHL specimens cured under wet/dry cycles and at 95%RH	112
Figure 6.25: Honeycomb formation observed in specimens cured under wet/dry cycles and detail	
Figure 6.26: CSH needle-like formations observed in specimens cured at 95%RH	113
Figure 6.27: Highly gelatinous hydraulic phases in specimens cured at 95%RH	113
Figure 6.28: Secondary fiber and needle-like hydraulic phases.....	114
Figure 6.29: Expanded honeycomb formations in specimens healed for 90 days.....	114
Figure 6.30: Layers of well-formed calcite crystals are precipitated alongside dense networks of fiber-like hydraulic phases, in specimens healed under wet/dry cycles.....	114
Figure 6.31: Conglomerates of needle-like formations in NHL specimens cracked after 30 days of curing.	115
Fig 6.32: Needle-like formations in NHL specimens cracked after 30 days of curing and healed for 90 days.	116

Figure 6.33: Analysis of the secondary products performed by EDAX revealed the two main groups formed in the examined specimens.	117
Figure 6.34: First-step, fiber-like or “low-density” CSH forms a continuous layer	119
Figure 6.35: Second-step needle-like CSH hydration products and detail.....	119
Figure 6.36: Second-step honeycomb CSH formations	119
Figure 6.37: Typical patterns of calcium carbonate formations of varying size and morphology.....	120
Figure 6.38: Secondary formed calcite in LP mortars completely filling a micro crack (left). Chemical characterization of secondary calcite was also determined by EDAX analysis (right).	121
Figure 6.39: Fiber-like secondary hydraulic phases bridging micro-cracks of ~30 and ~70 μm after prolonged healing period.	122
Figure 6.40: Secondary formed calcite in NHL mortars after ten (left-NHL730cy) and thirty wet-dry cycles (right-NHL790cy).	122
Figure 6.41: Secondary formed calcite in LP mortars after ten (left-LP1430) and thirty wet-dry cycles (right-LP1490). It was observed that the precipitation of calcite advances with additional cycles.	123
Figure 7.1: Damage profiles generated by different types of strain; (a) flexural, (b) compressive, (c) tensile and (d) cutting.....	128
Figure 7.2: Localized damage formed by the application of hertzian stress	131
Figure 7.3: Specimens were locally damaged by hertzian contact stress and were subsequently measured as to their residual strength by three point bending test	131
Figure 7.4: Timeline of curing and healing periods	132
Figure 7.5: Damage degree calculated by UPV after incremental loads applied by hertzian stress on NHL 3030 specimens.	133
Figure 7.6: Loading curves obtained during three-point bending tests and damage degree calculated by three-point bending tests after incremental loads applied by hertzian stress. ...	133
Figure 7.7 (Left): Flexural strength values of NHL specimens, damaged at 15 days. The 30 days healing process in elevated humidity conditions resulted in a significant recovery of their strength. Representative loading curves obtained during three-point bending tests.....	138
Figure 7.8: Flexural strength values of NHL specimens damaged at 30 and 240 days and healed for a 30 day healing period in elevated humidity conditions.	138
Figure 7.9: Flexural strength values of healed LP specimens damaged at 15 days 30 and 90 days respectively and healed for a 30 day healing period in elevated humidity conditions...	140
Figure 7.10: Representative loading curves obtained during three-point bending tests specimens damaged after 30 day curing and healed for another 30 days.....	141
Figure 7.11: Flexural strength values of NHL specimens, damaged at 30 days (left) and subsequently cured for 30 (left) or 210 (right) day healing period respectively under high humidity conditions (95%RH).	142
Figure 7.12: Flexural strength values of LP specimens, damaged at 90 days and subsequently cured for 30 (left) or 90 (right) days under high humidity conditions (95%RH).....	142

List of Publications and Conference contributions

• List of Peer-reviewed publications

- 2017 Amenta, M., Karatasios, I., Maravelaki, P., & Kilikoglou, V. The role of aggregate characteristics on the performance optimization of high hydraulicity restoration mortars- Submitted to the Construction and Building Materials Journal (under review)
- 2016 Amenta, M., Karatasios, I., Maravelaki, P., & Kilikoglou, V. (2016). Monitoring of self-healing phenomena towards enhanced sustainability of historic mortars. Applied Physics A, 122(5), 554.
<http://doi.org/10.1007/s00339-016-0064-1>
- 2014 M.Amenta., I.Karatasios, A. Kalagri, P. Maravelaki-Kalaitzaki, V.Kilikoglou, 2015. Mix Design Parameters of Restoration Mortars: The Effect of Aggregate Characteristics, in: Lollino, G., Manconi, A., Guzzetti, F., Culshaw, M., Bobrowsky, P., Luino, F. (Eds.), Engineering Geology for Society and Territory - Volume 5. Springer International Publishing, pp. 85–88.
- 2012 I. Karatasios, M. Amenta, M. Tziotziou and V. Kilikoglou. The effect of relative humidity on the performance of lime-pozzolan mortars, in : Historic Mortars: Characterisation, Assessment Conservation and Repair, Válek, Jan; Hughes, John J.; Groot, Caspar J. W. P. (Eds.), Springer (RILEM Bookseries), 2012, pp. 303-312.

• List of Conference contributions

- 2017 “ Study of Self-healing phenomena in historic mortars ”, M. Amenta, I. Karatasios, N.Maravelaki, V. Kilikoglou, 11th National Scientific Conference of Chemical Engineering, Thessaloniki, 25 - 27 May 2017
- 2015 “Morphology of self-healing products in nhl and lime-pozzolan mortars”, M. Amenta, I. Karatasios, N.Maravelaki, V. Kilikoglou, 15th EMABM, Delft, the Netherlands, 16-19 June 2015.
- 2015 “Study of Self-healing phenomena in traditional lime-based mortars”, M. Amenta, I. Karatasios, N.Maravelaki, V. Kilikoglou, Conservation of Cultural Heritage ,Challenges and Reviews Athens 25-29 May 2015
- 2015 “Monitoring of self-healing phenomena towards enhanced sustainability of conservation mortars”-Amenta M., Karatasios I., Kalagri A., Maravelaki- Kalaitzaki P., Kilikoglou V. E-MRS 2015 Spring Meeting, Lille Grand Palais, May 11-15, 2015
- 2014 “Mix design parameters of restoration mortars-The effect of aggregate characteristics“ Amenta M., Karatasios I., Kalagri A., Maravelaki-Kalaitzaki P., Kilikoglou V.- in XII IAEG Congress, Torino 2014
- 2013 “Deterioration mechanisms of lime-pozzolan and NHL mortars due to sulfate attack” M. Amenta, I. Karatasios, A. Kalagri, V. Kilikoglou. 3rd Historic Mortars Conference, 11-14 September 2013, Glasgow, Scotland

- 2013 “The phenomenon of self-healing in ancient mortars” M. Amenta, I. Karatasios, A. Kalagri, V. Kilikoglou. 6th Symposium on Archaeometry "Cultural influences on the expression of technical skills in the Mediterranean", Hellenic Society for Archaeometry, 16-18 May 2013, Acropolis Museum - Athens.
- 2012 I. Karatasios, A. Kalagri, M. Amenta, V. Kilikoglou Study and application of restoration mortars: From the Lab to the Field . 3rd Conference of the Society for Research and Promotion of Scientific Restoration of Monuments 1-3 November 2012. Athens
- 2012 “The historic mortars under the microscope: Study and interpretation of their microstructural characteristics” A. Kalagri, I. Karatasios, M. Amenta, M. Zerlentis, V. Kilikoglou. 3rd Conference of the Society for Research and Promotion of Scientific Restoration of Monuments 1-3 November 2012. Athens

• **Workshops and seminars attended**

- 2015 OPTO-CH POLITEIA 2015 workshop, at IESL-FORTH, Heraklion, Crete, , concerning Materials analysis with Optical Spectroscopy (LIBS, Raman), Optical coherence metrology for structural diagnosis, Imaging and mapping; multispectral, multi-photon and THz, Laser cleaning
- 2013 NARNIA- Marie Currie training network 3 days Training Course organized at NCSR Demokritos concerning Thermal and mechanical properties of archaeological ceramics (Official language: English)
- 2013 CHARISMA– 2 weeks training course on stone conservation – organized under the framework of the *Oriented-training courses on advanced methodologies* planned by FP7 CHARISMA project – at the Cultural Heritage Agency of the Netherlands in Amsterdam (Official language: English)
- 2011 NARNIA- Marie Currie training network 3 days Training Course organized at NCSR Demokritos concerning Physical and Chemical Properties of clays and archaeological ceramics (Official language: English)
- 2009 3rd Residential Summer School on Conservation Science-Chemistry and Cultural Heritage - Preservation of cultural heritage Lifelong Learning / Erasmus /Intensive Program at Aristotle University of Thessaloniki (Official language: English)
- 2008 NCSR Demokritos, 2008 Summer School. 3-days workshop on cutting edge technologies and applications in the field of materials science. Participation in the Special Workshop on Cultural Heritage Technologies. Athens - Greece